DISSERTATION

INVESTIGATION OF CATIONIC CONTRAST-ENHANCED COMPUTED TOMOGRAPHY FOR THE EVALUATION OF EQUINE ARTICULAR CARTILAGE

Submitted by

Bradley B. Nelson

Department of Clinical Sciences

In partial fulfillment of the requirements

For the Degree of Doctor of Philosophy

Colorado State University

Fort Collins, Colorado

Fall 2017

Doctoral Committee:

Advisor: Christopher E. Kawcak
Co-Advisor: Laurie R. Goodrich

C. Wayne McIlwraith
Mark W. Grinstaff
Myra F. Barrett

ABSTRACT

INVESTIGATION OF CATIONIC CONTRAST-ENHANCED COMPUTED TOMOGRAPHY FOR THE EVALUATION OF EQUINE ARTICULAR CARTILAGE

Osteoarthritis and articular cartilage injury are substantial problems in horses causing joint pain, lameness and decreased athleticism resonant of the afflictions that occur in humans. This debilitating joint disease causes progressive articular cartilage degeneration and coupled with a poor capacity to heal necessitates that articular cartilage injury is detected early before irreparable damage ensues. The use of diagnostic imaging is critical to identify and characterize articular cartilage injury, though currently available methods are unable to identify these early degenerative changes.

Cationic contrast-enhanced computed tomography (CECT) uses a cationic contrast media (CA4+) to detect the early molecular changes that occur in the extracellular matrix. Glycosaminoglycans (GAGs) within the extracellular matrix are important for the providing the compressive stiffness of articular cartilage and their degradation is an early event in the development of osteoarthritis. Cationic CECT imaging capitalizes on the electrostatic attraction between CA4+ and GAGs; exposing the proportional relationship between the amount of GAGs present within and the amount of CA4+ that diffuses into the tissue. The amount of CA4+ that resides in the tissue is then quantified through CECT imaging and estimates tissue integrity through nondestructive assessment. Despite the emergence of this promising technology to capture quantitative information on articular cartilage quality, cationic CECT has not been

thoroughly investigated in equine tissues *in vitro* or *in vivo,* nor has it been investigated in *in vivo* in any large animal or human subjects.

This compilation of studies was designed to critically examine the capacity of cationic CECT to provide quantitative information on articular cartilage quality across a continuum of disease states in horses while dually serving as a translational model to showcase its potential application in humans. The first experiments successfully characterized the diffusion properties of CA4+ into equine articular cartilage *in vitro* and *in vivo*, and also established the femoropatellar joint as the optimum joint for use in the subsequent *in vivo* experimental models. These initial studies also established preliminary evidence of the safety of CA4+ on articular tissues.

The experimental *in vivo* equine impact model delivered a contusive force to articular cartilage that successfully instituted degeneration of the extracellular matrix components and decreased tissue stiffness. This subtle degradation was discernable from healthy articular cartilage using cationic CECT imaging (microCT). *In vivo*, the clinical cationic CECT attenuation demonstrated fair correlations with the biochemical, mechanical and histologic staining measures, though there was not sufficient delineation among groups to detect significant differences between disease states. Further investigations are warranted to determine how focal sites of injury can be identified from the resolution limited by current CT technology.

The second *in vivo* experimental study generated reparative and degenerative articular cartilage to provide comparisons with healthy tissue. The cationic CECT method, using microCT and clinical scanners, demonstrated an ability to distinguish between these groups of varying

articular cartilage quality. Though the results were promising, this study revealed the complexity of detecting subtle articular cartilage injury in a solitary imaging examination owing to the inherent biochemical and biomechanical variation that exists across articular surfaces. However, this study confirmed the successful monitoring of articular cartilage through longitudinal examinations.

Overall, this collection of studies established that cationic CECT imaging *in vitro* and *in vivo* is capable of distinguishing articular cartilage across a spectrum of disease states exemplifying its utility in the comprehensive evaluation of equine articular cartilage. Further work of how this technique compares to other quantitative diagnostic imaging techniques and optimization strategies for routine use are required. Nonetheless, the results of this work reveal the excellent potential of cationic CECT imaging to be incorporated into research and clinical investigations in horses and highlight the feasible translation of this work into human tissues.

ACKNOWLEDGEMENTS

There are many individuals who have been essential in allowing me to complete this work. First and foremost, I acknowledge my graduate committee especially Drs. Chris Kawcak and Laurie Goodrich for serving as my advisors and permitting me to chase my research and clinical interests in orthopedic surgery and articular cartilage imaging. Their immeasurable efforts in providing me with the opportunities and skills necessary to accomplish this work and for my professional development as a clinician scientist are greatly appreciated. I would also like to thank Dr. C Wayne McIlwraith for his valuable advice regarding the *in vivo* models and in his overall guidance throughout this graduate work and in supporting my long-term career goals. I thank Dr. Myra Barrett, who was very encouraging and generously welcomed a surgeon into her diagnostic imaging domain. A special thanks to Dr. Mark Grinstaff whose cationic contrast agent provided the cornerstone of this work, and who helped diversify my research training experience by letting me join his laboratory in Boston.

A very special thanks to Jen (Suddreth) Daniels and the entire Equine Orthopaedic Research Center staff for their care of the research horses and in providing support for the countless early mornings that were required for the *in vivo* studies. I would also like to thank the Equine Orthopaedic Research Center laboratory personnel: specifically Nikki Phillips for her guidance and assistance with laboratory assays and troubleshooting histology staining protocols and Dr. John Kisiday for his guidance with the hydroxyproline assay. I also would like to thank Jeff Stewart, Anthony Nguyen and Chris Schmit, the diagnostic imaging technologists who assisted with the clinical CT and MR imaging.

I am incredibly grateful for my colleagues and mentors in Boston directed by Dr. Mark Grinstaff whose assistance and encouragement substantially improved the caliber of this work. Dr. Janne T.A. Mäkelä, Dr. Rachel Stewart, Taylor Lawson, Dr. Benjy Cooper and Dr. Brian Snyder all welcomed me into their laboratory space at Boston University and the Beth Israel Deaconess Medical Center broadening my knowledge of cartilage biomechanics, imaging analysis and chemistry while providing the equipment necessary to accomplish the goals of this work. A particular thanks to Drs. Amit Patwa and Jon Freedman who literally synthesized gallons of CA4+ for use in these experiments.

I would also like to thank Dr. Valerie Moorman for performing lameness examinations and for her continued guidance, friendship and encouragement throughout my graduate training. I also acknowledge Dr. Katie Seabaugh for performing lameness examinations and for her general support. I thank Dr. Ali Daniel for his friendship, inspiration and discussions about clinical cases and for reinforcing my interest in clinical practice, and Dr. Holly Stewart for her never-ending optimism and reassurance during these last couple of years.

I also extend a special thanks to my parents and brother, Judy, Rod and Tim Nelson for their continued support throughout my veterinary and post-graduate training and for their encouragement as I pursue my career goals.

TABLE OF CONTENTS

CHAPTER 1:

THE ROLE OF ADVANCED DIAGNOSTIC IMAGING IN ARTICULAR CARTILAGE EVALUATION[i]

Introduction

Osteoarthritis (OA) is a well-recognized and prevalent joint disease in horses that leads to debilitating joint pain, lameness and decreased athletic performance.[1-3] The impact of this disease is widespread throughout the equine industry and incurs significant financial costs.[1,3] Projected estimates from nearly 20 years ago revealed that lameness associated costs in horses were approximately $700 million annually and 60% of these costs were estimated to be related to OA.[1] This incurable disease instigates persistent pain that leads to early retirement and in some instances requires humane euthanasia. A recent survey by the American Association of Equine Practitioners given to equine veterinarians revealed that OA is one of the most important diseases requiring further research.[3] Not only limited to horses, OA is also an important human health concern. An estimated 27 million adults have clinical symptoms attributed to OA and a projected 10% of the United States population will be afflicted with symptomatic knee OA by the age of 60.[4,5] Costs associated with OA are estimated at $189 billion annually and these costs are not inclusive of lost wages or decreased mobility.[6] Through decreased mobility and joint pain humans with OA also experience decreased athleticism and may ultimately require artificial joint replacement.[7,8] The similarity in disease prevalence between these two species provides an

[i]This chapter is published in part: Nelson BB, Goodrich LR, Barrett MF, Grinstaff MW, Kawcak CE. Use of contrast media in computed tomography and magnetic resonance imaging in horses: techniques, adverse events, and opportunities. *Equine Vet J* 2017, 49 410–424.

opportunity to use equine research models to investigate new diagnostic and treatment methods to improve our understanding of this debilitating disease in horses while establishing a platform to promote translational research that simultaneously benefits humans.

The pathogenesis of OA is complex and may involve some or all of the structures that compose and surround the joint. Repetitive or single trauma could lead to inflammation of the peri-articular soft tissues (*e.g.* synovium and capsule), remodeling of the subchondral bone, ligamentous injury leading to joint instability or defects of joint congruency (*e.g.* fractures) that elicit abnormal stresses on normal articular cartilage.[9-11] Developmental articular cartilage defects including osteochondrosis could also initiate the degeneration of articular cartilage under normal physiologic joint loading conditions. Although there is variation in the underlying cause of OA, the disease is very complex and may involve multiple joint structures with complex pathobiological processes. Nonetheless, all attributes of injury lead to a progressive degeneration of articular cartilage.[12]

Pathophysiology of articular cartilage injury

Articular (hyaline) cartilage is vital joint tissue functioning to provide a smooth gliding surface between opposing subchondral bone surfaces and is integral to confer a near frictionless motion during joint movement. Articular cartilage is a viscoelastic tissue composed of chondrocytes suspended within an extracellular matrix (ECM).[13] The ECM is a complex tissue, but is comprised of three main components: proteoglycans, collagens, and water. Water makes up approximately 70% of the ECM on a wet weight basis. Excluding water (dry weight basis), the remainder of ECM components are 50% collagen, 35% proteoglycans, 10% glycoproteins, and

5% minerals, lipids and other miscellaneous substances.[13] The concentrations of ECM constituents and chondrocytes differ between zonal distributions of the tissue.[11] Compared with deeper layers, the superficial (tangential) zone of articular cartilage has the lowest concentration of proteoglycans, the highest density of chondrocytes and collagen is more densely packed and arranged parallel to the joint surface, counteracting the shear and tensile forces that occur at the articular surface. Extending into the intermediate (transitional) and deep (radiate) zones, chondrocyte size and proteoglycan concentrations increase, collagen density and water content decrease, and the orientation of collagen fibers shifts from parallel to perpendicular to the articular surface.[11,14]

Proteoglycans exist predominantly (85%) in the form of aggrecan (proteoglycan molecules attached to a hyaluronan backbone), although several minor proteoglycans also exist.[11] The proteoglycan molecules consist of a core protein with hundreds of glycosaminoglycan (GAG) polysaccharide side chains. The three predominant GAGs on aggrecan are chondroitin-4 sulfate, chondroitin-6-sulfate and keratan sulfate. The high numbers of sulfated and carboxyl groups on GAGs confer an overall negative charge to the tissue that leads to repulsion of adjacent GAG molecules while also promoting the attraction of sodium and water. The diffusion into and the retention of water in the ECM occurs because of two different processes: 1) the strong osmotic pressure present from polymer solutions (due to sodium content in the ECM) pulls water into the tissue, and 2) the (negative) charged contribution of GAGs, which are governed by Gibbs-Donnan equilibrium, lead to electrostatic attraction of the positive pole on the hydrogen atoms of water molecules.[15] These two processes draw in water and collagen functions to retain it, which confines a positive pressure inside of the tissue. This positive pressure affords the compressive

stiffness of articular cartilage that is endured during joint loading. Since GAGs are essentially fixed in place because of the strong charge this is termed fixed charge density.[11]

Collagen is also an important substance in the ECM with type II collagen predominating. Type II collagen forms a highly organized and cross-linked meshwork that restrains the large aggrecan molecules.[16] Type XI collagen is found within fibrils and type IX collagen (technically classified as both a proteoglycan and a collagen because of the presence of chondroitin sulfate) is integrated into the fibril surface of collagen allowing for interactions with other matrix constituents.[17] This interface facilitates the retention of proteoglycans and water and also forms covalent cross-links with type II collagen stabilizing the ECM network.[17] The positive pressure within the ECM facilitated by proteoglycans does not lead to cartilage swelling because of collagen network retaining the proteoglycans and water in the tissue.

While high proteoglycan and collagen content in articular cartilage is beneficial for tissue strength and integrity, there is natural variability. Proteoglycan and collagen distributions vary across joint surfaces depending upon the biomechanical forces normally inherent to that location, age, athletic activity or become altered as an adaptive response.[18-29] With increasing age, GAGs, water, and chondrocyte density decreases, causing a relatively higher collagen content than in juveniles.[19,24] Experimental studies have shown that the degree of athletic activity and specific joints influence articular cartilage physiology differently. Non-strenuous exercise influences a reversible, though considered beneficial, increase in GAG while strenuous activity decreases articular cartilage stiffness, and causes surface fibrillation, chondrocyte cluster formation and thickening of the calcified cartilage layer in carpal joints.[30-33] Adaptive thickening of hyaline

cartilage in the third carpal bone occurs following strenuous exercise.[24,34] In the metacarpophalangeal joint, exercise increases chondrocyte viability and proteoglycan content compared to controls,[35] but does not markedly affect articular cartilage structure or function.[36]

An early event in OA is the loss of GAGs from the ECM. This loss and degeneration leads to a reduction in the overall fixed charge density of the tissue and in effect causes less attraction of water compared to undamaged tissue. The overall reduction of negative charge lowers water attraction in the ECM and also leads to a decrease in compressive stiffness during joint loading. As articular cartilage is compressed during joint loading, the water normally confined to the ECM is partly expelled from the tissue. The amount of water expelled is directly related to the health and biochemical constituent concentrations of the tissue with decreasing proteoglycan and collagen content increasing hydraulic permeability.[37] With the increased ease of water expulsion and degeneration of components that draw and retain water within the ECM, the tissue becomes weaker and more susceptible to damage even under normal loading forces.

In early OA, there is also an increase in tissue hydration, which seems counterintuitive based on the decrease in electrostatic attraction that occurs following GAG loss. However, articular cartilage swelling does not occur because of the loss of GAGs, but because of the breakdown of the collagen network or its constitutive connections to GAGs permitting the tissue to swell.[38] The breakdown of bonds between type IX and type II collagen may also play a role by loosening this stable network and allowing for the previously confined ECM to swell until type II collagen in the superficial layer halts further expanse. With breakdown of collagen and proteoglycan bonds, there is increased space in the ECM (relative to non-degenerate ECM) and proteoglycan

structures unwind and expose more negative charges on the GAG molecules available to bind water thereby causing ECM swelling.[39] Nonetheless, during joint loading the respective decrease in negative charge and lower osmotic pressure in the ECM leads to water escaping more easily than in healthy tissue. The alteration in GAG content in early OA also leads to a sharper pressure gradient between adjacent cartilaginous zones and puts higher stresses on the superficial layers of collagen. Once the collagen layer becomes disrupted, the articular cartilage tissue swells due to a loss of tensile strength.[40,41] After the superficial layer is compromised, further joint loading contributes to additional GAG loss in deeper portions of the tissue leading to successive migration of the sharp pressure gradient into deeper cartilaginous zones, promoting further degeneration. These early biochemical changes in proteoglycans and collagens build over time and cause progressive deterioration of the tissue until macroscopic surface fibrillation occurs, which then promotes partial and full thickness articular cartilage loss and subchondral bone exposure.

Though articular cartilage is a vital tissue, a complex relationship exists between all articular tissues and the joint is considered as a whole organ. The tissue that must work in synergy with articular cartilage is the subchondral bone. Articular cartilage and the subchondral bone are connected through the calcified cartilage layer. The subchondral bone plate is porous and permits microvasculature and small solutes to extend into the calcified cartilage layer and provide a source of extrinsic healing to the avascular and aneural articular cartilage.[42] Beneath the subchondral bone plate is the more metabolically active subchondral trabecular bone network that provides shock absorption and maintains joint shape.[10] The communication exchange between articular cartilage and bone is critical and damage to any of the structures can promote

the development and progression of OA.[43,44] Injury to the subchondral bone is observed as sclerosis, increased vascular invasion, advancement and duplication of the tidemark, and thickening with microcrack formation of calcified cartilage.[45,46] The trabecular bone responds to injury through increased separation between trabecular septae and decreased volume and thickness while continued inflammation and injury promote the development of bone marrow and cystic lesions.[44] As stated earlier many other structures (*e.g.* synovial membrane, intra-articular and peri-articular ligaments) are involved in the pathogenesis of joint disease. The synovial membrane produces synovial fluid generating lubricity but also releases inflammatory mediators that lead to progressive joint deterioration. Intra- and periarticular ligaments provide joint stability and restrict the course of motion by keeping opposing articular cartilage surfaces together and avoiding high impact forces that would develop with joint laxity. Injury of these supportive structures that normally hold the joint together leads to alterations in joint loading and promotes joint tissue destruction.

Despite having three different repair strategies (*i.e.* intrinsic, extrinsic and matrix flow), articular cartilage healing is inherently poor. Even under optimal conditions, articular cartilage does not regenerate hyaline (type II) cartilage and instead produces fibrocartilage (Type III collagen), which is substantially weaker than normal (hyaline) articular cartilage. Coupled with a poor healing capacity and the progressive deterioration that occurs in OA, the detection of articular cartilage in its early stages of injury are critical to provide clinicians with the best opportunity to implement successful treatment strategies and improve patient outcomes. As such, there are numerous diagnostic imaging methods available that are used in attempts to detect articular cartilage injury.

Diagnostic imaging of articular cartilage

With the many articular structures that are involved in the development of OA, the use of diagnostic imaging is paramount to evaluate all joint tissues. However, the ability of imaging modalities to highlight articular cartilage and expose early degenerative conditions still remains a substantial challenge.[47] Before reviewing the advanced techniques (magnetic resonance imaging [MRI] and computed tomography [CT]) used for articular cartilage and joint evaluation, the more commonly employed methods will be discussed along with their limitations.

Radiography, lacking the ability to show articular cartilage directly, is used to evaluate joints for indirect signs consistent with OA including periarticular osteophytes, subchondral bone lysis or sclerosis, osteochondral fragmentation, or joint space narrowing.[48,49] Although these radiographic findings are consistent with OA, they do not confirm damage to articular cartilage. Despite the inability to directly image articular cartilage, the rapidity and easy access to this modality explains its first-line status for joint injury evaluation in both horses and humans. In horses (and humans) joint space narrowing is commonly used as an indirect measure of articular cartilage integrity; however, false identification can occur with inappropriate patient positioning and joint loading during acquisition.[50] Despite its shortcomings, radiography is a fast and readily available modality that still has clinical usefulness today for the screening of joint disease but nonetheless is incapable of highlighting early articular cartilage injury.

Ultrasonography shows articular cartilage and other joint soft tissues directly at a low cost while avoiding ionizing radiation. The good spatial and contrast resolution of joint tissues and rapid multi-planar assessment highlights the benefit of this technology. The physical properties of

sound limit penetration of ultrasound echoes through air and bone, anisotropy of the ultrasound beam angle can influence articular cartilage appearance and the technique is operator-dependent.[51,52] However, the high spatial resolution and rapid multiplanar assessment is useful to detect subtle alterations at the osteochondral junction and has been shown to supersede radiography for the detection of osteochondosis in the femoral trochlea of horses.[53,54] Deep articular structures obscured by a bone or gas interface severely limit the capabilities of this modality to detect articular cartilage injury. Though insensitive for early articular cartilage injury, the high detection of other joint tissue injuries (*e.g.* synovial membrane thickening, intra- and peri-articular ligament tearing, joint effusion, osteophyte formation) are clear advantages of ultrasound.[51,55,56] Despite improvements in ultrasound technology the detection of early articular cartilage degeneration or subtle morphologic change (including surface fibrillation) remains intangible.

Nuclear medicine techniques (*e.g.* 99m Technicium hydroxymethane diphosphonate scintigraphy, 18F-Fluoro-deoxy-glucose-positron emission tomography [PET]) are performed after the systemic injection of a radioisotope bound to a carrier that homes in on the region of interest.[57-64] In orthopedic applications these methods are used to detect regions of bone remodeling, inflammation and pain. There has been development of a tracer used in single photon emission tomography that binds to articular cartilage, but currently this has only been investigated *ex vivo*.[65] Although highly sensitive and capable of detecting physiologic change, nuclear medicine techniques have poor spatial resolution. This can be partially overcome with the use of hybrid technologies (PET-CT, PET-MRI). Regardless, the inability to detect articular cartilage injury limits its usefulness in patients with OA.

Computed tomography (CT) is a 3-dimensional imaging modality that permits sub-millimetric and volumetric assessment and is the modality of choice to evaluate cortical and trabecular bone architecture or soft tissue mineralizations.[49] Benefits of CT include rapid imaging especially with the advent of multi-slice and helical technology. Although CT involves the use of ionizing radiation, continuing advancements in technology have decreased the radiation exposure to patients. However, similar to radiography, the x-ray attenuation of articular cartilage is not distinguished from other intra-articular soft tissues without the administration of contrast media. Adjunctive methods have been adapted to CT to improve soft tissue contrast resolution and the most explored is the addition of contrast media, referred to as contrast-enhanced CT (CECT). In addition to CECT, PET, spectral CT, phase contrast x-ray CT and dual energy CT are new methods being investigated.[57-64] However aside from CECT,[56,66-73] there are sparse data on the use of these other methods in horses.

Magnetic resonance imaging

Magnetic resonance imaging (MRI) capitalizes on the magnetic resonance that occurs when certain atoms (*e.g.* hydrogen) that are capable of absorbing and emitting radiofrequency energy are placed in a magnetic field. Water and fat, both high in hydrogen are therefore mapped with MRI and conveys its use in articular cartilage imaging. Similar to CT, MRI provides volumetric assessment but with improved contrast resolution to identify soft tissue injuries. The applicability of MRI is very diverse with the implementation of different sequences that are used to highlight orthopedic tissues differently and therefore characterize different pathophysiological processes non-invasively. The most commonly used sequences for orthopedic imaging include T1-weighted fast spin echo (FSE), T2-weighted FSE, proton density (PD) and intermediate weighted

FSE and T1-weighted gradient echo (GRE).[74-77] Fat suppression techniques (*e.g.* short-tau inversion recovery [STIR] and fat-saturation of FSE) are commonly used to exclude the signal from fat to highlight other fluids (*e.g.* edema) and are an essential component of orthopedic imaging. Multiple proprietary sequence names have been developed but the large numbers available reveal that perfect sequence to image articular cartilage does not exist.[78,79]

The ability of MRI to provide volumetric and whole joint assessment without the use of ionizing radiation are advantages of articular cartilage imaging but due to the relatively high cost it is not widely used in the initial clinical assessment or during subsequent follow-up joint examinations in horses or humans.[49] Despite the recognized value of MRI, the evaluation of articular cartilage is still difficult in early disease states. Articular cartilage assessment is categorized as morphologic (qualitative) or compositional (also referred as biochemical or quantitative).[78,80,81] Some MRI sequences providing morphologic assessment (*e.g.* FSE) have lower spatial resolution than CT. Three-dimensional (3D) MRI techniques permit isotropic and sub-millimetric voxel dimensions improving upon this limitation. Similar to CT, 3D-MRI sequences can be reconstructed in multiple planes after a single acquisition but the decreased signal-to-noise and lower articular cartilage signal still potentially causes decreased diagnostic performance when compared to CT.[82,83]

Morphologic evaluation of articular cartilage is important to detect early degenerative changes and depict tissue health. Morphologic measurements are used to characterize health of the tissue though the efficacy of particular MRI sequences is reliant on cartilage thickness, joint curvature, spatial resolution and acquisition settings used.[74,84,85] Some studies have shown that articular

cartilage thickness measurements on MRI are not reliable and that volume averaging in thin articular cartilage decreases accuracy.[84,86-89] Additionally joint curvature, and the spatial resolution and acquisition settings used will impact the validity of measurements.[74,84,85] Articular cartilage thickness in the carpus, as measured with MRI, was highly correlated to histologic measurements,[84] but a human study concluded MRI measurements underestimated knee cartilage thickness.[89] Some studies also use measurements after tissue fixation (*e.g.* 10% formalin) and should address the shrinkage that occurs during histologic processing.[90] A study comparing equine metacarpo(tarso)phalangeal joint cartilage measurements with MRI, magnetic resonance arthrography and CT arthrography showed that no method correlated to postmortem measurements.[88] Typically, lower spatial resolution on MR (compared to CT) leads to more volume averaging and when performing measurements, voxel dimensions ≤1/3 of cartilage thickness will help minimize volume-averaging artifacts.[86,87] Despite the benefit of characterizing morphology through thickness measurements, these variables challenge the veracity of conclusions when using MRI.

In light of the complex interplay between articular cartilage and other joint tissues, whole joint scoring systems have been extensively reported in the human literature and when used by expert radiologists are reliable.[91-97] These scoring systems have emerged in the equine literature and are used in research settings to monitor the progression of OA.[98-100] Despite the improvement in global joint tissue evaluation, these morphologic methods are incapable of capturing the compositional changes that occur in the ECM during the early states of OA. With the poor capacity for articular cartilage to heal, the early detection of these degenerated components is critical to prevent tissue loss and joint deterioration. This has lead to the development of

adjunctive MRI techniques that are capable of assessing the molecular ECM components that become altered in early OA: GAGs, collagen and water.

Compositional assessment

MRI techniques that quantitate GAG content include delayed gadolinium enhanced MRI of cartilage (dGEMRIC), T1 rho (T1ρ), sodium MRI and GAG chemical exchange saturation transfer (gagCEST). The most researched compositional MRI technique is dGEMRIC.[66,101] This technique uses an intravenous or intraarticularly administered gadolinium-based contrast media (GCM) that congregates in articular cartilage. Commercial GCM are non-ionic or ionic in nature (Table 1.1). Negatively charged GCM partition into articular cartilage in direct proportion to the (negative) fixed charge density that is imposed by GAGs. Since there is a direct relationship between GAG content and compressive tissue strength, the MRI signal intensity in dGEMRIC reflects not only GAG content but has also been shown to reveal mechanical properties of the tissue.[102,103] Compared to undamaged tissue, degenerative articular cartilage takes in more GCM, which thus decreases the T1 relaxation time and MRI signal intensity.[104] Temporal assessments have also shown that dGEMRIC predicts OA progression.[105-108] However, reporting the MRI signal as an equivalent substitute for GAG content is more complicated and GCM diffusion is also influenced by collagen content, water diffusion trajectory, articular cartilage thickness and exercise.[79,101,109-111] Nonetheless, dGEMRIC still distinguishes healthy, degenerative and reparative articular cartilage using non-destructive assessment.[106,112]

There are only a few equine studies implementing dGEMRIC.[85,112,113] One study used dGEMRIC to predict metacarpophalangeal joint cartilage thickness and found when not contacted by

proximal phalanx cartilage, it had high accuracy and repeatability.[113] Despite the positive correlations, spatial resolution was limited and likely affected segmentation accuracy. The same group used dGEMRIC to quantify T1 signal in intact cadaver metacarpo(tarso)phalangeal joints.[85] They concluded a 60-120 minute delay optimized diffusion across joint surfaces, though would differ *in vivo* due to active joint metabolism. Intra- and inter-reader variability in this study was not assessed. Others have advocated shorter delays (1 min) with intravenous administration *in vivo*.[114] Menendez *et al.* used dGEMRIC *in vivo* in ponies to examine reparative cartilage instituted with gene therapy.[112] Reparative tissue had decreased signal compared to adjacent normal articular cartilage, paralleling findings in humans.[106] Additionally, a lower signal was observed in articular cartilage adjacent to poorly healed defects one year later, reflecting GAG loss in previously normal tissue.[112] Further studies in horses should investigate the repeatability of dGEMRIC to discern normal from degenerative articular cartilage in a variety of joints.

Similar to dGEMRIC, T1ρ reflects GAG content but without the necessity of contrast media.[80] The ECM is a motion-restricted environment for water and the T1ρ technique alters relaxation rates to discern water adjacent to GAGs from free water. Through a relationship with fixed charge density and GAG content, the technique reflects cartilage health and distinguishes disease states.[79,115] Similar to dGEMRIC, other ECM components (*e.g*. collagen fiber orientation and concentration) can influence T1ρ times.[79,116] Similar to hydrogen, sodium-23 has a magnetic dipole moment but differs in gyromagnetic ratio and precessional frequency.[117] Thus, specialized MRI receiver coils are tuned to capture the amount of sodium originating in the tissue. Recalling the electrostatic attraction of sodium to the negatively charged GAG molecules, sodium content

is also altered in OA after GAG loss and sodium MRI is capable of detecting this change.[118,119] gagCEST is a quantitative method that follows the protons in water bound to GAGs. Magnetization transfer is used to estimate this bound water as energy is transferred to free water. It has also been validated, though the complex analysis of signal limits its utility to research centers.[120,121]

Compositional MRI techniques that evaluate collagen content and structure include T2 / T2* mapping and ultrashort echo time. Aside from dGEMRIC, the T2 mapping technique is one of the most commonly researched methods and uses alternating echo times to produce proton relaxation times within each voxel of the imaging volume. During the early stages of OA, collagens first become anisotropic and then degrade allowing water to fill previously occupied space and increasing T2 relaxation times.[105] This alteration is detected with T2 mapping showcasing mechanical and histological attributes of normal, degenerative and reparative states of the tissue while being implemented as a method to provide longitudinal evaluation.[102,112,122-125] T2* mapping is similar to T2 mapping, though uses T2* relaxation times, which are more susceptible to magnetic field inhomogeneity and has lower sensitivity than T2 mapping.[126-129] As the moniker suggests, ultrashort echo time uses very short echo times in the MRI protocol to expose detail in tissues (*i.e.* deep articular cartilage and bone) that have too short of relaxation times to be distinguished with routine echo times used in orthopedic imaging.[105,130] The ultrashort echo time technique is repeatable but has reduced image quality and long scan times and has yet to be explored in equine tissues.[126]

Water is a critical component of ECM and MRI techniques (diffusion-weighted and diffusion-tensor imaging) are used to map the diffusion and trajectory of water, respectively.[121,131] Since water is drawn into the ECM by GAGs and is restrained in the tissue by collagen, measuring water diffusion and trajectory shows its mobility through the tissue characterizing the biochemical ECM milieu. Alteration in water permeation or movement through the tissue indicates tissue health and this information is provided by diffusion MRI. Though commonly applied in neuroimaging, its application in articular cartilage requires long scan times imparting its difficulty for standard use in orthopedic imaging.

With the advent of CECT, there is an ability to improve articular cartilage and soft tissue evaluation using CT technology. Using a similar basis as these compositional MRI methods, new techniques have been developed to improve articular cartilage imaging with CT and will be the focus of the remainder of this review.

Contrast-enhanced computed tomography

The CECT technique is where iodinated contrast medium (ICM) is administered systemically or regionally to enhance soft tissues and provide contrast resolution between soft tissues that have similar x-ray attenuation profiles on standard CT. Administration routes for ICM include arthrography, systemic intravenous administration, or regional intravascular administration with or without a tourniquet applied proximal to the site of injection.[68,70,72,73,132,133] Although these different methods are used to provide soft tissue enhancement in orthopedics, CT arthrography (CTA) is the most investigated for articular cartilage imaging. The use of CTA predates MRI technology and even today CTA is considered as the gold standard method for articular surface

evaluation in humans.[134-137] Other advantages of CT over MRI include lower cost, faster acquisition times, generally higher spatial resolution and higher accessibility.

Contrast media composition

There are many formulations of ICM available with varying physiochemical properties used in their classification (Table 1.1). The base structure of all ICM is a benzene ring with three iodine molecules (denoted as a monomer) and dimerization is process where two benzene rings are adjoined. The most notable ICM attributes include aqueous solubility, ionicity, osmolality, side chain modifications and viscosity.[66,138] Non-ionic (uncharged) ICM are the most commonly used in CT imaging today. Iodine, as an element with a high atomic number (and density), attenuates x-rays more than lower atomic number (and less dense) elements.[139] As iodine is the critical component in ICM that imparts x-ray attenuation, solutions are labeled in mg iodine/mL (mg I/mL) and are commercially available in varying concentrations (Table 1.1). Tissues attenuate x-rays based on their density, thickness and photon energies applied, but distinguishing between different tissue types with similar attenuating properties is challenging. However, after vascular injection, ICM highlight areas of increased vascular perfusion/permeability enabling differentiation of these similar tissues.[140,141] Since most ICM are small molecules (<2 kDa), they freely diffuse beyond the vascular endothelium[138] with <2% becoming intracellular.[140,142] Elimination of ICM is predominantly through the kidneys.[143,144] Although ICM do not undergo tubular reabsorption, the water and salt contained in solution are reabsorbed in the proximal renal tubules. In humans, the plasma half-life is ~2 hours with complete elimination within 20 hours[145] and this appears to be similar in horses.[143,144]

The overall charge on ICM is either negative (anionic) or positive (cationic), or the agent is neutral (non-ionic).[141] Commercially available ionic ICM are exclusively anionic and coordinated with meglumine or sodium. After administration, ionic ICM exert substantially more osmotic pressure in the biological system and are more likely to interact with cell membranes and peptides than non-ionic ICM.[67,138]

The osmolality (osmoles/kilogram) of a contrast medium depends upon its concentration, ionicity, dimerisation/oligomerisation and added solutes. High-osmolar ICM possess 5-8 times higher osmolality than normal equine plasma (280-290 mOsm/kg[146]). Low-osmolar ICM are 2-3 times higher than normal plasma and iso-osmolar ICM approximate it. High-osmolar ICM are more likely to cause adverse effects compared with low- and iso-osmolar ICM.[147,148] Recently, the use of ionic high-osmolar ICM in horses has largely declined due to higher complication rates and the availability of less expensive low-osmolar ICM. In general, ionic ICM simultaneously have high osmolarlity, though ioxaglate is a notable exception (low-osmolar, anionic ICM).

To decrease osmolality while maintaining equivalent or increasing iodine content per dose, ICM possessing two benzene rings and six iodine atoms (*i.e*. dimers) were developed. *In vitro*, higher cytotoxicity is observed with dimers than monomers[149] but *in vivo,* use of dimers causes fewer acute adverse events than monomers.[150] Although overall rates of delayed adverse events are similar for both, in humans, delayed cutaneous symptoms are more common with dimers (16.4%) than monomers (9.7%).[150]

Viscosity is determined by solution concentration, molecular shape and interactions between the ICM molecules and water.[141] Non-ionic ICM possess higher viscosity than ionic ICM because they do not dissociate in solution, and consequently, exhibit decreased osmolality.[151] High viscosity potentially leads to renal injury: resistance to renal tubular flow results in increased intratubular pressure, altering glomerular filtration rate and prolonged ICM contact promotes hypoperfusion and hypoxia.[152,153] For the purpose of this chapter, ICM will be discussed in the context of the agents ionicity.

Contrast media used in computed tomography

As discussed for MRI, CECT provides evaluation through morphologic or compositional measures. Morphologic tissue assessment with CECT requires that the ICM contacts and outlines articular cartilage permitting the distinction of its shape and contour from similar x-ray attenuating soft tissues. Commercially available non-ionic and anionic ICM have limited penetration into articular cartilage causing high x-ray attenuation of the joint space at the junction with the articular surface. Coupled with the high x-ray attenuation of bone, this leaves the hypoattenuating articular cartilage available for topographic evaluation. However, the conspicuity and clarity of articular cartilage will depend upon the concentration of ICM used. High-density objects including very concentrated ICM will cause streaking or blooming artifacts that decrease the ability to accurately evaluate articular cartilage.[67] Some investigators (including this author) prefer 30-40 mgI/mL,[56,154,155] while others use 100-150 mgI/mL successfully.[156,157]

Morphologic assessment using CTA includes evaluation of tissue contour, shape and surface topography and is reliant on sufficient contrast resolution to distinguish articular cartilage from

the synovial space, bone or abutting cartilage. Early detectable morphologic changes include focal fibrillation, fissuring and surface irregularity.[81] Subtle articular cartilage damage is also identified on CT as thickening (swelling) owing to a breakdown of the collagen network that normally restrains the tissue from expanding.[158,159] The depth and volume of articular cartilage are calculated from CTA to identify partial and full thickness defects.[158,160,161] Despite high accuracy,[162,163] thickness measurements are unable to reflect the entire articular surface. Average thickness over the entire joint or measurements of articular cartilage volume can overcome this limitation.[160] In an equine study, average articular cartilage thickness measurements using CTA in metacarpophalangeal joints did not consistently correlate to postmortem measurements,[88] and neither did other imaging methods (MRI and MR arthrography).[88] However, measurements at locations less susceptible to volume averaging were more accurate.[88] Another group similarly compared CTA to MRI and concluded that CTA had higher sensitivity and specificity to detect articular cartilage defects.[164] The contrasting results are explained through the varying spatial resolution, number of sites analyzed, methods to perform measurements and the diseased versus normal joints used between these studies.[88,164] With appropriate imaging resolution and positioning, measurements and lesion detection are more likely to be accurate, though joints with thin articular cartilage, such as the metacarpo(tarso)phalangeal joint, require caution during interpretation.

Anionic ICM

Despite the highly negative fixed charge density in articular cartilage ECM, many studies have shown that anionic ICM still diffuse into the tissue and do so in inverse proportion to GAG content (Figure 1.1).[165-172] After equilibration with ICM, the captured imaging signal from

microCT allows morphologic and depth-dependent assessment while also permitting measurement of tissue thickness and volume. The quantified CECT signal correlates to mechanical and histological properties in bovine, rat and human articular cartilage explants.[165,169,172-175] Studies have also shown that degenerative (GAG depleted) tissues are distinguishable with CECT under experimental and natural disease conditions.[165,166,176,177] These *in vitro* studies have validated the capacity for CECT using microCT to provide biochemical evaluation, though the spatial resolution with microCT is substantially higher (>10-fold) than that capable of clinical scanners. Nonetheless, investigators have examined the capacity for clinical scanners to quantify this biochemical information and have demonstrated that it is achievable in intact *ex vivo* human knee joint articular cartilage.[178] Additionally, a high correlation between CTA (using ioxaglate) and dGEMRIC was shown in humans with symptomatic knee pain.[179]

Cationic ICM

Exploiting the negative charge on GAG, cationic ICM were developed to overcome the repulsive property of anionic ICM with GAG and draw more ICM into the tissue. Joshi *et al.* reported on the synthesis of three different cationic ICM (+1, +2 and +4 charges) with comparisons between agents. The +1 (CA1+) and +2 (CA2+) charged compounds were synthesized as monomers, while the +4 charged (CA4+) compound was fashioned from the dimer ioxaglate. The positive charges on all cationic structures are bestowed from $NH3^{+}$ end groups. This study also showed CA4+ had the highest affinity for GAGs in rabbit articular cartilage compared with the other cationic analogues.[180] Comparative studies of cationic to anionic ICM have shown that captured cationic CECT signal (microCT) with CA4+ was 2.9 times higher than other anionic ICM

compounds at lower doses.[165,169] The higher amount of CA4+ and thus iodine that penetrates into articular cartilage causes the tissue to have higher x-ray attenuation than when anionic ICM is used (Figure 1.1). Other investigations have demonstrated significant correlations between CA4+ and GAG concentration (r = 0.79 - 0.93)[168,169,172,173,181] that surpass the correlations when using anionic ICM (r = -0.44 - 0.79).[168-171,173] Use of CA4+ in experimentally (chondroitinase) degraded articular cartilage showed ~5 times higher sensitivity in detecting degenerative tissue than anionic ICM.[168] There is also an appreciable decrease in cationic (CA4+) CECT attenuation in degenerative articular cartilage compared with healthy articular cartilage that similarly represents histological measures (Figure 1.2). Additionally, cationic (CA4+) attenuation significantly correlates to measured mechanical properties (equilibrium compressive modulus and coefficient of friction) of articular cartilage.[172,173,181]

The successes of these *in vitro* experiments have justified further investigations in animal research models. Importantly, preliminary investigations in small animal models have shown no adverse effects or toxicity to synovial tissues after CA4+ use.[182,183] The diffusion properties of anionic ICM into articular cartilage have been investigated *in vitro* (bovine explants) and *in vivo* (rats and rabbits).[168,182,184] The diffusion profile of CA4+ has also been explored in bovine explants and in rabbits *in vivo*.[168,182] Compared to CA4+, equilibrium is reached slightly faster with anionic ICM. The ability of cationic CECT using CA4+ to evaluate equine articular cartilage across disease states is unknown and requires further investigation.

The substantial impact of OA and the limited capacity of articular cartilage imaging methods to identify early injury are persistent concerns in horses as well as humans. Though there are

inherent differences in the biochemical and mechanical properties of humans and all research animal species, the horse has been established as an important translational research species.[185-187] Because of the synergistic connection between horses and humans, experimental disease models have emerged to improve the detection of articular cartilage injury and to explore new repair strategies under controlled conditions.[188] Cationic CECT is a promising new technology that has potential to transform how articular cartilage is evaluated. Using equine models in this work will establish the capacity of cationic CECT to characterize articular cartilage in horses and illustrate its potential use in humans.

Purpose of study

The evaluation of articular cartilage in horses and humans remains a diagnostic challenge and there is no established technique that provides sensitive assessment. As a quantitative method of articular cartilage evaluation, cationic CECT has shown considerable promise *in vitro* and in preliminary investigations in small animal models. While cationic CECT provides comprehensive information of articular cartilage physiology and mechanical attributes, its potential utility in equine tissue remains unclear. The purpose of this collection of studies is to determine the capacity of cationic CECT to characterize equine articular cartilage across a continuum of disease states, to determine its ability for *in vivo* use while concurrently serving as a translational research model and to establish its potential for articular cartilage imaging in humans.

Study Goals

The first objective of this group of studies was to determine the diffusion properties of CA4+ into equine articular cartilage and establish an experimental joint to be used for further investigation. The second objective was to determine the *in vivo* diffusion kinetics of CA4+ into articular cartilage and investigate its potential toxicity to equine articular tissues. A third objective was to investigate the ability of cationic CECT to identify early degenerative cartilage from healthy tissue using an *in vivo* impact model of subtle articular cartilage injury. The fourth objective was to determine the capacity of cationic CECT to distinguish equine articular cartilage across a continuum of disease states using an *in vivo* model of articular cartilage injury. To address these research objectives, the following hypotheses were generated.

Hypotheses

Hypothesis 1: The diffusion path of CA4+ into equine articular cartilage *in vitro* will increase with time and reach an equilibrated state.

Hypothesis 2: The partition and excretion course of CA4+ into articular cartilage *in vivo* will produce a predictable and consistent diffusion trajectory and will not cause toxicity to articular cartilage or the synovial membrane.

Hypothesis 3: Cationic CECT attenuation in subtly damaged articular cartilage created after impact injury will be distinguishable from normal healthy articular cartilage and will reflect biochemical and mechanical attributes of the tissue.

Hypothesis 4: Cationic CECT attenuation will be significantly different between reparative, degenerative, and normal equine articular cartilage and will indicate the biochemical and mechanical states of these tissues.

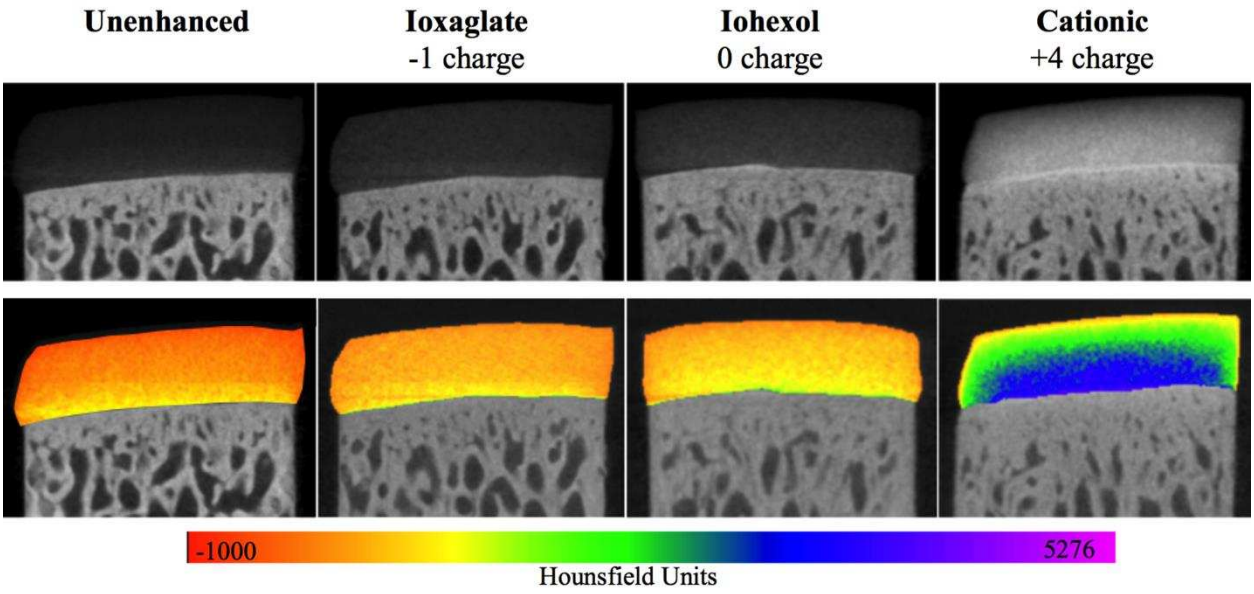

Figure 1.1 – Appearance of articular cartilage after equilibration in variably charged iodinated contrast media. The top row of images show equine osteochondral samples imaged using micro computed tomography without (unenhanced) and with iodinated contrast media. Administered contrast media include ioxaglate (-1 charge), iohexol (0 net charge) and cationic (+4 charge). The bottom row shows the same plugs as above with an applied color map overlying the articular cartilage (reported in Hounsfield units). Window width and level settings were kept identical for all images.

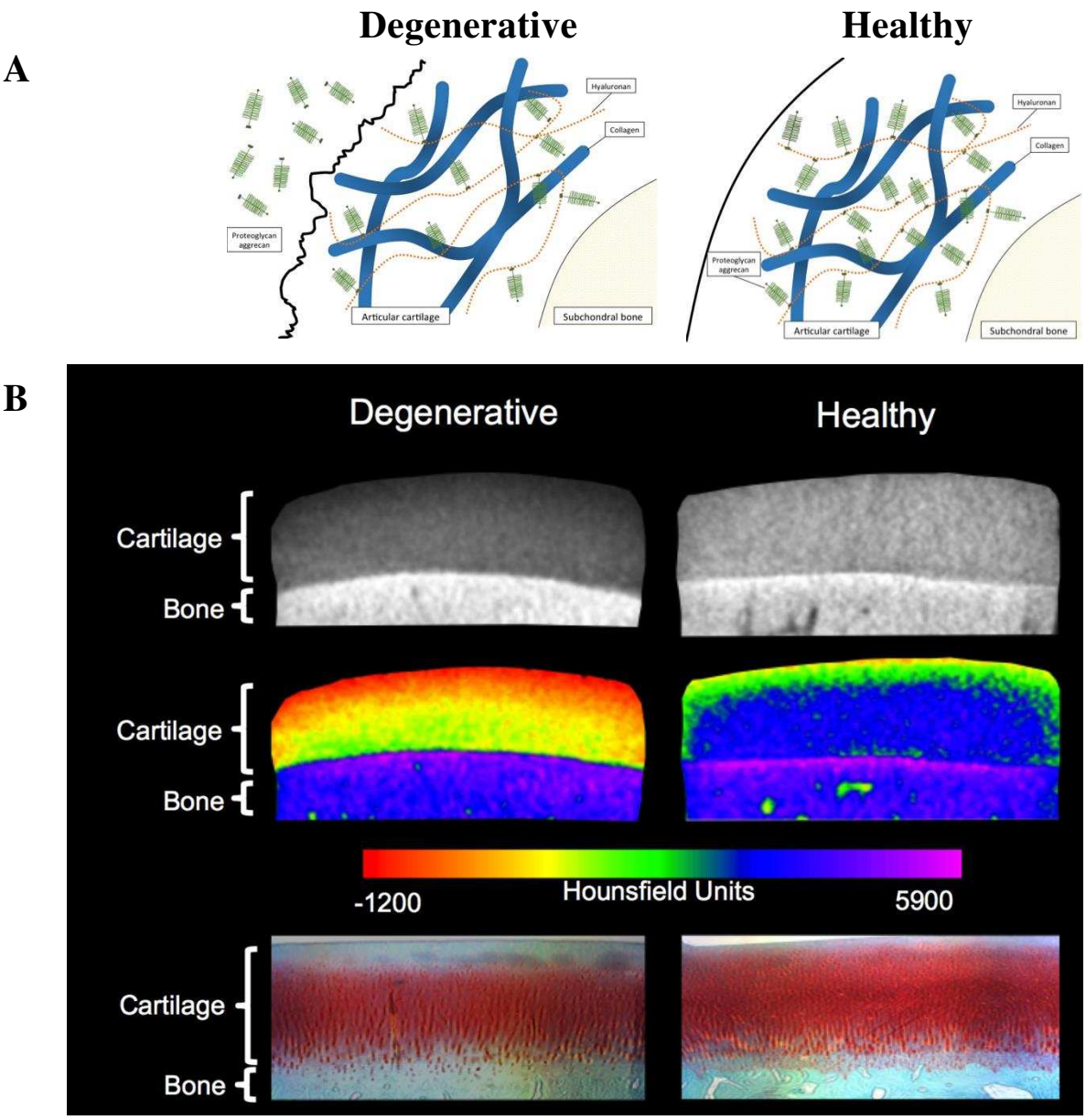

Figure 1.2 – (A) Pictorial diagrams of degenerative and normal articular cartilage. In degenerative articular cartilage, proteoglycans are depleted.[11] (B) Cationic (CA4+) contrast-enhanced computed tomography (CECT) of degenerative versus normal equine articular cartilage samples with comparative histology. The top row shows cationic CECT of osteochondral plugs collected from the equine femoropatellar joint surface. The degenerative plug was collected from a location adjacent to a full-thickness cartilage defect. The normal (healthy) sample was collected from a joint with no macroscopically damaged articular cartilage. The middle row shows the same micro CT scans as above with an applied color map to reveal the range of attenuation values within the tissues. The bottom row shows comparative histology (safranin-O fast green stain) of the same plugs after microCT imaging.

Table 1.1: Structural and physiochemical properties of iodinated and gadolinium contrast media. From Nelson *et al.*[66]
* Monomers have 1 benzene ring with 3 iodine atoms/molecule and dimers have 2 benzene rings with 6 iodine atoms/molecule
† Actual osmolality is reported at 300 mgI/mL (iodinated contrast media) or 0.5 mmol/mL (gadolinium contrast media) unless otherwise indicated in brackets
‡ Viscosity is measured at 37 °C and recorded in millipascal-seconds (mPa.s)
§ Risk categorisations of gadolinium contrast media are based upon recommendations from the European Society of Urogenital Radiology and the Federal Drug Administration. They are predominately made in regards to adverse renal events and are contra-indicated in humans with acute or chronic severe renal injury. These criteria should remain as guidelines, since risk assessments of different GCM have not been performed in horses.
¶ Remainder of elimination is through renal routes.
HOICM, high osmolar iodinated contrast media. LOICM, low-osmolar iodinated contrast media; IOICM; iso-osmolar iodinated contrast media; ECF, extracellular fluid

Contrast media	Commercial name	Structure*	Charge	Relative Osmolality	Actual Osmolality (mOsm/kg)†	Viscosity (mPa.s)‡	Comments§
Iodinated contrast media							
Amidotizoate	Urografin	Monomer	Ionic	HOICM	2100 [370mgI/mL]	8.9	Contraindicated for intrathecal use
Metrizoate	Isopaque	Monomer	Ionic	HOICM	1970	8.0	Contraindicated for intrathecal use
Iothalamate	Cysto-Conray II Conray 400	Monomer	Ionic	HOICM	1700 [325mgI/mL]	3.0	Contraindicated for intrathecal use
Diatrizoate	Renografin, Hypaque	Monomer	Ionic	HOICM	1500 [282mgI/mL]	4.0	Contraindicated for intrathecal use
Ioxithalamate	Telebrix	Monomer	Ionic	HOICM	1500	5.3	Contraindicated for intrathecal use
Iobitridol	Xenetix	Monomer	Non-Ionic	LOICM	915	6.0	
Iopentol	Imagopaque	Monomer	Non-Ionic	LOICM	810 [350mgI/mL]	6.5	
Iohexol	Omnipaque	Monomer	Non-Ionic	LOICM	750	6.7	
Ioversol	Optiray	Monomer	Non-Ionic	LOICM	700	5.5	
Iopromide	Ultravist	Monomer	Non-Ionic	LOICM	650	5.0	

Table 1.1 – continued

Contrast media	Commercial name	Structure*	Charge	Relative Osmolality	Actual Osmolality (mOsm/kg)†	Viscosity (mPa.s)‡	Comments§
Iopamidol	Iopamiro, Isovue	Monomer	Non-Ionic	LOICM	625	4.5	
Ioxilan	Oxilan	Monomer	Non-Ionic	LOICM	600	5.3	
Ioxaglate	Hexabrix	Dimer	Ionic	LOICM	600 [320mgI/mL]	7.5	
Iomeprol	Iomeron, Imeron	Monomer	Non-Ionic	LOICM	550	4.3	
Metrizamide	Amipaque	Monomer	Non-ionic	LOICM	484	7.1	
Iotrolan	Isovist	Dimer	Non-Ionic	IOICM	300	11.6	
Iodixonal	Visipaque	Dimer	Non-Ionic	IOICM	300	11.8	
Gadolinium contrast media							
Gadopentetate dimeglumine	Magnevist	Linear	Ionic	High	1960	2.9	High risk
Gadoversetamide	OptiMARK	Linear	Non-ionic	High	1100	2.0	High risk
Gadodiamide	Omniscan	Linear	Non-ionic	Low	750	1.4	High risk
Gadobenate dimeglumine	MultiHance	Linear	Ionic	High	1970	5.3	Intermediate risk; 4% biliary excretion¶
Gadofosveset trisodium	Vasovist, Ablavar	Linear	Ionic	Low	750 [0.25 mmol/mL]	2.7	Intermediate risk; 9% biliary excretion¶
Gadoxetate disodium	Primovist, Eovist	Linear	Ionic	Low	650 [0.25 mmol/mL]	1.2	Intermediate risk; 50% biliary excretion¶
Gadobutrol	Gadovist, Gadavist	Cyclic	Non-ionic	High	1600 [1 mmol/mL]	5.0	Low risk
Gadoterate meglumine	Dotarem, Magnescope	Cyclic	Ionic	High	1400	2.4	Low risk
Gadoteridol	ProHance	Cyclic	Non-ionic	Low	600	1.3	Low risk

REFERENCES

1. USDA. Lameness and Laminitis in U.S. horses. *National Animal Monitoring System USDA-APHIS: VS, Centers for Epidemiology and Animal Health*. Fort Collins, CO: http://www.aphis.usda.gov/animal_health/nahms/equine/downloads/equine98/Equine98_dr_Lameness.pdf #N318.0100, 2000;(accessed 1 October 2015).
2. Fubini SL, Erb HN, Freeman KP, et al. Prognostic factors affecting survival of 507 horses with joint disease: (1983 to 1990). *Can J Vet Res* 1999;63:253–260.
3. AAEP Foundation. Membership Equine Research Study. Lexington, KY: http://www.aaep.org/images/files/Research Study - Final - 10 07 09.pdf, 2009;(accessed 1 September 2013).
4. Richmond J, Hunter D, Irrgang J, et al. American Academy of Orthopaedic Surgeons clinical practice guideline on the treatment of osteoarthritis (OA) of the knee. *J Bone Joint Surg Am* 2010;92:990-993.
5. Lawrence RC, Felson DT, Helmick CG, et al. Estimates of the prevalence of arthritis and other rheumatic conditions in the United states. Part II. *Arthritis Rheum* 2008;58:26-35.
6. CDC. National and State Medical Expenditures and Lost Earnings Attributable to Arthritis and Other Rheumatic Conditions --- United States, 2003. *MMWR* 2007;56:4-7.
7. Gallo RA, Mosher TJ. Imaging of cartilage and osteochondral injuries: A case-based review. *Clin Sports Med* 2013;32:477-505.
8. Rankin EA, Alarcon GS, Chang RW, et al. NIH consensus statement on total knee replacement December 8-10, 2003. *J Bone Joint Surg Am* 2004;86:1328-1335.
9. McIlwraith CW, Frisbie DD, Kawcak CE. The horse as a model of naturally occurring osteoarthritis. *Bone Joint Res* 2012;1:297-309.

10. Kawcak CE, McIlwraith CW, Norrdin RW, et al. The role of subchondral bone in joint disease: a review. *Equine Vet J* 2001;33:120-126.
11. van Weeren PR. General anatomy and physiology of joints In: McIlwraith CW, Frisbie DD, Kawcak CE, et al., eds. *Joint Disease in the Horse* 2nd ed. St. Louis, MO: Elsevier, 2016;1-24.
12. McIlwraith CW. Traumatic arthritis and posttraumatic osteoarthritis in the horse In: McIlwraith CW, Frisbie DD, Kawcak CE, et al., eds. *Joint disease in the horse*. 2nd ed. St. Louis, MO: Elsevier, 2016;33-48.
13. Todhunter RJ. Anatomy and physiology of synovial joints In: McIlwraith CW,Trotter GW, eds. *Joint Disesase in the Horse*. Philadelphia, PA: Saunders, 1996.
14. Sophia Fox AJ, Bedi A, Rodeo SA. The basic science of articular cartilage. *Sports Health* 2009;1:461-468.
15. Maroudas A. Balance between swelling pressure and collagen tension in normal and degenerate cartilage. *Nature* 1976;260:808-809.
16. Poole AR, Pidoux I, Reiner A, et al. An immunoelectron microscope study of the organization of proteoglycan monomer, link protein, and collagen in the matrix of articular cartilage. *The Journal of Cell Biology* 1982;93:921-937.
17. Goldring M. Cartilage and chondrocytes In: Firestein G, Budd R, Gabriel S, et al., eds. *Kelley's Textbook of Rheumatology*. 9th ed. Philadelphia, PA: Elsevier Saunders, 2013;33-60.
18. Brama PAJ, Karssenberg D, Barneveld A, et al. Contact areas and pressure distribution on the proximal articular surface of the proximal phalanx under sagittal plane loading. *Equine Vet J* 2001;33:26-32.

19. Brommer H, Brama PA, Laasanen MS, et al. Functional adaptation of articular cartilage from birth to maturity under the influence of loading: a biomechanical analysis. *Equine Vet J* 2005;37:148-154.
20. Garcia-Seco E, Wilson DA, Cook JL, et al. Measurement of articular cartilage stiffness of the femoropatellar, tarsocrural, and metatarsophalangeal joints in horses and comparison with biochemical data. *Vet Surg* 2005;34:571-578.
21. Cluzel C, Blond L, Fontaine P, et al. Foetal and postnatal equine articular cartilage development: magnetic resonance imaging and polarised light microscopy. *Eur Cell Mater* 2013;26:33-48.
22. Jeffcott LB, Henson FM. Studies on growth cartilage in the horse and their application to aetiopathogenesis of dyschondroplasia (osteochondrosis). *Vet J* 1998;156:177-192.
23. Changoor A, Hurtig MB, Runciman RJ, et al. Mapping of donor and recipient site properties for osteochondral graft reconstruction of subchondral cystic lesions in the equine stifle joint. *Equine Vet J* 2006;38:330-336.
24. Firth EC. The response of bone, articular cartilage and tendon to exercise in the horse. *J Anat* 2006;208:513-526.
25. Brama PA, Tekoppele JM, Bank RA, et al. Functional adaptation of equine articular cartilage: the formation of regional biochemical characteristics up to age one year. *Equine Vet J* 2000;32:217-221.
26. Brama PA, TeKoppele JM, Bank RA, et al. Development of biochemical heterogeneity of articular cartilage: influences of age and exercise. *Equine Vet J* 2002;34:265-269.

27. Brama PA, TeKoppele JM, Bank RA, et al. Biochemical development of subchondral bone from birth until age eleven months and the influence of physical activity. *Equine Vet J* 2002;34:143-149.

28. Brama PA, Tekoppele JM, Bank RA, et al. Topographical mapping of biochemical properties of articular cartilage in the equine fetlock joint. *Equine Vet J* 2000;32:19-26.

29. te Moller NCR, van Weeren PR. How exercise influences equine joint homeostasis. *Vet J* 2017;222:60-67.

30. Murray RC, Janicke HC, Henson FM, et al. Equine carpal articular cartilage fibronectin distribution associated with training, joint location and cartilage deterioration. *Equine Vet J* 2000;32:47-51.

31. Murray RC, Smith RK, Henson FM, et al. The distribution of cartilage oligomeric matrix protein (COMP) in equine carpal articular cartilage and its variation with exercise and cartilage deterioration. *Vet J* 2001;162:121-128.

32. Murray RC, Whitton RC, Vedi S, et al. The effect of training on the calcified zone of equine middle carpal articular cartilage. *Equine Vet J Suppl* 1999:274-278.

33. Murray RC, Zhu CF, Goodship AE, et al. Exercise affects the mechanical properties and histological appearance of equine articular cartilage. *J Orthop Res* 1999;17:725-731.

34. Firth EC, Rogers CW. Musculoskeletal responses of 2-year-old Thoroughbred horses to early training. 7. Bone and articular cartilage response in the carpus. *N Z Vet J* 2005;53:113-122.

35. Dykgraaf S, Firth EC, Rogers CW, et al. Effects of exercise on chondrocyte viability and subchondral bone sclerosis in the distal third metacarpal and metatarsal bones of young horses. *Vet J* 2008;178:53-61.

36. Nugent GE, Law AW, Wong EG, et al. Site- and exercise-related variation in structure and function of cartilage from equine distal metacarpal condyle. *Osteoarthritis Cartilage* 2004;12:826-833.

37. Katta J, Stapleton T, Ingham E, et al. The effect of glycosaminoglycan depletion on the friction and deformation of articular cartilage. *Proceedings of the Institution of Mechanical Engineers, Part H: Journal of Engineering in Medicine* 2008;222:1-11.

38. Eyre DR, Weis MA, Wu JJ. Articular cartilage collagen: an irreplaceable framework? *Eur Cell Mater* 2006;12:57-63.

39. Athanasiou K, Darling E, Hu J. Articular cartilage pathology and therapies In: Athanasiou KA, Darling EM,Hu JC, eds. *Articular Cartilage*. Boca Raton, FL: Taylor & Francis Group, LLC, 2013;105-164.

40. Lai WM, Hou JS, Mow VC. A triphasic theory for the swelling and deformation behaviors of articular cartilage. *J Biomech Eng* 1991;113:245-258.

41. Bank RA, Soudry M, Maroudas A, et al. The increased swelling and instantaneous deformation of osteoarthritis cartilage is highly correlated with collagen degradation. *Arthritis & Rheumatism* 2000;43:2202-2210.

42. Arkill KP, Winlove CP. Solute transport in the deep and calcified zones of articular cartilage. *Osteoarthritis Cartilage* 2008;16:708-714.

43. Burr DB. The importance of subchondral bone in osteoarthrosis. *Curr Opin Rheumatol* 1998;10:256-262.

44. Li G, Yin J, Gao J, et al. Subchondral bone in osteoarthritis: insight into risk factors and microstructural changes. *Arthritis Res Ther* 2013;15:223.

45. Young DR, Richardson DW, Markel MD, et al. Mechanical and morphometric analysis of the third carpal bone of thoroughbreds. *Am J Vet Res* 1991;52.

46. Lacourt M, Gao C, Li A, et al. Relationship between cartilage and subchondral bone lesions in repetitive impact trauma-induced equine osteoarthritis. *Osteoarthritis Cartilage* 2012;20:572-583.

47. McIlwraith CW. Traumatic arthritis and posttraumatic osteoarthritis in the horse In: C.W. McIlwraith, D.D. Frisbie, C.E. Kawcak, et al., eds. *Joint Disease in the Horse* 2nd ed. St. Louis, MO: Elsevier, 2016;33-48.

48. Laverty S, Stover SM, Belanger D, et al. Radiographic, high detail radiographic, microangiographic and histological findings of the distal portion of the tarsus in weanling, young and adult horses. *Equine Vet J* 1991;23:413-421.

49. Roemer FW, Eckstein F, Hayashi D, et al. The role of imaging in osteoarthritis. *Best Pract Res Clin Rheumatol* 2014;28:31-60.

50. Contino EK, Barrett MF, Werpy NM. Effect of limb positioning on the radiographic appearance of the distal and proximal interphalangeal joint spaces of the forelimbs of horses during evaluation of dorsopalmar radiographs. *J Am Vet Med Assoc* 2014;244:1186-1190.

51. Barrett MF, Frisbie DD, McIlwraith CW, et al. The arthroscopic and ultrasonographic boundaries of the equine femorotibial joints. *Equine Vet J* 2012;44:57-63.

52. Barthez PY, Bais RJ, Vernooij JC. Effect of ultrasound beam angle on equine articular cartilage thickness measurement. *Vet Radiol Ultrasound* 2007;48:457-459.

53. Beccati F, Chalmers HJ, Dante S, et al. Diagnostic sensitivity and interobserver agreement of radiography and ultrasonography for detecting trochlear ridge osteochondrosis lesions in the equine stifle. *Vet Radiol Ultrasound* 2013;54:176-184.

54. Martel G, Forget C, Gilbert G, et al. Validation of the ultrasonographic assessment of the femoral trochlea epiphyseal cartilage in foals at osteochondrosis predilected sites with magnetic resonance imaging and histology. *Equine Vet J* 2017;doi: 10.1111/evj.12698. [Epub ahead of print].

55. Adrian AM, Barrett MF, Werpy NM, et al. A comparison of arthroscopy to ultrasonography for identification of pathology of the equine stifle. *Equine Veterinary Journal* 2017;49:314-321.

56. Nelson BB, Kawcak CE, Goodrich LR, et al. Comparison between computed tomographic arthrography, radiography, ultrasonography, and arthroscopy for the diagnosis of femorotibial joint disease in western performance horses. *Vet Radiol Ultrasound* 2016;57:387-402.

57. Spriet M, Espinosa P, Kyme AZ, et al. Positron emission tomography of the equine distal limb: exploratory study *Vet Radiol Ultrasound* 2016;57:630-638.

58. Sobal G, Velusamy K, Kosik S, et al. Preclinical evaluation of (99m)Tc labeled chondroitin sulfate for monitoring of cartilage degeneration in osteoarthritis. *Nucl Med Biol* 2016;43:339-346.

59. Rajendran K, Lobker C, Schon BS, et al. Quantitative imaging of excised osteoarthritic cartilage using spectral CT. *Eur Radiol* 2017;27:384-392.

60. Mallinson PI, Coupal TM, McLaughlin PD, et al. Dual-Energy CT for the Musculoskeletal System. *Radiology* 2016;281:690-707.

61. Spriet M, Espinosa P, Kyme AZ, et al. 18F-Sodium fluoride Positron Emission Tomography of the equine distal limb: Exploratory study in three horses. *Equine Vet J*:10.1111/evj.12719.

62. Nagarajan MB, Coan P, Huber MB, et al. Computer-aided diagnosis for phase-contrast X-ray computed tomography: quantitative characterization of human patellar cartilage with high-dimensional geometric features. *J Digit Imaging* 2014;27:98-107.

63. Nagarajan MB, Coan P, Huber MB, et al. Computer-aided diagnosis in phase contrast imaging X-ray computed tomography for quantitative characterization of ex vivo human patellar cartilage. *IEEE Trans Biomed Eng* 2013;60:2896-2903.

64. Omoumi P, Mercier GA, Lecouvet F, et al. CT arthrography, MR arthrography, PET, and scintigraphy in osteoarthritis. *Radiol Clin North Am* 2009;47:595-615.

65. Cachin F, Boisgard S, Vidal A, et al. First ex vivo study demonstrating that 99mTc-NTP 15-5 radiotracer binds to human articular cartilage. *Eur J Nucl Med Mol Imaging* 2011;38:2077-2082.

66. Nelson BB, Goodrich LR, Barrett MF, et al. Use of contrast media in computed tomography and magnetic resonance imaging in horses: Techniques, adverse events and opportunities. *Equine Vet J* 2017;49:410-424.

67. Pollard R, Puchalski S. CT contrast media and applications In: Schwarz T,Saunders JH, eds. *Veterinary Computed Tomography*. West Sussex, United Kingdom: John Wiley & Sons Ltd., 2011;57-65.

68. Puchalski SM. Advances in equine computed tomography and use of contrast media. *Vet Clin North Am Equine Pract* 2012;28:563-581.

69. Puchalski SM, Galuppo LD, Drew CP, et al. Use of contrast-enhanced computed tomography to assess angiogenesis in deep digital flexor tendonopathy in a horse. *Vet Radiol Ultrasound* 2009;50:292-297.

70. Puchalski SM, Galuppo LD, Hornof WJ, et al. Intraarterial contrast-enhanced computed tomography of the equine distal extremity. *Vet Radiol Ultrasound* 2007;48:21-29.

71. Puchalski SM, Snyder JR, Hornof WJ, et al. Contrast-enhanced computed tomography of the equine distal extremity. Proceedings of the 51st Annual Convention of the American Association of Equine Practitioners 2005;389-397.

72. Vallance SA, Bell RJ, Spriet M, et al. Comparisons of computed tomography, contrast-enhanced computed tomography and standing low-field magnetic resonance imaging in horses with lameness localised to the foot. Part 2: Lesion identification. *Equine Vet J* 2012;44:149-156.

73. Vallance SA, Bell RJ, Spriet M, et al. Comparisons of computed tomography, contrast enhanced computed tomography and standing low-field magnetic resonance imaging in horses with lameness localised to the foot. Part 1: anatomic visualisation scores. *Equine Vet J* 2012;44:51-56.

74. Gonzalez LM, Schramme MC, Robertson ID, et al. MRI features of metacarpo(tarso)phalangeal region lameness in 40 horses. *Vet Radiol Ultrasound* 2010;51:404-414.

75. King JN, Zubrod CJ, Schneider RK, et al. MRI findings in 232 horses with lameness localized to the metacarpo(tarso)phalangeal region and without a radiographic diagnosis. *Vet Radiol Ultrasound* 2013;54:36-47.

76. Werpy NM, Ho CP, Pease AP, et al. The effect of sequence selection and field strength on detection of osteochondral defects in the metacarpophalangeal joint. *Vet Radiol Ultrasound* 2011;52:154-160.

77. Olive J, d'Anjou MA, Alexander K, et al. Correlation of signal attenuation-based quantitative magnetic resonance imaging with quantitative computed tomographic measurements of subchondral bone mineral density in metacarpophalangeal joints of horses. *Am J Vet Res* 2010;71:412-420.

78. Pease A. Biochemical evaluation of equine articular cartilage through imaging. *Vet Clin N Am-Equine* 2012;28:637-646.

79. Crema MD, Roemer RW, Marra MD, et al. Articular cartilage in the knee: Current MR imaging techniques and applications in clinical practice and research. *Radiographics* 2011;31:37-62.

80. Potter HG, Black BR, Chong le R. New techniques in articular cartilage imaging. *Clin Sports Med* 2009;28:77-94.

81. Strickland CD, Kijowski R. Morphologic imaging of articular cartilage. *Magn Reson Imaging Clin N Am* 2011;19:229-248.

82. Ristow O, Stehling C, Krug R, et al. Isotropic 3-dimensional fast spin echo imaging versus standard 2-dimensional imaging at 3.0 T of the knee: artificial cartilage and meniscal lesions in a porcine model. *J Comput Assist Tomogr* 2010;34:260-269.

83. Notohamiprodjo M, Horng A, Pietschmann MF, et al. MRI of the knee at 3T: first clinical results with an isotropic PDfs-weighted 3D-TSE-sequence. *Invest Radiol* 2009;44:585-597.

84. Murray RC, Branch MV, Tranquille C, et al. Validation of magnetic resonance imaging for measurement of equine articular cartilage and subchondral bone thickness. *Am J Vet Res* 2005;66:1999-2005.

85. Carstens A, Kirberger RM, Velleman M, et al. Feasibility for mapping cartilage T1 relaxation times in the distal metacarpus3/metatarsus3 of thoroughbred racehorses using delayed gadolinium-enhanced magnetic resonance imaging of cartilage (dGEMRIC): normal cadaver study. *Vet Radiol Ultrasound* 2013;54:365-372.

86. Olive J. Distal interphalangeal articular cartilage assessment using low-field magnetic resonance imaging. *Vet Radiol Ultrasound* 2010;51:259-266.

87. Spriet M. Letter to the Editor. *Vet Radiol Ultrasound* 2014;55:5-6.

88. Porter EG, Winter MD, Sheppard BJ, et al. Correlation of articular cartilage thickness measurements made with magnetic resonance imaging, magnetic resonance arthrography, and computed tomographic arthrography with gross articular cartilage thickness in the equine metacarpophalangeal joint. *Vet Radiol Ultrasound* 2016;57:515-525.

89. Gomoll AH, Yoshioka H, Watanabe A, et al. Preoperative measurement of cartilage defects by MRI underestimates lesion size. *Cartilage* 2011;2:389-393.

90. An YH, Gruber HE. Introduction to experimental bone and cartilage histology In: An. Yuehuei H.,Martin KL, eds. *Handbook of Histology Methods for Bone and Cartilage*. New York, NY: Springer Science+Business Media, LLC, 2003;3-31.

91. Kornaat PR, Ceulemans RY, Kroon HM, et al. MRI assessment of knee osteoarthritis: Knee Osteoarthritis Scoring System (KOSS)--inter-observer and intra-observer reproducibility of a compartment-based scoring system. *Skeletal Radiol* 2005;34:95-102.

92. Peterfy CG, Guermazi A, Zaim S, et al. Whole-Organ Magnetic Resonance Imaging Score (WORMS) of the knee in osteoarthritis. *Osteoarthritis Cartilage* 2004;12:177-190.

93. Hunter DJ, Lo GH, Gale D, et al. The reliability of a new scoring system for knee osteoarthritis MRI and the validity of bone marrow lesion assessment: BLOKS (Boston Leeds Osteoarthritis Knee Score). *Ann Rheum Dis* 2008;67:206-211.

94. Hunter DJ, Guermazi A, Lo GH, et al. Evolution of semi-quantitative whole joint assessment of knee OA: MOAKS (MRI Osteoarthritis Knee Score). *Osteoarthritis Cartilage* 2011;19:990-1002.

95. Jungmann PM, Welsch GH, Brittberg M, et al. Magnetic resonance imaging score and classification system (AMADEUS) for assessment of preoperative cartilage defect severity. *Cartilage* 2017;8:272-282.

96. Roemer FW, Hunter DJ, Crema MD, et al. An illustrative overview of semi-quantitative MRI scoring of knee osteoarthritis: lessons learned from longitudinal observational studies. *Osteoarthritis Cartilage* 2016;24:274-289.

97. Lynch JA, Roemer FW, Nevitt MC, et al. Comparison of BLOKS and WORMS scoring systems part I. Cross sectional comparison of methods to assess cartilage morphology, meniscal damage and bone marrow lesions on knee MRI: data from the osteoarthritis initiative. *Osteoarthritis Cartilage* 2010;18:1393-1401.

98. Frisbie DD, McIlwraith CW, Kawcak CE, et al. Efficacy of intravenous administration of hyaluronan, sodium chondroitin sulfate, and N-acetyl-d-glucosamine for prevention or treatment of osteoarthritis in horses. *Am J Vet Res* 2016;77:1064-1070.

99. Kawcak CE, Frisbie DD, Werpy NM, et al. Effects of exercise vs experimental osteoarthritis on imaging outcomes. *Osteoarthritis Cartilage* 2008;16:1519-1525.

100. Smith AD, Morton AJ, Winter MD, et al. Magnetic resonance imaging scoring of an experimental model of post-traumatic osteoarthritis in the equine carpus. *Vet Radiol Ultrasound* 2016;57:502-514.

101. Hontoir F, Clegg P, Nisolle JF, et al. Magnetic resonance compositional imaging of articular cartilage: What can we expect in veterinary medicine? *Vet J* 2015;205:11-20.

102. Kurkijarvi JE, Nissi MJ, Kiviranta I, et al. Delayed gadolinium-enhanced MRI of cartilage (dGEMRIC) and T2 characteristics of human knee articular cartilage: topographical variation and relationships to mechanical properties. *Magn Reson Med* 2004;52:41-46.

103. Nieminen MT, Toyras J, Laasanen MS, et al. Prediction of biomechanical properties of articular cartilage with quantitative magnetic resonance imaging. *J Biomech* 2004;37:321-328.

104. Bashir A, Gray ML, Burstein D. Gd-DTPA2- as a measure of cartilage degradation. *Magn Reson Med* 1996;36:665-673.

105. Matzat SJ, Kogan F, Fong GW, et al. Imaging strategies for assessing cartilage composition in osteoarthritis. *Curr Rheumatol Rep* 2014;16:462.

106. Bekkers JE, Bartels LW, Benink RJ, et al. Delayed gadolinium enhanced MRI of cartilage (dGEMRIC) can be effectively applied for longitudinal cohort evaluation of articular cartilage regeneration. *Osteoarthritis Cartilage* 2013;21:943-949.

107. Multanen J, Rauvala E, Lammentausta E, et al. Reproducibility of imaging human knee cartilage by delayed gadolinium-enhanced MRI of cartilage (dGEMRIC) at 1.5 Tesla *Osteoarthritis Cartilage* 2009;17:559-564.

108. van Tiel J, Bron EE, Tiderius CJ, et al. Reproducibility of 3D delayed gadolinium enhanced MRI of cartilage (dGEMRIC) of the knee at 3.0 T in patients with early stage osteoarthritis. *Eur Radiol* 2013;23:496-504.

109. Noordin S, Winalski CS, Shortkroff S, et al. Factors affecting paramagnetic contrast enhancement in synovial fluid: effects of electrolytes, protein concentrations, and temperature on water proton relaxivities from Mn ions and Gd chelated contrast agents. *Osteoarthr Cartilage* 2010;18:964-970.

110. Burstein D, Velyvis J, Scott KT, et al. Protocol issues for delayed Gd(DTPA)(2-)-enhanced MRI (dGEMRIC) for clinical evaluation of articular cartilage. *Magn Reson Med* 2001;45:36-41.

111. Salo EN, Nissi MJ, Kulmala KAM, et al. Diffusion of Gd-DTPA2- into articular cartilage. *Osteoarthritis Cartilage* 2012;20:117-126.

112. Menendez MI, Clark DJ, Carlton M, et al. Direct delayed human adenoviral BMP-2 or BMP-6 gene therapy for bone and cartilage regeneration in a pony osteochondral model. *Osteoarthritis Cartilage* 2011;19:1066-1075.

113. Carstens A, Kirberger RM, Dahlberg LE, et al. Validation of delayed gadolinium-enhanced magnetic resonance imaging of cartilage and T2 mapping for quantifying distal metacarpus/metatarsus cartilage thickness in Thoroughbred racehorses. *Vet Radiol Ultrasound* 2013;54:139-148.

114. Saveraid TC, Judy CE. Use of intravenous gadolinium contrast in equine magnetic resonance imaging. *Vet Clin N Am Equine Pract* 2012;28:617-636.

115. Wang L, Regatte RR. T(1)rho MRI of human musculoskeletal system. *J Magn Reson Imaging* 2015;41:586-600.

116. Mlynarik V, Trattnig S, Huber M, et al. The role of relaxation times in monitoring proteoglycan depletion in articular cartilage. *J Magn Reson Imaging* 1999;10:497-502.

117. Bushberg JT, Seibert JA, Leidholdt EM, et al. Magnetic resonance imaging In: Mitchell CW, ed. *The Essential Physics of Medical Imaging*. Philadelphia, PA: Lippincott Williams & Wilkins, 2012;415-467.

118. Madelin G, Regatte RR. Biomedical applications of sodium MRI in vivo. *J Magn Reson Imaging* 2013;38:511-529.

119. Madelin G, Babb JS, Xia D, et al. Reproducibility and repeatability of quantitative sodium magnetic resonance imaging in vivo in articular cartilage at 3 T and 7 T. *Magn Reson Med* 2012;68:841-849.

120. Krusche-Mandl I, Schmitt B, Zak L, et al. Long-term results 8 years after autologous osteochondral transplantation: 7 T gagCEST and sodium magnetic resonance imaging with morphological and clinical correlation. *Osteoarthritis Cartilage* 2012;20:357-363.

121. Link TM, Neumann J, Li X. Prestructural cartilage assessment using MRI. *J Magn Reson Imaging* 2017;45:949-965.

122. Battaglia M, Rimondi E, Monti C, et al. Validity of T2 mapping in characterization of the regeneration tissue by bone marrow derived cell transplantation in osteochondral lesions of the ankle. *Eur J Radiol* 2011;80:e132-139.

123. David-Vaudey E, Ghosh S, Ries M, et al. T2 relaxation time measurements in osteoarthritis. *Magn Reson Imaging* 2004;22:673-682.

124. Lammentausta E, Kiviranta P, Toyras J, et al. Quantitative MRI of parallel changes of articular cartilage and underlying trabecular bone in degeneration. *Osteoarthritis Cartilage* 2007;15:1149-1157.

125. Welsch GH, Mamisch TC, Domayer SE, et al. Cartilage T2 assessment at 3-T MR imaging: in vivo differentiation of normal hyaline cartilage from reparative tissue after two cartilage repair procedures--initial experience. *Radiology* 2008;247:154-161.

126. Williams A, Qian Y, Chu CR. UTE-T2* mapping of human articular cartilage in vivo: a repeatability assessment. *Osteoarthritis Cartilage* 2011;19:84-88.

127. Marik W, Apprich S, Welsch GH, et al. Biochemical evaluation of articular cartilage in patients with osteochondrosis dissecans by means of quantitative T2- and T2-mapping at 3T MRI: a feasibility study. *Eur J Radiol* 2012;81:923-927.

128. Qian Y, Williams AA, Chu CR, et al. Multicomponent T2* mapping of knee cartilage: technical feasibility ex vivo. *Magn Reson Med* 2010;64:1426-1431.

129. Mamisch TC, Hughes T, Mosher TJ, et al. T2 star relaxation times for assessment of articular cartilage at 3 T: a feasibility study. *Skeletal Radiol* 2012;41:287-292.

130. Du J, Takahashi AM, Chung CB. Ultrashort TE spectroscopic imaging (UTESI): application to the imaging of short T2 relaxation tissues in the musculoskeletal system. *J Magn Reson Imaging* 2009;29:412-421.

131. Raya JG, Horng A, Dietrich O, et al. Articular cartilage: In vivo diffusion-tensor imaging. *Radiology* 2012;262:550-559.

132. Valdés-Martínez A. Computed tomographic arthrography of the equine stifle joint. *Vet Clin N Am-Equine* 2012;28:583-598.

133. Pollard RE, Puchalski SM. Reaction to intraarterial ionic iodinated contrast medium administration in anesthetized horses. *Vet Radiol Ultrasound* 2011;52:441-443.

134. Boven F, Bellemans M-A, Geurts J, et al. A comparative study of the patello-femoral joint on axial roentgenogram, axial arthrogram, and computed tomography following arthrography. *Skeletal Radiology* 1982;8:179-181.

135. Ihara H. Double-contrast CT arthrography of the cartilage of the patellofemoral joint. *Clin Orthop Relat Res* 1985:50-55.

136. Guermazi A, Hayashi D, Roemer FW, et al. Osteoarthritis: A review of strengths and weaknesses of different imaging options. *Rheum Dis Clin N Am* 2013;39:567-591.

137. Hayashi D, Roemer FW, Guermazi A. Imaging for osteoarthritis. *Ann Phys Rehabil Med* 2016;59:161-169.

138. Lusic H, Grinstaff MW. X-ray computed tomography contrast agents. *Chem Rev* 2013;113:1641-1666.

139. Bushberg JT, Seibert JA, Leidholdt EM, et al. Interaction of Radiation with Matter In: Mitchell CW, ed. *The Essential Physics of Medical Imaging*. 3rd ed. Philadelphia, PA: Lippincott Williams & Wilkins, 2012;33-59.

140. Pollard RE, Garcia TC, Stieger SM, et al. Quantitative evaluation of perfusion and permeability of peripheral tumors using contrast-enhanced computed tomography. *Invest Radiol* 2004;39:340-349.

141. Thomsen HS, Bellin MF, Jakobsen JA, et al. Contrast Media Classification and Terminology In: Thomsen HS,Webb JAW, eds. *Contrast Media: Safety Issues and ESUR Guidelines*. 3rd ed. New York, NY: Springer-Verlag, 2014;3-12.

142. Dawson P. Dynamic contrast-enhanced functional imaging with multi-slice CT. *Acad Radiol* 2002;9 Suppl 2:S368-370.

143. Satoh H, Abe S, Kato M, et al. Optimum conditions for serum clearance of iodixanol, applicable to the estimation of glomerular filtration rate in horses. *Vet Res Commun* 2011;35:463-468.

144. Wilson KE, Wilcke JR, Crisman MV, et al. Comparison of serum iohexol clearance and plasma creatinine clearance in clinically normal horses. *Am J Vet Res* 2009;70:1545-1550.

145. ACR Committee on Drugs and Contrast Media. *ACR manual on contrast media: version 101* American College of Radiology Website. http://www.acr.org/quality-safety/resources/?/media/37D84428BF1D4E1B9A3A2918DA9E27A3.pdf/. Published 2015. Accessed May 5, 2016, 2015.

146. Brownlow MA, Hutchins DR. The concept of osmolality: Its use in the evaluation of "dehydration" in the horse. *Equine Vet J* 1982;14:106-110.

147. Chalmers N, Jackson RW. Comparison of iodixanol and iohexol in renal impairment. *Br J Radiol* 1999;72:701-703.

148. Aspelin P, Aubry P, Fransson S-G, et al. Nephrotoxic effects in high-risk patients undergoing angiography. *New Engl J Med* 2003;348:491-499.

149. Heinrich MC, Kuhlmann MK, Grgic A, et al. Cytotoxic effects of ionic high-osmolar, nonionic monomeric, and nonionic iso-osmolar dimeric iodinated contrast media on renal tubular cells in vitro. *Radiology* 2005;235:843-849.

150. Schild HH, Kuhl CK, Hübner-Steiner U, et al. Adverse events after unenhanced and monomeric and dimeric contrast-enhanced CT: A prospective randomized controlled trial. *Radiology* 2006;240:56-64.

151. Seeliger E, Flemming B, Wronski T, et al. Viscosity of contrast media perturbs renal hemodynamics. *J Am Soc Nephrol* 2007;18:2912-2920.

152. Seeliger E, Sendeski M, Rihal CS, et al. Contrast-induced kidney injury: Mechanisms, risk factors, and prevention. *Eur Heart J* 2012;33:2007-2015.

153. Davidson C, Stacul F, McCullough PA, et al. Contrast medium use. *Am J Cardiol* 2006;98:42K-58K.

154. Gendler A, Keuler NS, Schaefer SL. Computed tomographic arthrography of the normal canine elbow. *Vet Radiol Ultrasound* 2015;56:144-152.

155. Vanderperren K, Ghaye B, Snaps FR, et al. Evaluation of computed tomographic anatomy of the equine metacarpophalangeal joint. *Am J Vet Res* 2008;69:631-638.

156. Bergman EHJ, Puchalski SM, van der Veen H, et al. Computed tomography and computed tomography arthrography of the equine stifle: Technique and preliminary results in 16 clinical cases Proceedings of the 53rd Annual Convention of the American Association of Equine Practitioners 2007;46-55.

157. Gray SN, Puchalski SM, Galuppo LD. Computed tomographic arthrography of the intercarpal ligaments of the equine carpus. *Vet Radiol Ultrasound* 2013;54:245-452.

158. Omoumi P, Michoux N, Roemer FW, et al. Cartilage thickness at the posterior medial femoral condyle is increased in femorotibial knee osteoarthritis: a cross-sectional CT arthrography study (Part 2). *Osteoarthritis Cartilage* 2015;23:224-231.

159. Broom ND. Abnormal softening in articular cartilage: its relationship to the collagen framework. *Arthritis Rheum* 1982;25:1209-1216.

160. Wang Y, Wluka AE, Jones G, et al. Use magnetic resonance imaging to assess articular cartilage. *Ther Adv Musculoskelet Dis* 2012;4:77-97.

161. Siebelt M, van Tiel J, Waarsing JH, et al. Clinically applied CT arthrography to measure the sulphated glycosaminoglycan content of cartilage. *Osteoarthritis Cartilage* 2011;19:1183-1189.

162. Allen BC, Peters CL, Brown NAT, et al. Acetabular cartilage thickness: Accuracy of three-dimensional reconstructions from multidetector CT arthrograms in a cadaver study. *Radiology* 2010;255:544-552.

163. Wyler A, Bousson V, Bergot C, et al. Hyaline cartilage thickness in radiographically normal cadaveric hips: comparison of spiral CT arthrographic and macroscopic measurements. *Radiology* 2007;242:441-449.

164. Hontoir F, Nisolle JF, Meurisse H, et al. A comparison of 3-T magnetic resonance imaging and computed tomography arthrography to identify structural cartilage defects of the fetlock joint in the horse. *Vet J* 2014;199:115-122.

165. Bansal PH, Joshi NS, Entezari V, et al. Contrast enhanced computed tomography can predict the glycosaminoglycan content and biomechanical properties of articular cartilage. *Osteoarthritis Cartilage* 2010;18:184-191.

166. Xie L, Lin ASP, Levenston ME, et al. Quantitative assessment of articular cartilage morphology via EPIC-microCT. *Osteoarthritis Cartilage* 2009;17:313-320.

167. Palmer AW, Guldberg RE, Levenston ME. Analysis of cartilage matrix fixed charge density and three-dimensional morphology via contrast-enhanced microcomputed tomography. *Proc Natl Acad Sci U S A* 2006;103:19255-19260.

168. Bansal PN, Joshi NS, Entezari V, et al. Cationic contrast agents improve quantification of glycosaminoglycan (GAG) content by contrast enhanced CT imaging of cartilage. *J Orthop Res* 2011;29:704-709.

169. Bansal PN, Stewart RC, Entezari V, et al. Contrast agent electrostatic attraction rather than repulsion to glycosaminoglycans affords a greater contrast uptake ratio and improved quantitative CT imaging in cartilage. *Osteoarthritis Cartilage* 2011;19:970-976.

170. Kallioniemi AS, Jurvelin JS, Nieminen MT, et al. Contrast agent enhanced pQCT of articular cartilage. *Phys Med Biol* 2007;52:1209-1219.

171. Kulmala KAM, Karjalainen HM, Kokkonen HT, et al. Diffusion of ionic and non-ionic contrast agents in articular cartilage with increased cross-linking--contribution of steric and electrostatic effects. *Med Eng Phys* 2013;35:1415-1420.

172. Lakin BA, Grasso DJ, Shah SS, et al. Cationic agent contrast-enhanced computed tomography imaging of cartilage correlates with the compressive modulus and coefficient of friction. *Osteoarthritis Cartilage* 2013;21:60-68.

173. Lakin BA, Ellis DJ, Shelofsky JS, et al. Contrast-enhanced CT facilitates rapid, non-destructive assessment of cartilage and bone properties of the human metacarpal. *Osteoarthritis Cartilage* 2015;23:2158-2166.

174. Aula AS, Jurvelin JS, Toyras J. Simultaneous computed tomography of articular cartilage and subchondral bone. *Osteoarthritis Cartilage* 2009;17:1583-1588.

175. Mittelstaedt D, Xia Y. Depth-dependent glycosaminoglycan concentration in articular cartilage by quantitative contrast-enhanced micro–computed tomography. *Cartilage* 2015;6:216-225.

176. Xie L, Lin AS, Guldberg RE, et al. Nondestructive assessment of sGAG content and distribution in normal and degraded rat articular cartilage via EPIC-microCT. *Osteoarthritis Cartilage* 2010;18:65-72.

177. Xie L, Lin AS, Kundu K, et al. Quantitative imaging of cartilage and bone morphology, reactive oxygen species, and vascularization in a rodent model of osteoarthritis. *Arthritis Rheum* 2012;64:1899-1908.

178. Siebelt M, van Tiel J, Waarsing JH, et al. Clinically applied CT arthrography to measure the sulphated glycosaminoglycan content of cartilage. *Osteoarthritis Cartilage* 2011;19:1183-1189.

179. Hirvasniemi J, Kulmala KAM, Lammentausta E, et al. In vivo comparison of delayed gadolinium-enhanced MRI of cartilage and delayed quantitative CT arthrography in imaging of articular cartilage. *Osteoarthritis Cartilage* 2012:434-442.

180. Joshi NS, Bansal PN, Stewart RC, et al. Effect of contrast agent charge on visualization of articular cartilage using computed tomography: exploiting electrostatic interactions for improved sensitivity. *J Am Chem Soc* 2009;131:13234-13235.

181. Lakin BA, Patel H, Holland C, et al. Contrast-enhanced CT using a cationic contrast agent enables non-destructive assessment of the biochemical and biomechanical properties of mouse tibial plateau cartilage. *J Orthop Res* 2016;34:1130-1138.

182. Stewart RC, Bansal PN, Entezari V, et al. Contrast-enhanced CT with a high-affinity cationic contrast agent for imaging ex vivo bovine, intact ex vivo rabbit and in vivo rabbit cartilage. *Radiology* 2013;266:141-150.

183. Stewart RC, Patwa AN, Lusic H, et al. Synthesis and preclinical characterization of a cationic iodinated imaging contrast agent (CA4+) and its use for quantitative computed tomography of ex vivo human hip cartilage. *J Med Chem* 2017;60:5543-5555.

184. Piscaer TM, Waarsing JH, Kops N, et al. In vivo imaging of cartilage degeneration using microCT-arthrography. *Osteoarthritis Cartilage* 2008;16:1011-1017.

185. Frisbie DD, Cross MW, McIlwraith CW. A comparative study of articular cartilage thickness in the stifle of animal species used in human pre-clinical studies compared to articular cartilage thickness in the human knee. *Vet Comp Orthop Traumatol* 2006;19:142-146.

186. Kol A, Arzi B, Athanasiou KA, et al. Companion animals: Translational scientist's new best friends. *Sci Transl Med* 2015;7:1-8.

187. Malda J, de Grauw JC, Benders KEM, et al. Of Mice, Men and Elephants: The Relation between Articular Cartilage Thickness and Body Mass. *PLOS ONE* 2013;8:e57683.

188. McIlwraith CW, Fortier LA, Frisbie DD, et al. Equine models of articular cartilage repair. *Cartilage* 2011;2:317-326.

CHAPTER 2:

DEVELOPMENT OF CATIONIC CONTRAST-ENHANCED COMPUTED TOMOGRAPHY IN EQUINE ARTICULAR CARTILAGE

Introduction

Joint disease is substantial problem in horses and subtle articular cartilage injuries at the onset of osteoarthritis are difficult to detect using currently available diagnostic imaging methods.[1] Quantitative imaging techniques developed for use in computed tomography (CT) and magnetic resonance imaging (MRI) have been shown to better characterize articular cartilage properties with higher sensitivity than methods that rely on morphologic assessment.[2-4] Particularly, the development of contrast-enhanced CT (CECT) has expanded the options for articular cartilage evaluation in horses in research settings and clinical practice.[5-10] Compared to MRI, the lower cost, faster acquisition times, generally higher spatial resolution and wider accessibility make CECT a promising modality to investigate articular cartilage in horses.[11,12]

All commercially available iodinated contrast media (ICM) are negatively charged or uncharged and therefore have limited penetration into articular cartilage due to the repulsive nature of negatively charged glycosaminoglycans (GAGs) in the extracellular matrix.[13-15] However, the high x-ray attenuation from the ICM in the joint space and from the subchondral bone provides high contrast resolution from the low x-ray attenuating articular cartilage, which permits assessment of morphology and surface topography. Despite minimal penetration of anionic ICM into the articular cartilage matrix, the high concentrations administered facilitate measurement of

CECT signal to provide quantitative information on the amount that penetrates the tissue and therefore indicates glycosaminoglycan content and mechanical properties.[13-16]

Exploiting the negatively charged environment of articular cartilage extracellular matrix, a novel cationic ICM (CA4+) was developed with positively charged side chain adjustments to make it more electrostatically attracted to and cause higher diffusivity of CA4+ into the tissue than anionic ICM.[17,18] Because CA4+ diffuses in direct proportion to the negative fixed charge density of the extracellular matrix, the measured CECT signal on microCT is also predictive of GAG content through non-destructive methods.[16-20]

Most studies investigating cationic CECT have been performed on tissue explants.[16-20] Therefore it is important to determine which equine specific joints are best suited for cationic CECT evaluation using intact joints. Though there are many equine joints available that could be chosen to investigate cationic CECT, the following three joints were selected because of their high frequency of developing joint disease and/or their use in experimental joint disease models. The metacarpo(tarso)phalangeal and middle carpal joints were selected for *ex vivo* evaluation because they are frequent locations of traumatic joint injury in the horse. The femoropatellar joint compartment was selected because it is frequently used in experimental articular cartilage healing research studies.[21,22]

In vitro experimentation has revealed the trajectory of CA4+ diffusion into non-equine cartilage.[20] Despite the similar articular cartilage attributes across mammalian species, there are clear anatomic and physiologic differences in constituents between species that prevent a direct

extrapolation of previous research studies to equine tissue.[23-25] Therefore, the diffusion trajectory of CA4+ into equine articular cartilage requires determination.

The objectives of this study were: 1) to compare the appearance of equine articular cartilage on anionic and cationic CECT and to determine the best joint suited for *in vivo* use in future investigations of cationic CECT and 2) to determine the diffusion properties of CA4+ into equine cartilage. The first hypothesis was that CA4+ would provide a better observation of articular cartilage tissue in all *ex vivo* joints than anionic ICM. The second hypothesis was that the diffusion path of CA4+ into equine articular cartilage would rapidly increase with time and reach an equilibrated state.

Materials and Methods

Synthesis of CA4+

The CA4+ solution was synthesized as previously described.[18] Briefly, a tri-iodinated precursor, 5-amino-2,4,6-triiodoisophthalic acid, was combined with thionyl chloride and evaporated to produce a solid followed by dissolving in tetrahydrofuran and malonyl chloride. After drying, the compound was reacted with mono-Boc protected ethylenediamine and was finally deprotected with trifluoroacetic acid to produce CA4+ as a solid (61% yield)(Figure 2.1). The final agent solid was solubilized in deionized water to the desired concentration and osmolality and pH were adjusted as necessary. Concentrations of 8 mg I/mL with 400 mOsm at pH = 7.4 were standard.[18] The molecular weight and size of CA4+ is 1,354.03 g/mol with a length of 29 Angstroms (Å) and width of 18 Å.[18]

Comparison of cationic to anionic CECT (Experiment 1)

A juvenile and skeletally mature two year-old horse was euthanized for reasons unrelated to joint disease. Immediately after euthanasia, the metacarpophalangeal, middle carpal and femoropatellar joints were injected with two different ICM: the three left-sided joints with ioxaglate (Hexabrix, 320 mg I/mL, 600 mOsm/kg, Mallinckrodt, Hazelwood, MO) and the three right joints with CA4+ (8 mg I/mL, 400 mOsm, pH=7.4). The ioxaglate was diluted with deionized water to a final concentration of 40 mg I/mL. The volume of injection was approximately 25 mLs for the metacarpophalangeal and middle carpal joints and 100 mLs for the femoropatellar joint using established joint injection approaches.[26] After injection all joints underwent full range of motion (*e.g.* flexion and extension) ten times to distribute each ICM throughout the joint and improve diffusion into articular cartilage.[27] All joints were then incubated at 20 °C to permit equilibration.

Postcontrast CECT scans were performed using a 16-slice multi-detector scanner (Gemini TF Big Bore PET/CT scanner, helical CT x-ray tube with an 85 cm bore, Philips Healthcare, Andover, MA) at 12, 21, and 36 hours after injection. Imaging acquisition settings were: 140 kVp, 500 mAs, 0.4–0.6 pitch, 35 cm field-of-view, 1024 x 1024 matrix. The CECT imaging data were reconstructed at 0.8 mm thickness x 0.8 mm increment (bone filter) for adequate bone resolution and 2.0 mm thickness x 1.0 mm increment (standard filter) to increase signal-to-noise ratio for soft tissue evaluation. The images were imported into commercial image viewing software (iSite PACS Radiology, v.3.6.134, Foster City, CA) for analysis. Multiplanar reconstructions were performed for all joints with particular focus on the transverse, sagittal, and dorsal plane projections.

The conspicuity and clarity of structures in each joint at each time point were graded subjectively for the ability to identify and distinguish articular cartilage from the joint space and the subchondral bone. The quality of articular cartilage visibility in each joint was determined to establish the feasibility of segmentation (estimated segmentation accuracy) from other articular structures and therefore provide an estimation of signal quantification accuracy. The subjective assessments (conspicuity, clarity and estimated segmentation accuracy) were defined by one of the following grades: poor, fair, good and excellent.

Diffusion kinetics of CA4+ in equine osteochondral plugs (Experiment 2)

Equine osteochondral plug specimens were harvested from a three year-old horse without macroscopic evidence of joint disease or articular cartilage defects. The soft tissues were dissected away from the femur and a stationary band saw was used to separate the femoral condyles from the remaining portions of the femur. The articular cartilage was saturated with 0.9% saline during the experiment to prevent desiccation of the tissue. The femoral condyles were placed in a vice and a 7 mm (internal diameter) diamond-tipped cylindrical coring drill bit (Starlite Industries, Bryn Mawr, PA) attached to a drill press (Delta Power Equipment Company, Anderson, SC) was used to remove osteochondral plugs. To prevent tissue heating, constant irrigation with water was performed through the core of the drill bit. Once complete, the osteochondral plugs were immediately irrigated with 400 mOsmol/kg saline to prevent hypotonic desiccation from the water lavage. Three osteochondral plugs were each acquired from the medial and lateral femoral condyles (n = 6)(Figure 2.2A). Each osteochondral plug was stored at 4 °C in 400 mOsmol/kg saline with a preservative cocktail containing a protease inhibitor,

antibiotic and antimycotic (5 mM EDTA; 5 mM Benzamidine HCl, Sigma-Aldrich, St. Louis, MO; 1x Gibco® Antibiotic-Antimycotic, Life Technologies, Carlsbad, CA).

The CA4+ contrast media (8 mgI/mL) was prepared in Nanopure water (Barnstead™ NanoPure™, Thermo Fisher Scientific, Waltham, MA), adjusted to a pH of 7.4 with sodium hydroxide and adjusted to 400 mOsmol/kg using sodium chloride to replicate the pH and osmolality of normal synovial fluid.[28] After the baseline (T0) scan, the fixture with secured plugs (excluding the tube of deionized water) was submerged in 90 mLs of CA4+ (8 mg I/mL).

At each successive diffusion time point after baseline, the fixture was removed from the CA4+ solution and the cartilage was lightly blotted with gauze to remove excess CA4+. The fixture with the osteochondral plugs was then scanned at the same baseline microCT settings stated previously. The fixture was scanned at 0.5 (T0.5), 1 (T1), 2 (T2), 3 (T3), 4 (T4), 6 (T6), 8 (T8), 12 (T12), 16 (T16), 20 (T20) and 24 (T24) hours after T0. The duration of microCT scans (~40 minutes per scan acquisition) was not included in the total time of CA4+ submersion.

The CT images were converted to digital imaging and communications in medicine (DICOM) format and imported to commercial processing software (Analyze, version 12.0, Biomedical Imaging Resource, Mayo Clinic, Rochester, MN). The articular cartilage from each plug at each time point was digitally segmented from the subchondral bone and air using a semi-automatic threshold-based algorithm with manual verification to ensure accurate cartilage segmentation of the tissue volume. The mean CT attenuation values were converted to linear attenuation

coefficients and then to Hounsfield Units (HU) using the deionized water scanned in the respective microCT acquisition (Equation 2.1).[11]

$$\mathrm{HU} = 1000 \cdot \left(\frac{\mu_x - \mu_{water}}{\mu_{water}}\right) \quad \text{Equation 2.1}$$

Where μ_x is the linear attenuation of the segmented cartilage and μ_{water} is the linear attenuation of water in the respective scan.

Data and statistical analysis

Continuous data are reported as mean ± standard deviation. The diffusion of CA4+ into cartilage was determined by plotting the mean cationic CECT attenuation at each time point for each plug. Diffusion data of each plug were then fit to a curve using a nonlinear least-square regression (Equation 2.2)[29] in MATLAB (R2017a, Mathworks, Natick, MA). Goodness-of-fit of the curve was determined by the coefficient of determination.

$$CT_{diff} = CT_{max} \cdot \left[1 - e^{-t/\tau}\right] \quad \text{Equation 2.2}$$

Where CT_{diff} is the CT attenuation at 63.2% of equilibrium, CT_{max} is the maximum CT attenuation at equilibrium, t is the diffusion time, and τ is the time to reach 63.2% of maximum CT attenuation.

As the diffusion data were not normally distributed as determined by a Shapiro-Wilk test, the Wilcoxon signed rank test was used to determine if there was a difference in τ values between medial and lateral condyle samples. Statistical analysis was performed using commercial

software (SAS University Edition, v. 9.2, SAS Institute Inc., Cary, NC) and significance was defined as $P < 0.05$.

Results

Comparison of cationic to anionic CECT (Experiment 1)

In general visibility of articular cartilage was easier and more obvious in the femoropatellar joint compared to the metacarpophalangeal and middle carpal joints for both the anionic and cationic ICM (Figure 2.3). The articular cartilage was observably thicker in the femoropatellar joint than the other joints and therefore the contrast media facilitated an easier distinction between this tissue and the subchondral bone and joint space.

Anionic ICM (ioxaglate) injected joints

The joints injected with ioxaglate caused a hyperattenuation of x-rays that was of similar intensity to the subchondral bone. This provided a good delineation of articular cartilage from surrounding joint structures in the metacarpophalangeal and middle carpal joints and excellent delineation in the femoropatellar joint (Figure 2.3A). At 12 hours, the clarity of the articular cartilage was fair for the metacarpophalangeal and middle carpal joints and good for the femoropatellar joint, though this assessment was dependent upon the joint surface. Increasing curvature of the articular surface particularly in the metacarpophalangeal and middle carpal joints lead to a decrease in articular cartilage clarity. Estimated segmentation accuracy in the metacarpophalangeal joint was fair to good, in the middle carpal joint was fair and in the femoropatellar joint was good to excellent. These ioxaglate ICM grades were prevalent at the 12-

hour time point and the conspicuity, clarity and prediction of segmentation accuracy were qualitatively scored identically at the 21 and 36 hour time points.

Cationic ICM (CA4+) injected joints

As opposed to the ioxaglate injected joints, the joints injected with CA4+ showed a hypoattenuating synovial space relative to the subchondral bone (Figure 2.3B). The conspicuity and clarity of articular cartilage increased with incubation time. In the joints incubating for 12 hours, the articular cartilage was marginally visible. The conspicuity and clarity of the articular cartilage in the metacarpophalangeal and middle carpal joints was poor and in the femoropatellar joint it was fair at 12 hours after CA4+ injection. The predictive segmentation accuracy was poor for the metacarpophalangeal and middle carpal joints and fair to good for the femoropatellar joint. At the 21 and 36 hour time points, the conspicuity, clarity and estimated segmentation accuracy improved for all joints. At 36 hours, the conspicuity and clarity of articular cartilage in the metacarpophalangeal and middle carpal joints slightly increased to fair, while in the femoropatellar joint it increased to good-excellent. The predicted segmentation accuracy for the metacarpophalangeal and middle carpal joints was fair and in the femoropatellar joint it was excellent.

Diffusion kinetics of CA4+ in equine osteochondral plugs (Experiment 2)

The amount of CA4+ that diffused into the articular cartilage explants increased gradually over the 24-hour experimental period. The diffusion pathway of CA4+ started radially from the cut edges and surface extending into the central and deep articular cartilage layers of the sample over time (Figure 2.4). There was no further increase in cationic CECT signal (maximum cationic

CECT attenuation) in the medial articular cartilage samples after 20 hours and in the lateral samples after 16 hours (Figure 2.5). In the medial articular cartilage samples, the mean difference in cationic CECT attenuation between the T16 and T20 time points was 29.7 HUs, representing <1% change of full equilibration following an additional four hours of submersion. The mean ± standard deviation diffusion time constant, τ, was 2.66 ± 0.68 hours ($R^2 > 0.95$ for each plug). The diffusion equation that represented all equine plugs was $CT_{diff} = 2953 (1 - e^{-16/2.66})$ with $R^2 = 0.97$. There was no significant difference in τ values between the medial and lateral femoral condyles (P = 0.11).

Discussion

The data from this experiment did not support the first hypothesis; that articular cartilage was better observed with cationic ICM than anionic ICM CECT. In the first experiment, the femoropatellar joint was determined to have the best visibility of articular cartilage for both the ioxaglate and CA4+ injections compared to the metacarpophalangeal and middle carpal joints. In analyzing the appearance of articular cartilage with anionic and cationic ICM, there were clear differences between groups. In the anionic (ioxaglate) ICM injected joints the articular cartilage appearance did not change over time. The ioxaglate caused increased attenuation in the joint space and a clear delineation of articular cartilage could be observed at the first CECT scan (12 hrs). This appearance caused a stark contrast between tissues with ioxaglate, whereas, there was a more subtle gradient change in grey scale values in the articular cartilage exposed to CA4+. The lack of joint metabolism in *ex vivo* tissue and the lack of penetration of anionic ICM because of electrostatic repulsion between ioxaglate and articular cartilage explains the persistence of contrast media in the synovial space and the lack of observable difference between time points.

In the CA4+ joints, there was a clear time effect on articular cartilage appearance. At 12 hours, there was minimal penetration into the tissue that could be seen on the CECT images. However, this increased at the 21- and 36-hour time points, albeit with minimal change between 21 and 36 hours. This suggests that the diffusion of CA4+ into *ex vivo* articular cartilage requires more than 12 hours for complete diffusion. In explant experiments, equilibration data for bovine osteochondral plugs show that the majority of CA4+ diffusion occurs within 6 hours. The explant plugs are capable of radial diffusion, whereas, intact *ex vivo* joints only permit surface diffusion. This could explain the observed time differences. Additionally, the explant plugs were imaged with microCT compared with the *ex vivo* joints, which were scanned with a clinical CT scanner. Differences in image resolution and the medium that surrounds cartilage (air versus synovial fluid) required by the each system also influences articular cartilage appearance. Despite the high affinity of CA4+ for negatively charged articular cartilage compared to ioxaglate, the depth (distance) of diffusion to reach equilibrium would be expected to take longer to reach equilibrium than anionic ICM.[20,30]

The differences in articular cartilage thickness between joints and orientation of the articular cartilage relative to the CT gantry influenced the appearance of the tissue. In the metacarpophalangeal and middle carpal joints, the articular cartilage is thin (~0.7 – 1 mm) compared to the femoropatellar joint (1 – 3 mm).[23,31,32] Though the in-plane resolution of the CT scan (0.34 - 0.34 mm) was capable of sufficient spatial resolution to clearly outline this tissue thickness, the smallest achievable slice thickness with this multidectector CT was 0.8 mm. This is smaller than is typically recommended for thickness measurements and causes decreased accuracy because of volume averaging (*i.e*. there are multiple, variably attenuating tissues that

occupy the voxel and the measured CT signal represents an average of all tissues within the space).[32,33] Unfortunately, a substantial portion of the articular cartilage's thickness in the metacarpophalangeal and middle carpal joints relative to the limb's axis, required placement in the same plane (z-dimension) that would be required *in vivo*. While flexing and manipulating the limb in order to alter this position and move the thickness of the tissue out of the z-plane was considered, the goal of using this experiment to guide future *in vivo* use of CECT would then be futile. Conversely, the thicker articular cartilage in the femoropatellar joint and the orientation of the articular cartilage relative to the CT gantry permitted easier evaluation of articular cartilage. There are also documented variations in proteoglycan and collagen content between articular surfaces that could influence CA4+ diffusion. Therefore, the lower ability to image thin articular cartilage may be more of a manifestation of positioning and internal biochemistry rather than the inability of CECT to accurately show articular cartilage because of varying thicknesses.

Despite the ability to discern articular cartilage in the ioxaglate injected metacarpophalangeal and middle carpal joints, there were frequently bloom and beam hardening artifacts that caused heterogeneity in the appearance of the tissue across the surface. Beam hardening occurs because of selective resorption of low energy photons from the polychromatic x-ray beam along a dense surface leading to a drop in attenuation when these values are calculated during the reconstruction process. Bloom artifacts typically occur with concentrated ICM use.[34] The metacarpophalangeal and middle carpal joint surfaces are both susceptible to these artifacts and are confounded by the thin articular cartilage at those locations. High iodine concentrations of ioxaglate promote the development of these artifacts and lower concentrations will reduce the risk of these artifacts permitting more reliable evaluation.[6,34,35] Even low iodine concentrations

coupled with thin articular cartilage can make these adverse effects more likely to occur and were observed in some metacarpophalangeal and middle carpal joints. While the femoropatellar joint showed articular cartilage the best, further investigation of cationic CECT *in vivo* is required to determine the diffusion course of CA4+ in the face of active joint metabolism.

In the second experiment, the hypothesis was supported by the data. The diffusion course in equine articular cartilage plugs reached a steady state after approximately 16 hours of diffusion with the majority of the increase in cationic CECT attenuation occurring in the first six hours. In an experiment using identical methodology with bovine osteochondral plugs, most of CA4+ diffusion also occurred by six hours.[20] The diffusion time constant in this study was 2-3 hours and diffusion equilibrium is considered at ~4-5 x τ.[36] For equine femoral condyle cartilage, this would be approximately 12 – 15 hours. However, the diffusion time constant (τ values) differed between studies with the equine plugs taking longer to reach this threshold compared to bovine plugs.[20] Despite similar methodology and CA4+ concentrations, differences in tissue volume and articular cartilage constituents (*e.g.* chondrocyte density, GAG content) between species could explain these differences.[23,24] In this experiment, three extra time points were acquired after four hours of diffusion and this could have influenced the nonlinear mixed-effects model used in determining this equilibration time. Another difference was that this study did not normalize CECT attenuation to reservoir concentrations. In that study,[20] this was performed to provide consistency for the comparisons between ioxaglate and CA4+ diffusion. Samples of the reservoir were collected throughout the course of this experiment; however, there was no change in cationic CECT attenuation from baseline to the end point. Hence, this was not determined to be a critical factor in the results and this normalization procedure was not performed.

Similar to observations from Stewart *et al.*, it is suspected that this course of CA4+ diffusion does not reflect *in vivo* conditions. Osteochondral plugs permit diffusion from the surface and radially from the cut edges, whereas, intact cartilage would not permit radial diffusion without adjacent tissue loss. An adjustment to this methodology to prevent this radial diffusion and better replicate *in vivo* conditions would be to place cyanoacrylate glue on the transected edges and this has been shown to restrict CA4+ diffusion to the superficial zone (data not shown).[30] These differences between *in vitro* and *in vivo* tissue could influence the time the tissue needs to reach equilibrium. However, as has been observed with delayed gadolinium enhanced magnetic resonance imaging of cartilage, equilibration in articular cartilage tissue may not be necessary to use quantitative imaging methods successfully.[37]

There was no significant difference in diffusion profiles between medial and lateral femoral condyle samples. However the small sample size resulting from biopsies collected from a single horse lead to low statistical power. Considering that thicker articular cartilage takes significantly longer for CA4+ to equilibrate than thinner articular cartilage, its reasonable that these results could not be assumed in different joints.[38] Further experiments are required to determine if there is a true difference in cationic CECT attenuation between these two locations incorporating the different biochemical properties and thickness of articular cartilage.

In conclusion, the femoropatellar joint was deemed to be an optimal joint to perform further *in vivo* experimentation with cationic CECT as compared with the metacarpophalangeal and middle carpal joints. The diffusion experiment showed that explanted cartilage should be permitted at least 15 hours of CA4+ submersion to reach equilibrium.

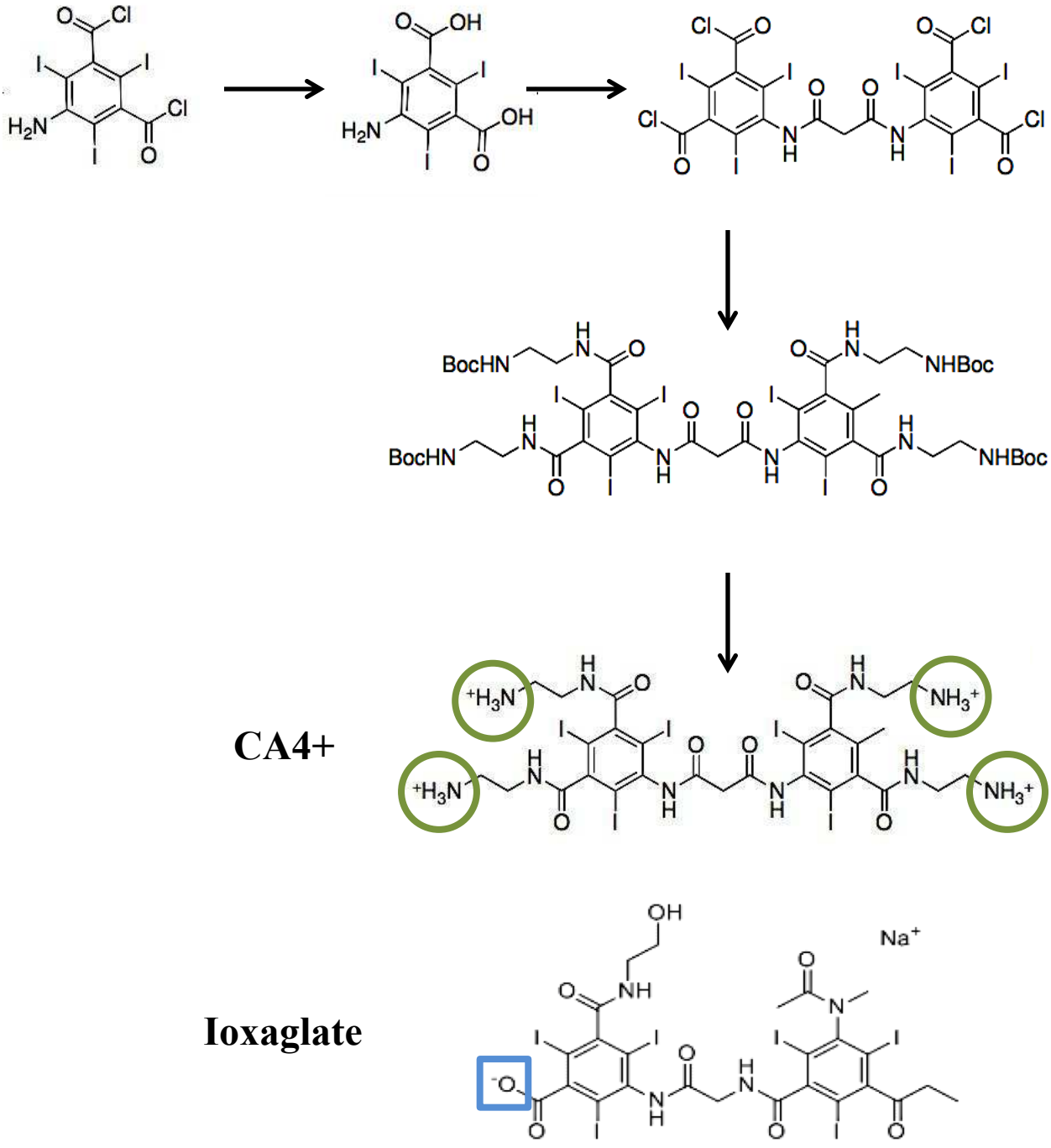

Figure 2.1 – Chemical synthesis scheme showing the four-step process used to produce the cationic contrast medium CA4+.[18] The chemical structure of ioxaglate, the commercially available (Hexabrix, Mallinckrodt Inc., Hazelwood, MO) iodinated contrast media, that CA4+ was modeled after is shown for comparison. Positive charges on CA4+ are indicated with green circles and the negative charge on ioxaglate with a blue square.

A

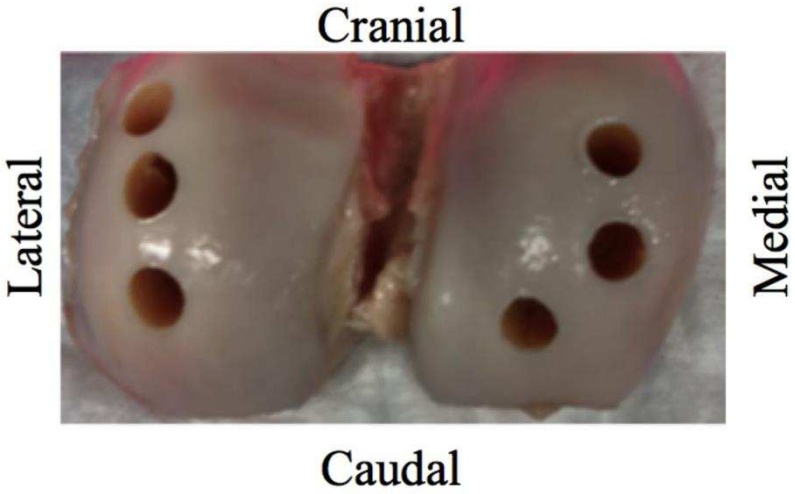

B

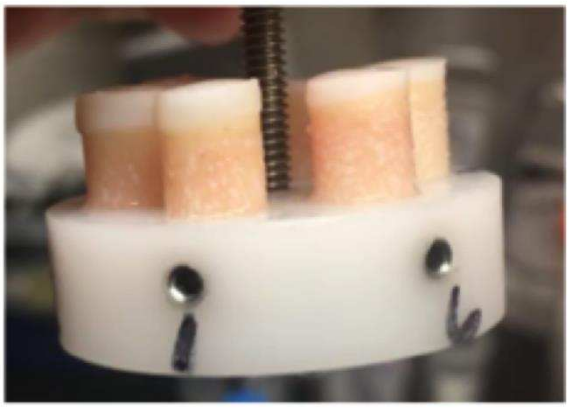

Figure 2.2 – (A) Locations of 7 mm osteochondral plugs collected from the medial and lateral femoral condyles for use in the *in vitro* CA4+ diffusion experiment. (B) The fixture used to systematize the micro computed tomography scans.

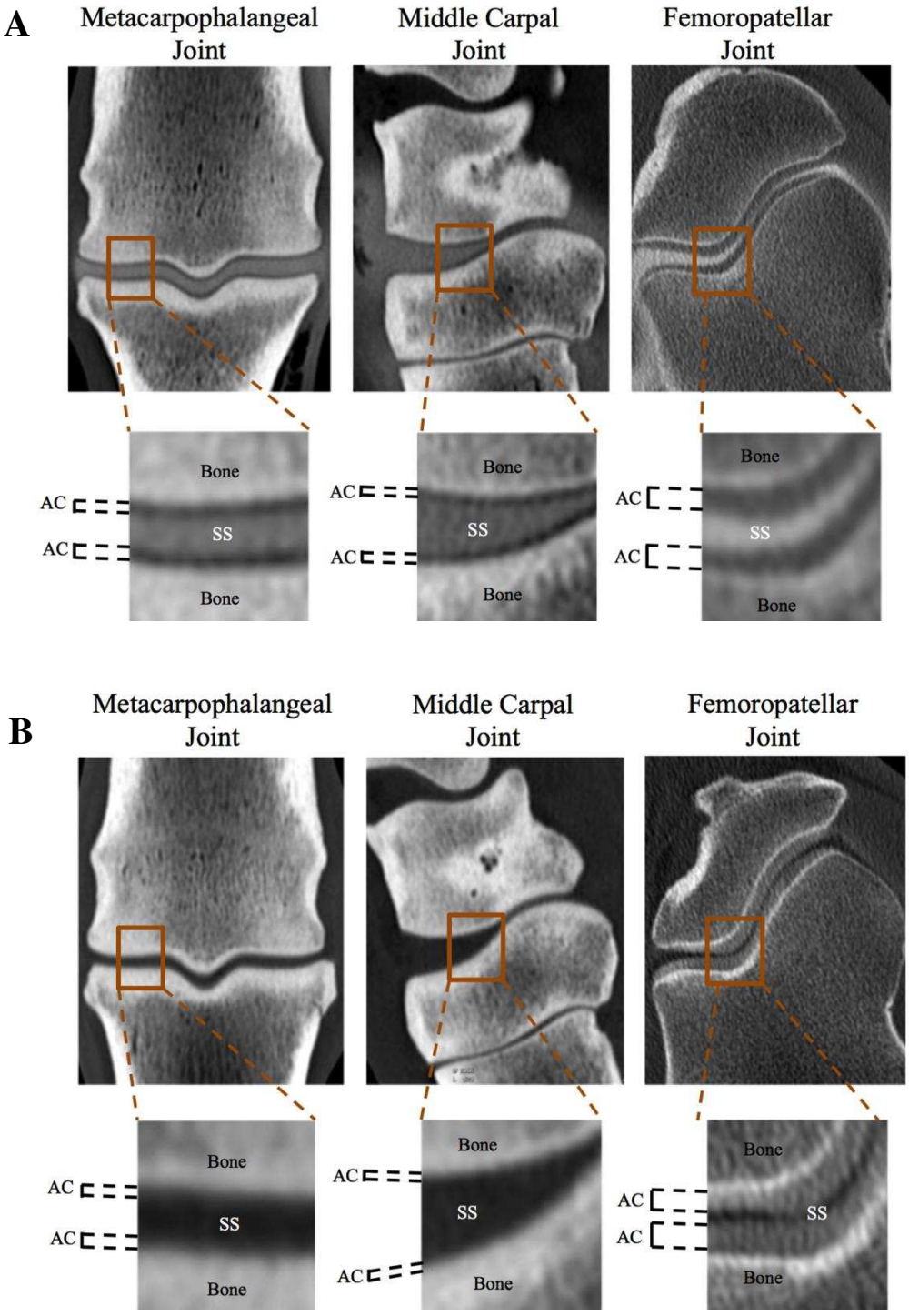

Figure 2.3 – A) Depiction of articular cartilage on contrast-enhanced computed tomography after intra-articular injection with anionic (A) and cationic (B) iodinated contrast media. The metacarpophalangeal joint is shown in the dorsal plane, the middle carpal joint in the sagittal plane and the femoropatellar joint in the transverse plane. The boxes below each image are magnified sections to highlight the interface between the synovial space (SS), articular cartilage (AC) and subchondral bone in each image.

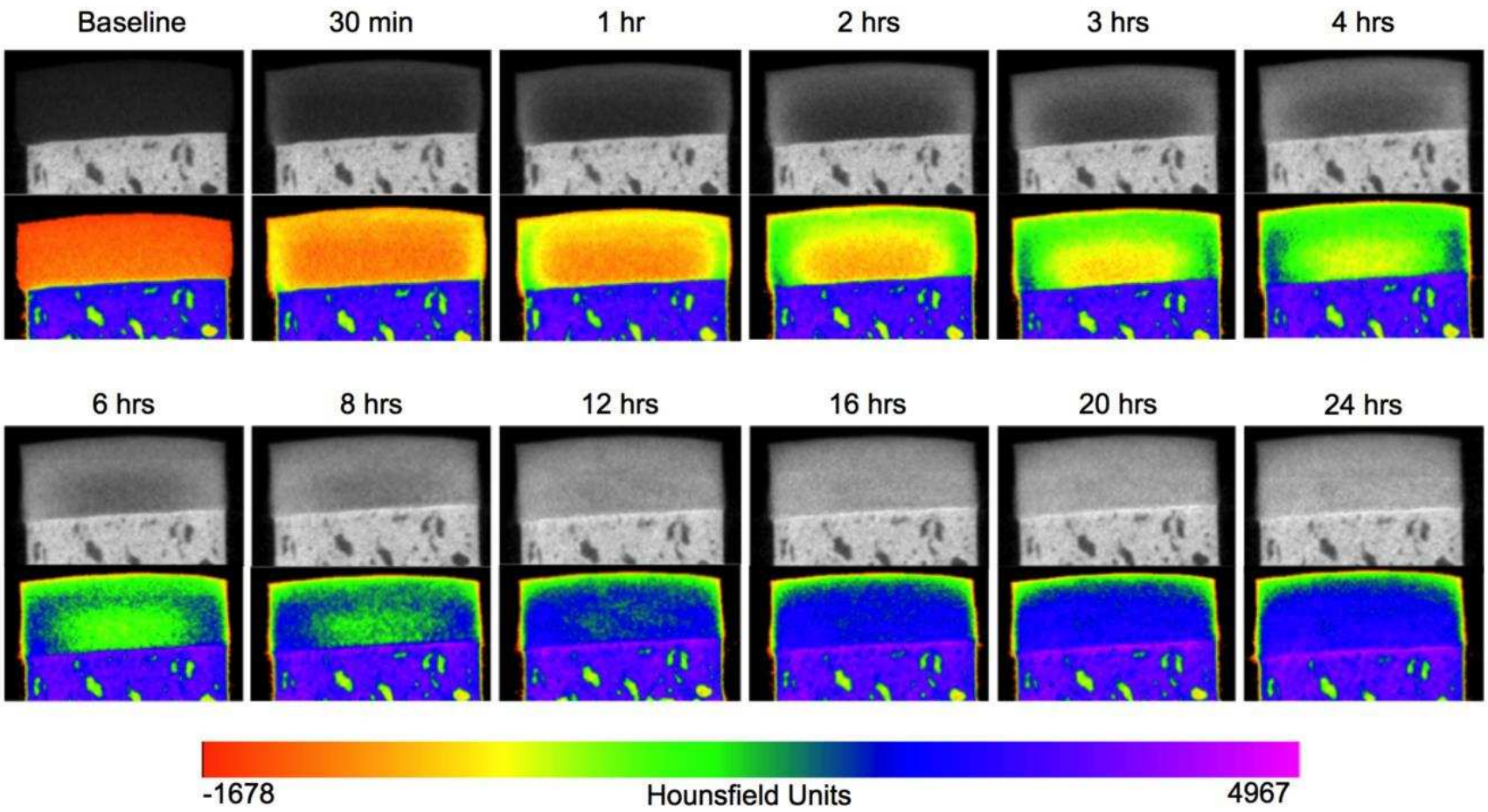

Figure 2.4 – Diffusion trajectory of CA4+ into equine articular cartilage as indicated by micro computed tomography. All images are taken from a single osteochondral plug (medial femoral condyle sample). The top image at each time point is in standard grey scale and the bottom image is after application of a color map to highlight differences in attenuation. For all images, window width and leveling were kept consistent.

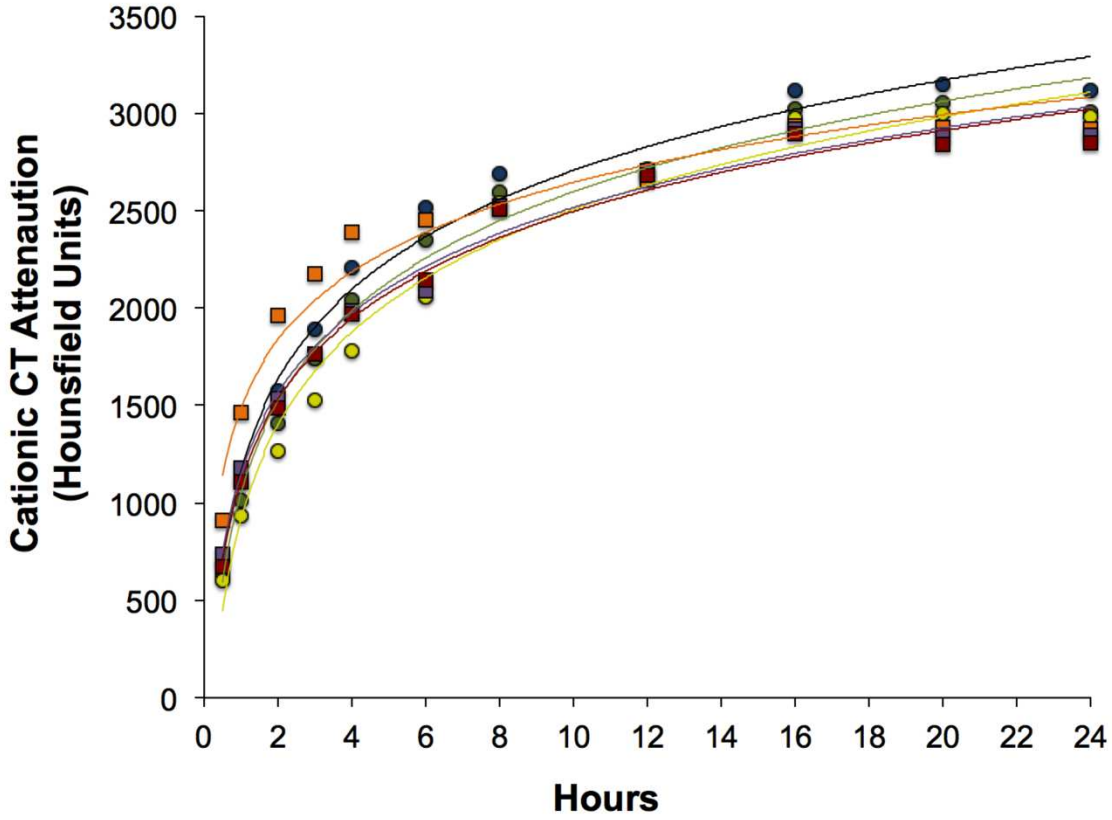

Figure 2.5 – Plotted course of CA4+ diffusion in equine articular cartilage from osteochondral plugs harvested from the femoral condyles of a 3 year-old horse without observable articular cartilage damage (circles = medial condyle plugs, squares = lateral condyle plugs). The plugs were submerged in CA4+ (8 mgI/mL, 400 mOsm/kg, pH=7.4) and sequentially imaged with micro computed tomography after each elapsed time of CA4+ diffusion.

REFERENCES

1. McIlwraith CW. Traumatic arthritis and posttraumatic osteoarthritis in the horse In: C.W. McIlwraith, D.D. Frisbie, C.E. Kawcak, et al., eds. *Joint Disease in the Horse* 2nd ed. St. Louis, MO: Elsevier, 2016;33-48.
2. Guermazi A, Alizai H, Crema MD, et al. Compositional MRI techniques for evaluation of cartilage degeneration in osteoarthritis. *Osteoarthritis Cartilage* 2015;23:1639-1653.
3. Pease A. Biochemical evaluation of equine articular cartilage through imaging. *Vet Clin N Am-Equine* 2012;28:637-646.
4. Potter HG, Black BR, Chong le R. New techniques in articular cartilage imaging. *Clin Sports Med* 2009;28:77-94.
5. Nelson BB, Goodrich LR, Barrett MF, et al. Use of contrast media in computed tomography and magnetic resonance imaging in horses: Techniques, adverse events and opportunities. *Equine Vet J* 2017;49:410-424.
6. Nelson BB, Kawcak CE, Goodrich LR, et al. Comparison between computed tomographic arthrography, radiography, ultrasonography, and arthroscopy for the diagnosis of femorotibial joint disease in western performance horses. *Vet Radiol Ultrasound* 2016;57:387-402.
7. Puchalski SM. Advances in equine computed tomography and use of contrast media. *Vet Clin North Am Equine Pract* 2012;28:563-581.
8. Puchalski SM, Bergman EHJ. Computed tomography arthrography for the diagnosis of equine femorotibial lameness in h 137 horses: 2007 to 2012. 59th Annual Convention of the American Association of Equine Practitioners 2013;228.

9. Vallance SA, Bell RJ, Spriet M, et al. Comparisons of computed tomography, contrast-enhanced computed tomography and standing low-field magnetic resonance imaging in horses with lameness localised to the foot. Part 2: Lesion identification. *Equine Vet J* 2012;44:149-156.

10. Vallance SA, Bell RJ, Spriet M, et al. Comparisons of computed tomography, contrast enhanced computed tomography and standing low-field magnetic resonance imaging in horses with lameness localised to the foot. Part 1: anatomic visualisation scores. *Equine Vet J* 2012;44:51-56.

11. Bushberg JT, Seibert JA, Leidholdt EM, et al. Computed tomography In: Mitchell CW, ed. *The Essential Physics of Medical Imaging*. Philadelphia, PA: Lippincott Williams & Wilkins, 2012;312-374.

12. Bushberg JT, Seibert JA, Leidholdt EM, et al. Magnetic resonance imaging In: Mitchell CW, ed. *The Essential Physics of Medical Imaging*. Philadelphia, PA: Lippincott Williams & Wilkins, 2012;415-467.

13. Bansal PH, Joshi NS, Entezari V, et al. Contrast enhanced computed tomography can predict the glycosaminoglycan content and biomechanical properties of articular cartilage. *Osteoarthritis Cartilage* 2010;18:184-191.

14. Xie L, Lin AS, Guldberg RE, et al. Nondestructive assessment of sGAG content and distribution in normal and degraded rat articular cartilage via EPIC-microCT. *Osteoarthritis Cartilage* 2010;18:65-72.

15. Xie L, Lin ASP, Levenston ME, et al. Quantitative assessment of articular cartilage morphology via EPIC-microCT. *Osteoarthritis Cartilage* 2009;17:313-320.

16. Lakin BA, Ellis DJ, Shelofsky JS, et al. Contrast-enhanced CT facilitates rapid, non-destructive assessment of cartilage and bone properties of the human metacarpal. *Osteoarthritis Cartilage* 2015;23:2158-2166.
17. Bansal PN, Joshi NS, Entezari V, et al. Cationic contrast agents improve quantification of glycosaminoglycan (GAG) content by contrast enhanced CT imaging of cartilage. *J Orthop Res* 2011;29:704-709.
18. Joshi NS, Bansal PN, Stewart RC, et al. Effect of contrast agent charge on visualization of articular cartilage using computed tomography: exploiting electrostatic interactions for improved sensitivity. *J Am Chem Soc* 2009;131:13234-13235.
19. Lakin BA, Grasso DJ, Shah SS, et al. Cationic agent contrast-enhanced computed tomography imaging of cartilage correlates with the compressive modulus and coefficient of friction. *Osteoarthritis Cartilage* 2013;21:60-68.
20. Stewart RC, Bansal PN, Entezari V, et al. Contrast-enhanced CT with a high-affinity cationic contrast agent for imaging ex vivo bovine, intact ex vivo rabbit and in vivo rabbit cartilage. *Radiology* 2013;266:141-150.
21. Kol A, Arzi B, Athanasiou KA, et al. Companion animals: Translational scientist's new best friends. *Sci Transl Med* 2015;7:1-8.
22. McIlwraith CW, Fortier LA, Frisbie DD, et al. Equine models of articular cartilage repair. *Cartilage* 2011;2:317-326.
23. Frisbie DD, Cross MW, McIlwraith CW. A comparative study of articular cartilage thickness in the stifle of animal species used in human pre-clinical studies compared to articular cartilage thickness in the human knee. *Vet Comp Orthop Traumatol* 2006;19:142-146.

24. Malda J, de Grauw JC, Benders KEM, et al. Of Mice, Men and Elephants: The Relation between Articular Cartilage Thickness and Body Mass. *PLOS ONE* 2013;8:e57683.
25. Hoemann CD. Molecular and biochemical assays of cartilage components In: De Ceuninck F, Sabatini M,Pastoureau P, eds. *Cartilage and Osteoarthritis*. Totowa, New Jersey: Humana Press, 2004;127-156.
26. Baxter GM, Stashak TS. Perineural and intrasynovial anesthesia In: Baxter GM, ed. *Adams and Stashaks Lameness in Horses*. Ames, IA: Wiley-Blackwell, 2011;173-202.
27. Entezari V, Bansal PN, Stewart RC, et al. Effect of mechanical convection on the partitioning of an anionic iodinated contrast agent in intact patellar cartilage. *J Orthop Res* 2014;32:1333-1340.
28. Shanfield S, Campbell P, Baumgarten M, et al. Synovial fluid osmolality in osteoarthritis and rheumatoid arthritis. *Clin Orthop Relat Res* 1988:289-295.
29. Bursac PM, Freed LE, Biron RJ, et al. Mass transfer studies of tissue engineered cartilage. *Tissue Eng* 1996;2:141-150.
30. Stewart R. A diagnostic imaging technique and therapeutic strategy for early osteoarthritis. *College of Engineering*. Boston, MA: Boston University, 2014;180.
31. Porter EG, Winter MD, Sheppard BJ, et al. Correlation of articular cartilage thickness measurements made with magnetic resonance imaging, magnetic resonance arthrography, and computed tomographic arthrography with gross articular cartilage thickness in the equine metacarpophalangeal joint. *Vet Radiol Ultrasound* 2016;57:515-525.
32. Carstens A, Kirberger RM, Dahlberg LE, et al. Validation of delayed gadolinium-enhanced magnetic resonance imaging of cartilage and T2 mapping for quantifying distal

metacarpus/metatarsus cartilage thickness in Thoroughbred racehorses. *Vet Radiol Ultrasound* 2013;54:139-148.

33. Spriet M. Letter to the Editor. *Vet Radiol Ultrasound* 2014;55:5-6.
34. Gendler A, Keuler NS, Schaefer SL. Computed tomographic arthrography of the normal canine elbow. *Vet Radiol Ultrasound* 2015;56:144-152.
35. Vanderperren K, Ghaye B, Snaps FR, et al. Evaluation of computed tomographic anatomy of the equine metacarpophalangeal joint. *Am J Vet Res* 2008;69:631-638.
36. Byun S, Tortorella MD, Malfait A-M, et al. Transport and equilibrium uptake of a peptide inhibitor of PACE4 into articular cartilage is dominated by electrostatic interactions. *Arch Biochem Biophys* 2010;499:32-39.
37. Salo EN, Nissi MJ, Kulmala KAM, et al. Diffusion of Gd-DTPA2- into articular cartilage. *Osteoarthritis Cartilage* 2012;20:117-126.
38. Stewart RC, Patwa AN, Lusic H, et al. Synthesis and preclinical characterization of a cationic iodinated imaging contrast agent (CA4+) and its use for quantitative computed tomography of ex vivo human hip cartilage. *J Med Chem* 2017;60:5543-5555.

CHAPTER 3:

INVESTIGATION OF CATIONIC CONTRAST MEDIA DIFFUSION INTO EQUINE ARTICULAR CARTILAGE *IN VIVO* AND THE POTENTIAL TOXICITY OF CA4+ TO ARTICULAR TISSUES

Introduction

Articular cartilage degeneration is an early indication of osteoarthritis and progression of the disease is inevitable as the intrinsic healing capability of this tissue is limited.[1-3] Although the use of magnetic resonance imaging (MRI) has improved the detection of articular cartilage injury, there is still a relative lack of sensitive diagnostic methods for detecting early biochemical change and further research is indicated to improve the diagnosis of early osteoarthritis.[4] Recently, the gantry diameter in some computed tomography (CT) scanners has increased, allowing the equine stifle to fit within the CT gantry.[5] When compared to MRI, CT has superior spatial resolution and scans are performed in minutes compared to an hour with MRI. Although both modalities allow for volumetric assessment, reconstruction algorithms provide for improved multi-planar evaluation with CT.[4] Contrast enhanced computed tomography (CECT) is a method where an iodinated contrast medium (ICM) is injected into the joint to outline specific tissues. If CECT imaging could be used to evaluate articular cartilage, it would provide an alternative to MRI evaluation with significantly faster scan times and improved resolution.

Glycosaminoglycans (GAGs) are predominant polysaccharides in the extracellular matrix of articular cartilage. In the early stages of osteoarthritis, the loss of GAGs is one of the first signs

of articular cartilage degeneration.[6] When traditional (anionic) ICM are injected into the joint, the articular cartilage surface is outlined but due to the negative charges on GAGs the contrast is repelled limiting diffusion into the tissue. Conversely, a cationic contrast medium with 4 positive charges (CA4+) has been synthesized and has high uptake into articular cartilage, allowing for the estimation of cartilage GAG content through cationic CECT imaging.[7-9] Initial successes in the use of cationic CECT to predict GAG content and equilibrium compressive modulus have been documented using explanted articular cartilage. While these methods have established the time needed for CA4+ to reach equilibrium in articular cartilage *ex vivo* (Chapter 2), active joint metabolism would affect these diffusion rates. Therefore, investigation of CA4+ diffusion *in vivo* is required to determine the optimal time needed after joint injection to perform the cationic CECT scan before experimental *in vivo* models are performed.

Another critical component that requires investigation before *in vivo* use is to determine the potential toxicity of CA4+ on joint tissues. Administration of CA4+ (via intravenous and intra-articular routes) has recently been documented.[10] In rats, increasing dosing volumes of CA4+ (24 mg I/mL) did not cause adverse effects in hepatic or renal function and >95% was excreted within 24 hours similar to other iodinated contrast media.[10-13] Another experimental small animal model showed that there was no toxicity of CA4+ to articular cartilage or synovial membrane after two injections over a 1-month period in rabbits.[14] At euthanasia, there were no signs of gross inflammation and the lack of neutrophilic inflammation in synovial fluid supported no acute toxic effects of CA4+.[14] However, the articular cartilage thickness in the rabbit is significantly less than in the horse and there may be differences in joint tissue responses to CA4+ between species.[15,16] Before CA4+ can be used in further *in vivo* studies, it must be more

critically evaluated in the horse to document any potential adverse effects after exposure to joint tissues.

The objectives of this study were: 1) to determine the *in vivo* diffusion trajectory of intra-articular delivery of CA4+ and to optimize the timing of CECT scanning after injection, and 2) to investigate the potential toxicity of CA4+ on joint tissues. The first hypothesis was that the cationic CECT attenuation would change over time and show a consistent and maximum value to optimize the timing of CECT scans after CA4+ injection. The second hypothesis was that after repeated exposure to CA4+ there would not be detrimental effects on clinically measured outcomes or articular tissues.

Materials and Methods

In vivo diffusion of CA4+ into femoropatellar joint cartilage (Experiment 1)

Three horses were used to determine the diffusion of CA4+ into femoropatellar joint cartilage *in vivo*. All experimental protocols were evaluated and approved by the Institutional Animal Care and Use Committee at Colorado State University (Protocol ID: 14-5119A, approval 6/24/2014). The femoropatellar joint was selected over the metacarpophalangeal and carpal joints because of its thicker articular cartilage and the improved observation of cationic CECT attenuation in this joint cartilage compared to the other joints (Chapter 2). The ages of the horses were 2 years (horse 1), 15 years (horse 2) and 5 years (horse 3). The CA4+ was synthesized as described previously (Chapter 2) and made into two concentrations (8 mg I/mL and 24 mg I/mL) though both solutions had identical osmolality (400 mOsm/kg) and pH (7.4).[9] The femoropatellar joint was injected with 100 mLs of CA4+ under aseptic conditions using a suprapatellar approach.

The base of the patella was palpated proximal to the lateral femoropatellar ligament and an 18 ga 3.5 inch spinal needle was advanced in a lateromedial and slightly distal angle to penetrate the suprapatellar recess of the femoropatellar joint. The stylet was removed and the CA4+ was injected.

Cationic CECT scans were performed using a 16-slice multi-detector scanner (Gemini TF Big Bore PET/CT scanner, helical CT x-ray tube with an 85 cm bore, Philips Healthcare, Andover, MA) at specific time points after CA4+ injection. The CA4+ concentrations and scan times after injection for each horse were as follows:

- Horse 1 (8 mg I/mL): 1, 2, 3, 4 and 24 hours after CA4+ injection
- Horse 2 (24 mg I/mL): 3, 4, 5 and 6 hours after CA4+ injection
- Horse 3 (24 mg I/mL): 3, 4, 5 and 6 hours after CA4+ injection

Imaging acquisition settings for all scans were: 140 kVp, 500 mAs, 0.4–0.6 pitch, 35 cm field-of-view, 1024 x 1024 matrix. The CT studies were reconstructed at 0.8 mm thickness x 0.8 mm increment (bone filter) and 2.0 mm thickness x 1.0 mm increment (standard filter). The images were imported into commercial imaging software (iSite PACS Radiology, v.3.6.134, Foster City, CA). Multiplanar reconstructions were performed in all joints in transverse, sagittal, and dorsal plane projections. The different concentrations between horses were used because of low attenuation values obtained after the first horse and higher concentrations were expected to increase the range of attenuation values. Also, different horse ages were used to investigate the potential effect of age related articular cartilage changes on cationic CECT attenuation.

All cationic CECT imaging data were also imported into and evaluated with commercial imaging software (Analyze, version 12.0, Biomedical Imaging Resource, Mayo Clinic, Rochester, MN). The articular cartilage of the medial and lateral trochlear ridges were manually segmented from the subchondral bone and joint space by generating regions of interest (ROIs)(Figure 3.1). The lateral trochlear ridge cartilage was divided into two ROIs (superficial [sLTR] and deep [dLTR] lateral trochlear ridge), while the medial trochlear ridge (MTR) with thinner articular cartilage was segmented as a single ROI. The mean ± standard deviation cationic CECT attenuation of each ROI was recorded at each time point. Line graphs were constructed to follow the diffusion path of CA4+ over time at each location. These data were evaluated to determine the time at which maximum cationic CECT attenuation occurred within each ROI location for each horse.

Assessment of potential toxicity of CA4+ to synovial tissues (Experiment 2)

A two year-old horse without hindlimb lameness, femoropatellar joint effusion or radiographic evidence of joint disease was used to investigate the potential toxicity of CA4+ to synovial tissues. One femoropatellar joint was randomly assigned (by coin toss) to receive CA4+ ICM, while the opposite joint received 1x phosphate buffered saline (PBS). Each femoropatellar joint was injected with the respective solution at baseline and then every two weeks thereafter until the study endpoint at four months (eight injections total per joint).

Clinical assessments

Assessments of hindlimb lameness were made subjectively by using a 0 to 5 scale and joint effusion was subjectively graded on a 0 to 4 scale (0 = none, 1 = slight, 2 = mild, 3 = moderate, 4 = severe).[17,18] Both of these clinical assessments preceded arthrocentesis and joint injection

procedures at baseline and at all subsequent time points (every two weeks thereafter) to prevent confounding those assessments. For arthrocentesis and joint injection procedures the horse was sedated with xylazine hydrochloride (0.3 mg/kg IV) and butorphanol tartrate (0.1 mg/kg IV). Once sedated, both femoropatellar joints were aseptically prepared using betadine scrub and alcohol. Synovial fluid was aspirated from the distolateral aspect of the femoropatellar compartment using a lateral approach.[19] Synovial aspiration was performed using established palpable landmarks, though when synovial fluid could not be successfully aspirated, an ultrasound-guided approach was used. Once collected, an aliquot (~500 μL) of synovial fluid was placed into a tube with ethylenediaminetetraacetic acid (EDTA) for cytologic analysis and the remainder placed into a serum tube for assessment of total protein, glycosaminoglycan (GAG) and prostaglandin E_2 (PGE_2). After synovial fluid aspiration, 100 mLs of fluid was injected into the respective femoropatellar joint (Right: CA4+ [24 mg I/mL, 400 mOsm/kg, pH=7.0]; Left: 1x PBS). Then, the horse was allowed to recover from sedation and resumed normal activity.

Synovial fluid evaluation

After aspiration, the collected sample of synovial fluid was visually examined and subjectively graded for its color and clarity. Placing a drop between two fingers and observing the length of the string as the fingers were separated assessed the viscosity of the fluid. This subjective assessment of viscosity was graded as normal or as a mild, moderate or severe decrease in viscosity. Cytologic analysis was performed using a commercial analyzer (Heska, HemaTrue, Cuattro, Loveland, CO) and reported as total leukocyte concentrations along with the percentage of neutrophils in the synovial fluid sample. Total protein (TP) concentrations were determined by

placing a drop of aspirated synovial fluid on a refractometer immediately after collection. The synovial fluid placed in serum tubes was centrifuged at 1000 G for 10 minutes and the supernatant was collected and frozen at -80 °C until all samples were obtained. Clinical and synovial fluid assessments were repeated every two weeks until the end of the experiment (four months after baseline).

The frozen aliquots of synovial fluid were thawed in preparation for GAG and PGE_2 quantitation. The GAG samples were analyzed using the 1,9-dimethylmethylene blue (DMMB) assay after papain digestion.[20] The DMMB assay was performed using a standard curve generated with known concentrations of chondroitin C sulfate. Samples were prepared in triplicate and read on a microplate reader (SpectraMax M3, Molecular Devices, Sunnyvale, CA), set at a wavelength of 530 nm. Using a fit quadratic curve, the mean absorbance of all samples was determined and a mean calculated for each sample. The PGE_2 quantitation was performed by first extracting it from synovial fluid through use of C2 columns (Amprep mini-columns ethyl C2 columns, GE Healthcare Co, Pittsburgh, PA). Then, the samples were processed using a commercial assay kit with a minimum detection rate of 13.4 pg/mL (Enzo Life Sciences Inc., Farmingdale, NY). Samples were run in duplicate and read on a microplate reader set at a wavelength of 405 nm. The mean value was reported for each sample. Samples from the DMMB and PGE_2 assays were repeated if the standard curve $R^2 < 0.9$ or if the coefficient of variation between replicates was > 0.1.

Postmortem evaluation

At four months, the horse was humanely euthanized with an overdose of pentobarbital (88 mg/kg IV). Immediately after euthanasia, both femoropatellar joints were dissected to examine the appearance of the synovial membrane and articular cartilage. The synovial membrane was subjectively evaluated for evidence of inflammation and/or thickening. The articular cartilage was examined for signs of surface injury or defects and were graded on the International Cartilage Repair Society (ICRS) scale.[21]

Three samples of synovial membrane were collected per joint and placed in 10% formalin in preparation for histologic processing. Synovial membrane samples were collected from the lateral aspect of the femoropatellar joint in proximity to the site of arthrocentesis, from the suprapatellar recess and from the medial aspect of the joint. The femoral trochlea was removed from the femur using a band saw. Samples of osteochondral tissue were then collected from the femoral trochlea and patella using a diamond bladed saw (EXAKT 300 CP, Exact Technologies, Inc., Oklahoma City, OK) using constant water irrigation to prevent tissue heating. Two osteochondral samples (1.5 mm thickness) were each cut from the medial and lateral trochlear ridges of the femur, trochlear groove and articular surfaces of the patella in each joint. One sample from each site was placed in 1x PBS for chondrocyte viability assessment, while a second sample was stored in 10% formalin for histologic analysis. Assessment of chondrocyte viability was performed using a commercial assay (Live/Dead Viability/Cytotoxicity Kit, Life Technologies, Grand Island, NY). Mixtures of calcein acetoxymethyl ester (1:2000) and ethidium bromide homodimer (1:3000) in PBS were added to plate wells with the osteochondral tissue and were incubated for 30 minutes in the dark at 20 °C.[22] The tissue was then examined

under an inverted and automated confocal microscope (Olympus IX83, Olympus Life Science, Center Valley, PA) equipped with a digital camera acquisition system. Microscopic images were captured of the entire sample (superficial through deep zones) at 10X magnification and collected in a Z-stack of 10 images (20 μms between stack images). Images were analyzed using commercial software (Count & Measure module, CellSens Dimension v.1.16, Olympus Life Science). Viable and non-viable cells were counted separately through an automated protocol after establishing an intensity and threshold-based segmentation. The same protocol and threshold process was instituted over all samples. The percentage of live cells out of the total number of counted cells was reported for each tissue site.

After five days in 10% formalin, the osteochondral samples were decalcified in EDTA (Formical-2000, Statlab, McKinney, TX) for seven days and were then rinsed in 1x PBS prior to undergoing further histologic processing (Appendix I.1). Samples of synovial membrane were maintained in 10% formalin until histologic processing. After tissue processing, both the synovial membrane and osteochondral tissue samples were embedded in paraffin and using a microtome (Leica RM2255, Leica Biosystems, Buffalo Grove, IL), 5 μm sections were prepared on microscope slides. The synovial membrane and osteochondral samples were each stained with hematoxylin and eosin and a slide of the osteochondral samples was stained with safranin-O fast green (SOFG)(Appendix I.2). Control tissues (bovine trachea and equine osteochondral samples) were stained with all groups to control for variation in staining intensity across batches.

The sections of synovial membrane were scored by a blinded single investigator for grades of cellular infiltration, intimal hyperplasia, and subintimal vascularity, edema and fibrosis (grade 0

– 4; 0 = normal, 4 = marked) using the Osteoarthritis Research Society International (OARSI) scoring system.[23] Sections of articular cartilage and bone were also scored on the OARSI scoring system. Articular cartilage was scored for grades of chondrocyte necrosis, chondrone (cluster) formation, cartilage fibrillation/fissuring, focal cell loss and SOFG uptake (grades 0 – 4; 0 normal, 4 = marked/severe). The subchondral bone was graded for levels of osteochondral lesions, subchondral bone remodeling and osteochondral splitting.[23] The grades of osteochondral lesions range from 0 – 4 (0 = normal, 4 = ulcerated) and the other categories range from 0 – 3 (0 = normal, 3 = severe).[23] Articular cartilage sections evaluated for SOFG stain uptake were also individually scored in region-specific locations (tangential, intermediate, radiate territorial and radiate interterritorial zones). A cumulative OARSI score was calculated ranging from 0 – 20. The OARSI scoring system was chosen over other histological scoring systems because it better designates early states of osteoarthritis and was designed for use with equine tissue.[24-26]

Data and statistical analysis

Categorical data was reported as median (interquartile range [IQR] or range) and continuous data reported as mean ± standard deviation (s.d.). The determination of a Normal distribution of each outcome parameter was made using the Shapiro-Wilk test. Synovial fluid parameters (GAG, PGE_2, TP, leukocytes, neutrophils) were compared between CA4+ and control joints and over time using a repeated measures mixed model ANOVA. Ordinal outcome variables (lameness, joint effusion) were analyzed using ordered logistic regression. Multiple comparisons were addressed using posthoc Tukey-Kramer adjustments. Cell viability comparisons were made between CA4+ and control joints using a paired t-test and histology (synovium and articular cartilage) scores were made using a Wilcoxon signed rank test. Statistical analysis was

performed using SAS (University Edition, v. 9.2, SAS Institute Inc., Cary, NC) and significance was defined as $P<0.05$.

Results

In vivo diffusion of CA4+ into femoropatellar joint cartilage (Experiment 1)

The articular cartilage was visible at every time point in all horses, though the distribution of CA4+ diffusion varied across joint surfaces. The MTR and superficial portions of the LTR were readily observed at the first time point in all scans. The deep portions of the lateral trochlear ridge and femoral groove were typically devoid of CA4+, though this changed over time in subsequent cationic CECT scans. Over time this portion of articular cartilage became visible (Figure 3.1B) indicating deeper diffusion with longer CA4+ exposure. There were specific differences in cationic CECT attenuation within each individual horse.

In horse 1 (using 8 mg I/mL CA4+), the mean cationic CECT attenuation of all three sites (MTR, sLTR and dLTR) over time concentrated around 200 HUs (Figure 3.2A). The cationic CECT attenuation averaging over all time points in the MTR, sLTR and dLTR were 194 ± 54, 173 ± 32 and 213 ± 51 HUs, respectively. The maximum cationic CECT attenuation in the MTR (210 ± 26 HUs) and dLTR (250 ± 36 HUs) was at 3 hours after injection, while in the sLTR (200 ± 51 HUs) the maximum was at 1 hour after injection. After 24 hours, the cationic CECT attenuation returned to the attenuation of unenhanced articular cartilage (~100 HUs).

In horse 2 (using 24 mg I/mL CA4+), the cationic CECT attenuation averaging over all time points centered around 350 HUs (MTR: 293 ± 55 HUs, sLTR: 338 ± 36 HUs and dLTR: 488 ±

70 HUs). The maximum cationic CECT attenuation in the MTR (327 ± 45 HUs) was at 3 hours, in the sLTR (367 ± 43 HUs) it was at 4 hours and in the dLTR (509 ± 72 HUs) it was at 5 hours after CA4+ injection (Figure 3.2).

In horse 3, the mean cationic CECT attenuation centered around 350 HUs (MTR: 299 ± 47 HUs, sLTR: 255 ± 42 HUs, dLTR: 427 ± 62 HUs). The maximum cationic CECT attenuation in all sites (MTR: 318 ± 42 HUs, sLTR: 278 ± 39 HUs, dLTR: 472 ± 62 HUs) was at 5 hours post CA4+ injection (Figure 3.2).

Assessment of potential toxicity of CA4+ to synovial tissues (Experiment 2)

Clinical assessments

The horse tolerated all arthrocentesis and joint injection procedures without incident. There were no observable adverse reactions to the horse's comfort, attitude or ambulation after any of the injections. The median (range) lameness score over the course of the experiment was 0 (0 – 1) in the CA4+ joint and 0 (0 – 0) in the control joint. The median synovial effusion score was 1 (0 – 2) for both the CA4+ and control joints. There were no significant differences in lameness or synovial effusion scores over time (P = 0.99 and P = 0.55, respectively) or between the CA4+ and control joints (P = 0.99 and P = 0.68, respectively).

Synovial fluid evaluation

The results of synovial fluid TP and leukocyte assessments at each time point are shown in Table 3.1. There were no significant differences in either synovial fluid parameter between groups or over time. There was no decrease in synovial fluid viscosity in any of the samples and the color

of the aspirate was consistently clear aside from two samples in the CA4+ group (at weeks 8 and 10), which were observed to be slightly cloudy. Hemorrhage was commonly encountered in the sample aspirates though was not consistently related to a specific joint and was not cumulative over time (Table 3.1). Synovial fluid concentrations of GAG and PGE_2 are shown in Figure 3.3. There were no significant differences between synovial fluid GAG and PGE_2 between joints or over time.

Postmortem evaluation

The macroscopic appearance of the articular surfaces in both the CA4+ and control joints did not show evidence of gross inflammation. The synovial membrane was not visibly thickened in either joint. The articular cartilage was smooth and congruous throughout all articular surfaces with no apparent surface irregularities (ICRS score 0) observed in either joint. In the control joint, there was some discolored (red) articular cartilage at the distal aspect of the lateral trochlear ridge of the femur at the same level where arthrocentesis procedures were performed but there was no alteration in the integrity of the articular surface.

Mean chondrocyte viability of the articular cartilage samples was 84.7 ± 3.9% in the CA4+ joint and 82.8 ± 5.9% in the control joint and were not significantly different between joints (P=0.67)(Figure 3.4). Non-viable cells were commonly observed at the articular cartilage surface (superficial zone) in both joints.

The histological scores of synovial membrane were not significantly different between CA4+ and PBS injected joints for any individual parameter or as a cumulative total on the OARSI scale

(Table 3.2). The median scores of vascularity and subintimal edema and fibrosis were moderately elevated in both joints. There were no differences in articular cartilage scores between the CA4+ and PBS injected joints (Table 3.3).

Discussion

The *in vivo* diffusion experiment showed that there is regional variation in CA4+ partitioning across joint surfaces and over time. Regardless of the time imaged, the medial trochlear ridge and superficial portions of the lateral trochlear ridge were well highlighted by the CA4+ contrast media. However, the deep portions of the lateral trochlear ridge and the femoral groove frequently had lower attenuations. By increasing the time of CA4+ exposure, cationic CECT attenuation also increased in these deeper portions of articular cartilage. The difference between medial and lateral trochlear ridge diffusion was attributed to the disparities in tissue thickness and volume between these locations in the equine stifle.[15] Thicker articular cartilage will increase the time needed for CA4+ to diffuse into the tissue.[10]

There were disparities in cationic CECT appearance between horses that could have been due to differences in CA4+ concentration, tight articulation caused by the medial patellar ligament, age or anesthetic timing. The difference in the magnitude of cationic CECT attenuation between horse 1 and the other two horses is explained by the two different CA4+ concentrations administered. While 8 mgI/mL was initially chosen in the preliminary experiments to investigate cationic CECT there was only a 2-fold increase over baseline (unenhanced) articular cartilage. Despite this concentration being sufficient to outline articular cartilage, when the CT attenuation was quantified, this relatively low value was suspected to substantially limit the range of

detection when degenerative tissue was imaged. Since the iodine concentration is directly proportional to CT attenuation, the iodine concentration was increased in subsequent horses to increase the range of CT attenuation values. The equine stifle is held tightly together by the patellar, cruciate and collateral ligaments. As such the compression on articular cartilage caused during full extension (required position on the CT table) can alter the diffusion of CA4+ into compressed portions of articular cartilage (data not shown). However, the location on the medial trochlear ridge was not observably altered in these scans.

The variation in age or joint metabolism rates between horses also could have influenced cationic CECT attenuation. While horse 1 and 3 were both juvenile, horse 2 was middle aged (15 years old). The use of different ages in these experiments was intentional to investigate the potential effect of age on subsequent attenuation values. Age has been associated with a decline in GAGs, water, and chondrocyte density with relative increases in collagen content when compared to juvenile articular cartilage.[27,28] With lower GAG content, the cationic CECT attenuation would decrease due to lower attraction of CA4+. However in this experiment, the oldest horse (horse 2) comparatively had the highest cationic CECT attenuation. Possible explanations include there was no difference in articular cartilage biochemistry across the three horses because of the low prevalence of degenerative and osteoarthritic cartilage in the femoropatellar compartment compared to other weight bearing joints (*e.g.* femorotibial joints). Another potential explanation could be that the articular cartilage swelling that occurs after anisotropy and breakdown of the collagen network permitted more CA4+ to build in the tissue. Biochemical analyses of these joint tissues were not performed and thus these conclusions remain speculative. A limitation of this study was that a density phantom was not used to standardize CT attenuation values between

horses and thus comparisons between horses should be interpreted with caution due to decreased accuracy of CT measurements. Nonetheless, age was not an influential factor in cationic CECT attenuation in this subset of horses.

The timing of anesthesia was different between horse 1 and horses 2 and 3. Since horse 1 was anesthetized after 1 hour this limited the time of CA4+ contact with articular cartilage compared to the other horses that were not placed into lateral recumbency until 3 hours after CA4+ injection. The suprapatellar recess is a large compartment in the horse. Despite filling the joint with 100 mLs of CA4+ (approximate capacity of the femoropatellar joint), when the horse is placed in lateral recumbency, the contrast media may recede away from the femoral trochlea and sequester in the suprapatellar recess. Considering all of these factors and the proposed location of future articular cartilage defects on the medial trochlear ridge, four hours after CA4+ injection was determined to provide the most consistent time to perform the cationic CECT scan.

In the second experiment, there were no adverse consequences attributed to the CA4+ contrast media on the clinical, synovial fluid, articular cartilage and synovial membrane outcomes when compared to the PBS control. Over the course of the nine bi-weekly injections, there was a slight increase in synovial effusion in both joints as determined by palpation. The lack of a difference in effusion scores between groups implies that no short-term detrimental effects occurred. The slight increase in synovial effusion in both joints could be explained by the repeated penetration of the joint compartment and injection of a large fluid volume (CA4+ or PBS) stimulating the production of synovial fluid or the resultant inflammation from repeated puncture caused altered joint clearance.

The results of the synovial fluid assessments did not indicate inflammation or articular toxicity following exposure to CA4+. Bertone *et al* investigated the use of a similar PGE_2 assay on equine synovial fluid. They established a threshold of 62.5 pg/mL as the minimum threshold to classify joint disease.[29] Additionally Frisbie *et al.* showed that baseline PGE_2 concentrations in the middle carpal joints of horses averaged 100 pg/mL.[20] Though variability in the assays and joints used could contribute to differences between these two studies and prevented establishing a definitive threshold, the values observed from the joints in this study suggest a lack of joint inflammation.[20,29] The response of repeated synovial fluid GAG concentrations in the femoropatellar joint of horses have not previously been characterized. A study investigating an experimental impact model of osteoarthritis in the femorotibial joint showed that there was a significant and transient decrease in synovial fluid GAG in the first 54 days after impact injury that then began to increase.[30] Other investigators have documented this same response in other joints.[31-33] The effect of repeated arthrocentesis has been shown to increase synovial fluid GAG and PGE_2 concentrations and a general trend of this same effect was observed in this horse.[20,34] The lack of a significant difference between joints suggests CA4+ use was not detrimental; however, the low number of samples and joints used in this experiment precludes further conclusions.

Despite the lack of a significant difference between the CA4+ and control joints for all articular cartilage histologic parameters, there was an elevation in synovial membrane histology scores in both joints. The median vascularity and subintimal edema and fibrosis parameters were scored as moderately increased. To the author's knowledge this high frequency of joint injections over a short time on synovial membrane outcomes have not been documented. The injection of PBS in

the control joint was meant to investigate this potential effect. Since PBS is a physiologic fluid with a more similar osmolality (315 mOsm/kg) and pH (7.4) to synovial fluid than 0.9% saline (285 mOsm/kg and 5.5, respectively), it was suspected to be innocuous.[35,36] However, PBS still has a slightly lower osmolality than joint fluid (400 mOsm/kg) and it has been proposed that higher osmolality joint irrigation solutions may prevent chondrocyte necrosis.[37] Regardless, the lack of a difference between groups suggests there are not detrimental effects of CA4+ and that these responses are a consequence of the study design and repetitive joint injections. The results of this chapter support further *in vivo* use of CA4+ and cationic CECT to investigate articular cartilage in horses, though the low sample numbers warrant continued assessments of CA4+ on the potential toxicity to articular tissues in subsequent experiments.

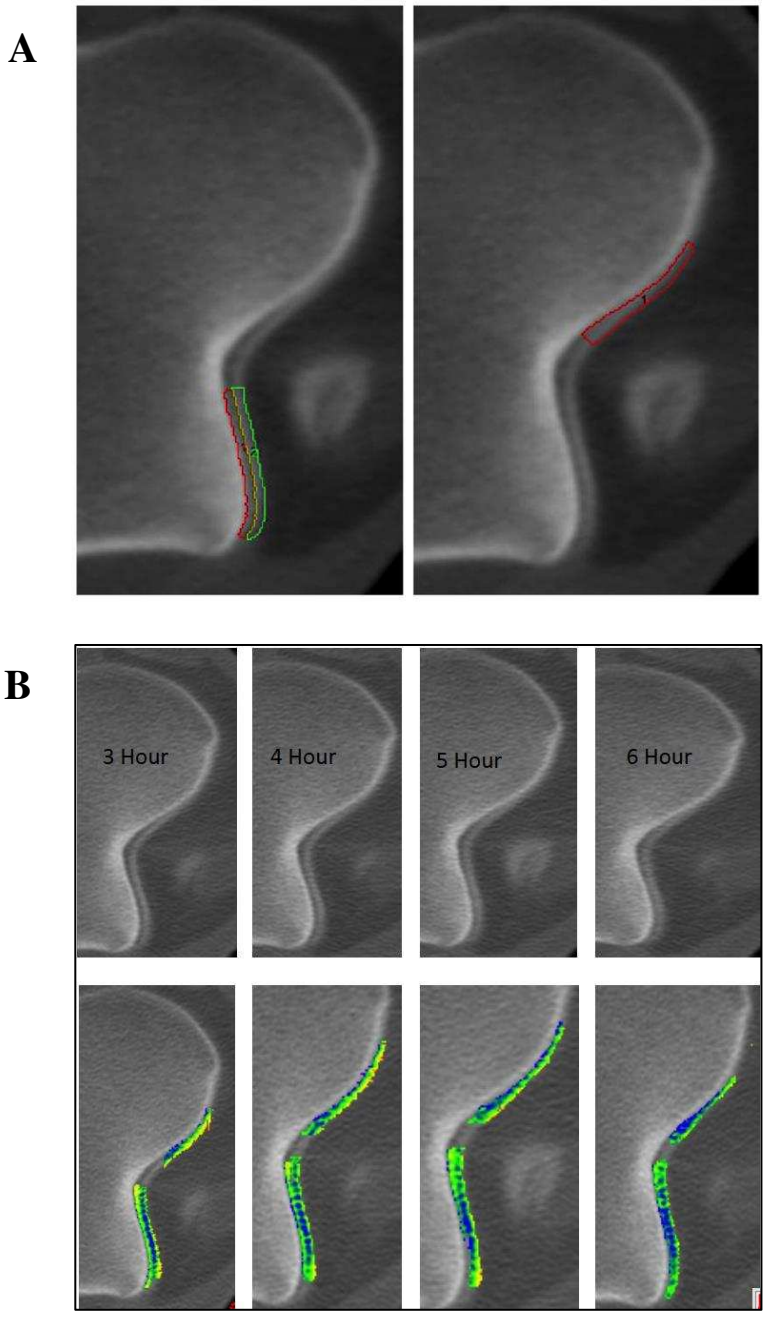

Figure 3.1 – A) Transverse plane cationic CECT image in horse 2 demonstrating the regions of interest (ROIs) used in the plotting of CA4+ diffusion *in vivo*. The left image shows the lateral trochlear ridge ROI separated into superficial (green) and deep (red) segments. The right image shows the location sampled on the medial trochlear ridge. B) Transverse plane cationic CECT images of horse 2 at each acquisition time point (3, 4, 5 and 6 hours after CA4+ injection). The top row of images show the standard grey scale images and the images below depict the ROIs overlaid with a color map to highlight changes in attenuation values.

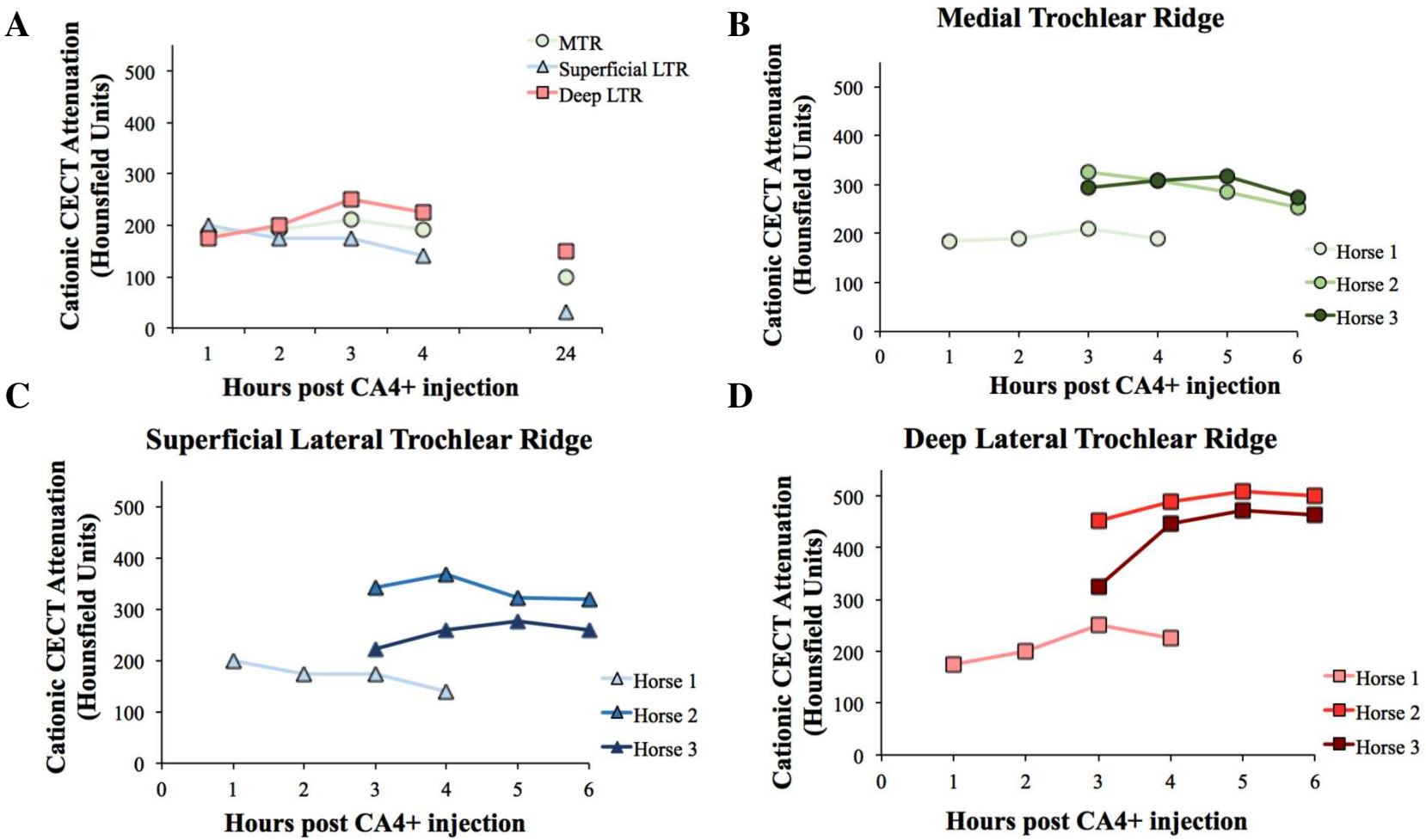

Figure 3.2 – A) The plotted diffusion trajectory of CA4+ into equine femoropatellar cartilage sites (horse 1). Mean cationic contrast-enhanced computed tomography (CECT) attenuation indicates the measured signal within the segmented region of interest at each femoropatellar joint location. Hours 1 – 4 were recorded under a signal anesthetic period. The horse was recovered from anesthesia and scanned 24 hours after the first CA4+ injection. The comparison of the captured data at the time points collected in all 3 horses are shown in the accompanying graphs and are grouped by sample location (B, medial trochlear ridge [MTR]; C, superficial lateral trochlear ridge [LTR]; D, deep LTR). Horse 2 and 3 had cationic CECT performed at 3, 4, 5 and 6 hours after CA4+ injection.

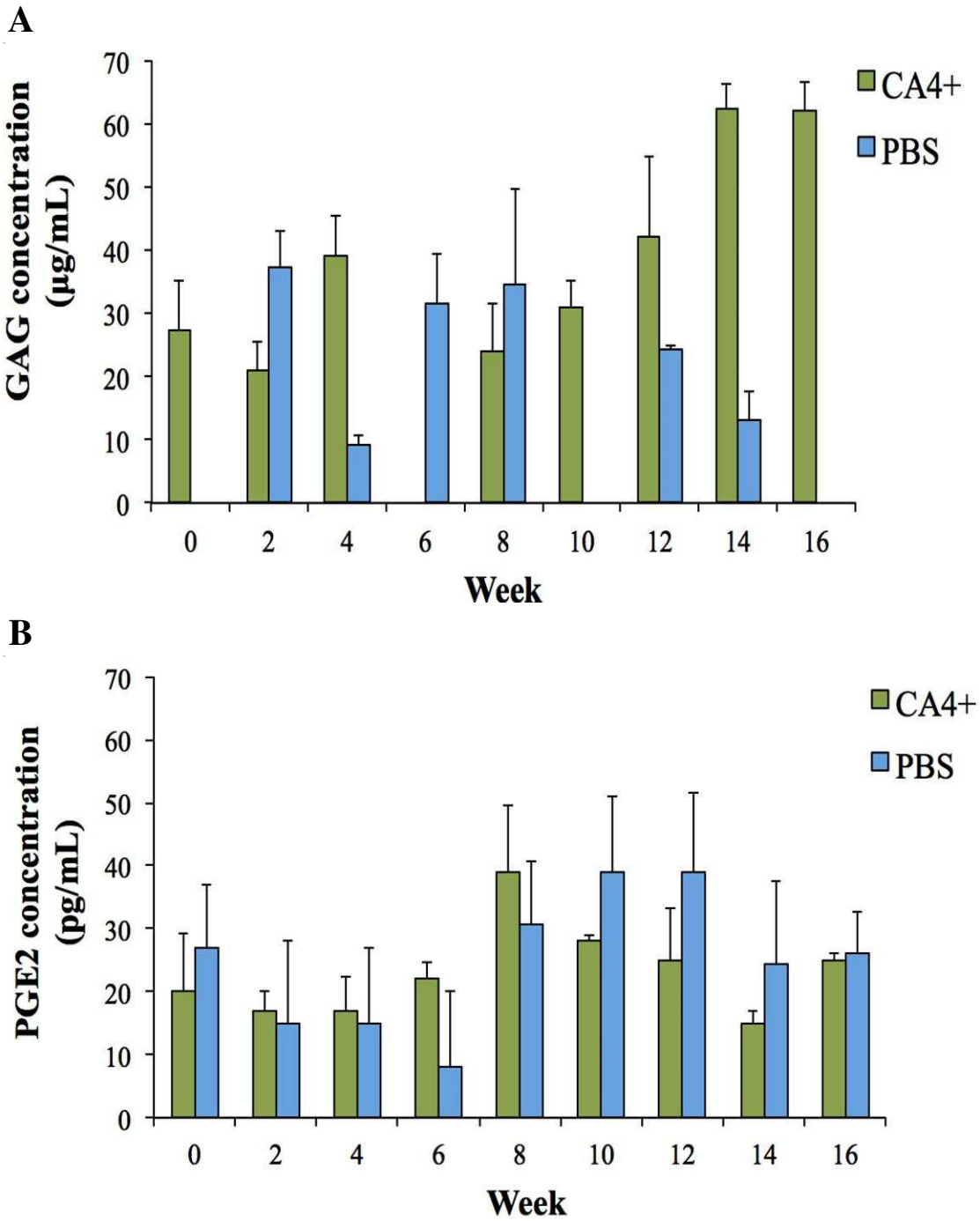

Figure 3.3 – Mean ± standard deviation synovial fluid concentrations of (A) glycosaminoglycan (GAG) and (B) prostaglandin E_2 (PGE_2) concentrations following the repeated injection of 100 mLs of CA4+ or phosphate buffered saline (PBS) in one horse. Week 0 is baseline and precedes any exposure to CA4+ or PBS. At each subsequent time point, the joint injection immediately followed each synovial aspirate without removing the needle. Each joint was only administered the same substance (*i.e.* not a crossover designed experiment) over the experiments duration. There was no significant difference in synovial fluid GAG or PGE_2 between groups or over time.

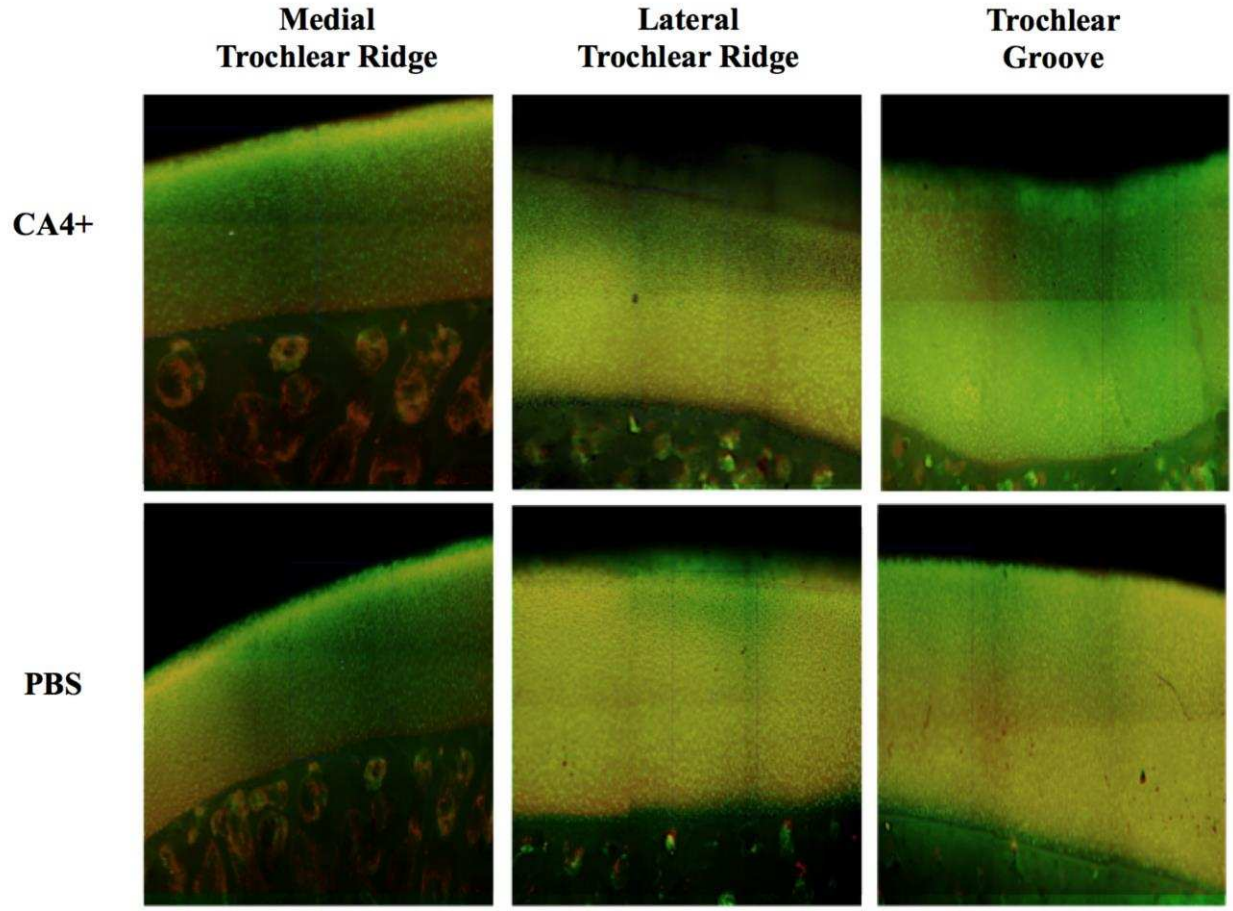

Figure 3.4 – Microscopy images showing chondrocyte viability staining of articular cartilage samples collected following the repeated (bi-weekly) injection of 100 mLs of CA4+ or phosphate buffered saline (PBS) in a horse over a 4-month period. Viable cells fluoresce green and dead cells stain red.

Table 3.1 – Results of total protein and leukocyte concentrations in synovial fluid aspirates after the repeated administration of CA4+ or PBS (control) in a horse. + mild hemorrhage, ++ moderate hemorrhage, +++ severe hemorrhage, -- Insufficient volume for analysis, *Statistical comparisons were made using an analysis of variance (ANOVA).

Time Point	**Total protein concentration (g/dL)**		**Leukocyte concentration (10^6/μL) [% neutrophils]**	
	CA4+ Joint	Control Joint	CA4+ Joint	Control Joint
Baseline (week 0)	2.2 +	3.2 +++	--	200 [25.0%]
2 weeks	3.0	2.4	1800 [21.2%]	500 [27.7%]
4 weeks	2.2	3.0 +	500 [16.7%]	2000 [44.0%]
6 weeks	3.2 ++	4.0 +++	200 [25.0%]	--
8 weeks	3.0	2.2 ++	500 [19.2%]	200 [25.0%]
10 weeks	2.4	2.4 ++	500 [18.6%]	600 [25.1%]
12 weeks	1.8 +	2.2	400 [35.9%]	400 [24.8%]
14 weeks	2.8 +	2.8 +	1100 [46.8%]	1600 [25.1%]
16 weeks	2.4 +	3.0 ++	300 [23.5%]	--
*Statistical comparisons**				
Between joints	P = 0.28		P = 0.58 [P = 0.87]	
Over time	P = 0.23		P = 0.87 [P = 0.91]	

Table 3.2 – Median (range) histological scores of synovial membrane sampled after repeated bi-weekly administration of CA4+ or PBS (control) in a horse over a 4-month period. Histological scores were made using the Osteoarthritis Research Society International (OARSI) scoring system; NC, P-value was not calculable because of identical values across parameters. Statistical comparisons were made using a Wilcoxon signed rank test.

OARSI parameter	**CA4+ joint**	**PBS joint**	**P - value**
Cellular Infiltration	2 (1 – 2)	1 (1 – 1)	0.16
Vascularity	3 (2 – 4)	3 (2 – 4)	1.0
Intimal hyperplasia	1 (1 – 1)	1 (1 – 1)	NC
Subintimal edema	3 (3 – 3)	2 (1 – 3)	0.17
Subintimal fibrosis	3 (2 – 4)	3 (2 – 4)	NC
Cumulative score	11 (11 – 13)	10 (9 – 11)	0.17

Table 3.3 – Median (interquartile range) histological scores of articular cartilage sampled after repeated bi-weekly administration of CA4+ or PBS (control joint) in a horse over a 4-month period. Histological scores were made using the Osteoarthritis Research Society International (OARSI) scoring system. SOFG, safranin-O fast green; NC, P-value not calculable because of identical values across parameters. Statistical comparisons are made using a Wilcoxon signed rank test.

OARSI parameter	**CA4+ joint**	**PBS joint**	**P - value**
Chondrocyte necrosis	1.5 (1 – 2)	3.5 (3.25 – 3.75)	0.16
Cluster formation	0 (0 – 0)	0 (0 – 0)	NC
Surface fibrillation	0.5 (0 – 1)	1 (0.5 – 1.5)	0.32
Focal cell loss	0.5 (0 – 1)	1.5 (1.25 – 1.75)	0.32
SOFG	1 (0.75 – 1)	1 (1 – 1)	NC
Cumulative OARSI score	3.5 (2.75 – 4)	7 (6.5 – 7.5)	0.18
Superficial zone SOFG	1.5 (0.75 – 2.25)	1 (0 – 2.25)	0.32
Middle zone SOFG	0.5 (1 – 1.5)	0 (0 – 0.5)	0.32
Deep zone territorial SOFG	0.5 (1 – 1.5)	0 (0 – 0.5)	0.32
Deep zone interterritorial SOFG	0.5 (1 – 1.5)	0.5 (0 – 1.5)	0.65
Cumulative SOFG score	4.5 (2.25 – 6.75)	0.75 (1.5 – 4)	0.65
Osteochondral lesions	1 (1 – 1.25)	2 (1 – 2)	0.99
Subchondral bone remodeling	0.5 (0 – 1)	0 (0 – 0.5)	0.32
Osteochondral splitting	0 (0 – 0)	0 (0 – 0)	NC
Cumulative bone score	1.5 (1 – 2.25)	2 (1 – 2.5)	0.78

REFERENCES

1. Fubini SL, Erb HN, Freeman KP, et al. Prognostic factors affecting survival of 507 horses with joint disease: (1983 to 1990). *Can J Vet Res* 1999;63:253–260.
2. Frisbie DD, and McIlwraith, CW. Evaluation of gene therapy as a treatment for equine traumatic arthritis and osteoarthritis. *Clin Orthop Relat Res* 2000;379(suppl 379):S273–S287.
3. CDC. National and State Medical Expenditures and Lost Earnings Attributable to Arthritis and Other Rheumatic Conditions --- United States, 2003. *MMWR* 2007;56:4-7.
4. Roemer FW, Eckstein F, Hayashi D, et al. The role of imaging in osteoarthritis. *Best Pract Res Clin Rheumatol* 2014;28:31-60.
5. Valdés-Martínez A. Computed tomographic arthrography of the equine stifle joint. *Vet Clin N Am-Equine* 2012;28:583-598.
6. Maldonado M, Nam J. The role of changes in extracellular matrix of cartilage in the presence of inflammation on the pathology of osteoarthritis. *Biomed Res Int* 2013;2013:1-10.
7. Bansal PH, Joshi NS, Entezari V, et al. Contrast enhanced computed tomography can predict the glycosaminoglycan content and biomechanical properties of articular cartilage. *Osteoarthritis Cartilage* 2010;18:184-191.
8. Bansal PN, Joshi NS, Entezari V, et al. Cationic contrast agents improve quantification of glycosaminoglycan (GAG) content by contrast enhanced CT imaging of cartilage. *J Orthop Res* 2011;29:704-709.
9. Joshi NS, Bansal PN, Stewart RC, et al. Effect of contrast agent charge on visualization of articular cartilage using computed tomography: exploiting electrostatic interactions for improved sensitivity. *J Am Chem Soc* 2009;131:13234-13235.

10. Stewart RC, Patwa AN, Lusic H, et al. Synthesis and preclinical characterization of a cationic iodinated imaging contrast agent (CA4+) and its use for quantitative computed tomography of ex vivo human hip cartilage. *J Med Chem* 2017;60:5543-5555.
11. ACR Committee on Drugs and Contrast Media. *ACR manual on contrast media: version 101* American College of Radiology Website. http://www.acr.org/quality-safety/resources/?/media/37D84428BF1D4E1B9A3A2918DA9E27A3.pdf/. Published 2015. Accessed May 5, 2016, 2015.
12. Satoh H, Abe S, Kato M, et al. Optimum conditions for serum clearance of iodixanol, applicable to the estimation of glomerular filtration rate in horses. *Vet Res Commun* 2011;35:463-468.
13. Wilson KE, Wilcke JR, Crisman MV, et al. Comparison of serum iohexol clearance and plasma creatinine clearance in clinically normal horses. *Am J Vet Res* 2009;70:1545-1550.
14. Stewart RC, Bansal PN, Entezari V, et al. Contrast-enhanced CT with a high-affinity cationic contrast agent for imaging ex vivo bovine, intact ex vivo rabbit and in vivo rabbit cartilage. *Radiology* 2013;266:141-150.
15. Frisbie DD, Cross MW, McIlwraith CW. A comparative study of articular cartilage thickness in the stifle of animal species used in human pre-clinical studies compared to articular cartilage thickness in the human knee. *Vet Comp Orthop Traumatol* 2006;19:142-146.
16. McIlwraith CW, Fortier LA, Frisbie DD, et al. Equine models of articular cartilage repair. *Cartilage* 2011;2:317-326.

17. American Association of Equine Practitioners. *Guide for veterinary service and judging of equestrian events*. Lexington, KY: American Association of Equine Practitioners, 1991.

18. Frisbie DD, Bowman SM, Colhoun HA, et al. Evaluation of autologous chondrocyte transplantation via a collagen membrane in equine articular defects – results at 12 and 18 months. *Osteoarthritis and Cartilage* 2008;16:667-679.

19. Hendrickson DA, Nixon AJ. Comparison of the cranial and a new lateral approach to the femoropatellar joint for aspiration and injection in horses. *J Am Vet Med Assoc* 1994;205:1177-1179.

20. Frisbie DD, Al-Sobayil F, Billinghurst RC, et al. Changes in synovial fluid and serum biomarkers with exercise and early osteoarthritis in horses. *Osteoarthritis and Cartilage* 2008;16:1196-1204.

21. Brittberg M, Winalski CS. Evaluation of cartilage injuries and repair. *J Bone Joint Surg* 2003;85-A:58-69.

22. Edwards RB, Lu Y, Cole BJ, et al. Comparison of radiofrequency treatment and mechanical debridement of fibrillated cartilage in an equine model. *Vet Comp Orthop Traumatol* 2008;21:41-48.

23. McIlwraith CW, Frisbie DD, Kawcak CE, et al. The OARSI histopathology initiative - recommendations for histological assessments of osteoarthritis in the horse. *Osteoarthritis and Cartilage* 2010;18:S93-S105.

24. Mankin HJ. Biochemical and metabolic aspects of osteoarthritis. *Orthop Clin North Am* 1971;2:19-31.

25. Mainil-Varlet P, Van Damme B, Nesic D, et al. A new histology scoring system for the assessment of the quality of human cartilage repair: ICRS II. *Am J Sports Med* 2010;38:880-890.

26. Pauli C, Whiteside R, Heras FL, et al. Comparison of cartilage histopathology assessment systems on human knee joints at all states of osteaorthritis development. *Osteoarthritis and Cartilage* 2012;20:476-485.

27. Brommer H, Brama PA, Laasanen MS, et al. Functional adaptation of articular cartilage from birth to maturity under the influence of loading: a biomechanical analysis. *Equine Vet J* 2005;37:148-154.

28. Firth EC. The response of bone, articular cartilage and tendon to exercise in the horse. *J Anat* 2006;208:513-526.

29. Bertone AL, Palmer JL, Jones J. Synvoial fluid cytokines and eicosanoids as markers of joint disease in horses. *Vet Surg* 2001;30:528-538.

30. Bolam C, Hurtig, MB, Cruz, A, and McEwen, BJE. Characterization of experimentally induced post-traumatic osteoarthritis in the medial femorotibial joint of horses. *Am J Vet Res* 2006;67:433-447.

31. Oke SL, Hurtig MB, Keates RA, et al. Assessment of three variations of the 1,9-dimethylmethylene blue assay for measurement of sulfated glycosaminoglycan concentrations in equine synovial fluid. *Am J Vet Res* 2003;64:900-906.

32. Palmer JL, Bertone AL, McClain H. Assessment of glycosaminoglycan concentration in equine synovial fluid as a marker of joint disease. *Can J Vet Res* 1995;59:205-212.

33. Todhunter RJ, Fubini SL, Freeman KP, et al. Concentrations of keratan sulfate in plasma and synovial fluid from clinically normal horses and horses with joint disease. *J Am Vet Med Assoc* 1997;210:369-374.

34. van den Boom R, van de Lest CH, Bull S, et al. Influence of repeated arthrocentesis and exercise on synovial fluid concentrations of nitric oxide, prostaglandin E2 and glycosaminoglycans in healthy equine joints. *Equine Vet J* 2005;37:250-256.

35. Dechant JE, Symm WA, Nieto JE. Comparison of pH, lactate, and glucose analysis of equine synovial fluid using a portable clinical analyzer with a bench-top blood gas analyzer. *Vet Surg* 2011;40:811-816.

36. Shanfield S, Campbell P, Baumgarten M, et al. Synovial fluid osmolality in osteoarthritis and rheumatoid arthritis. *Clin Orthop Relat Res* 1988:289-295.

37. Amin AK, Huntley JS, Simpson AHRW, et al. Increasing the osmolarity of joint irrigation solutions may avoid injury to cartilage: A pilot study. *Clin Orthop Relat Res* 2010;468:875-884.

CHAPTER 4:

EVALUATION OF CATIONIC CONTRAST-ENHANCED COMPUTED TOMOGRAPHY USING AN *IN VIVO* EQUINE IMPACT MODEL OF ARTICULAR CARTILAGE INJURY

Introduction

The impact of joint disease and osteoarthritis are well recognized in horses and these conditions incur significant costs.[1-3] Joint injury leads to progressive inflammation and ultimately damage to articular cartilage with an early mark being the loss of glycosaminoglycan (GAG) content.[4,5] The disease is ultimately progressive as articular cartilage healing is limited. Therefore, early detection of osteoarthritis is critical to successful therapeutic strategies. Currently, MRI is the gold standard imaging method to evaluate articular cartilage in horses and humans.[6-8] However, this method can lead to false positive results and becomes increasingly difficult if not impossible to evaluate higher on the limb of the horse due to the large muscle mass and decreased MRI coil diameters available.[7] With the advent of multi-slice computed tomography (CT), costs and scan length have decreased while having improved spatial resolution and larger gantry diameters compared to MRI.[9,10] A more sensitive method to evaluate articular cartilage is warranted in horses and the use of CT is a promising technology to investigate new cartilage imaging techniques.

Contrast agents are administered intra-articularly to outline articular structures for x-ray based imaging including contrast-enhanced computed tomography (CECT). Anionic, iodinated contrast

media (ICM) diffuse into the extracellular matrix (ECM) of articular cartilage. The limited amount that enters the ECM is dependent upon the fixed negative charge present in the ECM from GAGs; the negative charge repels the anionic charged ICM.[4,11] With GAG loss in the early stages of osteoarthritis, the fixed charge density decreases permitting more contrast agent to enter the ECM despite its negative charge.[4,11] Conversely, cationic contrast agents such as CA4+ are positively charged and are electrostatically attracted to the negatively charged GAGs, which consequently results in higher diffusion and is a more sensitive technique for imaging articular cartilage.[4] Cationic CECT attenuation is directly proportional to the GAG content within cartilage and this is due to the higher partitioning of CA4+ inside the ECM than anionic ICM.[11,12]

Investigations of cationic CECT imaging *in vitro* have confirmed its utility in bovine, human, and rabbit articular cartilage explants[12-17] and its preliminary use in equine tissue has been promising (Chapter 2 & unpublished observations). Its *in vivo* use in rabbits has also been encouraging.[16] Despite these favorable results, the use of cationic CECT in subtly damaged equine articular cartilage corresponding to early stage osteoarthritis requires investigation as well as determine its ability for *in vivo* use.

Many experimental equine models of joint disease exist and are typically used to investigate emerging joint therapies.[18-28] Impact models of articular cartilage injury are a subset of these experimental models and are used to replicate the contusive injury that initiates post traumatic osteoarthritis.[18,28-36] A few *in vivo* equine impact models have been developed to investigate the

initiation and progression of post traumatic osteoarthritis under the premise that the injury will replicate naturally occurring osteoarthritis.[18,28]

The objectives of this study were to determine the ability of cationic CECT to distinguish subtly damaged from normal articular cartilage and also to determine its capability as an *in vivo* diagnostic method. The first hypothesis of this study was that cationic CECT attenuation distinguishes between subtly damaged and normal articular cartilage and also reflects the biochemical and mechanical attributes of the tissue. The second hypothesis was that cationic CECT can be successfully implemented *in vivo* and is predictive of articular cartilage quality.

Materials and Methods

The use of the custom impact device has been reported and it has been previously applied to the equine femoral trochlea *ex vivo*.[18,28,37] However, modifications have since been made to the impactor system hardware and thus preliminary testing was required to optimize the adjusted settings on the device before *in vivo* use.

Impact force optimization to induce articular cartilage injury (Experiment 1)

This preliminary experiment was divided into two portions. The objective of the first portion of this testing experiment was to calibrate the impactor and establish the variability at each gradation setting. The objective of the second portion was to use that data to apply a range of impact forces to articular cartilage *ex vivo* and to ascertain the degree of articular cartilage injury caused with each impact force.

Calibration testing

The spring-loaded impactor has a 6.45 mm diameter plane-ended tip with rounded edges. Using a 1-inch thick red oak wood sample, which has similar mechanical properties as articular cartilage (M. Hurtig, personal communication), impact forces were delivered (six per gradation). The impactor tip was aligned perpendicular to the surface of the red oak sample and then the spring was pulled back to the appropriate gradation setting and locked in place. Then, the trigger was released while the impactor was stabilized at the impactor tip-red oak interface to prevent shearing during discharge. After firing, the impact stresses were derived from measurements collected from a calibrated piezoelectric force transducer (Model 218C, PCB Piezotronics, Depew, NY, USA) secured between the impactor shaft and tip. The transducer was connected to a charge amplifier (Model 421A11, PCB Piezotronics, Depew, NY, USA) with a data acquisition card (Model USB6009, National Instruments) and LABVIEW software. The transducer signal was sampled at 48 kHz and the impact stress calculated by normalizing peak force to the cross-sectional area of the impactor tip, 32.7 mm^2.[37] These data were used to generate the six levels of impact force (range 0 – 71 MPa) tested in the *ex vivo* experiment.

Ex vivo testing

The femur from a horse euthanized for reasons other than joint disease was collected within one hour of euthanasia and with no observed (macroscopic) articular cartilage lesions of the trochlear surface. The femoral trochlea was removed with a hacksaw and fixed to an osteochondral autograft transfer system workstation platform (Arthrex, AR4013, Naples, FL)(Figure 4.1). The articular cartilage was lavaged using 0.9% saline for the duration of the experiment to prevent desiccation. The impactor tip was aligned to the articular surface at 36 predetermined and

randomized locations over the trochlear surface (Figure 4.1). Immediately after applying each delivered impact, an 8 mm tissue biopsy punch (Integra Miltex, Inc, Plainsboro, NJ) was used to core a circular portion of articular cartilage, while the attachment to the subchondral bone remained intact. After all sites were impacted and cored, the articular cartilage was removed from the subchondral bone with a scalpel blade and evaluated for tissue architecture and cell viability distributions using a commercial assay kit (LIVE/DEAD Viability/Cytotoxicity Kit, Life Technologies™, Grand Island, NY). The circular articular cartilage discs were transected in half (semicircle sample) to ensure efficient diffusion of the cellular stains throughout the tissue and to microscopically image the center of the impacted cartilage. Mixtures of calcein acetomethoxyester (1:2000) and ethidium homodimer (1:3000) in 1x PBS were added to plate wells with articular cartilage tissue and incubated for 1 hour in the dark at 20 °C. A scalpel blade was used to cut a thin (~ 1 mm) portion of articular cartilage immediately prior to microscopy to facilitate examination of all articular cartilage zones. The tissue was then examined under a fluorescence microscope equipped with a digital camera acquisition system (QImaging, MicroPublisher, 5.0 RTC, Surrey, Canada). The images were evaluated subjectively to determine the depth of injury and regional chondrocyte death at each delivered impact site to establish the degree and distribution of articular cartilage injury following impact.

In vivo delivery of articular cartilage impacts (Experiment 2)

All experimental protocols were evaluated and approved by the Institutional Animal Care and Use Committee at Colorado State University (Protocol ID: 14-4924A, approval 3/28/2014). Four juvenile and skeletally mature horses (aged 2-4 years) were included in the study. Prior to inclusion all horses had lameness examinations demonstrating a lack of lameness and

femoropatellar joint compartment effusion. Radiographs were taken to exclude horses that had evidence of joint disease (*e.g.* osteophytes, subchondral bone defects, sclerosis or lysis). Prior to surgery, baseline lameness examinations with full limb flexion tests graded on the AAEP scale[38] and assessment of femoropatellar joint effusion was performed on a 5-point scale (0 = none, 4 = severe effusion) by an observer blinded to limb allocation.[39]

Density phantom

There is inherent variability in CT attenuation values (Hounsfield units, HUs) between different acquisitions on the same scanners over time.[40-42] To counteract this problem, density phantoms are imaged concurrently to standardize and improve HU accuracy and also serve as a method to convert CT attenuation to biologically relevant (usually bone mineral density) concentrations.[43,44] A customized density phantom was created for use in the *in vivo* portion of this study and was composed of 3 core constituents at varying concentrations (CA4+ contrast media [0.75, 1.5, 3, 6, 12 and 24 mg I/mL], iohexol contrast media [Omnipaque-350, GE healthcare, Princeton, NJ] [9.4, 18.8, 37.5, 75, 150 and 300 mg I/mL] and calcium hydroxyapatite [CaHA, Computerized Imaging Reference Systems, Norfolk, VA] [400, 800, 1000 and 1500 mg CaHA/cm^3])(Figure 4.2). These density phantom components were used to standardize clinical cationic CECT attenuation over multiple scans while permitting conversion to biologically relevant tissue concentrations. Circular regions of interest (63 mm^2) were sampled at the same location on the phantom and carried over 10 slices. The mean value (HU) of each concentration cylinder in each component was plotted against the known concentration of that cylinder. The data was plotted, a regression line was created and the coefficient of determination was used to establish linear fit.

Clinical cationic CECT examination

Based on the results of the *in vivo* diffusion trajectory experiment (Chapter 3), CA4+ was prepared as previously described at a concentration of 24 mg I/mL (400 mOsmol/kg, pH = 7.4).[11] Before inducing articular cartilage injury, a baseline cationic CECT examination was performed on both femoropatellar joints in each horse. Prior to each cationic CECT scan, each horse was sedated (detomidine hydrochloride and butorphanol tartrate: each 0.01 mg/kg IV) and both femoropatellar joints were aseptically prepared with betadine scrub and alcohol. Starting with the left femoropatellar joint, a synovial fluid sample was aspirated via lateral approach[45] and aliquots were placed into EDTA and serum tubes for cytologic and biochemical analysis, respectively. With the needle still in place 100 mLs of CA4+ was injected. Twenty minutes later the right femoropatellar joint underwent an identical protocol. The time delay was made to permit repositioning of the horse on the CT table between scan acquisitions. After the bilateral injections, the horse recovered from sedation and was placed in stall confinement until cationic CECT examination.

Approximately 3.5 hours after CA4+ injection, general anesthesia was induced with ketamine (2.2 mg/kg IV) and diazepam (0.1 mg/kg IV) and maintained on isoflurane in 100% oxygen. The horse was placed in left lateral recumbency with the left leg tied in extension on the CT table.[9,10] The custom density phantom was placed 5 cm distal to the tibial tuberosity and aligned parallel to the CT gantry. Then, the cationic CECT scan was acquired four hours after CA4+ injection. The cationic CECT parameters of all acquisitions were: 140 kVp, 550 mAs, 0.8 mm x 0.8 mm slice thickness, 30 cm field of view, 1024 x 1024 matrix, 0.6 helical pitch facilitating in-plane resolution of 0.292 x 0.292 mm. The CT data was reconstructed with a sharp (B70f)

reconstruction bone kernel (0.8 mm slice thickness) for improved spatial resolution and bone detail and as a soft tissue reconstruction kernel (2 mm slice thickness) to improve signal-to-noise ratios. After the left stifle was scanned, the horse was alternated into right lateral recumbency and the right stifle was scanned with the same protocol as described for the left ensuring the acquisition time was four hours after CA4+ was injected into the right femoropatellar joint. At the study endpoint (70 days after impact), the cationic CECT examination of both stifles was repeated.

Arthroscopic procedure to impact articular cartilage

After baseline cationic CECT examination, the horse was moved to the surgical suite, placed in dorsal recumbency and routinely prepared for aseptic surgery. After sterile draping, both femoropatellar joints were examined arthroscopically.[46] One stifle in each horse was randomly assigned (block randomization using Microsoft Excel) to receive the impacted defects while the contralateral limb was sham-operated to confirm no damaged articular cartilage. Immediately following arthroscopic camera insertion, examination of the observable trochlear and patellar articular cartilage surfaces was performed. An 18-gauge spinal needle was used to triangulate positioning of the instrument portal on the medial trochlear ridge of the femur, proximal and lateral to the arthroscopic portal. A stab incision (1 cm) was made using an #11 blade to enter the femorotibial joint. The impactor tip was inserted into the incision and applied to the proximal articular surface of the medial trochlear ridge of the femur. The impactor tip was applied evenly to the articular cartilage surface to efficiently deliver the impact while minimizing the risk for shearing (Figure 4.3). Nine, 41 MPa force impacts were then delivered to the proximal medial trochlear ridge in a stellate pattern (Figure 4.3). An 18-ga spinal needle was used to mark the

regions at a site away from the impacted location (at the trochlear groove) to ensure the impact sites could be identified at *postmortem* evaluation. Following the delivery of all impacts, the impactor tip and arthroscope were removed and the skin incisions closed routinely using 2-0 nylon in a simple interrupted pattern. Covaderm bandages were applied over the surgical incisions and the horse recovered from general anesthesia. After surgery, the horse was maintained on stall confinement (12 x 12 feet) until the incisions were healed 12 days after surgery at which time the sutures were removed. The horses were then turned out to a large paddock for free exercise until the end of the study.[23]

Synovial fluid assessment

The total protein of synovial fluid was measured using a refractometer and recorded in g/dL. Then, the remaining fluid was centrifuged at 1,000 G for 10 minutes. The supernatant was aspirated, stored in a micro-centrifuge tube and frozen at -80 °C until further biochemical analysis. Total leukocyte cell counts were determined from the EDTA sample using a benchtop hematology analyzer and leukocyte differential percentages were calculated. If a limited amount of fluid was obtained (<1 mL), then the sample in the serum tube was prioritized.

Biochemical analysis of the synovial fluid included determination of GAG content using the 1,9-dimethylmethylene blue (DMMB) binding assay and prostaglandin E_2 (PGE_2) concentrations using a commercially available immunoassay kit (Enzo Life Sciences, Inc. Farmingdale, NY).[5,47,48] The frozen aliquots of synovial fluid were thawed and the GAG samples were analyzed using the DMMB assay after papain digestion.[5] The DMMB assay was performed using a standard curve generated with known concentrations of chondroitin C sulfate. Samples

were prepared in triplicate and read on a microplate reader (SpectraMax M3, Molecular Devices, Sunnyvale, CA), set at a wavelength of 530 nm. Using a quadratic curve fit, the mean absorbance of all samples was determined and a mean calculated for each sample. The PGE_2 quantitation was performed by first extracting it from synovial fluid through use of C2 columns (Amprep mini-columns ethyl C2 columns, GE Healthcare Co, Pittsburgh, PA). Then, the samples were processed using a commercial assay kit with a minimum detection rate of 13.4 pg/mL (Enzo Life Sciences Inc., Farmingdale, NY). Samples were run in duplicate and read on a microplate reader set at a wavelength of 405 nm. A mean value was reported for each sample. Samples from the DMMB and PGE_2 assays were repeated if the standard curve $R^2 < 0.9$ or if the coefficient of variation between replicates was > 0.1.

Clinical assessments

After baseline, lameness examinations and assessments of femoropatellar joint effusion were repeated every two weeks by the same blinded investigator until the end of the study as described above. Synovial fluid aspirates were also repeated every 2 weeks until the end of the study and were analyzed as described above.

Postmortem assessments

At the study endpoint (70 days after impact), the cationic CECT examination of both stifles was repeated and the horse was euthanized under general anesthesia (pentobarbital 86 mg/kg IV). The stifles were removed by transecting the femur and tibia at the mid-diaphyseal regions preserving the soft tissues over the stifle. Postmortem MRI examinations were performed with a 1.5 Tesla MRI (GE Signa 9.1 LX MR instrument, GE Healthcare, Waukesha, WI) using the

following sequences: proton density (with and without fat suppression), T2-weighted, and T1-weighted fast spin echo and T1-weighted spoiled gradient recalled echo. Proton density sequences were also generated at oblique transverse planes to improve spatial resolution at the curvilinear surface of the medial trochlear ridge of the femur, which is susceptible to volume averaging. After MRI, the stifles were then subsequently frozen at -20 °C until microCT analysis and mechanical testing.

Each stifle was thawed individually and underwent all mechanical testing and microCT imaging assessments to prevent the tissue degradation that could occur following multiple freeze-thaw cycles. After thawing, synovial membrane and osteochondral plug biopsies were collected from each joint. Samples of synovial membrane were collected and placed in 10% formalin. Osteochondral plug biopsies (7 mm internal diameter) were collected along the medial (5 plugs) and lateral (5 plugs) trochlear ridge surfaces using a diamond tipped cylindrical coring drill bit (Starlite Industries, Bryn Mawr, PA) attached to a drill press (Delta Power Equipment Company, Anderson, SC). The articular cartilage was lavaged with water to prevent overheating of the tissue during osteochondral coring. After coring, samples were then immediately lavaged with 400 mOsmol/kg saline to regain normal tonicity. Each osteochondral biopsy was graded macroscopically on the Outerbridge[49] and international cartilage repair society (ICRS)[50] scoring systems to classify macroscopic articular cartilage damage.

After each osteochondral plug was removed and macroscopically scored, it was allowed to equilibrate overnight with 0.9% saline in a preservative cocktail containing protease inhibitors, antibiotics, and antimycotics (5 mM Benzamidine HCl, 5 mM EDTA both of Sigma-Aldrich, St.

Louis, MO; 1x Antibiotic-Antimycotic, Life Tech, Carlsbad, CA) at room temperature to remove any residual CA4+ present within articular cartilage at the time of euthanasia. After saline equilibration, mechanical testing was performed.

Mechanical testing

The compressive stiffness of articular cartilage is attributed to GAGs and from a fluid phase permitting free flow diffusion of water and solutes in and outside of the tissue, while the dynamic elastic response results mainly from the interstitial fluid resisting tissue loading and collagen fibril network resisting tensile forces and shape alterations.[51,52] Articular cartilage degeneration reduces the equilibrium compressive (Young's) modulus (EM) and dynamic (Young's) modulus (DM).[51,52] A stress-relaxation compressive regimen was performed on each osteochondral plug biopsy. On the day of and prior to mechanical testing, the thickness of the articular cartilage on each osteochondral biopsy was determined with microCT (μCT40, Scanco Medical AG, Brüttisellen, Switzerland) using the following parameters: 70 kVp, 113 μA, 300 ms integration time and 36-μm isotropic voxel resolution. The imaging data was converted to DICOM format and imported into Analyze (AnalyzeDirect, Overland Park, KS). Object maps of the articular cartilage volume were created using a semi-automatic threshold-based algorithm. Using the line profile tool, automated sampling of 400 locations across the entire plug volume was performed. The sampled regions were averaged and converted from voxel dimensions to generate an average articular cartilage thickness of the sample.

Each plug was rigidly clamped in a mechanical testing apparatus (Enduratec3230, BOSE, Eden Prairie MN) and a compressive pre-load was applied to the articular cartilage surface

(unconfined compression) using a nonporous ultrahigh molecular weight polyethylene) platen while immersed in 400 mOsm/kg saline solution. The stress-relaxation regimen for each plug consisted of four incremental 5% compressive strain steps (0.333 %/sec) with stress relaxation (45 minutes) between strain steps. A collection rate of 10 Hz was used to record the force and displacement data, and a linear fit to stress versus strain at each equilibrium step was used to calculate EM and incremental DM[53] for each cartilage specimen using a custom program (MATLAB, R2017a, Mathworks, Natick, MA).

Cationic CECT (microCT)

While cationic CECT (microCT) has been shown to reflect healthy articular cartilage (Chapter 2 & unpublished data), this method was performed in this study to validate the cationic CECT method in degenerative articular cartilage. After mechanical testing, all osteochondral plugs were immersed in CA4+ (24 mg I/mL, approximately 20 times the articular cartilage volume) for 24 hours at 20 °C, known to exceed the required equilibration time under these settings (Chapter 2).[16] Then, the plugs were imaged using microCT at the same above settings. The cationic CECT images were converted into DICOM format and imported into Analyze® software). A semi-automatic threshold-based segmentation procedure was performed with manual correction to ensure accurate segmentation of the articular cartilage volume from the subchondral bone and air. The cationic CECT signal intensity in each osteochondral plug was converted into the linear attenuation coefficients and then to Hounsfield units (HUs) using a sample of deionized water concurrently scanned with the plugs (Equation 2.1). The mean HU for each articular cartilage plug was recorded.

After microCT, the osteochondral plugs were again equilibrated overnight in saline with the preservative solution to remove any residual CA4+ that could contribute to inaccuracy in forthcoming assessments of GAG content. The cartilage of each circular biopsy was bisected and the articular cartilage from one side was removed from the subchondral bone using a scalpel blade, while the remaining cartilage portion (still attached to bone) was placed in 10% formalin in preparation for histologic analysis. The portion of removed cartilage was again cut in half. One portion (1/4 of total cartilage surface) was minced and placed in a tube assigned for GAG evaluation while the other quarter portion was similarly prepared for assessment of total collagen content. All samples were weighed to determine a hydrated (wet) weight, and were then lyophilized for 24 hours and weighed again to determine dry weight. The samples were stored at -80 °C until further biochemical analysis.

Bone morphometric analysis

Bone morphometry calculations were performed using the microCT scan data collected for the determination of articular cartilage thickness (equilibrated in saline) that preceded mechanical testing using commercial software (ScancoMedical, Brüttisellen, Switzerland). A circular ROI (180 pixel diameter, 32.98 mm^2) was generated in the subchondral trabecular bone of each osteochondral plug starting 1.8 mm (10 slices) beneath the subchondral bone plate and extending distally 50 slices. The same automated threshold algorithm was used for all plugs to exclude air from bone (467 to 3000 mg HA/cm^3). Trabecular parameters were reported as bone volume fraction (BV/TV), trabecular number (Tb.N), thickness (Tb.Th), and separation (Tb.Sp) and bone mineral (BMD) and tissue mineral (TMD) density using the direct 3D method.[54] The subchondral bone plate was segmented from the articular cartilage and trabecular bone using a

threshold-based segmentation with manual adjustment (Analyze® software). Linear attenuation values from the segmented bone were converted into mineral density units (mg HA/cm^3) and the volume of the subchondral bone was reported (mm^3). The thickness of the segmented subchondral bone plate was performed using the line profile tool automating the subchondral bone plate thickness of the entire plug at 400 sampled locations, which were then reported as a mean thickness.

Biochemical and histological analyses

The biochemical content (GAG and total collagen) of the articular cartilage from each osteochondral biopsy was determined using the DMMB and hydroxyproline assays, respectively. For GAG quantitation, the lyophilized cartilage was removed from the -80 °C freezer and digested in papain (1 mg/mL) overnight at 65 °C. The papain digestion solution was made in a mixture of 50 mM NaH_2PO_4, 5 mM EDTA and 2 mM dithiothreitol adjusted to a pH of 6.8. The digested samples were evaluated with the DMMB assay as described under synovial fluid evaluation, though were first diluted 1:20 with incomplete (without papain) digestion buffer to more closely be in the center of the generated standard chondroitin sulfate curve. The mean GAG concentration of each sample was standardized to the sample's wet weight. For determination of total collagen content, the lyophilized articular cartilage was also digested in papain. The sample was diluted 1:20 and hydrolyzed with an equal volume of 12.1 N HCl for 16 hours in a dry oven at 110 °C.[55] The samples were then evaporated on a heating block set at 60 °C overnight. The samples along with known hydroxyproline standard concentrations were pipetted into a tissue culture plate in duplicate. Chloramine T reagent was added to the samples and hydroxyproline standards and were incubated for 20 minutes at 25 °C. The 4-dimethyl-aminobenzaldehyde

reagent was added to all samples and standards and the plate incubated at 60 °C for 15 minutes followed by 5 minutes at 25 °C. Then the plate was read at 550 nm. The hydroxyproline concentrations for each sample were determined from the standard curve and reported as a mean of the duplicate samples. Total collagen was determined from hydroxyproline using an established conversion (13.2 mg hydroxyproline /100 mg collagen type II)[56] and standardized to dry weight.

Histologic evaluation

The osteochondral and synovial membrane samples were prepared routinely for histologic evaluation. After seven days in 10% formalin the osteochondral samples were transferred to 70% ethanol until decalcification. The osteochondral samples were then decalcified in EDTA (Formical-2000, Statlab, McKinney, TX) for seven days and then rinsed in 1x PBS prior to undergoing further histologic processing (Appendix I.1). After processing (Appendix I.1), both the synovial membrane and osteochondral tissue samples were embedded in paraffin and using a microtome (Leica RM2255, Leica Biosystems, Buffalo Grove, IL), 5 μm sections were prepared on microscope slides. The synovial membrane and osteochondral samples were each stained with hematoxylin and eosin and a second slide of the osteochondral samples was stained with safranin-O fast green (SOFG)(Appendix I.2). Control tissues (bovine trachea and equine osteochondral samples) were stained with all groups to control for variation across batches.

The sections of synovial membrane were scored for grades of cellular infiltration, intimal hyperplasia, and subintimal vascularity, edema and fibrosis (grade 0 – 4; 0 = normal, 4 = marked) using the Osteoarthritis Research Society International (OARSI) scoring system.[57]

Sections of articular cartilage and bone were also scored on the OARSI scoring system. Articular cartilage was scored for grades of chondrocyte necrosis, chondrone (cluster) formation, cartilage fibrillation/fissuring, focal cell loss and SOFG uptake (grades 0 – 4; 0 normal, 4 = marked/severe). The subchondral bone was graded for levels of osteochondral lesions, subchondral bone remodeling and osteochondral splitting.[57] The grades of osteochondral lesions range from 0 – 4 (0 = normal, 4 = ulcerated) and the other categories range from 0 – 3 (0 = normal, 3 = severe).[57] Articular cartilage sections evaluated for SOFG stain uptake were also individually scored in region-specific locations (tangential, intermediate, radiate territorial and radiate interterritorial zones). Cumulative scores were calculated for the OARSI score (range 0 – 20), SOFG score (0 – 16) and bone score (0 – 10). The OARSI scoring system was chosen over other histological scoring systems because it has been documented to better designate early stages of osteoarthritis and was designed for use in equine tissue; both elements important for this study.[58-60]

Clinical cationic CECT evaluation

Following removal of all osteochondral plug biopsies, the cored mask of the femoral trochlea was imaged with a cone beam CT system (Pegaso, Epica Medical Innovations, San Clemente, California) to provide a template for accurate comparisons between the biochemical mechanical and histological data to clinical imaging (cationic CECT and MRI) parameters. The cone beam CT settings were 70 kVp, 70 mA, 5 ms, 220.8 mm field of view and 736 x 736 matrix, permitting isotropic voxel dimensions of 0.3 mm^3. Using the 3-D voxel registration module, the post-coring mask from each joint was manually aligned over each respective clinical imaging scan. Using this template, an object map was generated consisting of digitally segmented

articular cartilage over the same location where osteochondral plugs were removed. This generated object map was applied to all scans performed on the same limb. When applied to the clinical data set, the segmented ROIs were manually verified to ensure the captured volume only contained articular cartilage and not the subchondral bone or other soft tissues. The cationic CECT attenuation was measured and reported in HUs and the volume (mm^3) and area (mm^2) from the ROIs were recorded. Density phantom correction was performed for each of the three components (CA4+, iohexol and CaHA) to account for CT attenuation drift between scans. A sample of the joint space (233 mm^3) was also segmented to normalize articular cartilage attenuations contrast media concentrations remaining in the synovial fluid.[61]

MRI evaluation

The same post-coring mask scan used in the clinical cationic CECT scans was also co-registered with the MRI images. Generating cursors in the trabecular bone provided a way to create an object map at same location where the osteochondral plugs were removed and avoided influencing the MRI appearance of tissues during subjective assessment. These object maps were applied to each MRI sequence and acquisition plane. A board certified radiologist blinded to group allocation (impact versus control joint) performed all scoring. The articular cartilage at each site was subjectively scored for volume/fill (0: 100%, 1:75 to <100%, 2: 50 to <75%, 3: 25 to <50%, 4: <25% fill), and for T2 and T1 signal intensity (0: none, 1: mild, 2: moderate, 3: severe). The subchondral bone signal intensity was scored on the PD with fat saturation (PDFS) sequence (0: none, 1: mild, 2: moderate, 3: severe) and the amount of trabecular bone sclerosis (0: none, 1: mild, 2: moderate, 3: severe).

Data and Statistical analysis

Categorical data were reported as median ± interquartile (IQR) range and continuous data as mean ± standard deviation (s.d.). Continuous data were evaluated for normality, by using a Shapiro Wilk test and visually using histograms and quantile-quantile plots. Nonparametric tests were used in the event data were not normally distributed. Comparisons of continuous variables were performed using a Spearman rank correlation. The strength of correlation was reported based on an established scale with a minor naming modification – slight: 0.0 to 0.20, fair: 0.21 to 0.40, moderate: 0.41 to 0.60, strong: 0.61 to 0.80, very strong: 0.81 to 1.0.[62]

By joint analysis

Ordinal data (lameness and synovial effusion assessments) were compared between impact and control joints using ordered logistic regression. Synovial fluid parameters (TP, leukocyte, neutrophils, GAG, PGE_2) were compared between joints using a repeated measures mixed-effects model ANOVA with the horse as a random effect. Synovial membrane histology scores were compared between joints using a Wilcoxon signed rank test.

By site analysis

Two locations (impact and remote sites) were categorized within the impact and control joints (Figure 4.4). The impact site in the impact joint defines the location of the delivered impact, while in the control joint this site is used as a specific control to address the inherent variability that occurs across the femoropatellar articular surface.[63,64] MRI scores were evaluated at these sample locations using Fisher's exact test.

Articular cartilage (microCT, GAG, EM, DM, histology) and bone morphometry measures were analyzed by comparing the impact to remote sites between impact and control joints using a mixed-effects model ANOVA with the horse as a random effect. Pairwise comparisons were made after Tukey-Kramer adjustment if more than three comparisons were made. Histological samples were also compared to the imaging parameters after establishing a threshold of injury determined by receiver operator characteristic (ROC) curve analysis. Histological scores were identified as impacted based on their location at the impact site and confirmed to decline in GAG and EM. Using the ROC curve, the maximum Youden index was determined to establish a threshold of impacted articular cartilage damage. The sensitivity and specificity are reported along with the area under the curve of the ROC model. Statistical analyses were performed using commercial software (SAS University Edition, v. 9.2, SAS Institute Inc., Cary, NC) and significance was defined as $P<0.05$.

Results

Impact force optimization to induce articular cartilage injury (Experiment 1)

In the calibration testing, the recorded impact forces had almost exclusively < 10% coefficient of variation. The five forces determined to provide a diffuse testing range are shown in Figure 4.5. In the *ex vivo* testing experiment, the 52 and 70 MPa force impacts all induced a palpable defect on the articular surface (Figure 4.1 – C). The lower impact forces (<52 MPa) did not cause macroscopically visible or palpable defects in the cartilage. The cell viability staining showed a directly proportional increase in surface injury with impact force starting at 27 MPa. Articular cartilage surface cracking started to occur in the samples with 41 MPa applied force with

extension into the middle zone. The degree of fissuring increased in the 52 and 71 MPa injury groups (Figure 4.5).

In vivo delivery of articular cartilage impacts (Experiment 2)

No major adverse events were encountered during the clinical cationic CECT scans or impact surgeries. No horses showed evidence of lameness after CA4+ injection or after recovering from general anesthesia.

Synovial fluid assessment

Results of synovial fluid parameters are shown in Table 4.1 – A-C and Figure 4.6. There were no significant differences between the impact and control joints or over time for any of the measured parameters.

Clinical assessments

There were no differences between impact and control joints for lameness and synovial effusion or overtime (Figure 4.7).

Postmortem assessments

Macroscopic inspection of the articular surfaces at the impacted sites revealed minor surface irregularities (Figure 4.8). The impacted sites also showed slight blistering with some sites having a red discoloration to the tissue. Articular cartilage at these locations were graded as ICRS = 1 and OB = 1, while locations in the remote sites in the impact joint and all surfaces of

the control joints were scored 0 for both systems. No other signs of articular cartilage injury or osteoarthritis were detected in the impact or control joints.

Mechanical testing

There was a significant effect of sample location on EM ($P = 0.0035$). In the impact joints, the mean EM at the impact sites approached a significant difference compared to the remote sites ($P = 0.06$). The mean EM was lower at the impact location in the impact joints than at this location in the control joints ($P = 0.006$)(Figure 4.9). There was no significant difference in EM in the remote sites between the impact and control joints. There were no significant effects of sample location on DM at any of the 5% incremental strain steps (Figure 4.10).

Cationic CECT (microCT)

There was a significant effect of sample location on cationic CECT attenuation (microCT)($P = 0.0004$). In the impact joints, the mean cationic CECT attenuation at the impact site was significantly lower than the remote sites ($P < 0.0001$)(Figures 4.9 and 4.11). The mean cationic CECT attenuation was lower at the impact location in the impact joint when compared to this location in the control joint ($P = 0.015$). There was no significant difference in the remote sites between the impact and control joints.

Cationic CECT attenuation (microCT) had a very strong and significant correlation with GAG ($\rho = 0.82$, $P < 0.0001$) and EM ($\rho = 0.80$, $P < 0.0001$)(Figure 4.12). In the impact joints, this very strong correlation with GAG and EM persisted (both $\rho = 0.85$, $P < 0.0001$). In the control joints, the strength of the correlation of cationic CECT attenuation with GAG and EM slightly declined

($\rho = 0.80$, $P < 0.0001$; and $\rho = 0.79$, $P < 0.0001$; respectively). There was a significant correlation between total collagen and cationic CECT attenuation ($\rho = -0.32$, P 0.007). Correlations between cationic CECT attenuation and bone morphometry measures are shown in Table 4.2.

Bone morphometric analysis

There were no significant differences in bone morphometry parameters between sample locations (Table 4.3).

Biochemical analyses

There was a significant effect of sample location on GAG content ($P = 0.005$). In the impact joints, the mean GAG concentration at the impact site was significantly lower than the remote sites ($P = 0.0012$) (Figure 4.9). The mean GAG concentration at the impact site was lower in the impact joint than at this site in the control joint ($P = 0.015$). There was no significant difference between the remote sites between the impact and control joints. There was no significant effect of sample location on total collagen content ($P = 0.18$)(Figure 4.9).

Histologic evaluation

The median (IQR) scores of the synovial membrane in the impact joints were: cellular infiltration 0 (0 – 0), vascularity 1 (0.75 – 1), intimal hyperplasia 0 (0 – 0.25), subintimal edema 0 (0 – 0), subtintimal fibrosis 0 (0 – 0), cumulative score 2.5 (1.75 – 3) and in the control joints were: cellular infiltration 0 (0 – 0), vascularity 1 (0.75 – 1.25), intimal hyperplasia 0 (0 – 0), subintimal edema 0 (0 – 0), subtintimal fibrosis 1 (0 – 2), cumulative score 3.5 (2.75 – 4.25). There were no

significant differences in synovial membrane assessments between the impact and control joints (cellular infiltration, $P = 0.99$; vascularity, $P = 0.32$; intimal hyperplasia, $P = 0.32$; subintimal edema, $P = 0.99$; subintimal fibrosis, $P = 0.16$; cumulative score, $P = 0.09$).

Cationic CECT attenuation (microCT) was significantly correlated with the majority of the individual OARSI scoring components and cumulative scores (Table 4.4). Table 4.5 shows comparisons of histologic parameters between sample locations. There was a significant effect of cationic CECT attenuation (microCT) with many OARSI score parameters (chondrocyte necrosis, $P < 0.0001$; cluster formation, $P = 0.0004$; surface fibrillation, $P = 0.036$; focal cell loss, $P = 0.012$; SOFG, $P < 0.0001$; cumulative score, $P = 0.0002$)(Figure 4.13). There was also a significant effect of cationic CECT attenuation (microCT) on SOFG zonal and cumulative scores (all $P < 0.0001$)(Figure 4.14) but not on bone scores (Figure 4.15).

The ROC curve analysis generated from the cumulative OARSI score revealed a maximum Youden index of 9.18 (90% sensitivity, 86% specificity, area under the curve = 0.923) and established a threshold of 10 to define impact injured articular cartilage (Figure 4.16). Using this threshold, the mean ± s.d. cationic CECT attenuation was 2152 ± 353 in samples with a cumulative OARSI score ≥ 10, while it was 2659 ± 513 in samples scoring < 10 ($P = 0.037$).

Clinical cationic CECT evaluation

At the endpoint scans, there was not a significant correlation between uncorrected clinical cationic CECT attenuation and GAG content. However, there was a significant correlation when cationic CECT attenuation was corrected to CA4+ concentrations ($\rho = 0.25$, $P = 0.036$), but not

when corrected to iohexol or CaHA (Figure 4.17). There was not a significant correlation between uncorrected clinical cationic CECT attenuation and EM. When corrected to iohexol concentrations, EM was significantly correlated to clinical cationic CECT attenuation ($\rho = 0.32$, $P = 0.006$). Clinical cationic CECT attenuation after CA4+ and CaHA correction were not significantly correlated to EM. There was a significant effect of articular cartilage volume on sample location at baseline ($P = 0.0005$) and endpoint ($P = 0.0007$). Comparisons of articular cartilage volume in the impact and remote sites were significantly different in the impact joint (baseline, $P = 0.0008$; end point, $P = 0.002$).

Cumulative OARSI articular cartilage score was not significantly correlated to end point clinical cationic CECT attenuation irrespective of density phantom correction. The cumulative SOFG score was significantly correlated to cationic CECT attenuation after CA4+ ($\rho = -0.26$, $P = 0.027$), iohexol ($\rho = -0.40$, $P = 0.0006$) and CaHA ($\rho = -0.25$, $P = 0.032$) correction (Figure 4.18). Most individual zonal SOFG scores were also significantly correlated to clinical cationic CECT attenuation (Table 4.5).

A comparison of baseline to end point scans showed there were no significant differences in cationic CECT attenuation for either reconstruction algorithm (0.8 mm bone or 2mm standard). Correlations between the 0.8 mm bone and 2 mm standard algorithms are shown in Figure 4.19. Normalizing the cationic CECT attenuation to synovial fluid concentrations or to articular cartilage volume did demonstrate a significant difference between time points. There was no significant difference between time points with the ROC defined threshold or in articular cartilage volume.

MRI evaluation

MRI scores at the sample locations were not significantly different (articular cartilage fill, P = 0.22; morphology, P = 0.5; T2 signal, P = 0.79; T1 signal, P = 0.82; bone sclerosis, P = 0.21). No sections had increased PDFS signal intensity in the subchondral bone beneath the articular cartilage sites. Using the ROC defined criteria to indicate articular cartilage impact injury, there were no significant differences in MRI scores (articular cartilage fill, P = 0.25; morphology, P = 0.5; T2 signal, P = 0.50; T1 signal, P = 0.42; bone sclerosis, P = 0.12). There was no difference in cationic CECT attenuation between MRI scores (Figures 4.21 & 4.22).

Discussion

The first experiment established a level of impact that consistently invoked injury to the superficial and middle zones of articular cartilage without macroscopic fissuring. This contusive impact would avoid articular incongruities and articular cartilage fractures that could promote high local stress at that location potentially leading to more severe lesions than sought for this experimental model. Other experimental impact studies in other species document lower impact forces (~25 MPa) are needed to establish disease.[35,65-67] While delivered *ex vivo*, this experiment established the degree of injury that would be initiated after impactor discharge and also gave credence to using the 41-MPa impact force *in vivo*. While the cell viability stain showed the level of chondrocyte necrosis after impact, there is potential chondrocyte recovery *in vivo*.[68-70]

In the *in vivo* experiment, the delivered impact resulted in biochemical, mechanical and histological changes in articular cartilage associated with degeneration. However, the *in vivo* model did not incite severe joint disease as indicated by the lack of clinical, synovial fluid, bone

morphometry, and histologic bone and synovium responses that commonly occur with osteoarthritis.[5,18,47,71,72] Contrary to the results of a similarly designed study applying 60 MPa force to the medial femoral condyle, this study did not incite severe injury or established a broad spectrum of articular cartilage injury.[18] Their use of a weight bearing joint compartment, longer study duration, and higher impact forces applied that caused deeper injury, all likely contributed more substantial damage in their model.[18,73] All of these factors would be more likely to contribute to the progression of fulminant joint disease after impact. Despite the higher impact forces and more substantial injury inflicted, lameness was also transient in the Bolam *et al.* study; hence the lack of observable lameness in this study was not unexpected. In addition to the lack of a difference in synovial membrane scores between joints, the low histologic scores indicate minimal joint inflammation. These low scores in both joints lead further confidence to the conclusion that the high scores observed in the safety experiment (Chapter 3) were caused by the high frequency and large volumes of injected solutions and not directly related to CA4+.

A slight decrease in synovial GAG and increase in PGE_2 could be seen over time in this study, though was not significantly different between joint groups. Perhaps with higher impact force or a longer duration this model could progress to more severe disease. Bolam *et al.* showed that there was a significant and transient decrease in synovial fluid GAG in the first 54 days after impact injury followed by a progressive increase.[18] Other investigators have documented this same observation.[74-76] The initial decline is due to chondrocyte death, followed by a hypertrophic response in adjacent, undamaged cells.[75,77] Reported as a concentration, the synovial fluid GAG values are potentially influenced by the size of the joint compartment and the quantity of synovial effusion (Chapter 3). The synovial fluid volume was not quantified and the minor

articular cartilage injury inflicted in this study could have precluded a detectible difference in these synovial fluid biomarkers.

In support of the first hypothesis, cationic CECT (microCT) distinguishes between subtly damaged and normal articular cartilage, reflecting the biochemical, mechanical and histologic attributes of the tissue. The strong correlations of cationic CECT attenuation (microCT) with GAG and EM have been demonstrated in other *in vitro* studies of normal and chemically degenerated (chondroitinase) articular cartilage.[12-17] This study showed that mechanical injury to articular cartilage that more closely resembles natural osteoarthritis etiology, is detectable with cationic CECT attenuation (microCT) and also correlates with histologic measures. The DM data did have a significant (global effect) on sample location but individual comparisons were not significant after adjusting for multiple comparisons. This insinuates that the sample size and methods used were insufficient to detect these differences. Further studies are required to confirm this speculation. There was also no significant difference in the amount of total collagen in the impacted vs normal articular cartilage; however, there was a trend for an increase in total collagen in the impact sites and this would be consistent with declining GAG content (and weight) while maintaining collagen content.[78,79] Additionally, this decrease in imaging signal reflects the decline in biochemical, mechanical and histologic tissue properties. Non-destructive imaging methods such as cationic CECT hold promise to detect early articular cartilage injury.

The sampling locations in this study were selected to investigate not only the effect of the impact site, but also to search for any regional changes that occur in locations away from the impact site. With the small number of horses used and the subtle disease inflicted, this meant binning medial

(distal) and lateral trochlear ridge samples within the remote location group. Because of this sampling process and the variation that exists across the femoropatellar surface, establishing a definitive threshold of injury using GAG content or EM would be difficult to achieve.[63,64] Coupled with sites for sample location, the process of portioning articular cartilage for biochemical and histologic assessments was a source of variability in measured assessments. While the imaging and mechanical testing assessments were made on the entire plug, GAG and total collagen content were quarter portions and the histologic specimen was a half portion of the total sample. Sample averaging normal and damaged cartilage in the same plug also would lower the magnitude of difference between groups. This sampling protocol was used to permit comparisons between the biochemical, mechanical and histologic data from the same location. These divisions lend variability to these outcome values and the strength of correlations and effects could have improved without this segregation. Nonetheless, significant correlations were detected between the microCT imaging parameters and biochemical and mechanical data and permitted achieving the study objectives.

The histologic comparisons to cationic CECT attenuation (microCT) showed significant correlations with chondrocyte necrosis, focal cell loss and SOFG staining along with the cumulative OARSI articular cartilage score. Chondrocyte necrosis and focal cell loss are recognized as a continuum of disease.[57] Not surprisingly, the loss of chondrocytes (the source of GAG production) would prevent GAG replenishment in the ECM. The link between cationic CECT and SOFG are explained by the same mechanism of action between CA4+ and the safranin-O dye. Both are cationic compounds that bind proportionally to the negatively charged GAGs in the ECM.[80] However, the severe loss of proteoglycan content can prevent the dye from

binding in histologic specimens in spite of the presence of keratan and chondroitin sulfate.[81] In cationic CECT this may not occur because of the entire articular cartilage volume is still available permitting water collection and therefore CA4+ into the tissue despite low electrostatic attraction, whereas, the ethanol steps after safranin-O staining can elute the stain (Appendix I.2).

Though there is evidence in support of the second hypothesis using microCT, the use of clinical cationic CECT was not as robust. The co-registration methods facilitated consistency in comparing the results of bench top laboratory assessments to the clinical imaging data sets. As mentioned previously, the partitioning of samples from each plug may have contributed to the variability encountered with the clinical scanner but to a higher degree than would be expected on microCT. Despite these divisions, a similar decrease in performance between these imaging techniques has been recognized.[82] There is decreased spatial and contrast resolution, number of voxels per region-of-interest, signal-to-noise ratio, and range of attenuation values in clinical CT compared with microCT. There was a significant correlation between the two different algorithms (0.8 mm sharp [bone] and 2 mm standard) used to reconstruct the clinical data; however, only 2/3 of the variation ($R^2 \approx 0.67$) from one algorithm is explained by the other. This observation imparts the necessity of choosing and standardizing appropriate algorithms when quantifying cationic CECT attenuation. In this study, identical object maps were applied over both scan algorithms. Thus, volume averaging and individual computer processing methods will cause variation if these points are not considered in future studies. Further studies should also look into efficacy in different joints, animal age and athletic disciplines.

Despite these limitations, with density phantom correction some significant correlations between clinical cationic CECT and the biochemical, mechanical and histological outcomes were established. Addressing the variability that exists across CT scans is reinforced by this study where uncorrected attenuation values were inaccurate until adjusted to the density phantom concentrations.[40-44] Three different components in this customized phantom were used to expand the diversity of adjustments. However, the linear regression applied to each density phantom component highlighted variation. The CaHA component had consistent ($R^2 > 0.99$) coefficient of determinations, while CA4+ was typically lower ($R^2 > 0.97$) and iohexol ($R^2 > 0.95$) had the lowest coefficients of determination. The CaHA was a commercially produced solid density, while the others were dilutions of synthesized (CA4+) and commercial (iohexol) contrast media. Despite both contrast media having the same units, the iohexol concentrations had a higher range and potentially caused decreased accuracy when the linear fit was applied compared to CA4+. These small differences in variation between density phantom components can impart large inconsistencies across the clinical scan data.

The significant fair correlation of end point clinical cationic CECT attenuation with GAG and with EM echoes similar findings to microCT. The significant negative correlation between clinical cationic CECT attenuation with SOFG staining is explained by the inverse relationship of these two measures. Increasing SOFG score on the OARSI scale is associated with lower matrix staining and therefore lower GAG content. Lower cationic CECT attenuation occurs because of decreased CA4+ binding to GAG. Comparing the clinical data between groups did not reveal significant differences in cationic CECT attenuation. In the baseline scans, there was a significant effect of location (impact versus remote locations) in the impact joints. This could be

explained by the varied articular cartilage volumes that compose these groups.[63] At the endpoint, there was no longer a significant difference between these locations. While direct conclusions cannot be made, the loss of a significant difference could indicate a detectable change in articular cartilage volume or CECT attenuation. Yet, individual statistical comparisons could not establish a difference in articular cartilage volume between these sites and the significance of this observation remains unclear. The low number of horses and subtle injury inflicted likely contributed to low detection rates and further investigations are required before a more substantive conclusion can be made.

Importantly, ICM concentration varies based on individual joint excretion rates or disease states. Altering synovial fluid volumes can cause dilution effects and normalization of CT signal improves measurement consistency.[61] Hirvasniemi *et al.* normalized contrast media concentrations to that within articular cartilage in attempt to standardize joint metabolism variation across individual subjects.[61] In this study, an attempt was made to determine if this standardization would improve the clinical results. However, there is a substantial difference between anionic and cationic ICM. Anionic ICM more consistently remains in the synovial space allowing higher attenuation values to be monitored, while the lower iodine concentration in CA4+ quickly penetrates articular cartilage and leaves the joint space after 4 hours (Chapter 2 & 3) and segmentation of the joint space would reflect (unenhanced) soft tissue attenuations. The attempt at normalizing CA4+ concentration was not successful herein, though if shorter durations between CA4+ injection and CT imaging are pursued, this should be revisited.

No serious events occurred to the horses during the cationic CECT scans *in vivo*. However, mild extravasation of CA4+ was commonly observed. Extravasation of contrast media in the periarticular tissues is not uncommon and occurs with arthrography in humans and horses.[10,83,84] The periarticular extravasation that occurred in these horses quickly resolved and did not cause a problem to the horse similar to that observed with anionic ICM extravasation.[84] Periarticular extravasation could be avoided by use of a more proximal injection site. However, the lateral (distal) approach was chosen to permit sampling of synovial fluid for subsequent analysis that is not reliably attainable with other approaches.[45] Extravasation could have decreased the concentration of CA4+ with further dilution from synovial fluid volume, though did not appear to affect penetration of CA4+ into articular cartilage on the CT scans. Some portions of articular cartilage did not have full diffusion up to the subchondral bone as seen in Chapter 3. Despite the exact timing of scan acquisition after injection, individual joint excretion rates, extravasation, and altering synovial fluid volumes could have been factors that varied cationic CECT attenuation values *in vivo*.

In conclusion, this impact model successfully produced subtle articular cartilage injury that was distinguishable from normal articular cartilage by using cationic CECT imaging. The significant correlations with clinical cationic CECT to the biochemical, mechanical and histologic outcomes is promising for this technique to extend into the clinic though the repeatability of these results and ability to detect healing cartilage tissue require further investigation.

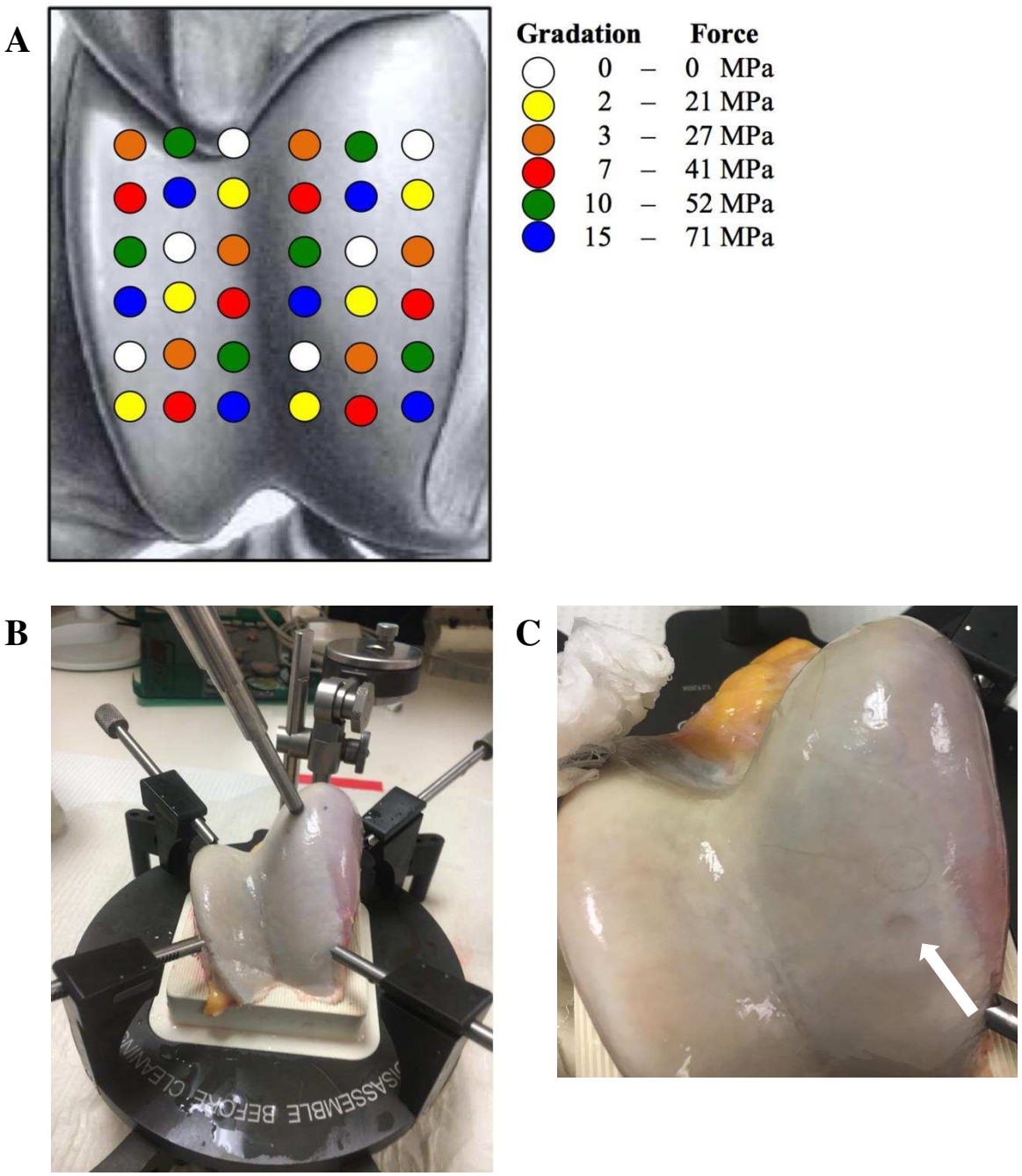

Figure 4.1 – A) Distribution of planned impact forces applied to induce superficial cartilage injury. The lateral trochlear ridge is on the left and the proximal aspect of the trochlea to the top. The circular dots represent the locations of the applied impact force (dots are not to scale). B) Experimental set up using the osteochondral autograft transfer system workstation platform with the impactor applied to the medial trochlear ridge of the femur. C) Macroscopic examination of the articular cartilage on the femoral trochlea after the first (farthest right) column of impacts were delivered. The arrow points to an area of cartilage that received a 52 MPa impact. Note the observable depression.

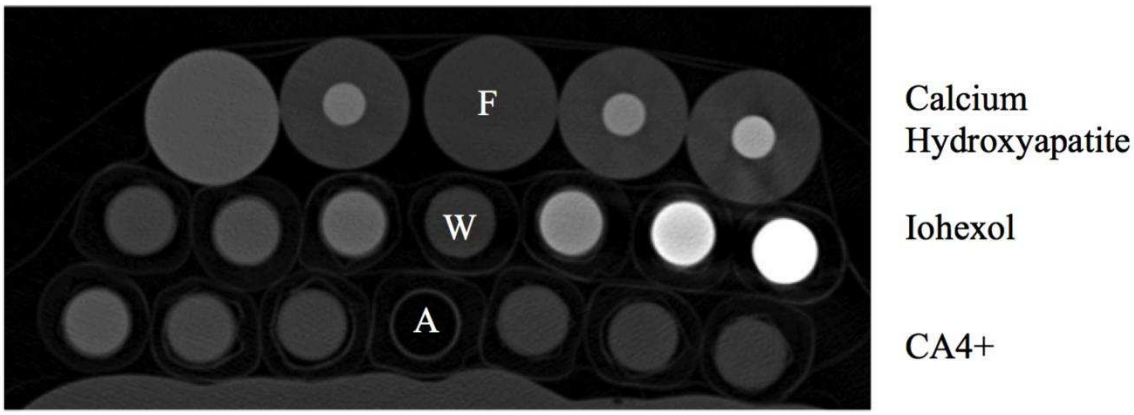

Figure 4.2 – Computed tomography image of the customized density phantom created for this study. Top row – calcium hydroxyapatite (CaHA) concentrations (left to right): 400, 800, (adipose, F), 1000 and 1500 mg CaHA/cm^3. Middle row – iohexol concentrations (left to right): 9.4, 18.8, 37.5, (water, W), 75, 150 and 300 mg I/mL. Bottom row – CA4+ concentrations (left to right): 24, 12, 6, (air, A), 3, 1.5, 0.75 mgI/mL.

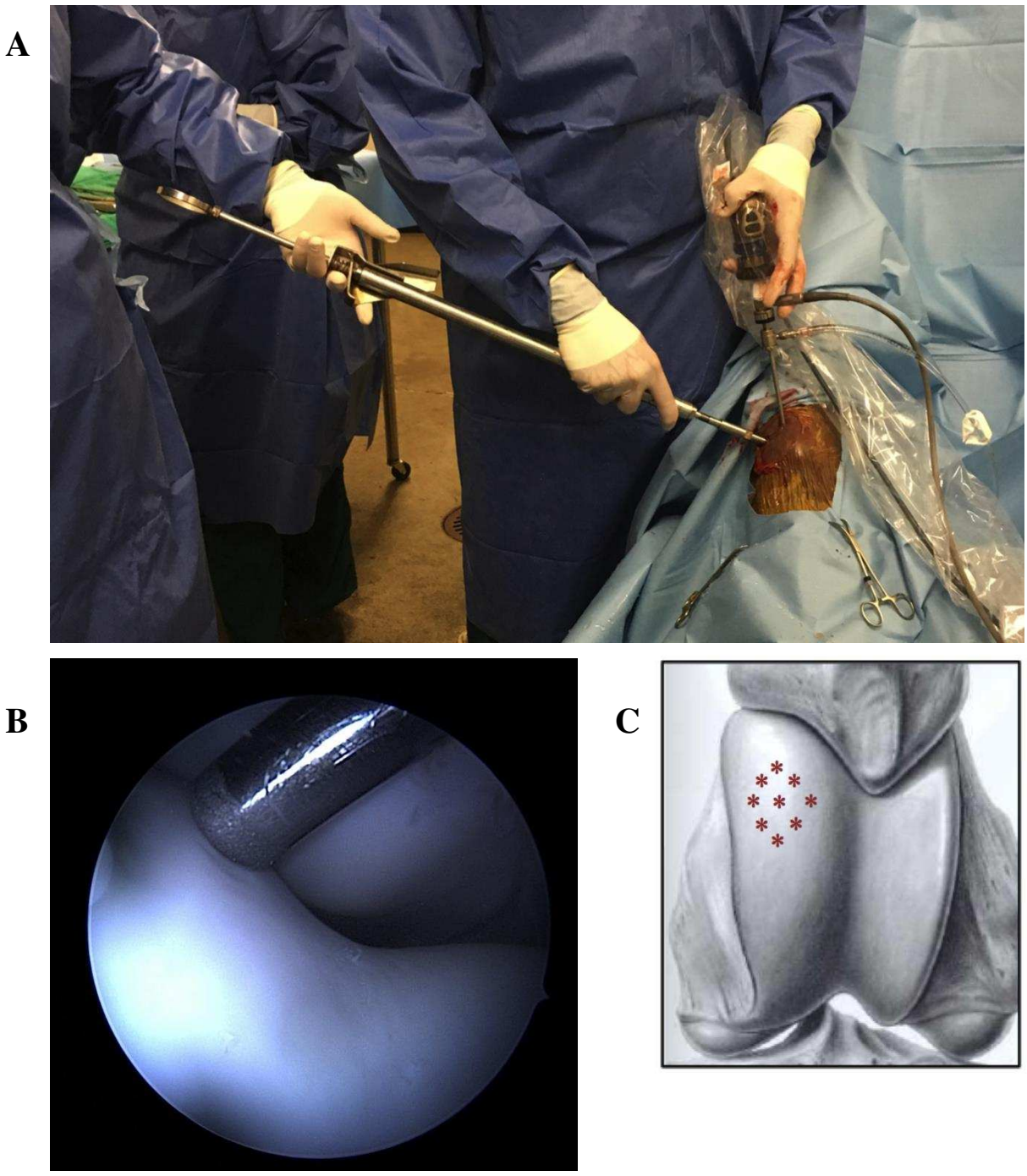

Figure 4.3 – A) Locations of the arthroscopic and impact device portals used *in vivo*. B) Arthroscopic view of the medial trochlear ridge of the femur after an impact was delivered. C) Diagram of the stellate pattern used to deliver nine contusive impacts to the medial trochlear ridge of the femur.

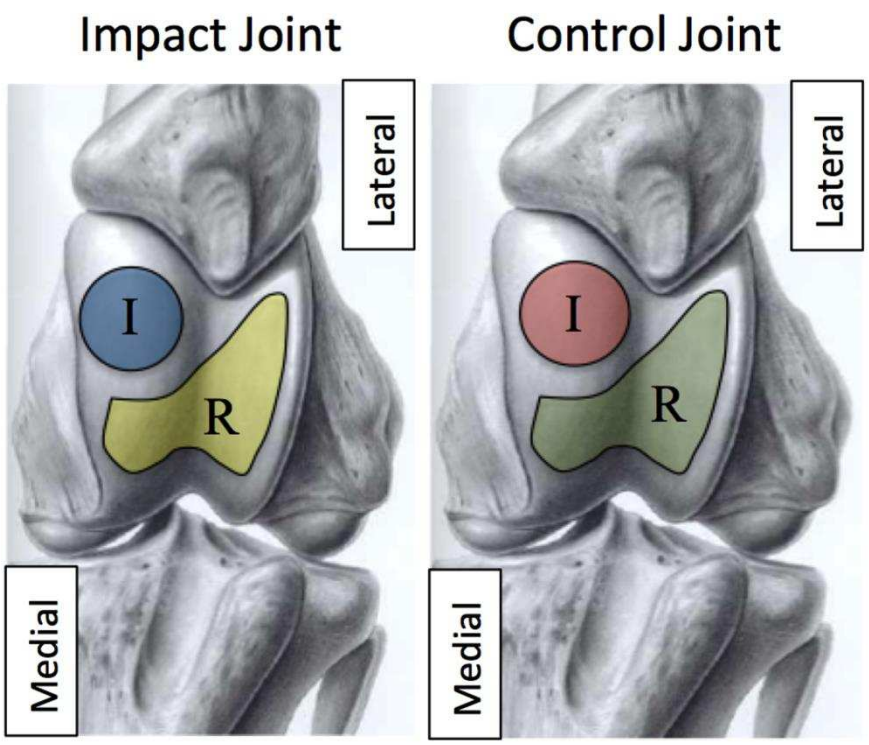

Figure 4.4 – Sampling locations across the femoropatellar joint surfaces where osteochondral biopsies were collected. The impacted sites were collected from the medial trochlear ridge in both impact and control joints. I, impact site; R, remote site.

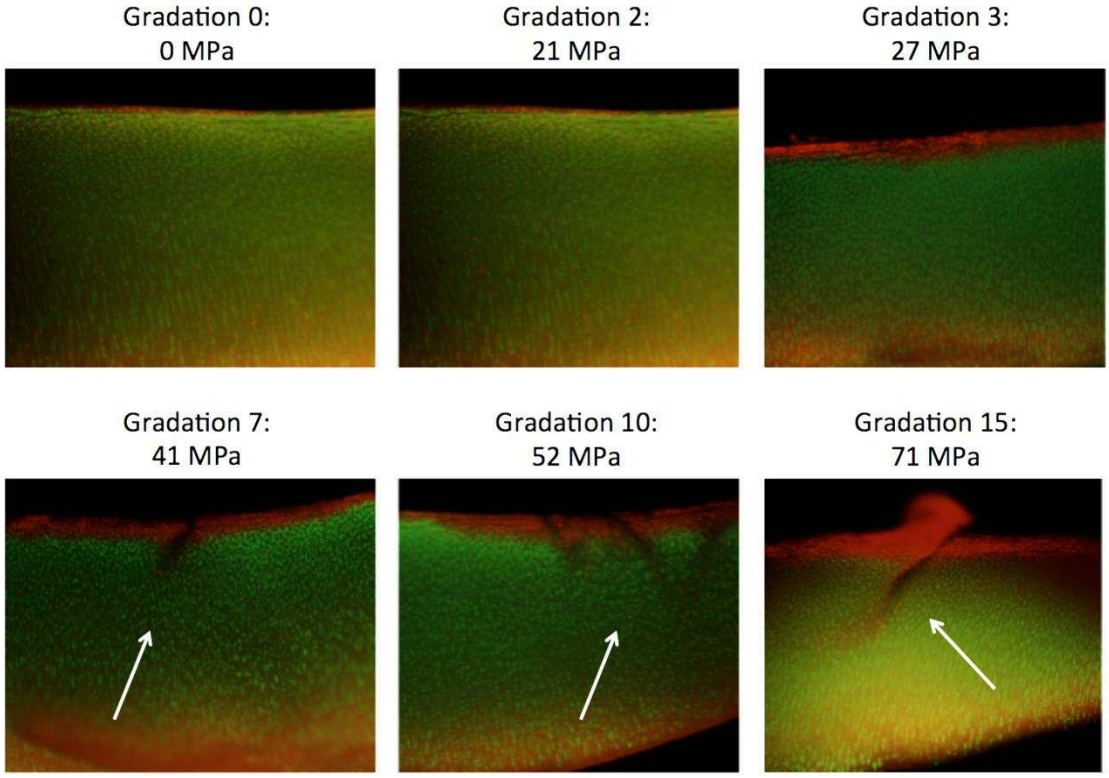

Gradation	Mean (MPa)	Standard Deviation	Coefficient of Variation
0	0	0	-
2	21	2.9	14.0%
3	27	2.3	8.5%
7	41	2.8	6.8%
10	52	1.3	2.5%
15	71	5.7	8.0%

Figure 4.5 – Chondrocyte viability staining images showing the degree of injury to articular cartilage after application of different impact forces *ex vivo*. The superficial zone is to the top of all images and was the location of where the impact was delivered. Viable cells stain green and red cells red. The arrows point to articular cartilage cracking visible after impact. The table shows the mean, standard deviation and coefficient of variation in the impact gradations used in the *ex vivo* study.

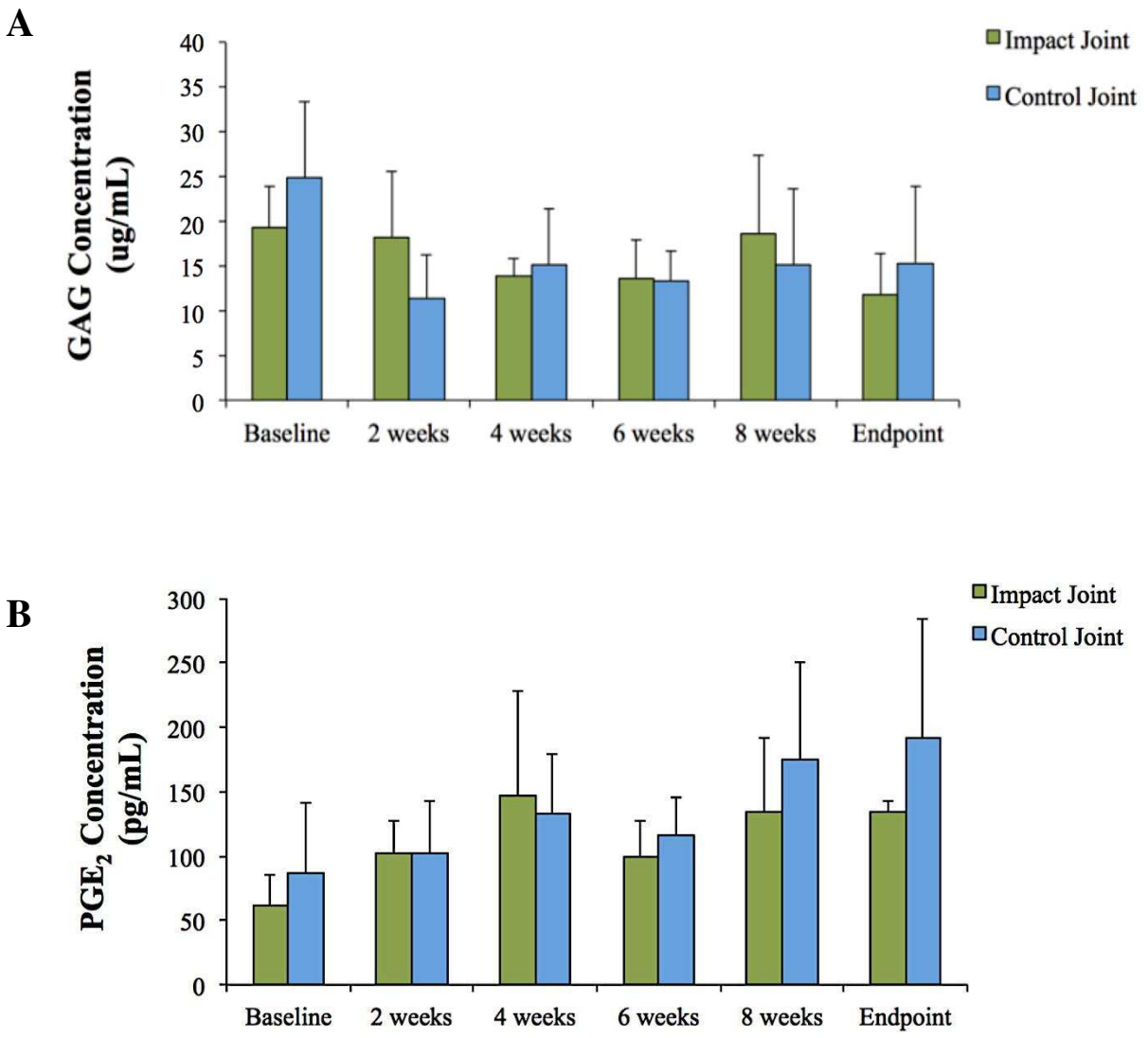

Figure 4.6 – Mean ± standard deviation synovial fluid (A) glycosaminoglycan (GAG) and (B) prostaglandin E_2 (PGE_2) concentrations in impact and control joints in four horses over the course of two months. After baseline, nine 41-MPa force impacts were delivered under arthroscopic guidance to the medial trochlear ridge of the femur in the impact joints, while the control joints were sham-operated. There were no significant differences between joints or over time in either variable.

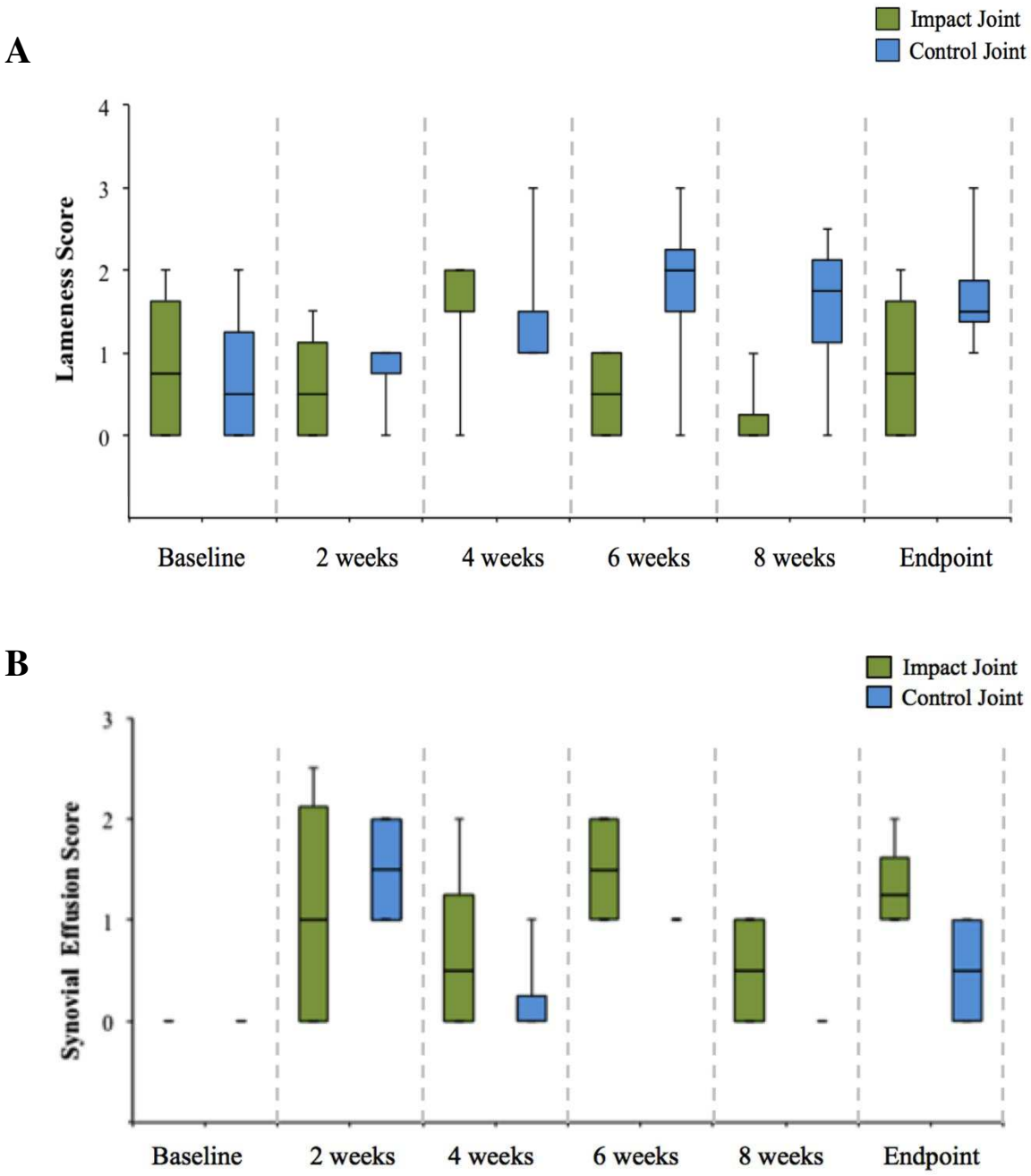

Figure 4.7 – Box and whisker plots of the lameness (A) and synovial effusion (B) scores in the impacted and control joints. Baseline values are recorded prior to impact. Results of ordered logistic regression indicate no significant differences between impact and control joints or over time in lameness or joint effusion scores.

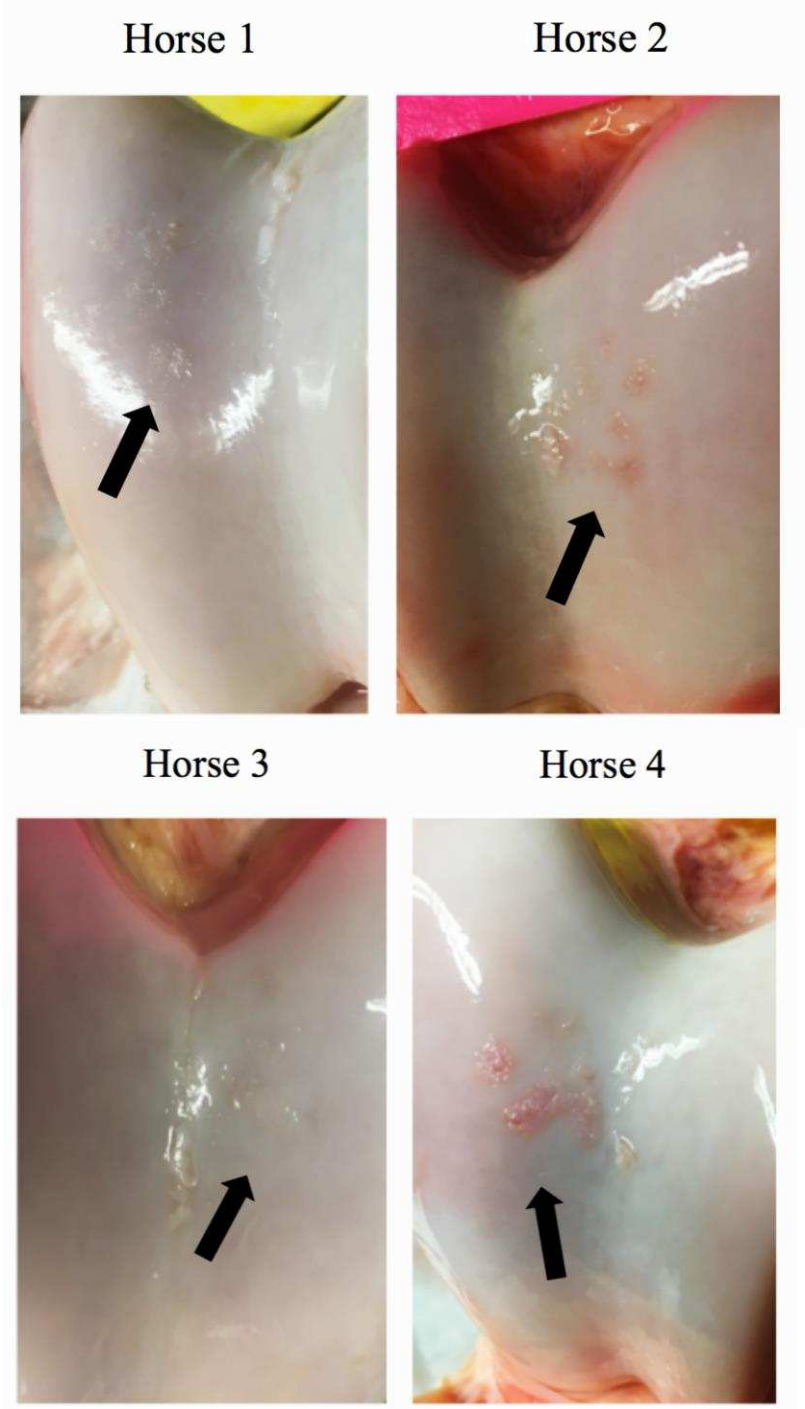

Figure 4.8 – Postmortem photographs of the femoral trochlea two months after impact was delivered to the medial trochlear ridge of the femur.

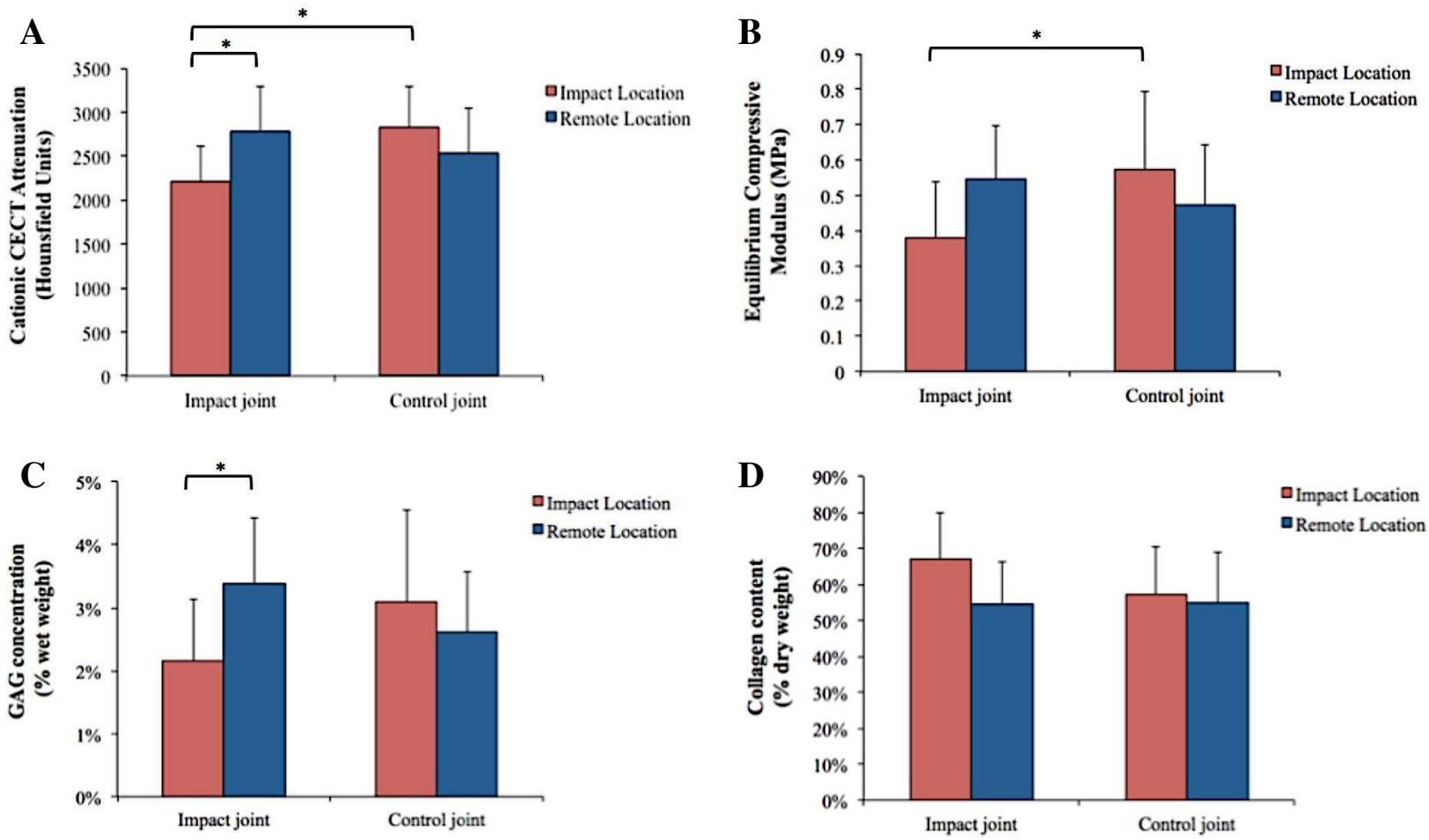

Figure 4.9 – Mean ± standard deviation of (A) cationic CECT attenuation (microCT), (B) equilibrium compressive modulus, (C) glycosaminoglycan (GAG) content and (D) total collagen content grouped by site (impact vs remote) and joint (impact vs control). *P < 0.05

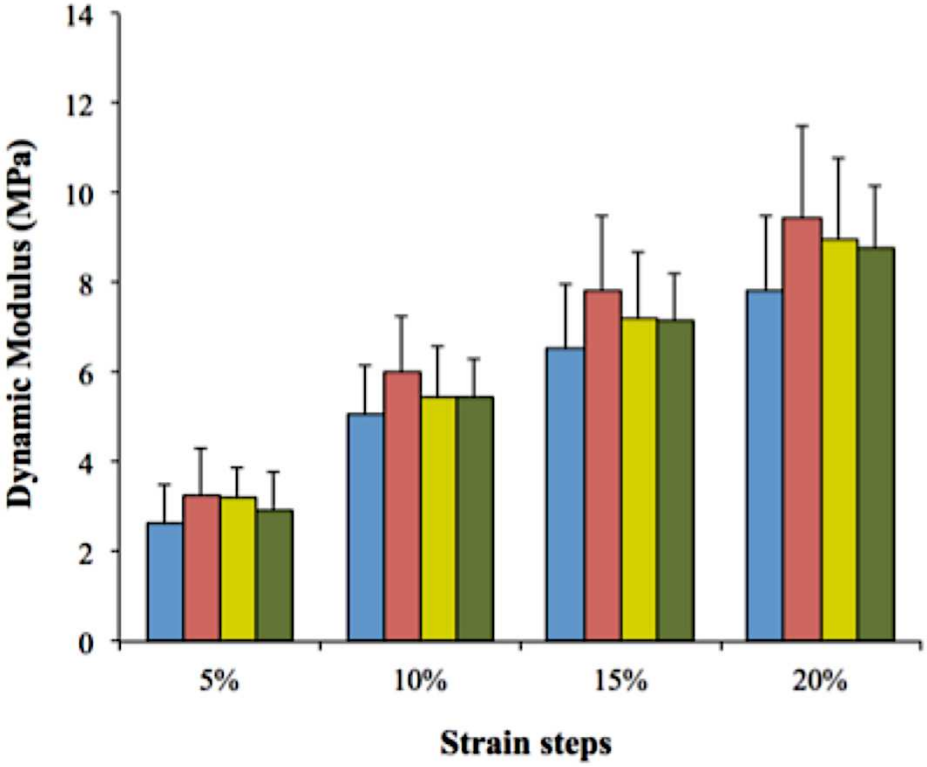

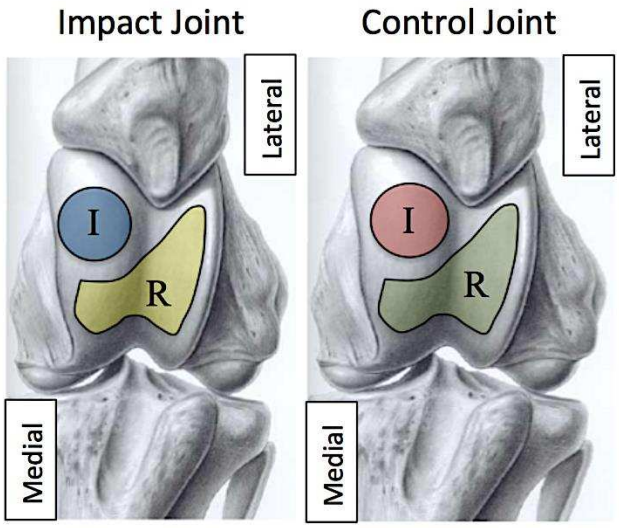

Figure 4.10 – Mean ± standard deviation of dynamic modulus values by sample location and by % strain. There were no significant differences in dynamic modulus between sample locations.

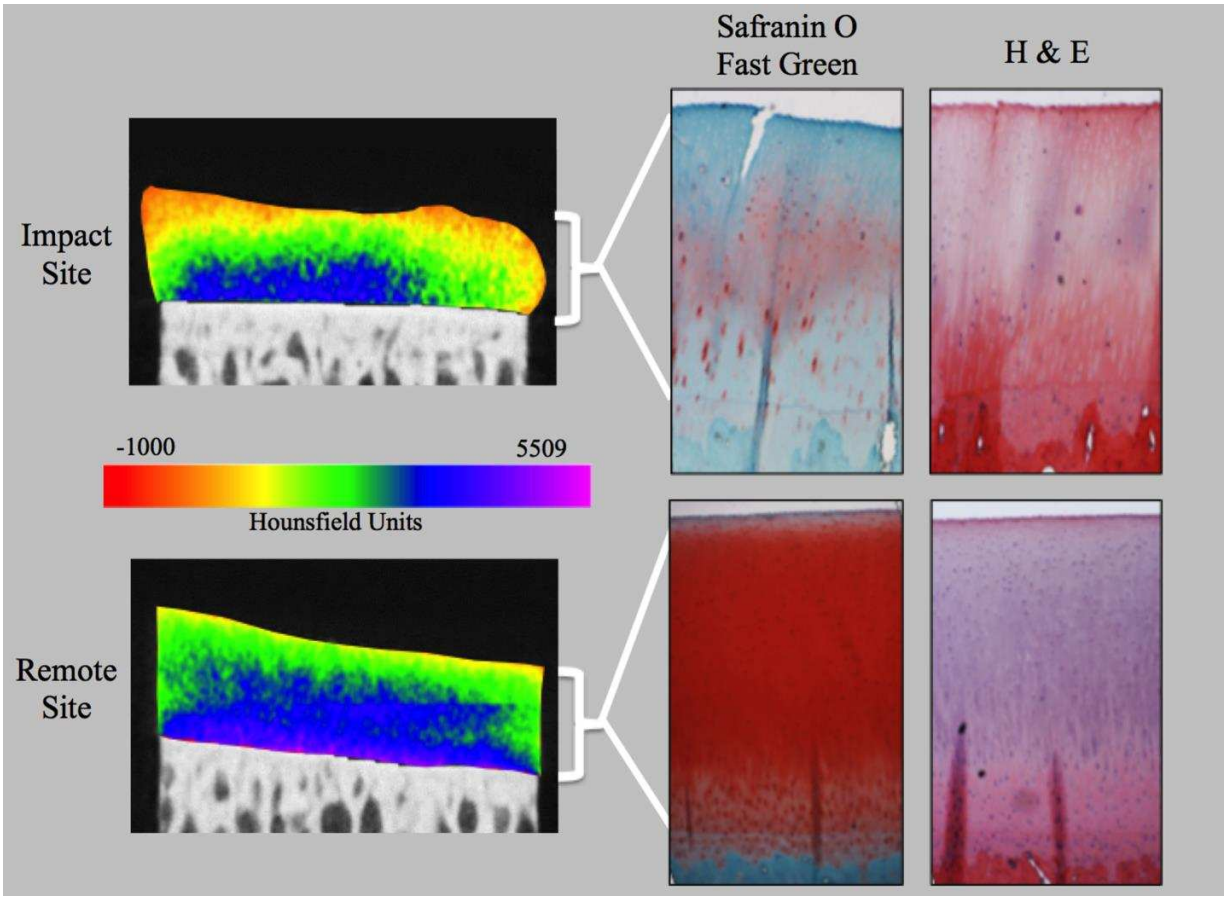

Figure 4.11 – Schematic showing representative samples of two osteochondral biopsy plugs imaged with cationic CECT (microCT). Both samples were collected two months after mechanical impact was delivered to the impact sample, while the remote sample was at a location away from the impact. A color map is applied to show the difference in attenuation values between samples. Comparative histology images are shown to the right of the associated plug. Safranin O fast green stain highlights proteoglycans while hematoxylin and eosin (H & E) shows tissue architecture and cellular morphology.

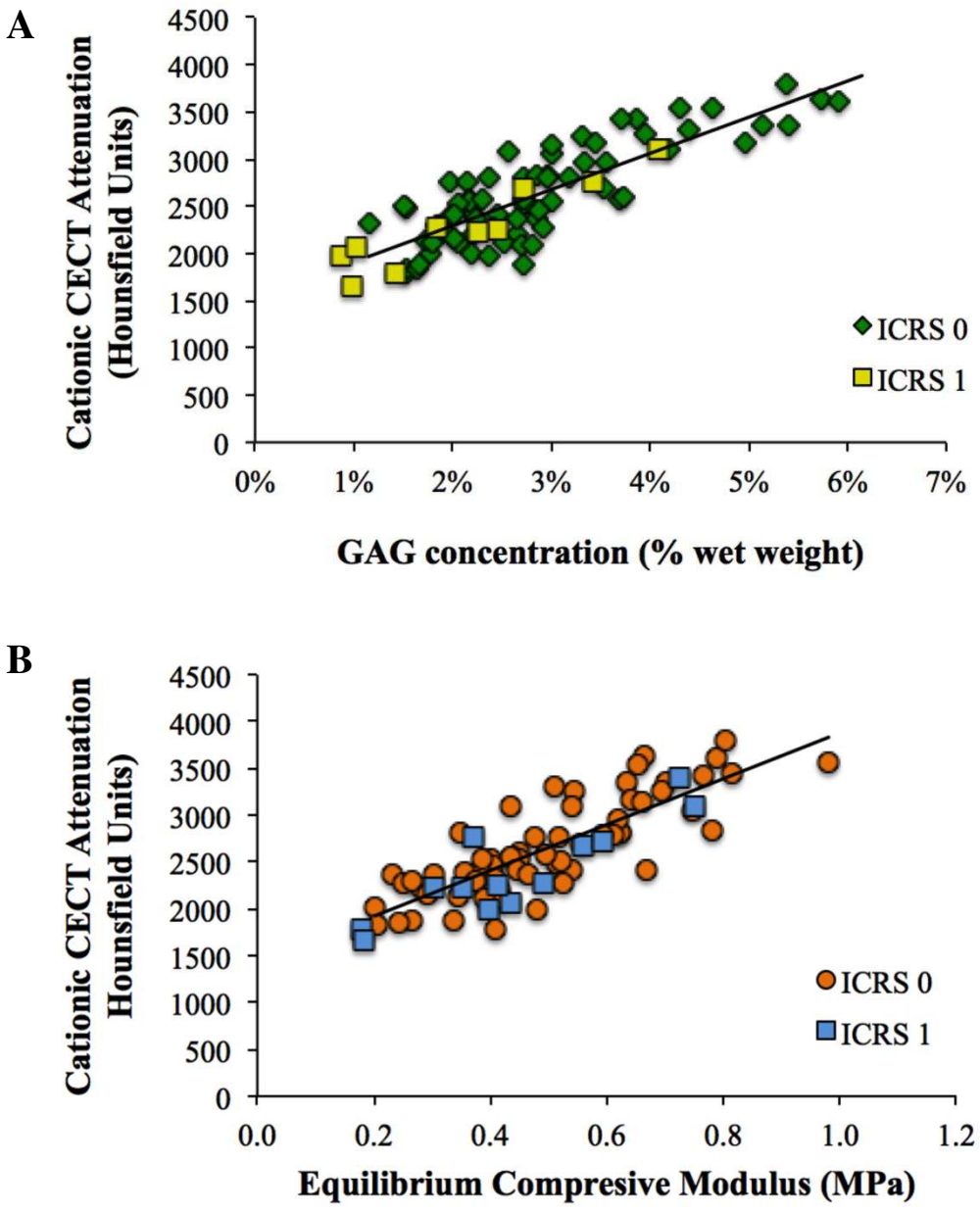

Figure 4.12 – Scatterplots of cationic CECT attenuation (microCT) versus (A) glycosaminoglycan (GAG) content and (B) equilibrium compressive modulus. Data points are assigned by ICRS score.

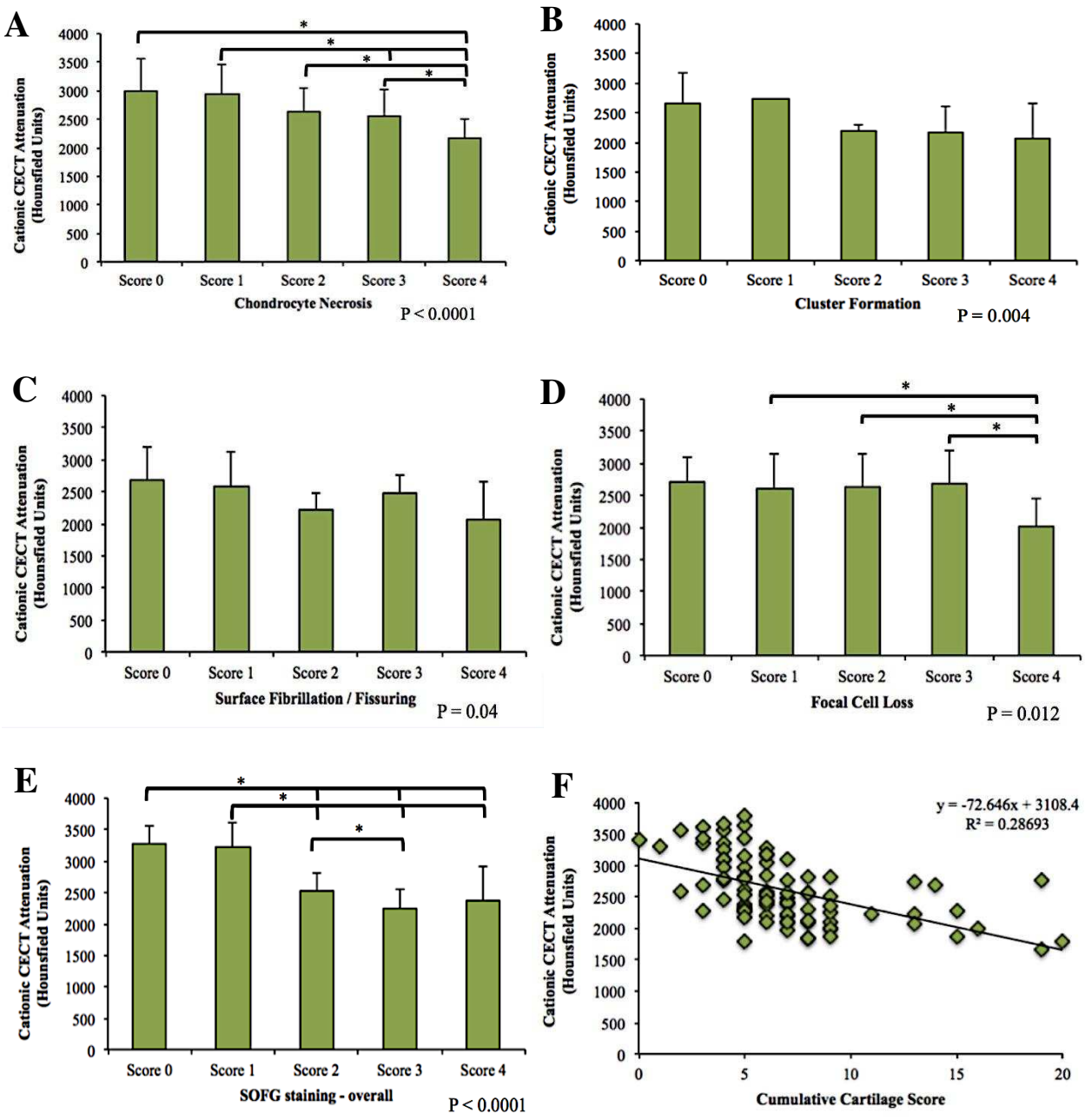

Figure 4.13 – (A – E) Mean ± s.d. cationic CECT attenuation (microCT) at each score level of the OARSI histologic scoring system.[57] The P-value in the lower right corner of each graph shows the fixed effects (overall) significance level for that variable. Asterisks and brackets above each bar graph indicate significant differences ($P < 0.05$) between scores and are adjusted for multiple comparisons using a Tukey-Kramer adjustment. (F) Scatterplot of cationic CECT attenuation (microCT) versus cumulative OARSI score.

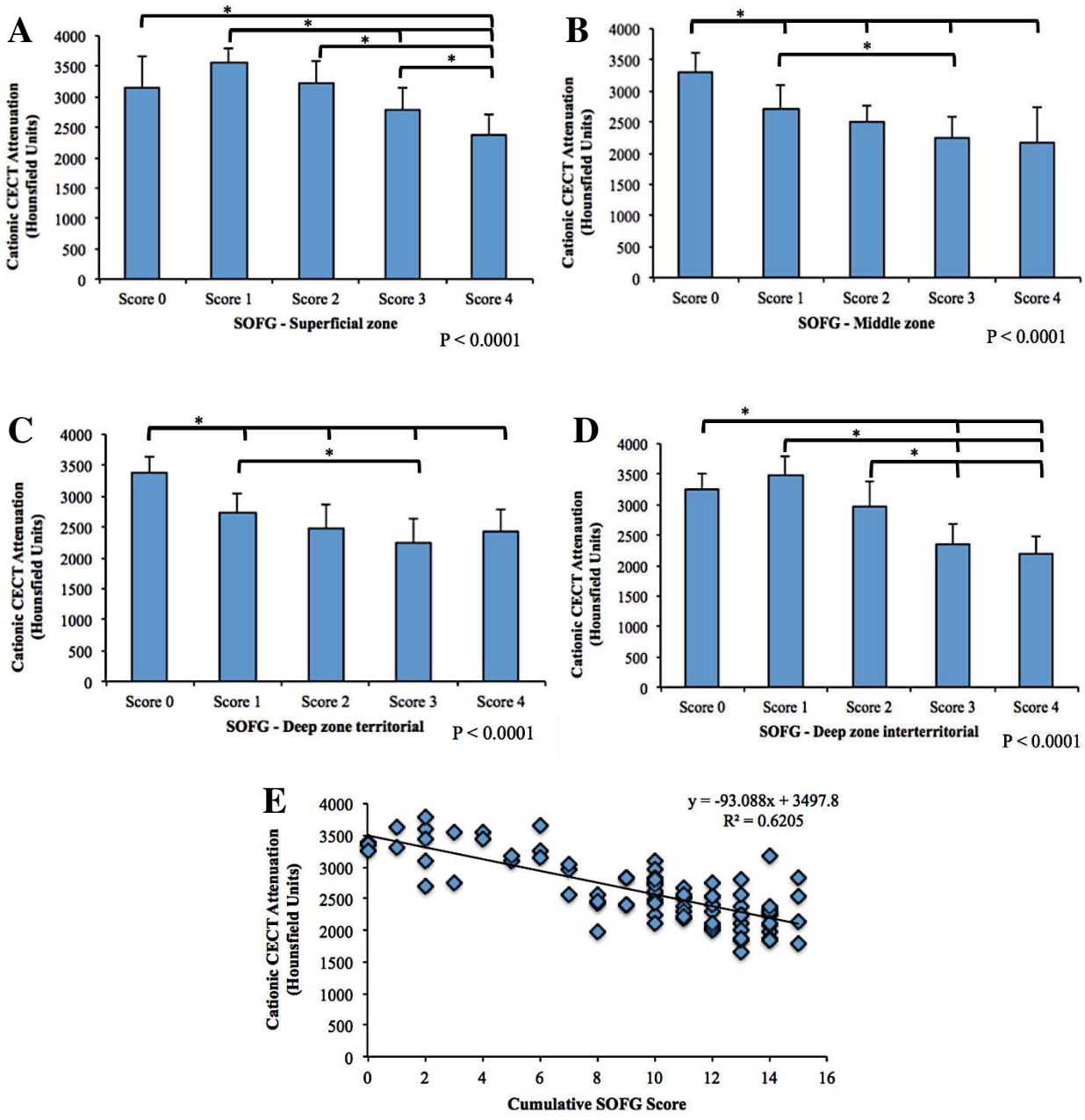

Figure 4.14 – (A – D) Mean ± s.d. cationic CECT attenuation (microCT) at each score level of safranin-O fast green (SOFG) within the respective articular cartilage zone of the OARSI histologic scoring system.[57] The P-value in the lower right corner of each graph shows the fixed effects (overall) significance level for that variable. Asterisks and brackets above each bar graph indicate significant differences ($P < 0.05$) between scores and are adjusted for multiple comparisons using a Tukey-Kramer adjustment. (E) Scatterplot of cationic CECT attenuation (microCT) versus cumulative safranin-O fast green (SOFG) score.

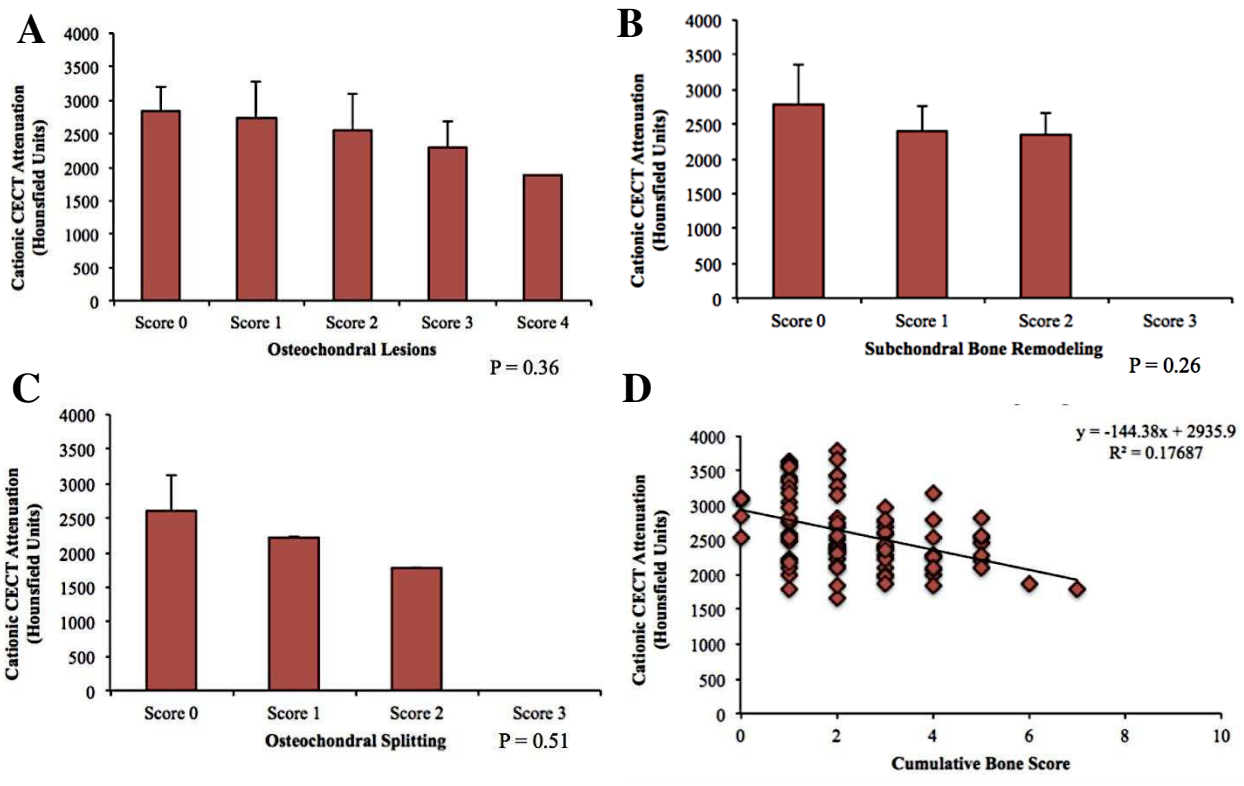

Figure 4.15 – (A – C) Mean ± s.d. cationic CECT attenuation (microCT) at each score level of the OARSI histologic bone score.[57] The P-value in the lower right corner of each graph shows the fixed effects (overall) significance level for that variable. (D) Scatterplot of cationic CECT attenuation (microCT) versus cumulative OARSI bone score. There were no significant effects of the OARSI bone score components on cationic CECT attenuation.

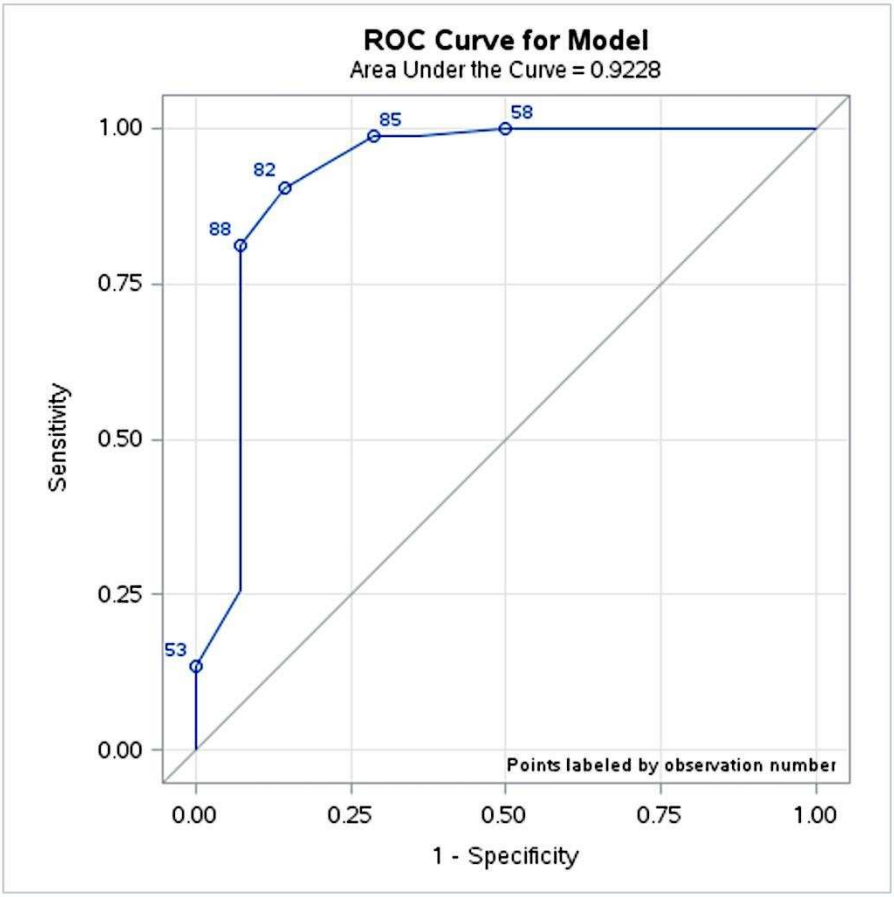

Figure 4.16 – Receiver operating characteristic curve used to establish a threshold of articular cartilage injury as defined by the OARSI histologic (cumulative) score. Maximum Youden index = 9.18 (point 82 on the graph).

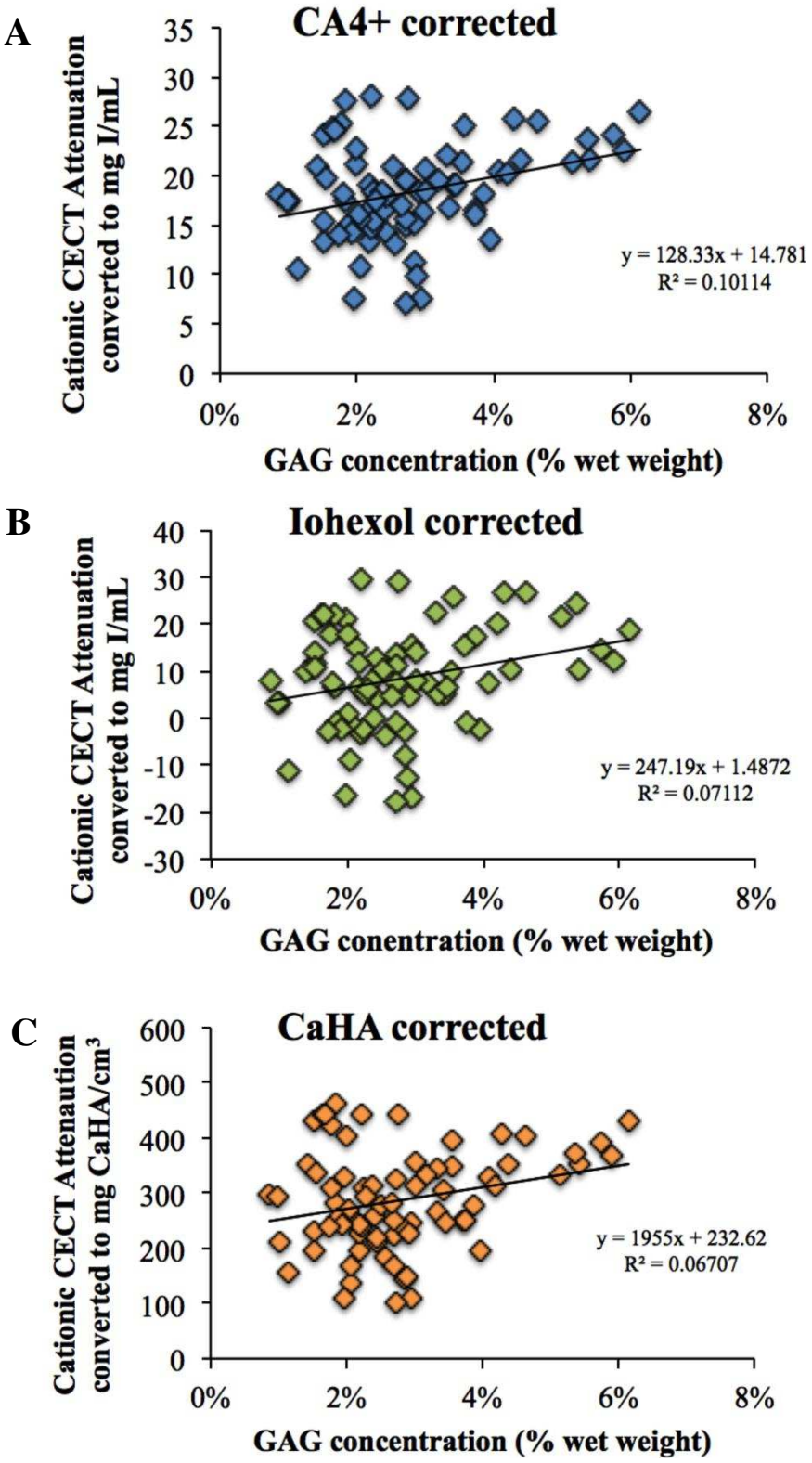

Figure 4.17 – Scatterplots of clinical cationic CECT attenuation versus glycosaminoglycan (GAG) content after correction to concentrations of (A) CA4+, (B) iohexol and (C) calcium hydroxyapatite (CaHA).

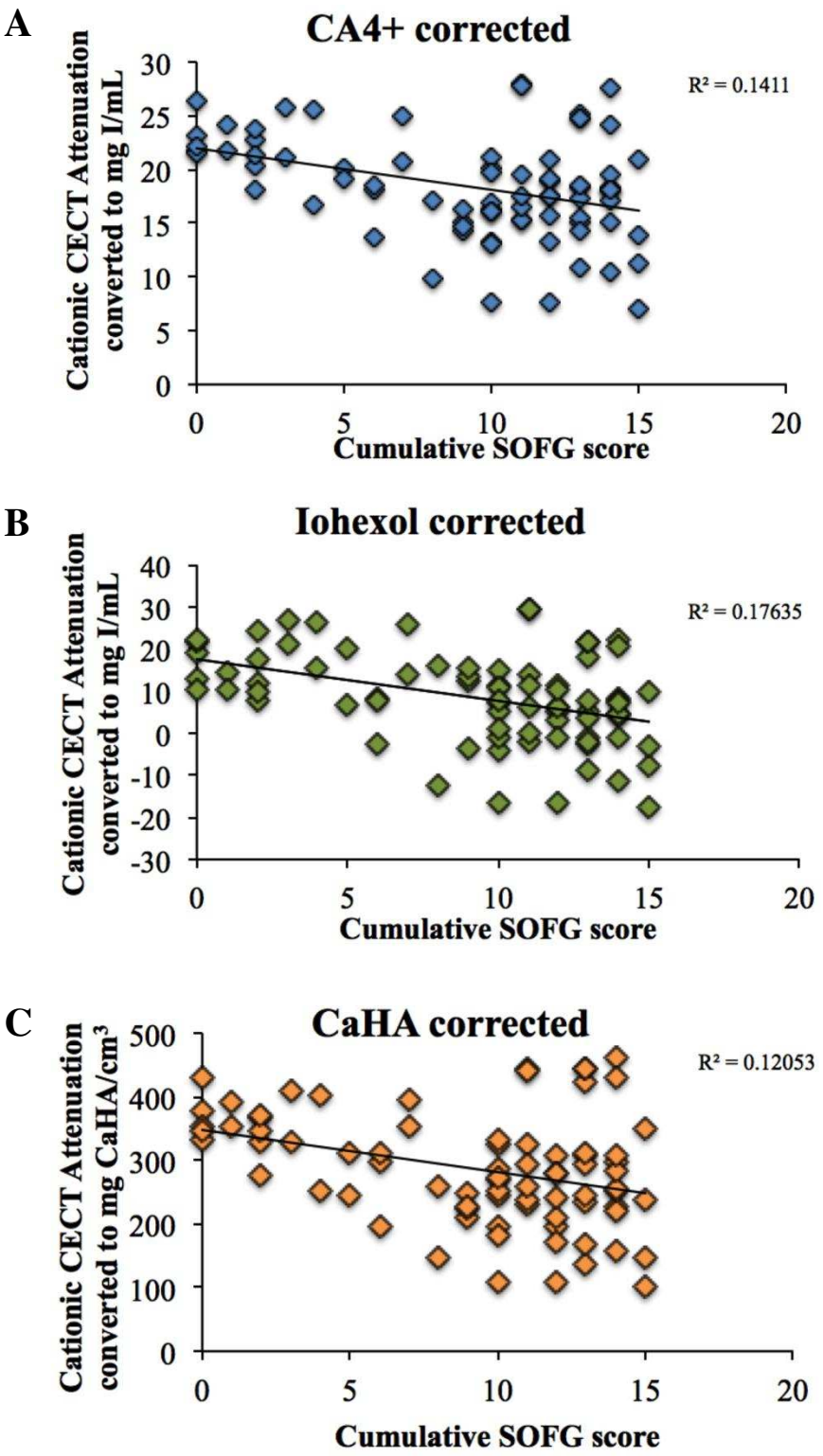

Figure 4.18 – Scatterplots of clinical cationic CECT attenuation versus cumulative safranin-O fast green (SOFG) scores after correction to concentrations of (A) CA4+, (B) iohexol and (C) calcium hydroxyapatite (CaHA).

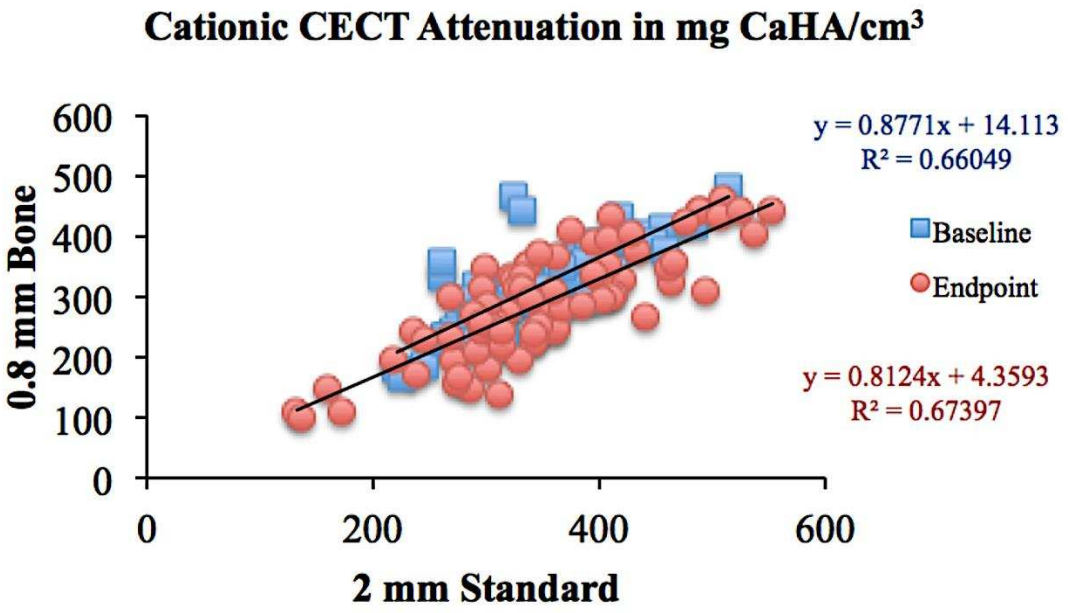

Figure 4.19 – Comparison of CT reconstruction algorithms used for cationic CECT imaging. Baseline data points are from all joints prior to impact injury and endpoint show the joints after impact.

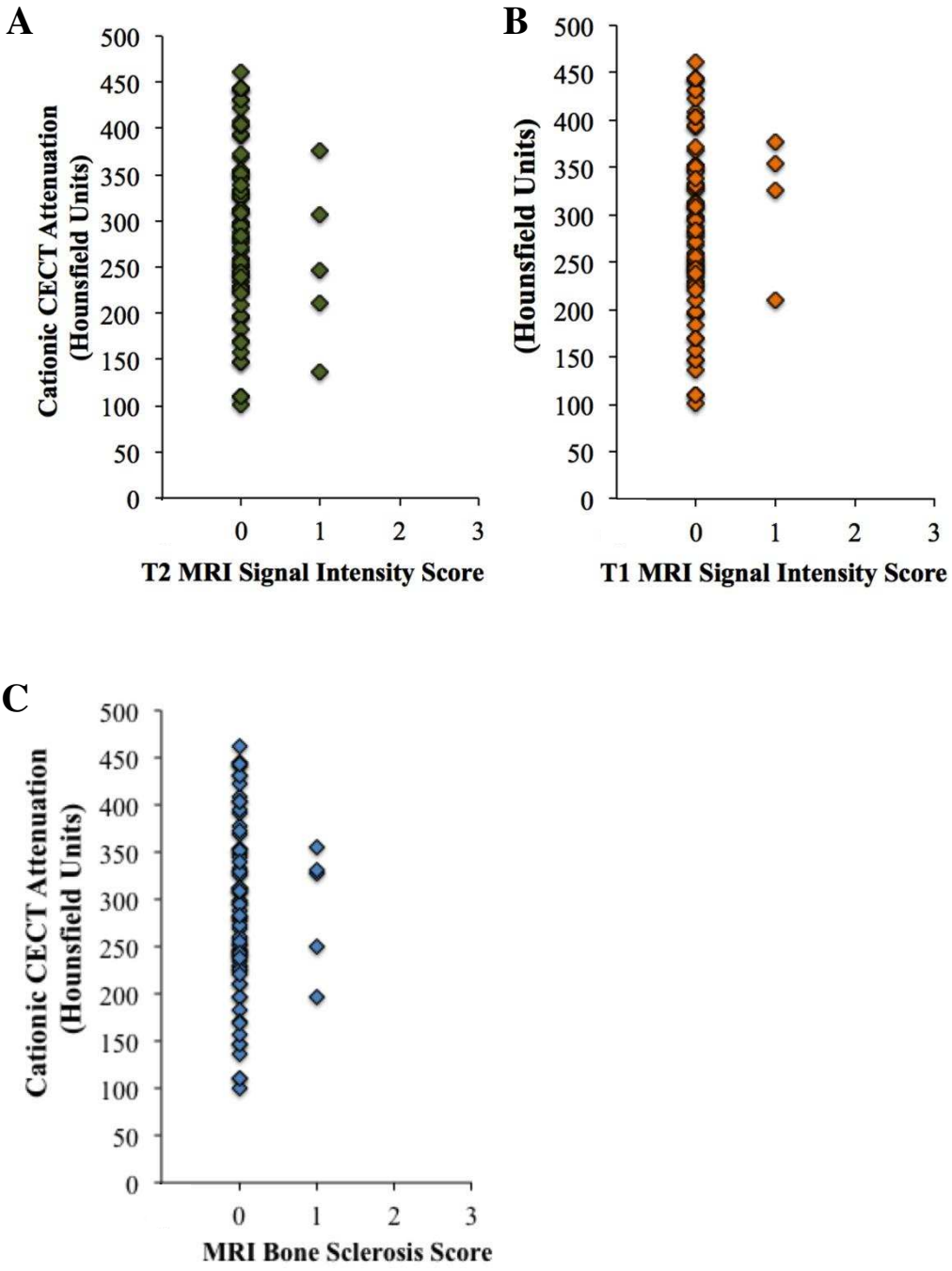

Figure 4.20 – Comparison of clinical cationic CECT attenuation values (0.8 mm sharp [bone] algorithm) to MRI scores. A) T2 signal intensity. B) T1 signal intensity. C) Bone sclerosis.

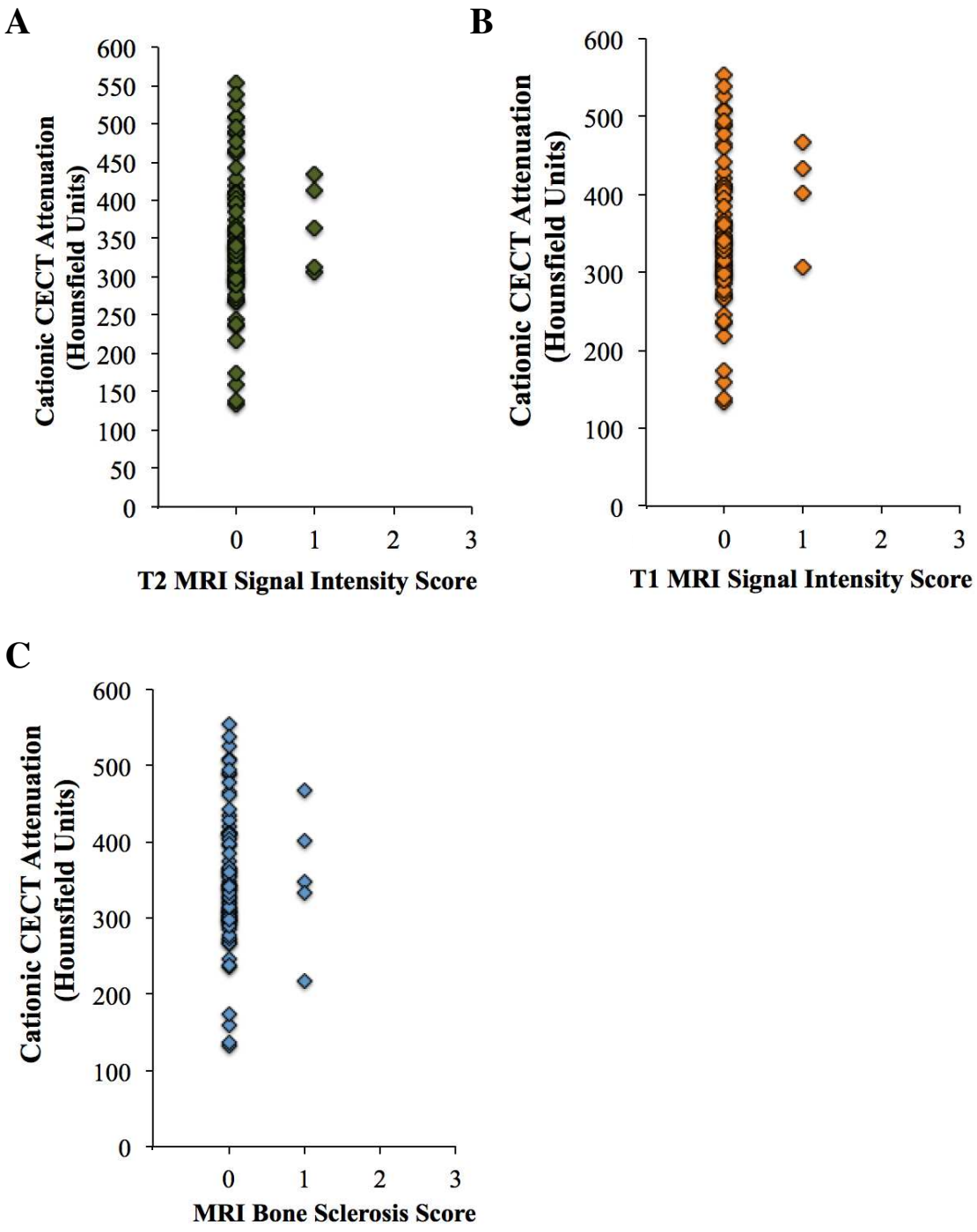

Figure 4.21 – Comparison of clinical cationic CECT attenuation values (2 mm standard algorithm) to MRI scores. A) T2 signal intensity. B) T1 signal intensity. C) Bone sclerosis.

Table 4.1A – Mean ± standard deviation synovial fluid total protein concentrations in four horses after articular cartilage impact (impact joint) compared to the non-impacted control joint.

Time Point	**Total protein concentration (g/dL)**	
	Impact Joint	Control Joint
Baseline (0 weeks)	1.93 ± 0.15	1.8 ± 0.54
2 weeks	2.3 + 0.53	1.95 ± 0.19
4 weeks	2.68 ± 1.22	2.25 ± 0.38
6 weeks	1.9 ± 0.82	2.35 ± 0.97
8 weeks	1.95 ± 0.82	2 ± 0.82
Endpoint	2 ± 0	1.7 ± 0.42

Table 4.1B – Mean ± standard deviation synovial fluid leukocyte concentrations in four horses after articular cartilage impact (impact joint) compared to the non-impacted control joint.

Time Point	**Leukocyte concentration (10^6/μL)**	
	Impact Joint	Control Joint
Baseline (0 weeks)	--	--
2 weeks	933 ± 379	12,200
4 weeks	600	600
6 weeks	500 ± 100	370 ± 120
8 weeks	400 ± 265	525 ± 585
Endpoint	--	400 ± 141

Table 4.1C – Mean ± standard deviation synovial fluid neutrophil percentage in four horses after articular cartilage impact (impact joint) compared to the non-impacted control joint.

Time Point	**Neutrophils (% of leukocytes)**	
	Impact Joint	Control Joint
Baseline (0 weeks)	--	--
2 weeks	46.9 ± 8.8	56.7
4 weeks	53.9	41.4
6 weeks	43.9 ± 5.9	44.4 ± 12.5
8 weeks	40 ± 0.1	40.2 ± 5.2
Endpoint	--	24.4 ± 3.5

Table 4.2 – Mean +/- standard deviation measurements of bone morphometry grouped by sampling location. BV, bone volume; TV, total volume; Tb.N, trabecular number; Tb.Th, trabecular thickness; Tb.Sp, trabecular separation; TMD, tissue mineral density; HA, hydroxyapatite; BMD, bone mineral density. There were no significant differences between joint locations for any parameter (all P>0.05) as determined with a mixed model ANOVA.

Parameter	**Impact Joint**		**Control Joint**		**P - value**
Sample location	Impact	Remote	Impact	Remote	
BV/TV	0.524 ± 0.102	0.667 ± 0.134	0.540 ± 0.062	0.626 ± 0.151	0.48
Tb.N (No./mm)	2.320 ± 0.180	2.675 ± 0.432	2.531 ± 0.132	2.517 ± 0.353	0.08
Tb.Th (mm)	0.234 ± 0.047	0.291 ± 0.067	0.222 ± 0.025	0.262 ± 0.066	0.60
Tb.Sp (mm)	0.375 ± 0.046	0.295 ± 0.071	0.331 ± 0.030	0.315 ± 0.088	0.22
Trabecular bone TMD ($mgHA/cm^3$)	729.4 ± 13.2	728.6 ± 19.3	732.9 ± 22.6	731.3 ± 21.9	
Trabecular BMD ($mgHA/cm^3$)	490 ± 61.8	507.0 ± 77.2	492.8 ± 79.9	532.5 ± 93.5	0.90
Subchondral bone volume (mm^3)	13.1 ± 4.5	15.9 ± 5.3	12.0 ± 3.3	14.6 ± 6.4	0.38
Subchondral bone density ($mgHA/cm^3$)	655.9 ± 51.3	663.5 ± 42.7	658.4 ± 50.3	643.9 ± 51.7	0.33
Subchondral bone thickness (mm)	0.354 ± 0.101	0.415 ± 0.133	0.320 ± 0.109	0.378 ± 0.165	0.46

Table 4.3 – Spearman rank correlations between cationic CECT attenuation (microCT) with biochemical and bone parameters. GAG, glycosaminoglycan; BV/TV, bone volume fraction; Tb.N, trabecular number; Tb.Th, trabecular thickness; Tb.Sp, trabecular spacing; BMD, bone mineral density; TMD, tissue mineral density.

Parameter	**Rho**	**P-value**
GAG concentration	0.82	<0.0001*
Equilibrium compressive modulus	0.80	<0.0001*
5% Dynamic modulus	0.53	<0.0001*
10% Dynamic modulus	0.33	0.006*
15% Dynamic modulus	0.32	0.007*
20% Dynamic modulus	0.33	0.005*
Total collagen	-0.32	0.007*
BV/TV	0.49	<0.0001*
Tb.N	0.56	<0.0001*
Tb.Th	0.41	0.0004*
Tb.Sp	-0.58	<0.0001*
Trabecular bone BMD	0.21	0.08
Trabecular bone TMD	0.09	0.45
Subchondral bone density	0.47	<0.0001*

Table 4.4 – Coefficients of determination and Spearman rank correlations between histologic OARSI parameters and cationic CECT attenuation (microCT). SOFG, safranin-O fast green; OC, osteochondral; SCB, subchondral bone. *P < 0.05.

Histologic parameter	**R^2**	**Rho**	**P-value**
Chondrocyte necrosis	0.26	-0.47	<0.0001*
Cluster formation	0.09	-0.3	0.005*
Fibrillation fissuring	0.07	-0.26	0.016*
Focal cell loss	0.02	-0.15	0.185
SOFG overall	0.56	-0.72	<0.0001*
Cumulative cartilage score	0.29	-0.65	<0.0001*
SOFG superficial	0.42	-0.63	<0.0001*
SOFG middle	0.59	-0.72	<0.0001*
SOFG deep territorial	0.46	-0.64	<0.0001*
SOFG deep interterritorial	0.51	-0.72	<0.0001*
Cumulative SOFG score	0.62	-0.72	<0.0001*
OC lesions	0.12	-0.41	0.0001*
SCB remodeling	0.13	-0.36	0.0007*
OC splitting	0.04	-0.2	0.07
Cumulative bone score	0.18	-0.46	<0.0001*

Table 4.5 – Effects of joints and sites on histologic scoring parameters in four horses eight weeks after receiving articular cartilage impact injury. [#]Histologic parameters were scored on the OARSI grading system. The effects on each histologic parameter were determined using [a]ordinal logistic regression or [b]multiple regression. The second column reports the significance level of each variable on the interaction between joint (impact & control) and site (impact & remote). The remaining columns report the P-values of the comparisons listed at the top of the column after posthoc Tukey-Kramer adjustment for multiple comparisons. *P < 0.05. P-values in parenthesis are shown with an approaching significant (0.05 > P < 0.1) effect on the joint-by-site interaction. SOFG, safranin-O fast green; OC, osteochondral; SCB, subchondral bone, NS, not significant (P > 0.05); NA, not applicable (joint-by-site interaction did not reach significance).

		Impact Joint	**Impact vs Control joint**	**Control Joint**	**Impact vs Control joint**
Histologic parameter[#]	**Joint-by-site interaction P-value**	**Impact vs remote site**	**Impact site**	**Impact vs remote site**	**Remote site**
Chondrocyte necrosis[a]	P = 0.004*	< 0.0001*	0.014*	NS	NS
Cluster formation[a]	P = 0.98	NA	NA	NA	NA
Fibrillation fissuring[a]	P = 0.91	NA	NA	NA	NA
Focal cell loss[a]	P = 0.01*	0.0007*	0.014*	NS	NS
SOFG overall[a]	P = 0.004*	0.017*	0.025*	NS	NS
Cumulative cartilage score[b]	P < 0.0001*	< 0.0001*	< 0.0001*	NS	NS
SOFG superficial[a]	P = 0.035*	NS	NS	NS	NS
SOFG middle[a]	P = 0.008*	0.018*	0.028*	NS	NS
SOFG deep territorial[a]	P = 0.26	NA	NA	NA	NA
SOFG deep interterritorial[a]	P = 0.04*	NS	NS	NS	NS
Cumulative SOFG score[b]	P = 0.09	(0.02*)	NS	NS	NS
OC lesions[a]	P = 0.043*	0.047*	NS	NS	NS
SCB remodeling[a]	P = 0.37	NA	NA	NA	NA
OC splitting[a]	P = 0.96	NA	NA	NA	NA
Cumulative bone score[b]	P = 0.07	NS	NS	NS	NS

Table 4.6 – Spearman rank correlations of histologic SOFG grades with clinical endpoint CECT after density phantom correction to CA4+, iohexol or calcium hydroxyapatite (CaHA). * P < 0.05

	CA4+ corrected		**Iohexol corrected**		**CaHA corrected**	
Histologic parameter	Rho	P	Rho	P	Rho	P-value
SOFG overall	-0.24	0.04*	-0.39	0.0008*	-0.24	0.05*
SOFG superficial	-0.3	0.01*	-0.27	0.03*	-0.26	0.03*
SOFG middle	-0.23	0.05*	-0.32	0.007*	-0.22	0.07
SOFG deep territorial	-0.28	0.02*	-0.46	0.0001*	-0.27	0.02*
SOFG deep interterritorial	-0.32	0.007*	-0.48	<0.0001*	-0.32	0.007*
Cumulative SOFG score	-0.26	0.027*	-0.40	0.0006*	-0.25	0.032*

REFERENCES

1. Fubini SL, Erb HN, Freeman KP, et al. Prognostic factors affecting survival of 507 horses with joint disease: (1983 to 1990). *Can J Vet Res* 1999;63:253–260.
2. Frisbie DD, and McIlwraith, CW. Evaluation of gene therapy as a treatment for equine traumatic arthritis and osteoarthritis. *Clin Orthop Relat Res* 2000;379(suppl 379):S273–S287.
3. CDC. National and State Medical Expenditures and Lost Earnings Attributable to Arthritis and Other Rheumatic Conditions --- United States, 2003. *MMWR* 2007;56:4-7.
4. Bansal PH, Joshi NS, Entezari V, et al. Contrast enhanced computed tomography can predict the glycosaminoglycan content and biomechanical properties of articular cartilage. *Osteoarthritis Cartilage* 2010;18:184-191.
5. Frisbie DD, Al-Sobayil F, Billinghurst RC, et al. Changes in synovial fluid and serum biomarkers with exercise and early osteoarthritis in horses. *Osteoarthritis and Cartilage* 2008;16:1196-1204.
6. Murray RC, Mair TS, Sherlock CE, et al. Comparison of high-field and low-field magnetic resonance images of cadaver limbs of horses. *Vet Rec* 2009;165:281-288.
7. Smith MA, Dyson SJ, Murray RC. Reliability of high- and low-field magnetic resonance imaging systems for detection of cartilage and bone lesions in the equine cadaver fetlock. *Equine Vet J* 2012;44:684–691.
8. Taylor C, Carballido-Gamio, J, Majumdar, S, Li, X. Comparison of quantitative imaging of cartilage for osteoarthritis: T2, T1ρ, dGEMRIC and contrast-enhanced computed tomography. *Mag Res Imag* 2009;27:779-784.

9. Valdés-Martínez A. Computed tomographic arthrography of the equine stifle joint. *Vet Clin N Am-Equine* 2012;28:583-598.
10. Nelson BB, Kawcak CE, Goodrich LR, et al. Comparison between computed tomographic arthrography, radiography, ultrasonography, and arthroscopy for the diagnosis of femorotibial joint disease in western performance horses. *Vet Radiol Ultrasound* 2016;57:387-402.
11. Joshi NS, Bansal PN, Stewart RC, et al. Effect of contrast agent charge on visualization of articular cartilage using computed tomography: exploiting electrostatic interactions for improved sensitivity. *J Am Chem Soc* 2009;131:13234-13235.
12. Bansal PN, Joshi NS, Entezari V, et al. Cationic contrast agents improve quantification of glycosaminoglycan (GAG) content by contrast enhanced CT imaging of cartilage. *J Orthop Res* 2011;29:704-709.
13. Lakin BA, Ellis DJ, Shelofsky JS, et al. Contrast-enhanced CT facilitates rapid, non-destructive assessment of cartilage and bone properties of the human metacarpal. *Osteoarthritis Cartilage* 2015;23:2158-2166.
14. Lakin BA, Grasso DJ, Shah SS, et al. Cationic agent contrast-enhanced computed tomography imaging of cartilage correlates with the compressive modulus and coefficient of friction. *Osteoarthritis Cartilage* 2013;21:60-68.
15. Lakin BA, Patel H, Holland C, et al. Contrast-enhanced CT using a cationic contrast agent enables non-destructive assessment of the biochemical and biomechanical properties of mouse tibial plateau cartilage. *J Orthop Res* 2016;34:1130-1138.

16. Stewart RC, Bansal PN, Entezari V, et al. Contrast-enhanced CT with a high-affinity cationic contrast agent for imaging ex vivo bovine, intact ex vivo rabbit and in vivo rabbit cartilage. *Radiology* 2013;266:141-150.
17. Stewart RC, Patwa AN, Lusic H, et al. Synthesis and preclinical characterization of a cationic iodinated imaging contrast agent (CA4+) and its use for quantitative computed tomography of ex vivo human hip cartilage. *J Med Chem* 2017;60:5543-5555.
18. Bolam C, Hurtig, MB, Cruz, A, and McEwen, BJE. Characterization of experimentally induced post-traumatic osteoarthritis in the medial femorotibial joint of horses. *Am J Vet Res* 2006;67:433-447.
19. Little CB, Zaki S. What constitutes an "animal model of osteoarthritis" – the need for consensus? *Osteoarthritis and Cartilage* 2012;20:261-267.
20. Elmesiry A, Seleim M, Cullis-Hill D. Iodoacetate and allogenous cartilage particles as models for arthritis induction in equine. *International Journal of Veterinary Science and Medicine* 2014;2:142-150.
21. McIlwraith CW, and Van Sickle, DC. Experimentally induced arthritis of the equine carpus: histologic and histochemical changes in the articular cartilage. *Am J Vet Res* 1981;42:209-217.
22. McIlwraith CW, Frisbie DD, Kawcak CE. The horse as a model of naturally occurring osteoarthritis. *Bone Joint Res* 2012;1:297-309.
23. McIlwraith CW, Fortier LA, Frisbie DD, et al. Equine models of articular cartilage repair. *Cartilage* 2011;2:317-326.

24. Nixon AJ, Begum L, Mohammed HO, et al. Autologous chondrocyte implantation drives early chondrogenesis and organized repair in extensive full- and partial-thickness cartilage defects in an equine model. *J Orthop Res* 2001;29:1121-1130.

25. Nixon AJ, Rickey E, Butler TJ, et al. A chondrocyte infiltrated collagen type I/III membrane (MACI implant) imporves cartilage healing in the equine patellofemoral joint model. *Osteoarthritis and Cartilage* 2015;23:648-660.

26. Ross TN, Kisiday JD, Hess T, et al. Evaluation of the inflammatory response in experimentally induced synovitis in the horse: a comparison of recombinant equine interleukin 1 beta and lipopolysaccharide. *Osteoarthritis Cartilage* 2012;20:1583-1590.

27. Frisbie DD, Kawcak CE, Baxter GM, Trotter GW, Powers BE, Lassen ED, McIlwraith CW. Effects of 6-alpha-methylprednisolone acetate on an equine osteochondral fraent exercise model. *Am J Vet Res* 1998;59:1619-1628.

28. Rickey EJ, Cruz AM, Trout DR, et al. Evaluation of experimental impact injury for inducing post-traumatic osteoarthritis in the metacarpophalangeal joints of horses. *Am J Vet Res* 2012;73:1540-1552.

29. Fischenich KM, Pauly HM, Button KD, et al. A study of acute and chronic tissue changes in surgical and traumatically-induced experimental models of knee joint injury using magnetic resonance imaging and micro-computed tomography. *Osteoarthritis Cartilage* 2017;25:561-569.

30. Fischenich KM, Button KD, DeCamp C, et al. Comparison of two models of post-traumatic osteoarthritis; temporal degradation of articular cartilage and menisci. *J Orthop Res* 2017;35:486-495.

31. Lee CM, Kisiday JD, McIlwraith CW, et al. Development of an in vitro model of injury-induced osteoarthritis in cartilage explants from adult horses through application of single-impact compressive overload. *Am J Vet Res* 2013;74:40-47.
32. Barton KI, Shekarforoush M, Heard BJ, et al. Use of pre-clinical surgically induced models to understand biomechanical and biological consequences of PTOA development. *Journal of Orthopaedic Research* 2017;35:454-465.
33. Brimmo OA, Pfeiffer F, Bozynski CC, et al. Development of a novel canine model for posttraumatic asteoarthritis of the knee. *J Knee Surg* 2016;29:235-241.
34. Novakofski KD, Berg LC, Bronzini I, et al. Joint-dependent response to impact and implications for post-traumatic osteoarthritis. *Osteoarthritis Cartilage* 2015;23:1130-1137.
35. Haut RC, Ide TM, De Camp CE. Mechanical responses of the rabbit patello-femoral joint to blunt impact. *J Biomech Eng* 1995;117:402-408.
36. Jeffrey JE, Gregory DW, Aspden RM. Matrix damage and chondrocyte viability following a single impact load on articular cartilage. *Arch Biochem Biophys* 1995;322:87-96.
37. Changoor A, Coutu JP, Garon M, et al. Streaming potential-based arthroscopic device is sensitive to cartilage changes immediately post-impact in an equine cartilage injury model. *J Biomech Eng* 2011;133:061005-061001-061009.
38. American Association of Equine Practitioners. *Guide for veterinary service and judging of equestrian events*. Lexington, KY: American Association of Equine Practitioners, 1991.
39. Frisbie DD, Bowman SM, Colhoun HA, et al. Evaluation of autologous chondrocyte transplantation via a collagen membrane in equine articular defects – results at 12 and 18 months. *Osteoarthritis and Cartilage* 2008;16:667-679.

40. Birnbaum BA, Hindman N, Lee J, et al. Multi-detector row CT attenuation measurements: assessment of intra- and interscanner variability with an anthropomorphic body CT phantom. *Radiology* 2007;242:109-119.

41. Lamba R, McGahan JP, Corwin MT, et al. CT Hounsfield numbers of soft tissues on unenhanced abdominal CT scans: variability between two different manufacturers' MDCT scanners. *AJR Am J Roentgenol* 2014;203:1013-1020.

42. Cropp RJ, Seslija P, Tso D, et al. Scanner and kVp dependence of measured CT numbers in the ACR CT phantom. *J Appl Clin Med Phys* 2013;14:4417.

43. Mao SS, Li D, Luo Y, et al. Application of quantitative computed tomography for assessment of trabecular bone mineral density, microarchitecture and mechanical property. *Clin Imaging* 2016;40:330-338.

44. Sekhon K, Kazakia GJ, Burghardt AJ, et al. Accuracy of volumetric bone mineral density measurement in high-resolution peripheral quantitative computed tomography. *Bone* 2009;45:473-479.

45. Hendrickson DA, Nixon AJ. Comparison of the cranial and a new lateral approach to the femoropatellar joint for aspiration and injection in horses. *J Am Vet Med Assoc* 1994;205:1177-1179.

46. McIlwraith CW, Nixon AJ, Wright IM. Diagnostic and surgical arthroscopy of the femoropatellar and femorotibial joints In: McIlwraith CW, Nixon AJ,Wright IM, eds. *Diagnostic and surgical arthroscopy in the horse*. 4th ed. New York: Mosby Elsevier, 2015;175-242.

47. Bertone AL, Palmer JL, Jones J. Synvoial fluid cytokines and eicosanoids as markers of joint disease in horses. *Vet Surg* 2001;30:528-538.

48. Farndale RW, Buttle DJ, Barrett AJ. Improved quantitation and discrimination of sulphated glycosaminoglycans by use of dimethylmethylene blue. *Biochim Biophys Acta* 1986;883:173-177.

49. Outerbridge RE. The etiology of chondromalacia patellae. *J Bone Joint Surg Br* 1961;43-B:752-757.

50. Brittberg M, Winalski CS. Evaluation of cartilage injuries and repair. *J Bone Joint Surg Am* 2003;85-A Suppl 2:58-69.

51. Mow V, Hayes W. *Basic Orthopaedic Biomechanics*. New York, NY: Raven Press Ltd., 1991.

52. Mow VC, Ratcliffe A, Poole AR. Cartilage and diarthrodial joints as paradigms for hierarchical materials and structures. *Biomaterials* 1992;13:67-97.

53. Park S, Hung CT, Ateshian GA. Mechanical response of bovine articular cartilage under dynamic unconfined compression loading at physiological stress levels. *Osteoarthritis and Cartilage*;12:65-73.

54. Bouxsein ML, Boyd SK, Christiansen BA, et al. Guidelines for assessment of bone microstructure in rodents using micro-computed tomography. *J Bone Miner Res* 2010;25:1468-1486.

55. Lippiello L, Hall D, Mankin HJ. Collagen synthesis in normal and osteoarthritic human cartilage. *J Clin Invest* 1977;59:593-600.

56. Venn M, Maroudas A. Chemical composition and swelling of normal and osteoarthrotic femoral head cartilage. I. Chemical composition. *Ann Rheum Dis* 1977;36:121-129.

57. McIlwraith CW, Frisbie DD, Kawcak CE, et al. The OARSI histopathology initiative - recommendations for histological assessments of osteoarthritis in the horse. *Osteoarthritis and Cartilage* 2010;18:S93-S105.

58. Mankin HJ. Biochemical and metabolic aspects of osteoarthritis. *Orthop Clin North Am* 1971;2:19-31.

59. Mainil-Varlet P, Van Damme B, Nesic D, et al. A new histology scoring system for the assessment of the quality of human cartilage repair: ICRS II. *Am J Sports Med* 2010;38:880-890.

60. Pauli C, Whiteside R, Heras FL, et al. Comparison of cartilage histopathology assessment systems on human knee joints at all states of osteaorthritis development. *Osteoarthritis and Cartilage* 2012;20:476-485.

61. Hirvasniemi J, Kulmala KA, Lammentausta E, et al. In vivo comparison of delayed gadolinium-enhanced MRI of cartilage and delayed quantitative CT arthrography in imaging of articular cartilage. *Osteoarthritis Cartilage* 2013;21:434-442.

62. Landis JR, Koch GG. The measurement of observer agreement for categorical data. *Biometrics* 1977;33:159-174.

63. Frisbie DD, Cross MW, McIlwraith CW. A comparative study of articular cartilage thickness in the stifle of animal species used in human pre-clinical studies compared to articular cartilage thickness in the human knee. *Vet Comp Orthop Traumatol* 2006;19:142-146.

64. Changoor A, Hurtig MB, Runciman RJ, et al. Mapping of donor and recipient site properties for osteochondral graft reconstruction of subchondral cystic lesions in the equine stifle joint. *Equine Vet J* 2006;38:330-336.

65. D'Lima DD, Hashimoto S, Chen PC, et al. Impact of mechanical trauma on matrix and cells. *Clin Orthop Relat Res* 2001:S90-99.

66. Thompson RC, Jr., Oegema TR, Jr., Lewis JL, et al. Osteoarthrotic changes after acute transarticular load. An animal model. *J Bone Joint Surg Am* 1991;73:990-1001.

67. Newberry WN, Zukosky DK, Haut RC. Subfracture insult to a knee joint causes alterations in the bone and in the functional stiffness of overlying cartilage. *J Orthop Res* 1997;15:450-455.

68. Komori T. Cell death in chondrocytes, osteoblasts, and osteocytes. *International Journal of Molecular Sciences* 2016;17:2045.

69. van Haaften EE, Ito K, van Donkelaar CC. The initial repair response of articular cartilage after mechanically induced damage. *Journal of Orthopaedic Research* 2017;35:1265-1273.

70. Voss JR, Lu Y, Edwards RB, et al. Effects of thermal energy on chondrocyte viability. *Am J Vet Res* 2006;67:1708-1712.

71. Pawson DJ, Glanzmann M, Luechinger R, et al. Quantitative morphometric patterns in cartilage and bone from the humeral heads of end-stage osteoarthritis patients. *Osteoarthritis and Cartilage* 2015;23:1377-1387.

72. Maerz T, Kurdziel M, Newton MD, et al. Subchondral and epiphyseal bone remodeling following surgical transection and noninvasive rupture of the anterior cruciate ligament as models of post-traumatic osteoarthritis. *Osteoarthritis Cartilage* 2016;24:698-708.

73. Gannon AR, Nagel T, Bell AP, et al. The changing role of the superficial region in determining the dynamic compressive properties of articular cartilage during postnatal development. *Osteoarthritis Cartilage* 2015;23:975-984.

74. Oke SL, Hurtig MB, Keates RA, et al. Assessment of three variations of the 1,9-dimethylmethylene blue assay for measurement of sulfated glycosaminoglycan concentrations in equine synovial fluid. *Am J Vet Res* 2003;64:900-906.

75. Palmer JL, Bertone AL, McClain H. Assessment of glycosaminoglycan concentration in equine synovial fluid as a marker of joint disease. *Can J Vet Res* 1995;59:205-212.

76. Todhunter RJ, Fubini SL, Freeman KP, et al. Concentrations of keratan sulfate in plasma and synovial fluid from clinically normal horses and horses with joint disease. *J Am Vet Med Assoc* 1997;210:369-374.

77. Adams ME, Matyas JR, Huang D, et al. Expression of proteoglycans and collagen in the hypertrophic phase of experimental osteoarthritis. *J Rheumatol Suppl* 1995;43:94-97.

78. Brommer H, Brama PA, Laasanen MS, et al. Functional adaptation of articular cartilage from birth to maturity under the influence of loading: a biomechanical analysis. *Equine Vet J* 2005;37:148-154.

79. Firth EC. The response of bone, articular cartilage and tendon to exercise in the horse. *J Anat* 2006;208:513-526.

80. Schmitz N, Laverty S, Kraus VB, et al. Basic methods in histopathology of joint tissues. *Osteoarthritis and Cartilage* 2010;18:S113-S116.

81. Camplejohn KL, Allard SA. Limitations of safranin 'O' staining in proteoglycan-depleted cartilage demonstrated with monoclonal antibodies. *Histochemistry* 1988;89:185-188.

82. Stewart R. A diagnostic imaging technique and therapeutic strategy for early osteoarthritis. Dissertation. *College of Engineering*. Boston, MA: Boston University, 2014; 1-180.

83. Jakobsen JA. Contrast media extravsation injury In: Thomsen HS,Webb JAW, eds. *Contrast Media: Safety Issues and ESUR Guidelines*. 3rd ed. New York, NY: Springer-Verlag, 2014;131-137.

84. Nelson BB, Goodrich LR, Barrett MF, et al. Use of contrast media in computed tomography and magnetic resonance imaging in horses: Techniques, adverse events and opportunities. *Equine Vet J* 2017;49:410-424.

CHAPTER 5:

EVALUATION OF CATIONIC CONTRAST-ENHANCED COMPUTED TOMOGRAPHY FOR THE LONGITUDINAL ASSESSMENT OF REPARATIVE AND DEGENERATIVE ARTICULAR CARTILAGE USING AN *IN VIVO* EQUINE CHONDRAL DEFECT MODEL

Introduction

Articular cartilage injury and the subsequent development of osteoarthritis are substantial concerns in horses and its detection and monitoring of healing remain a diagnostic challenge. One of the earliest changes in osteoarthritis is the loss of glycosaminoglycan (GAG) content within the extracellular matrix (ECM).[1,2] Alongside GAG degeneration and disruption of the collagen network, articular cartilage becomes structurally weaker with a decreased ability to resist joint loading forces.[3] This structural weakness leads to additional articular cartilage fibrillation, inflammation and further joint injury even with normal physiologic loading. The disease is progressive as intrinsic cartilage healing is limited. Therefore, detection of articular cartilage lesions prior to advanced joint degeneration is essential for successful therapy.[4] However, routine diagnostic methods cannot be used to detect this essential biochemical change, thereby limiting their usefulness for early detection.

Currently, MRI is the gold standard method for the evaluation and monitoring articular cartilage healing in horses and humans.[5-7] While MRI provides volumetric and whole joint assessment without ionizing radiation, its relatively high cost prevents widespread use in the initial clinical

assessment or during subsequent follow-up examinations to characterize the progression of healing.[8] Despite the recognized value of MRI, the evaluation of articular cartilage is still difficult in early disease states and can lead to false positive results.[4] It also becomes increasingly difficult if not impossible to evaluate higher portions of the horse's limb due to the large muscle mass surrounding the stifle and relatively small MRI coil diameters available.[6,9] Some specialized MRI sequences (delayed gadolinium enhanced MRI of cartilage (dGEMRIC) and T2 mapping) can be used to more thoroughly evaluate articular cartilage; however, both have limitations and do not overcome the longer scan time, relatively poorer resolution or ability to evaluate more proximal joints.[4] Although in most cases a safe procedure, general anesthesia is required for high-field (≥1.0 Tesla) MRI scans and are typically 45 – 60 minutes in duration. Therefore, a high-resolution imaging technique that can be used to assess articular cartilage matrix in a short time frame with high sensitivity is needed.

With the advent of multi-slice computed tomography (CT), costs and scan length have decreased while having improved spatial resolution compared to MRI.[10] Further benefits of CT include the ability to create multi-planar reconstructions after the patient has left the scanner. Reference lines can be orientated in an infinite number of locations to highlight areas of interest even after the scan has completed, while the plane captured with MRI is stationary and usually cannot be reconstructed without reducing spatial resolution. With higher spatial resolution and the larger gantry diameters, a more complete evaluation of proximal joints such as the stifle is possible with CT.[10,11]

Contrast agents are injected into the joint to outline articular structures for three dimensional imaging including contrast-enhanced computed tomography (CECT) and MR arthrography.[4] Anionic, iodinated contrast media (ICM) are injected intra-articularly and are capable of entering the articular cartilage ECM.[1] The amount of contrast agent that enters the ECM is dependent upon the fixed negative charge due to GAGs[1,12] and under normal circumstances (*i.e.* non-degenerative articular cartilage) repels the negatively charged anionic contrast. While anionic ICM vastly improves the contrast resolution of the CT image, evaluation of articular cartilage is still difficult, as only the surface can be evaluated.

Cationic ICM such as CA4+ are positively charged and are electrostatically attracted to the negatively charged GAGs allowing for higher uptake within the ECM. Since the measured cationic CECT attenuation is directly proportional to the amount of CA4+ present within the ECM it is also directly proportional to GAG content. Correlations between cationic CECT attenuation and GAG concentration are strong[13-17] and surpass those when using anionic ICM.[13-15,18,19] Cationic CECT attenuation also significantly correlates to measured mechanical properties (Chapter 4) and coefficient of friction of cartilage.[15-17] The successes of these *in vitro* experiments have justified further investigations in animal research models and have shown no adverse effects or toxicity to synovial tissues after CA4+ use (Chapters 3 & 4).[20,21] Despite these promising results, the ability for cationic CECT to characterize reparative tissue is unknown.

The objective of this study was to examine the capacity of cationic CECT to distinguish a continuum of articular cartilage disease states. The first hypothesis was that cationic CECT distinguishes between reparative, degenerative and normal equine articular cartilage, reflective of

the biochemical, mechanical, and histologic properties. The second hypothesis was that cationic CECT *in vivo* would distinguish these same disease states through sequential imaging examinations.

Materials and Methods

Study design

All *in vivo* experimental protocols were evaluated and approved by the Institutional Animal Care and Use Committee at Colorado State University (Protocol ID: 14-4907A, approval 3/28/2014). Seven juvenile and skeletally mature horses (aged 2-5 years) were included in the study. Prior to inclusion all horses had lameness examinations demonstrating a lack of lameness or femoropatellar joint compartment effusion. Radiographs were taken to exclude horses that had evidence of joint disease (*e.g.* osteophytes, subchondral bone defects, sclerosis or lysis). Prior to surgery, baseline lameness examinations with full limb flexion tests graded on the AAEP scale[22] and assessment of femoropatellar joint effusion was performed on a 5-point scale (0 = none, 4 = severe effusion) by an observer blinded to limb allocation.[23] The seven horses were allocated into two groups based on their duration in the study. Group I horses (n = 3) were enrolled for four months, while group II horses (n = 4) were enrolled for two months. These groups were created to establish varying levels of articular cartilage healing.

Clinical cationic CECT examination

The same customized density phantom created for the previous study (Chapter 4) was also used for this study. Briefly, varying concentrations of CA4+ contrast media (0.75, 1.5, 3, 6, 12 and 24 mg I/mL), iohexol contrast media (Omnipaque-350, GE healthcare, Princeton, NJ)(9.4, 18.8,

37.5, 75, 150 and 300 mg I/mL) and calcium hydroxyapatite (CaHA; Computerized Imaging Reference Systems, Norfolk, VA)(400, 800, 1000 and 1500 mg CaHA/cm^3) were used to standardize cationic CECT attenuation over multiple scans and permit conversion to biologically relevant tissue concentrations. Circular regions of interest (63 mm^2) were sampled at the same location on the phantom and were extended over 10 slices. The mean value (Hounsfield units, HUs) of each concentration cylinder from each component was plotted against the known concentration of the cylinder. A regression line was constructed with a coefficient of determination to establish the fit of the line.

The CA4+ was prepared as previously described (Chapter 3) at a concentration of 24 mg I/mL (400 mOsmol/kg, pH=7.4).[12] Before creating articular cartilage defects, baseline cationic CECT examinations were performed on both femoropatellar joints of each horse. Prior to each cationic CECT scan, each horse was sedated (detomidine hydrochloride and butorphanol tartrate: each 0.01 mg/kg IV) and both femoropatellar joints were aseptically prepared with betadine scrub and alcohol. Starting with the left femoropatellar joint, a synovial fluid sample was aspirated via lateral approach[24] and aliquots were placed into EDTA and serum tubes for cytologic and biochemical analysis, respectively. With the needle still in place 100 mLs of CA4+ was injected. Twenty minutes later the right femoropatellar joint underwent an identical protocol. The time delay was used to permit repositioning of the horse on the CT table between scan acquisitions. After the bilateral injections, the horse recovered from sedation and was placed in stall confinement until cationic CECT examination. The stent bandages were removed until after the cationic CECT examination because the compression of the cranial soft tissues influenced the intensity of attenuation in articular cartilage.

Approximately 3.5 hours after CA4+ injection, general anesthesia was induced with ketamine (2.2 mg/kg IV) and diazepam (0.1 mg/kg IV) and maintained on isoflurane in 100% oxygen. The horse was placed in left lateral recumbency with the left leg tied in extension on the CT table.[10,11] The custom density phantom was placed 5 cm distal to the tibial tuberosity and aligned parallel to the CT gantry. Then, the cationic CECT scan was acquired four hours after CA4+ injection. The cationic CECT parameters of all acquisitions were: 140 kVp, 550 mAs, 0.8 mm x 0.8 mm slice thickness, 30 cm field of view, 1024 x 1024 matrix, 0.6 helical pitch facilitating in-plane resolution of 0.292 x 0.292 mm. The CT data was reconstructed with a sharp (B70f) reconstruction bone kernel (0.8 mm slice thickness) for improved spatial resolution and bone detail and as a soft tissue reconstruction kernel (2 mm slice thickness) to improve signal-to-noise ratios. After the left stifle was scanned, the horse was alternated into right lateral recumbency and the right stifle was scanned with the same protocol as described for the left ensuring the acquisition time was four hours after CA4+ was injected into the right femoropatellar joint. The cationic CECT scans were repeated every 14 days until the study endpoint (Group I: nine scans per joint; Group II: five scans per joint). The clinical scans were identified in relation to defect creation as follows: baseline (T0) and two weeks (T1), four weeks (T2), six weeks (T3), eight weeks (T4), ten weeks (T5), 12 weeks (T6), 14 weeks (T7) and 16 weeks (T8) after defect creation.

Creation of chondral defects via arthrotomy

After the baseline cationic CECT examination, the horse was moved to the surgical suite, placed in dorsal recumbency and routinely prepared for aseptic surgery. A cranial arthrotomy was performed on both femoropatellar joints.[23] One femoropatellar (defect) joint in each horse was

randomly allocated (block randomization using Microsoft Excel) to receive two critically sized 15 mm circular chondral defects on the medial trochlear ridge of the femur.[23,25,26] The contralateral femoropatellar (control) joint in the same horse underwent arthrotomy to ensure no articular cartilage damage, though no defects were created. Of the two chondral defects in the defect joint, one was randomly assigned to have calcified cartilage retained (Repair 1), while the second defect had calcified cartilage removed (Repair 2). This was done to establish two reparative articular cartilage sample groups. The two chondral defects were separated from one another by 10 mm. Each defect was classified as proximal or distal and was also determined through block randomization approaches. Subchondral bone microfracture was not performed to avoid penetrating the subchondral bone plate and avoided the potential influence of the subchondral bone in the evaluation of cationic CECT.[27] The arthrotomy incision was closed in four layers (joint capsule – 2-0 polyglaction 910, deep and superficial fascia – 0 polyglactin 910, subcutaneous tissue – 2-0 polyglactin 910, all with continuous patterns; and skin with simple interrupted sutures of 2-0 nylon). Stent bandages were placed over the incision for anesthetic recovery and maintained until suture removal. Peri-operative antibiotics (ceftiofur sodium, 2.2 mg/kg IV q12hrs) were administered for 5 days. After surgery, the horse was maintained on stall confinement (12 x 12 feet) until the incisions were healed 12 days after surgery at which time the sutures were removed. The horses were then turned out to a large paddock for free exercise.[25]

Synovial fluid assessment

Immediately after collection, the total protein of synovial fluid was measured using a refractometer and recorded in g/dL. Then, the remaining fluid was centrifuged at 1,000 G for 10 minutes. The supernatant was aspirated, stored in a micro-centrifuge tube and frozen at -80 °C

until further biochemical analysis. Total leukocyte cell counts were determined from the EDTA sample using a benchtop hematology analyzer and leukocyte differential percentages were calculated. If a limited amount of fluid was obtained (<1 mL), then the sample in the serum tube was prioritized.

Biochemical analysis of the synovial fluid included determination of GAG content using the 1,9-dimethylmethylene blue (DMMB) binding assay and prostaglandin E_2 (PGE_2) concentrations using a commercially available immunoassay kit (Enzo Life Sciences, Inc. Farmingdale, NY).[2,28,29] The frozen aliquots of synovial fluid were thawed and the GAG samples were analyzed using the DMMB assay after papain digestion.[2] The DMMB assay was performed using a standard curve generated with known concentrations of chondroitin C sulfate. Samples were prepared in triplicate and read on a microplate reader (SpectraMax M3, Molecular Devices, Sunnyvale, CA), set at a wavelength of 530 nm. Using a fit quadratic curve, the mean absorbance of all samples was determined and a mean calculated for each sample. The PGE_2 quantitation was performed by first extracting it from synovial fluid through use of C2 columns (Amprep mini-columns ethyl C2 columns, GE Healthcare Co, Pittsburgh, PA). Then, the samples were processed using a commercial assay kit with a minimum detection rate of 13.4 pg/mL (Enzo Life Sciences Inc., Farmingdale, NY). Samples were run in duplicate and read on a microplate reader set at a wavelength of 405 nm. A mean value was reported for each sample. Samples from the DMMB and PGE_2 assays were repeated if the standard curve $R^2 < 0.9$ or if the coefficient of variation between replicates was > 0.1.

Clinical assessments

After baseline, lameness examinations and assessments of femoropatellar joint effusion were repeated every two weeks until the end of the study by the same blinded investigator as described above. Synovial fluid aspirates were also repeated every two weeks until the end of the study and analyzed as described above. Lameness and effusion assessments were always performed prior to arthrocentesis and joint injection procedures to avoid potential influences caused by those techniques.

Postmortem assessments

At the study endpoint, the cationic CECT examination of both stifles was repeated and the horse was euthanized under general anesthesia (pentobarbital 86 mg/kg IV). The stifles were removed by transecting the femur and tibia at the mid-diaphysis preserving the soft tissues over the stifle joint compartments. Postmortem MRI examinations were performed in a 1.5 Tesla MRI (GE Signa 9.1 LX MR instrument, GE Healthcare, Waukesha, WI) using the following sequences: proton density (with and without fat suppression), T2-weighted, and T1-weighted fast spin echo and T1-weighted spoiled gradient recalled echo. Proton density sequences with and without fat suppression were also generated at oblique transverse planes to improve spatial resolution at the curvilinear surface of the medial trochlear ridge of the femur, which is susceptible to volume averaging.

After MRI, the stifles were placed on a custom stand and arthroscopic examination of the femoropatellar joint was performed.[30] Arthroscopic scoring of each of the defects included: percent of repair tissue (0-4; 0%, 1-25%, 26-50%, 51-75%, 76-100%), cartilage and bone

attachment (0-4; normal, moderate, mild, slight, none), firmness (0-4; similar, slightly soft, mildly soft, moderately soft, markedly soft compared to normal articular cartilage), level (1-6; mildly recessed, slightly recessed, level, slightly elevated, mildly elevated, moderately elevated), International Cartilage Repair Society (ICRS) score (0-4; normal, nearly normal, abnormal <50% depth, severely abnormal >50% depth, severely abnormal – through subchodral bone),[31] Outerbridge score (0-4; normal, softening, partial thickness 1.5 cm diameter, fissuring >1.5 cm diameter, subchondral bone),[32] blood (1-3; fresh, old, none), shape (0-1; no increase, degeneration beyond defect), color (1-6; red, red/white, yellow, yellow/white, white/yellow, white), surface (1-4; non-undulating, slightly undulating, mildly undulating, moderately undulating) and grade (0-4; no tissue, poor, fair, good, excellent). During arthroscopic examination, three 4.5 mm diameter osteochondral biopsies (L50343786, Smith & Nephew Inc., Fort Worth, TX) were collected from the distal femoral trochlea (medial and lateral trochlear ridges and femoral groove) and a sample from the apex of the patella was collected with a Ferris-Smith rongeurs. These four samples were placed in 1x PBS for chondrocyte viability assessment. Samples of synovial membrane were collected from each joint with a Ferris smith rongeurs, placed in histology cassettes and put into 10% formalin. After arthroscopic scoring and biopsy sample collection, the arthroscopic portals were closed with 2-0 nylon and the stifle was frozen at -20 °C until further evaluation.

The tissues undergoing cell viability assessment were processed immediately following arthroscopic examination. A diamond tip bladed saw (EXAKT 300 CP, Exact Technologies, Inc., Oklahoma City, OK) was used to cut the osteochondral biopsies into 1.5 mm thickness samples using constant water irrigation to prevent tissue heating, followed by placement into 1 x

PBS. Assessment of chondrocyte viability was performed using a commercial assay (Live/Dead Viability/Cytotoxicity Kit, Life Technologies, Grand Island, NY). Mixtures of calcein acetoxymethyl ester (1:2000) and ethidium bromide homodimer (1:3000) in 1 x PBS were added to plate wells with the osteochondral tissue and were incubated for 30 minutes in the dark at 20 °C.[33] The tissue was then examined under an inverted and automated confocal microscope (Olympus IX83, Olympus Life Science, Center Valley, PA) equipped with a digital camera acquisition system. Microscopic images were captured of the entire sample (superficial through deep zones) at 10X magnification and collected in a Z-stack of 10 images (20 μms between stack images). Images were analyzed using commercial software (Count & Measure module, CellSens Dimension v.1.16, Olympus Life Science). Viable and non-viable cells were counted separately through an automated protocol after establishing an intensity and threshold-based segmentation. The same protocol and threshold process was instituted over all samples. The percentage of live cells out of the total number of counted cells was reported for each articular cartilage site.

Each stifle was thawed individually and all mechanical testing and microCT imaging assessments were performed prior to thawing the subsequent joint to prevent the tissue degradation that could occur following multiple freeze-thaw cycles. For each horse, the defect joint was processed first followed by the control joint in order to ensure biopsies were collected at similar locations within each horse. After thawing, osteochondral plug biopsies (7 mm internal diameter) were collected along the femoropatellar surfaces using a diamond tipped cylindrical coring drill bit (Starlite Industries, Bryn Mawr, PA) attached to a drill press (Delta Power Equipment Company, Anderson, SC) under constant water irrigation to prevent overheating. In the defect joints, 14 osteochondral cores were harvested; 2 within each defect, 2 immediately

adjacent to each defect (adjacent location), and 2 from the lateral trochlear ridge of the femur and 4 on the patella (2 medial and 2 lateral)(remote location). These same 14 biopsies were collected in the control joints at the same locations. In total, 196 osteochondral biopsy plugs were collected. After coring, each sample was immediately lavaged with 400 mOsmol/kg saline to regain normal tonicity. Each osteochondral biopsy was graded macroscopically on the Outerbridge[32] and ICRS[34] scoring systems for macroscopic cartilage damage. After each osteochondral plug was removed and macroscopically scored, it was allowed to equilibrate overnight with 0.9% saline in a preservative cocktail containing protease inhibitors, antibiotics, and antimycotics (5 mM Benzamidine HCl, 5 mM EDTA both of Sigma-Aldrich, St. Louis, MO; 1x Antibiotic-Antimycotic, Life Tech, Carlsbad, CA) at room temperature to remove any residual CA4+ present within articular cartilage at the time of euthanasia. After saline equilibration, mechanical testing was performed.

Mechanical testing

The compressive stiffness of articular cartilage is attributed to GAGs and from a fluid phase permitting free flow diffusion of water and solutes in and outside of the tissue. The dynamic elastic response results mainly from the interstitial fluid resisting tissue loading and collagen fibril network resisting tensile forces and shape alterations.[35,36] Articular cartilage degeneration reduces the equilibrium compressive (Young's) modulus (EM) and incremental dynamic (Young's) modulus (DM).[35,36] A stress-relaxation compressive regimen was performed on 12 samples from the defect joints and 8 from the control joints. The remote – lateral patella and defect samples in the control joints were not tested. The defect sites in the defect joint were tested though the measured results were below the threshold of detection (*i.e.* the 5 Newton (N)

preload overwhelmed reparative cartilage and measurements were reflective of the subchondral bone plate and were subsequently excluded). On the day of and prior to mechanical testing, the thickness of the articular cartilage on each osteochondral biopsy was determined with microCT (μCT40, Scanco Medical AG, Brüttisellen, Switzerland) using the following parameters: 70 kVp, 113 μA, 300 ms integration time and 36-μm isotropic voxel resolution. The imaging data was imported into MATLAB (R2017a, Mathworks, Natick, MA). The average thickness of the plug was determined by using nine circular regions-of-interest comprising ~2850 individual thickness measurements from the superficial surface to the subchondral bone using a customized program.

After the determination of articular cartilage thickness, each plug was rigidly clamped in a mechanical testing apparatus (Enduratec3230, BOSE, Eden Prairie MN) and a compressive 5 N pre-load was applied to the articular cartilage surface in unconfined compression using a nonporous ultrahigh molecular weight polyethylene platen while immersed in 400 mOsm/kg saline solution. The stress-relaxation regimen for each plug consisted of four incremental 5% compressive strain steps (0.333 %/sec) with stress relaxation (45 minutes) between strain steps. A collection rate of 10 Hz was used to record the force and displacement data, and a linear fit to stress versus strain at each equilibrium step was used to calculate the EM and incremental DM[37] for each cartilage specimen using a custom program (MATLAB).

Cationic CECT (microCT)

After mechanical testing, all osteochondral plugs were immersed in CA4+ (24 mg I/mL, approximately 20 times the articular cartilage volume) for 24 hours at 20 °C, known to exceed the required equilibration time under these settings (Chapter 2).[20] Then, the plugs were imaged

using microCT at the same above settings. The cationic CECT images were converted into DICOM format and imported into Analyze® software (version 12.0, Biomedical Imaging Resource, Mayo Clinic, Rochester, MN). A semi-automatic threshold-based segmentation procedure was performed with manual correction to ensure accurate segmentation of the articular cartilage volume from the subchondral bone and air. The cationic CECT signal intensity in each osteochondral plug was converted into the linear attenuation attenuation coefficients and then to Hounsfield units (HUs) using a sample of deionized water concurrently scanned with the plugs (Equation 2.1). The mean HU for each articular cartilage plug was recorded.

After microCT, the osteochondral plugs were again equilibrated overnight in saline with the preservative cocktail to remove any residual CA4+ that could contribute to inaccuracy in forthcoming assessments of GAG content. The cartilage of each circular biopsy was bisected and the articular cartilage from one side was removed from the subchondral bone using a scalpel blade, while the remaining cartilage portion (still attached to bone) was placed in 10% formalin in preparation for histologic analysis. The portion of removed cartilage was again cut in half. One portion (1/4 of total cartilage surface) was minced and placed in a tube assigned for GAG evaluation while the other quarter portion was similarly prepared for assessment of total collagen content. All samples were weighed to determine a hydrated (wet) weight and were then lyophilized for 24 hours and weighed again to determine dry weight. The samples were stored at -80 °C until further biochemical analysis.

Biochemical and histological analyses

The biochemical content (GAG and total collagen) of the articular cartilage from each osteochondral biopsy was determined using the DMMB and hydroxyproline assays, respectively. For GAG quantitation, the lyophilized cartilage was removed from the -80 °C freezer and digested in papain (1 mg/mL) overnight at 65 °C. The papain digestion solution was made in a mixture of 50 mM NaH_2PO_4, 5 mM EDTA and 2 mM dithiothreitol adjusted to a pH of 6.8. The digested samples were evaluated with the DMMB assay as described under synovial fluid evaluation, though were first diluted 1:20 with incomplete (without papain) digestion buffer to more closely be in the center of the generated standard chondroitin sulfate curve. The mean GAG concentration of each sample was standardized to a wet weight basis. For determination of total collagen content, the lyophilized articular cartilage was also digested in papain before undergoing the hydroxyproline assay.[38] The sample was diluted 1:20 and hydrolyzed with an equal volume of 12.1 N HCl for 16 hours in a dry oven set at 110 °C. The samples were evaporated on a heating block set at 60 °C overnight. The samples along with known hydroxyproline standard concentrations were pipetted into a tissue culture plate in duplicate. Chloramine T reagent was added to the samples and hydroxyproline standards and were incubated for 20 minutes at 25 °C. The 4-dimethyl-aminobenzaldehyde reagent was added to all samples and standards and the plate incubated at 60 °C for 15 minutes followed by 5 minutes at 25 °C. Then the plate was read at 550 nm. The hydroxyproline concentrations for each sample were determined from the standard curve and reported as a mean. Total collagen was determined from hydroxyproline using an established conversion (13.2 mg hydroxyproline /100 mg collagen type II)[39] and standardized to dry weight.

Histologic evaluation

The osteochondral and synovial membrane samples were prepared routinely for histologic evaluation. After seven days in 10% formalin the osteochondral samples were transferred into 70% ethanol until decalcification. The osteochondral samples were decalcified in EDTA (Formical-2000, Statlab, McKinney, TX) for seven days and then rinsed in 1 x PBS prior to undergoing further histologic processing. After processing (Appendix I.1), both the synovial membrane and osteochondral tissue samples were embedded in paraffin and using a microtome (Leica RM2255, Leica Biosystems, Buffalo Grove, IL), five μm sections were prepared on microscope slides. The synovial membrane and osteochondral samples were each stained with hematoxylin and eosin and a second slide of the osteochondral samples was stained with safranin-O fast green (SOFG)(Appendix I.2). Control tissues (bovine trachea and equine osteochondral samples) were stained with all groups to control for variation across batches.

The sections of synovial membrane were scored for grades of cellular infiltration, intimal hyperplasia, and subintimal vascularity, edema and fibrosis (grade 0 – 4; 0 = normal, 4 = marked) using the Osteoarthritis Research Society International (OARSI) scoring system.[40] The articular cartilage was graded on the ICRS II scale.[41] Briefly, each component (tissue morphology, matrix staining, cell morphology, chondrocyte clustering, surface architecture, basal integration, tidemark formation, subchondral bone abnormalities, inflammation, abnormal calcification, vascularization in repair tissue, superficial zone assessment, middle/deep zone assessment, and overall assessment) was graded on a continuous scale 0 – 100 (0 = poor, 100 = excellent) akin to a visual analog scale.[41]

Clinical cationic CECT evaluation

Following removal of all osteochondral plug biopsies, the cored mask of the femoral trochlea was imaged with a cone beam CT system (Pegaso, Epica Medical Innovations, San Clemente, California) to provide a template for accurate comparisons between the biochemical and histological data to imaging (cationic CECT and MRI) parameters. The cone beam CT settings were 70 kVp, 70 mA, 5 ms, 220.8 mm field of view and 736 x 736 matrix, permitting isotropic voxel dimensions of 0.3 mm^3. Using the 3-D voxel registration module (Analyze® software), the post-coring mask from each joint was manually aligned over each respective clinical imaging scan. Using this template, an object map was generated consisting of digitally segmented articular cartilage over the identical location where osteochondral plugs were removed. This generated object map was applied to all scans obtained on the same limb. The segmented ROIs were verified to ensure the captured volume only contained articular cartilage and not the subchondral bone or articular soft tissues. The cationic CECT attenuation was measured and reported in HUs and the volume (mm^3) and area (mm^2) from the ROIs were recorded. Density phantom correction was performed for each of the three components (CA4+, iohexol and CaHA) to account for CT attenuation drift between scans.

MRI evaluation

The same post-coring mask scan used in the clinical cationic CECT scans was also co-registered with the MRI images. Generating cursors in the trabecular bone provided a way to create an object map outlining the same location on the MRI images where the osteochondral plugs were removed to avoid influencing MRI interpretation during subjective assessment. These object maps were applied to each MRI sequence and acquisition plane. A board certified radiologist

blinded to group allocation (impact vs control joint) performed all scoring. The articular cartilage at each site was subjectively scored for volume/fill (0: 100%, 1: 75 to <100%, 2: 50 to <75%, 3: 25 to <50%, 4: <25% fill), trabecular bone sclerosis (0: none, 1: mild, 2: moderate, 3: severe) and for T2, T1 and PD with fat saturation signal intensity (0: none, 1: mild, 2: moderate, 3: severe).

Data and Statistical analysis

Categorical data were reported as median ± interquartile range (IQR) or range and continuous data as mean ± standard deviation (s.d.). Continuous data were evaluated for normality, by using a Shapiro Wilk test and visually using histograms and quantile-quantile plots. Nonparametric tests or log transformation methods were used in the event data were not normally distributed. Comparisons of continuous variables were performed using a Spearman rank correlation. The strength of correlation was reported based on an established scale with a minor naming modification – slight: 0.0 to 0.20, fair: 0.21 to 0.40, moderate: 0.41 to 0.60, strong: 0.61 to 0.80, very strong: 0.81 to 1.0.[42]

Continuous outcome variables were evaluated between and within joints using a mixed-effects model ANOVA with the individual horse as a random effect. When measurements were performed over time, the repeated measures were accounted for in the model. Ordinal outcome variables were evaluated using ordered logistic regression. The overall model P – value was examined first and if significant, multiple pairwise comparisons were evaluated with Tukey-Kramer adjustments if more than three comparisons were made. Synovial membrane histology scores were compared between joints using a Wilcoxon signed rank test. Cell viability

assessments were compared with a paired t-test. Horse group (I and II) designations were evaluated in all postmortem statistical assessments to determine the potential influence of this component of the study design. A significant difference was only detected in the vascularity component of the ICRS II histology score. Therefore, this group designation was not included as a covariate in further statistical analyses. Statistical analyses were performed using commercial software (SAS University Edition, v. 9.2, SAS Institute Inc., Cary, NC) and significance was defined as $P<0.05$.

Results

All surgical defects were created as expected without complication. One joint in one horse developed partial dehiscence of the arthrotomy incision 14 days after surgery. A passive (penrose) drain was placed along with local wound treatment. The incisional dehiscence healed by second intention over 2 weeks. All other incisions healed without incident.

Clinical cationic CECT examination

In one clinical cationic CECT scan in one horse, the CT table malfunctioned and the imaging scan had to be aborted. This scan was repeated 3 days later without complication. All other cationic CECT examinations were performed on exact two-week intervals as scheduled. Minimal but consistent periarticular extravasation was observed in the subcutaneous tissues surrounding the CA4+ injection site. This did not prevent full femoropatellar joint distention in any joint. All cases of CA4+ extravasation resolved within four hours and no horse showed signs of discomfort on palpation of the region. In two horses at the first time point (T1) there was subjectively a diffuse decrease in CT attenuation across all articular surfaces in both joints. This was

determined to be from the stent bandages being replaced after CA4+ injection. The cranial compression of soft tissues from the bandages was suspected to reduce CA4+ contact with the articular cartilage. When the stents were not replaced until after the cationic CECT scan was completed, this effect was not observed again.

Synovial fluid assessment

There was no significant difference in synovial fluid leukocyte counts or differential (lymphocytes, monocytes, or neutrophil) percentages between joint groups or over time (Table 5.1 – A - D). There was a significant difference in synovial fluid TP concentrations over time ($P = 0.0002$), but not between joint groups ($P = 0.49$)(Figure 5.1 – A). There was no significant difference in synovial fluid GAG or PGE_2 concentrations between groups or over time (Figure 5.1 – B & C).

Clinical assessments

In horse group I, two of the three horses exhibited a marked increase in synovial effusion scores in both defect and control joints. These severe grades were observed starting six to eight weeks after surgery and persisted until the group I endpoint at 16 weeks. Group II horses did not develop this same effect, though their effusion scores were gradually increasing in both defect and control joints similar to that observed in group I at the six to eight week time points. Ten out of 14 joints developed moderately sized seromas on the cranial aspect of the stifles centered over the arthrotomy incisions after the horses were allowed free exercise.

There was not a significant difference in lameness scores between joint groups (P = 0.10) or over time (P = 0.20)(Figure 5.2 – A). There was not a significant difference in synovial effusion scores between groups (P = 0.85), but there was a significant effect over time (P < 0.0001)(Figure 5.2 – B). There was no significant difference in the response to stifle flexion scores between groups (P = 0.32), but there was a significant change in scores over time (P = 0.001)(Figure 5.2 – C). There was no significant difference in stifle range of motion scores between groups (P = 0.54), but there was a significant effect over time (P < 0.0001)(Table 5.2 – D).

Postmortem assessments

Postmortem arthroscopy scores of the defects are shown in Table 5.2 and postmortem photographs at the time of osteochondral biopsy harvest are shown in Figure 5.3. In the repair 1 samples, there were minimal and irregular amounts of tissue filling the defects, while there was more complete filling of repair tissue in the repair 2 group samples. At postmortem assessment, the perimeter of the circular defects was irregular and visually different from the sharp edges observed at the end surgery indicative of peridefect deterioration. The articular cartilage adjacent to the defects was thinned and increased radially in thickness and in health as the distance from the defect increased. The articular surfaces of the patella and lateral trochlear ridge in the defect joints and in all surfaces of the control joints were smooth and healthy in appearance (ICRS = 0).

There was no significant difference in cell viability assessments between groups I and II. Mean cell viability measurements between the defect and control joints were not significantly different (87.5 ± 4.8% and 86.8 ± 5.5%, respectively)(P = 0.59). Aside from one component of the ICRS

II histology score (see below) none of the other microCT, GAG, mechanical or histologic data outcomes were significantly different between group I and II horses. Therefore, horse group was not included as a covariate in further statistical models.

Mechanical testing

The mechanical testing results from the repair 1 and 2 groups were not accurate. The mechanical testing protocol consistently compressed all reparative cartilage during the 5 N preload instituted to equilibrate the tissue before the stress-relaxation regimen began. Therefore, the measurements from these two groups were excluded restricting comparisons of mechanical data to the adjacent and remote samples in the defect and control joints. However, based on the geometry of the plug and the applied preload this suggests that the repair tissues from the defect joints have a compressive stiffness < 0.13 MPa.

There was a significant effect of sample location on EM ($P = 0.006$). In the defect joints, the adjacent samples had lower EM than remote samples ($P < 0.0001$)(Figure 5.4 – A). There was also a significant difference in EM between the defect and control joints at the adjacent sites ($P = 0.04$), but not at the remote sites ($P = 0.73$)(Figure 5.4 – A). There was a significant effect of sample location on DM at 5% strain ($P = 0.03$). In the defect joints, the adjacent samples had lower DM at 5% strain than remote samples ($P = 0.03$). There was a significant difference between the defect and control joints at all levels of strain in the adjacent sites (all $P \leq 0.03$), but not in the remote sites (Figure 5.4 – B & C).

Cationic CECT (microCT)

The CA4+ distribution throughout the articular cartilage samples varied based on disease state (Figure 5.5) and there was a significant effect of sample location on cationic CECT attenuation (microCT)($P < 0.0001$)(Figure 5.6 – A). In the defect joints, the mean cationic CECT attenuation between the repair 1 and repair 2 groups was not different, but there were significant differences between each defect and all other sample sites. The mean cationic CECT attenuation (microCT) in the defect joints was significantly lower than the control joints at each sample site except for the remote location (Figure 5.6 – A). There was a strong correlation between cationic CECT attenuation (microCT) and GAG content ($\rho = 0.76$, $P < 0.0001$) and EM ($\rho = 0.78$, $P < 0.0001$)(Figure 5.7 – A & B).

Biochemical analyses

There was a significant effect of sample location on GAG ($P < 0.0001$) and total collagen ($P = 0.04$) concentrations (Figure 5.6 – B & C). Grouping of these data by ICRS macroscopic score, shows ICRS scores 2 – 4 have very low cationic CECT attenuation and GAG content while scores 0 – 1 have a fair amount of overlap (Figure 5.7 – A & B). There was a significant effect of EM and GAG on cationic CECT attenuation (microCT)(both $P < 0.0001$).

Histologic evaluation

The vascularity component of the ICRS II histology score was significantly different between groups I and II. For the repair 2 tissue, the mean group II score was higher than group I ($P = 0.002$). The repair 1, adjacent and remote sample sites were not significantly different between group I and II ($P = 0.45$, $P = 0.99$, $P = 0.99$, respectively).

There was a significant effect of sample location on the following ICRS II scoring parameters: tissue morphology ($P < 0.0001$), matrix staining ($P < 0.0001$), cell morphology ($P < 0.0001$), chondrocyte clustering ($P < 0.0001$), surface architecture ($P < 0.0001$), basal integration ($P < 0.0001$), tidemark formation ($P < 0.0001$), subchondral bone abnormalities ($P < 0.0001$), abnormal calcification ($P = 0.002$), vascularization ($P < 0.0001$), surface assessment ($P < 0.0001$), mid/deep zone assessment ($P < 0.0001$) and overall assessment ($P < 0.0001$). There was no significant effect of sample location on the inflammation score ($P = 0.57$)(Appendix Figure II.1). When SOFG staining was analyzed by tissue depth, there was a significant effect of sample location on SOFG scores in the middle ($P < 0.0001$), deep territorial ($P = 0.004$) and deep interterritorial ($P = 0.003$) zones, but not in the superficial zone ($P = 0.06$)(Appendix Figure II.1). The majority of individual scoring components from the ICRS II system had significant moderate correlations with cationic CECT attenuation (microCT)(Table 5.3). These correlations from the defect joints and grouped by sample location are shown in Figure 5.8.

The median (IQR) synovial membrane scores in defect and control joints were: cellular infiltration (2 (1 – 2) and 2 (1.5 – 2.5), respectively), vascularity (2 (1 -2) and 2 (2 – 2), respectively), intimal hyperplasia (2 (1 – 2) and 2 (2 – 2), respectively), subintimal edema (1 (1 – 2) and 1 (0.5 – 2), respectively) and subintimal fibrosis (2 (1.5 – 2) and 2 (2 – 3), respectively). There were no significant differences in synovial membrane scores between joint groups.

Clinical cationic CECT evaluation

The clinical cationic CECT images all showed increased attenuation indicative of high uptake of CA4+ within articular cartilage. Articular cartilage from the femoral trochlea and patella were

consistently distinguishable from the subchondral bone and intraarticular soft tissues at all time points. In the defect joints, there was a void in articular cartilage attenuation at each defect location on the medial trochlear ridge at the week two scan. In the defect bed at two weeks, a hypoattenuating line relative to the joint soft tissues began to emerge at the subchondral bone interface with minimal enhancement with CA4+. Over the subsequent scans the attenuation in this location increased representative of CA4+ uptake and indicative of reparative tissue in the defect bed. From four weeks after defect throughout the end of the study, there was not a substantial change in cationic CECT attenuation in the reparative tissue.

Correction of clinical cationic CECT attenuation to the density phantom components revealed stronger correlations after conversion to CA4+ and CaHA concentrations than with iohexol. There was a significant moderate correlation between clinical and microCT cationic CECT attenuation ($\rho = 0.52$, $P < 0.0001$)(Table 5.4). When analyzed by defect and control joints, the correlation was stronger with defect joint data (Figure 5.9 – A). There was also a significant fair correlation between clinical cationic CECT attenuation and GAG content and EM ($\rho = 0.39$, $P < 0.0001$; $\rho = 0.36$, $P = 0.0003$; respectively)(Table 5.4 and Figure 5. 9 – B & C).

There was a significant moderate correlation between clinical cationic CECT attenuation and tissue morphology ($\rho = 0.57$, $P < 0.0001$), whereas most other ICRS II parameters had a significant fair correlation to clinical cationic CECT attenuation (Table 5.4). Comparing defect to control joints, there was a significant difference between clinical cationic CECT attenuation and GAG ($P < 0.0001$), EM ($P = 0.04$) and overall ICRS II histology score ($P = 0.0002$) (Figure 5.9).

Attempts to standardize clinical cationic CECT attenuation to articular cartilage volume did not improve the strength of correlations with other variables (data not shown).

Compared to the control joints, there was a decrease in clinical cationic CECT attenuation in defect joints at most time points after baseline (2, 4, 6, 8, 10, 12 and 16 weeks after surgery). There was also a significant difference in mean clinical CECT attenuation between defect and control joints at all time points except baseline and 10 weeks after surgery (Figure 5.10). Two weeks after defect, there was minimal cationic CECT attenuation in the defect, though this changed over time consistent with tissue emerging in the defect bed suggestive of reparative tissue (Figure 5.11). The locations adjacent to the defect had an observable decrease in cationic CECT attenuation over time despite maintaining similar tissue volume (Figure 5.11). The clinical cationic CECT attenuation in the sample sites of the defect joints showed significant differences between reparative tissue (repair 1 or 2 groups) and adjacent and remote samples at most time points (Figure 5.12). These differences were not significant at 10, 12, or 14 weeks, but again reemerged at 16 weeks after surgery.

Starting at six weeks after the creation of defects, there was a significant decrease in clinical cationic CECT attenuation in adjacent samples compared to the remote sites and this difference persisted through the eight week scan. Evaluating the individual sample sites over time, the largest change was observed at all time points after baseline in repair 1 and 2 groups and was also observed at six weeks after defect in the adjacent samples (Figure 5.13).

MRI evaluation

The articular cartilage defects were easily detected on MRI sequences. The lack of MRI signal changes in the control joints required the following analyses to be examined only within the defect joints. Though statistical comparisons could not reliably be made, there was a clear difference in the use of MRI to distinguish the defect joints from control joints. The mean T2 and T1 signal intensity scores in the repair 1 and 2 defects were scored higher in the defect joints compared to the scores from the PDFS sequence or subchondral bone sclerosis scores beneath the defects (Figure 5.14). While scores from within the defect were commonly different than the adjacent and remote sites, the mean scores were not significantly different between repair 1 and 2 groups for any sequence. The mean clinical cationic CECT attenuation was evaluated at each level of MRI intensity score (Figure 5.15). There was wide variation in clinical cationic CECT attenuation values across scores.

Discussion

The results of this experiment supported the first hypothesis that cationic CECT is capable of distinguishing articular cartilage across disease states. While other studies have examined cationic CECT in degenerative cartilage (Chapter 4),[13,43] this study showed that reparative tissue could be segregated from early degenerative and normal articular cartilage. Additionally, the cationic CECT attenuation values were highly associated with articular cartilage GAG content, EM and histologic scores, representing a way to distinguish articular cartilage quality based on internal biochemistry and structural and mechanical attributes. Notwithstanding the separation of reparative from degenerative and normal tissue, cationic CECT was unable to consistently distinguish between the repair 1 and 2 groups. Similarly, no individual ICRS II scoring

parameters or the overall scores were capable of distinguishing between these two repair groups. Therefore, the implored study design did not provide an opportunity to discern these two reparative groups using the outcomes measured in this study.

Another intriguing result of this study was cationic CECT attenuation (microCT) reflected many histological scoring components, particularly the scores reflecting regional depth. Since articular cartilage is a heterogeneous tissue, classification of its integrity as a conglomerate score or measure could impart inaccuracy. However, the results of this study show that the zonal characteristics were still estimated through the microCT. A more detailed investigation of depth dependent assessments measured with cationic CECT should be pursued. Similar to that observed in the impacted articular cartilage study (Chapter 4), the amount of SOFG staining in the ICRS II score was highly linked to cationic CECT attenuation owing to the similar mechanism of action of cationic molecules on GAG charge.[44] While histologically the reparative groups did not take in any SOFG stain, there was diffusion of CA4+ into these tissues on microCT. This disparity can be attributed to the differences between microCT and histology (volumetric vs planar assessment, effect of Gibbs-Donnan equilibrium attracting CA4+ with water into the tissue volume and the lack of evacuating CA4+ that potentially occurs with safranin –O dye in the ethanol steps of histological staining).[45,46] While it is logical for cationic CECT attenuation to reflect GAG content, additional correlations with other parameters outside of the extracellular matrix (*e.g.* chondrocytes, subchondral bone) are less clear. With the progressive nature of osteoarthritis the extension of injury beyond articular cartilage into bone is well documented and the chondrocytes that produce GAGs also degenerate with disease progression.[47-50] Considering the overlap that exists across histologic parameters and their

interaction with one another (*e.g.* co-linearity) throughout the disease process explains these significant correlations.

Contrary to the results from the impact study (Chapter 4), the individual zonal scores of SOFG staining with cationic CECT (microCT) attenuation were not as strong. The superficial zone was not significantly correlated to cationic CECT attenuation (microCT). The other zonal scores were significantly correlated with cationic CECT attenuation although were weak. This could be explained by a few factors. While the superficial zone inherently has lower amounts of GAG and therefore picks up less stain relative to deeper zones, the lack of SOFG uptake in the reparative group samples further complicates the distinction between reparative and healthy tissue groups. There is also variability between staining batches and subjectively, these samples had lower stain uptake than other tissues despite undergoing the same experimental protocol and histologic processing steps (Chapter 4). Different histologic scoring systems were used between studies; and the categorical grades used for the OARSI scale and continuous grades used in ICRS II could also explain this disparity.[40,41] Despite this perceived variation, the control tissue samples stained consistently across batches.

Collagens are responsible for preventing shear forces at the articular cartilage surface and DM is a mechanical measure representative of collagen content in the tissue.[51,52] While EM indicates the compressive strength of the tissue, the DM should reflect tensile strength.[51,52] The hydroxyproline assay was used to quantify total collagen content; however, there was not a significant correlation between this measurement and DM.[36] A potential explanation for this lack of association is in the sampling methods used for outcome analyses. While errors in performing

the hydroxyproline assay were considered, the amount of collagen detected in the assay were the amounts expected on a dry weight basis.[53] The portioning of tissues on each plug could explain this lack of a correlation between collagen and DM. Cationic CECT microCT imaging and mechanical testing assessments were made on the entire plug, whereas GAG, total collagen and histologic measurements were harvested from different portions of the plug. Therefore, a main assumption of this study was that the sampled portions were representative of the entire plug. This sampling protocol was used to permit comparisons across the biochemical, mechanical and histologic data of each biospy. However, these divisions lend variability to these outcome values and the strength of correlations and resultant effects could have improved without this division. Radial degeneration is recognized after full thickness defects are created.[54] Despite the significant correlations between GAG and cationic CECT attenuation and histological outcomes, the capacity for the hydroxyproline assay to reflect the DM measurement might be diminished using this particular study design.[38]

Concordant with the second hypothesis the *in vivo* application of (clinical) cationic CECT imaging distinguished articular cartilage across disease states by quantifying CT signal. Despite this promising distinction that echoes microCT evaluation, the loss of articular cartilage volume in the defects was detectable without the need for quantifying the attenuation values. However, one of the most interesting results of this study involved the detection of lower clinical cationic CECT attenuation in the adjacent defects compared to the remote sites starting at six weeks after defect, which did not have an appreciable difference in tissue volume. This detectable change signifies that degenerative tissue can be identified using the resolution employed by the clinical scanner. The lower attenuation in the adjacent samples in the defect joints is consistent with

lower GAG content and degeneration at the periphery of the defects that was confirmed in this study with the DMMB assay results.[54] At ten weeks after surgery, there were no longer significant differences between the defect and adjacent and remote groups. The most likely explanation was that there was a lower number of joints available for evaluation starting at 10 weeks (Group II end point was at eight weeks). Regardless, at 16 weeks significant differences between these groups re-emerged.

Interestingly, the clinical cationic CECT attenuation at two weeks was significantly lower than baseline for all sample locations. Then, at four weeks the mean cationic CECT attenuation increased. This decline was also observed in the remote samples that were not near damaged articular cartilage. Since all significant differences in remote samples over time were linked to the 2-week time point, a transient effect seemed likely and was suspected to be a consequence of recent surgery. All clinical CECT examinations were performed exactly at four hours after injection based on preliminary studies (Chapter 3). However, the surgical inflammation that occurs with arthrotomy and defect creation could have influenced joint metabolism rates. As such, the inflammation that occurs with osteoarthritis or the chronicity of injury may influence CA4+ diffusion times. Until further testing is performed to confirm or refute this possibility, cationic CECT scans are not recommended at two weeks after arthrotomy without recognizing a potential decline in measurement accuracy. Additional studies should explore the diffusion rates of CA4+ into articular cartilage and clearance in inflamed joints.

The *in vivo* chondral defect model produced a continuum of articular cartilage for evaluation as anticipated. Typically this model is used for investigation of cartilage healing.[23,25,26] While the

same surgical technique was replicated, the short duration of study is not standard practice for the investigation of long-term healing.[25] However, this study was designed to examine the capability of cationic CECT to detect articular cartilage injury and assess defect healing early in the disease process through longitudinal assessment. Despite the categorization as reparative tissue, the methods used for healing are not the optimal techniques to maximize healing. Subchondral bone microfracture and osteochondral allograft transplantation used in horses and humans would likely lead to better quality of repair tissue.[27,55] The reparative tissue that forms after the removal of calcified cartilage and following subchondral bone microfracture is fibrocartilage (type III collagen), while osteochondral transplantation re-institutes native hyaline (type II collagen) cartilage. There are clear mechanical and biochemical differences between these two tissue types.[51,56-58] The former method was selected in this study as it is more commonly used in equine articular cartilage repair strategies. While cationic CECT attenuation could be used to distinguish between fibrocartilage and degenerative and normal hyaline cartilage, further experiments are required to determine the ability to characterize the hyaline tissue from osteochondral allograft transplants and to classify healing endpoints after an appropriate duration of healing is permitted.[25,26]

Similar to the impact study, density phantoms of CA4+, iohexol and CaHA were included to perform transformation to biologically relevant units while simultaneously addressing variability across CT examinations. This study also showed that the CA4+ and CaHA density phantoms improved consistency across scans. The CaHA density chambers are solid components and are less affected by extrinsic factors (*e.g.* light exposure) that could degrade iodinated solutions over time. The CA4+ was chosen as a liquid medium that is directly related to the solution that

diffuses into articular cartilage. If investigating bone, the conversion units (mg I/mL) are not as relevant as mg CaHA/cm^3. Therefore if quantitative assessments of bone are also to be investigated in future studies, use of this CaHA density phantom should be considered.

The approach used for CA4+ injection was selected to provide a reliable way to aspirate synovial fluid from the femoropatellar joint that would not be attainable with other approaches.[24] Another benefit of this lateral technique was that it avoids damaging articular cartilage during needle placement. However, the ventral dependency of this location also makes it more likely to extravasate into the periarticular soft tissues because of the large injection volume and therefore pressure that builds up at the puncture site causing leakage. The suprapatellar approach used in Chapter 3 would likely prevent this complication if synovial fluid assessments were not required. Regardless, the periarticular extravasation did not appear to influence the quantitation of cationic CECT attenuation in this study similar to what was observed the previous experiment (Chapter 4).

An unanticipated consequence of the *in vivo* model was the severe femoropatellar joint effusion that developed in the Group I horses. Despite the lack of observable lameness, other assessments (response to stifle flexion and range of motion) were unmistakably altered. Because both hindlimbs were similarly affected, significant differences between joints were not detected, but were identified through the temporal assessments. While severe synovial effusion was not detected in the one horse that underwent the safety experiment and that also endured the same number of joint injections (Chapter 3), there was an adverse response of synovial membrane in the joints of this horse to repeated arthrocentesis and 100 mLs of injected fluid (CA4+ or PBS)

over four months. A key distinction from that study and this experiment, was the potential influence of surgical inflammation induced as a consequence of the arthrotomy procedure. While some inflammation is expected using any surgical model, the repeated joint injections and fast return to free exercise could have been factors in the development of increased joint effusion. The increased levels of PGE_2 detected in this study relative to that observed in Chapters 3 and 4 further support this conclusion. The high frequency of seroma formation also indicates that free turnout should be postponed until four weeks as used for other cartilage healing studies. While the joint was macroscopically determined to be normal at surgery, an oversight was that collection of synovial membrane was not performed before defects were created. This would have provided a baseline for comparison. Collectively the synovial membrane data from Chapters 3 - 5 suggest that the volume and repeated injections of CA4+ were the likely contributors to the increased synovial membrane responses and in this study were exacerbated by the arthrotomy procedure and fast return to free exercise. However, soft tissue histology scores have been observed to have increased cellular infiltrates after tenoscopic surgery using these short time periods.[59] The high frequency of injections used in this study exceeds the practical use in clinical cases. Nonetheless, the injection frequency used in this study should not be replicated without further investigation.

The comparisons between clinical cationic CECT and MRI showed that neither method was capable of distinguishing between repair 1 and 2 groups using this study design. The variation in healing responses and the small number of horses used in this study likely contributed to this inability to separate reparative groups. Observing the range of cationic CECT attenuation values within each MRI score, however, highlights the value of quantitative assessment. Direct

comparisons between cationic CECT and MRI are still difficult with this design. Cationic CECT was measured quantitatively, while assessments with MRI were categorical and routinely used in clinical and research examinations.[60-62] These different properties limit direct comparisons between the two modalities. Quantitative MRI techniques do exist and comparisons of these methods to cationic CECT warrant consideration.[4,63]

In summary, the results of this experiment showed that cationic CECT provides imaging measures that reflect tissue quality through non-destructive assessment and successfully distinguishes reparative from degenerative and healthy articular cartilage. This experiment also showed that cationic CECT is successfully used *in vivo* though further work is required to determine any long-term effects that could not be investigated with this study design. Regardless, this quantitative imaging technique shows considerable promise as an investigative tool for longitudinal assessment of articular cartilage and as a method to characterize articular cartilage injury across a range of disease states.

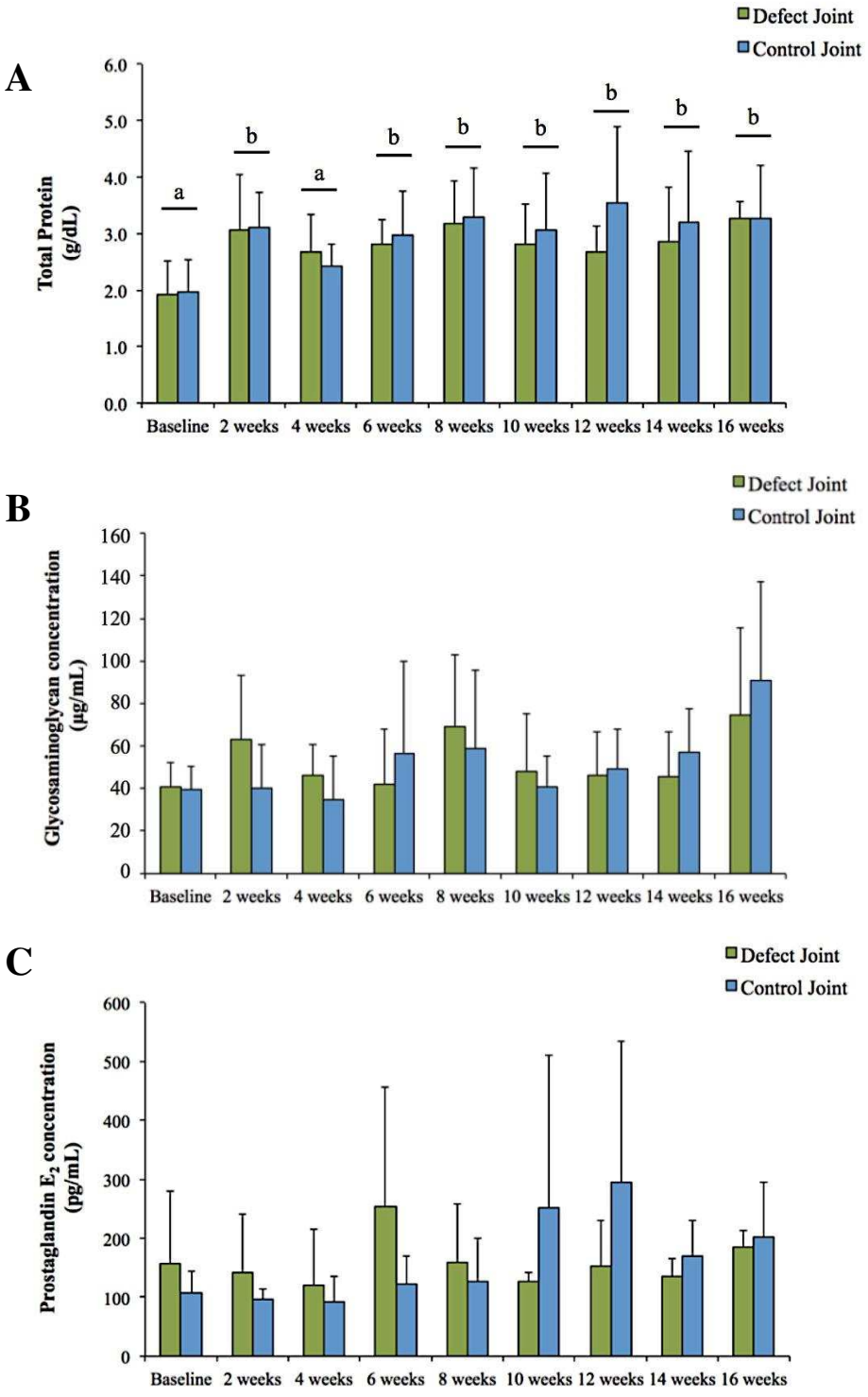

Figure 5.1 – Mean ± s.d. of synovial fluid parameters (A) total protein, (B) glycosaminoglycan and (C) prostaglandin E_2 concentrations compared between defect and control joints over time. There was no significant interaction between joint (defect vs. control) and time point. There was a significant main effect of time point on total protein. Different letters indicate a significant difference ($P < 0.05$) between time points.

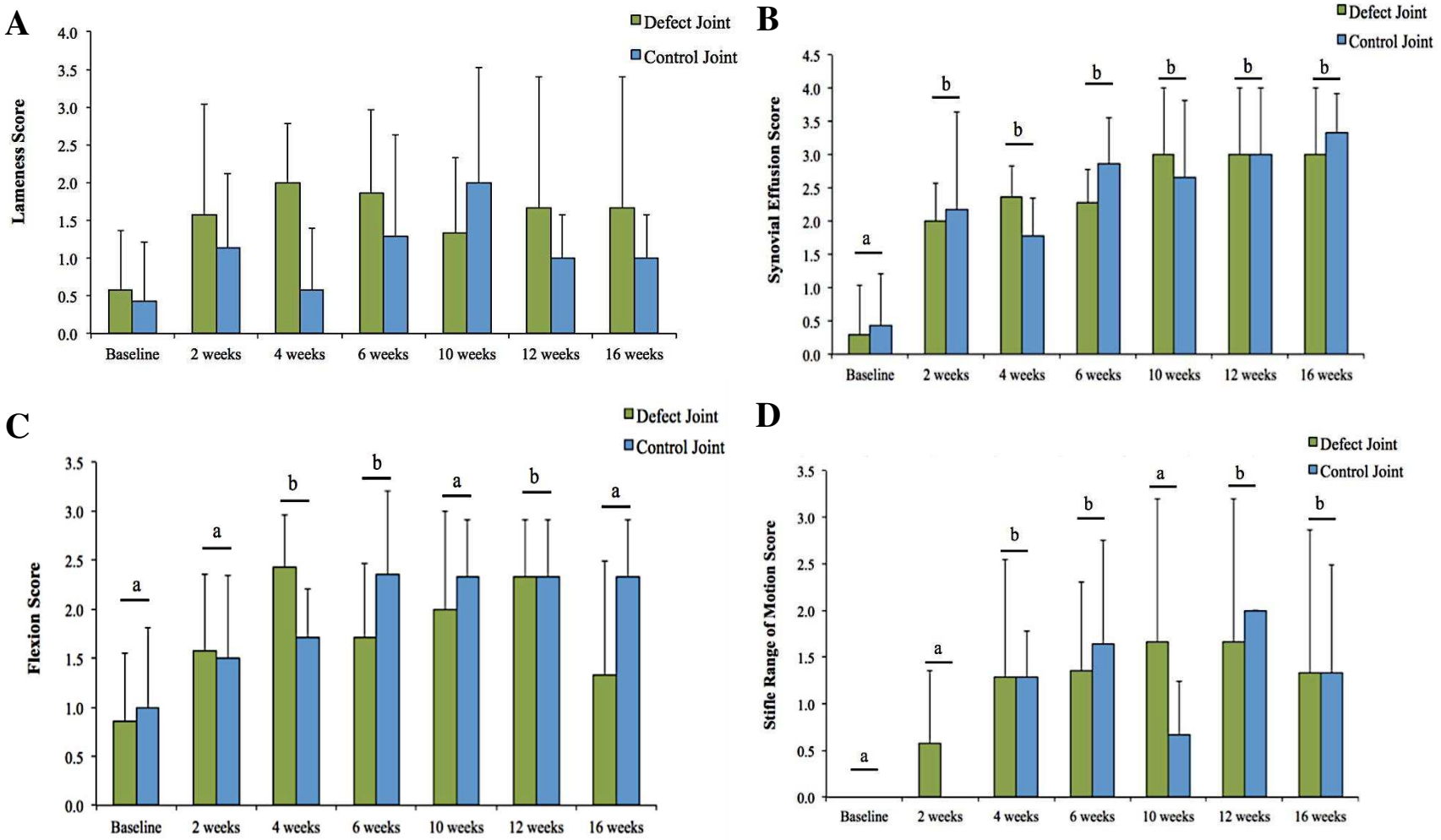

Figure 5.2 – Mean ± s.d. of clinical evaluation variables (A) lameness, (B) synovial effusion, (C) stifle flexion, and (D) stifle range of motion score. There was not a significant interaction between joint group (control vs defect) and time point level for any clinical evaluation variable. There was a significant main effect of time on synovial effusion, stifle flexion and stifle range of motion scores. Different letters indicate a significant difference ($P < 0.05$) between time points after Tukey-Kramer adjustment for multiple comparisons.

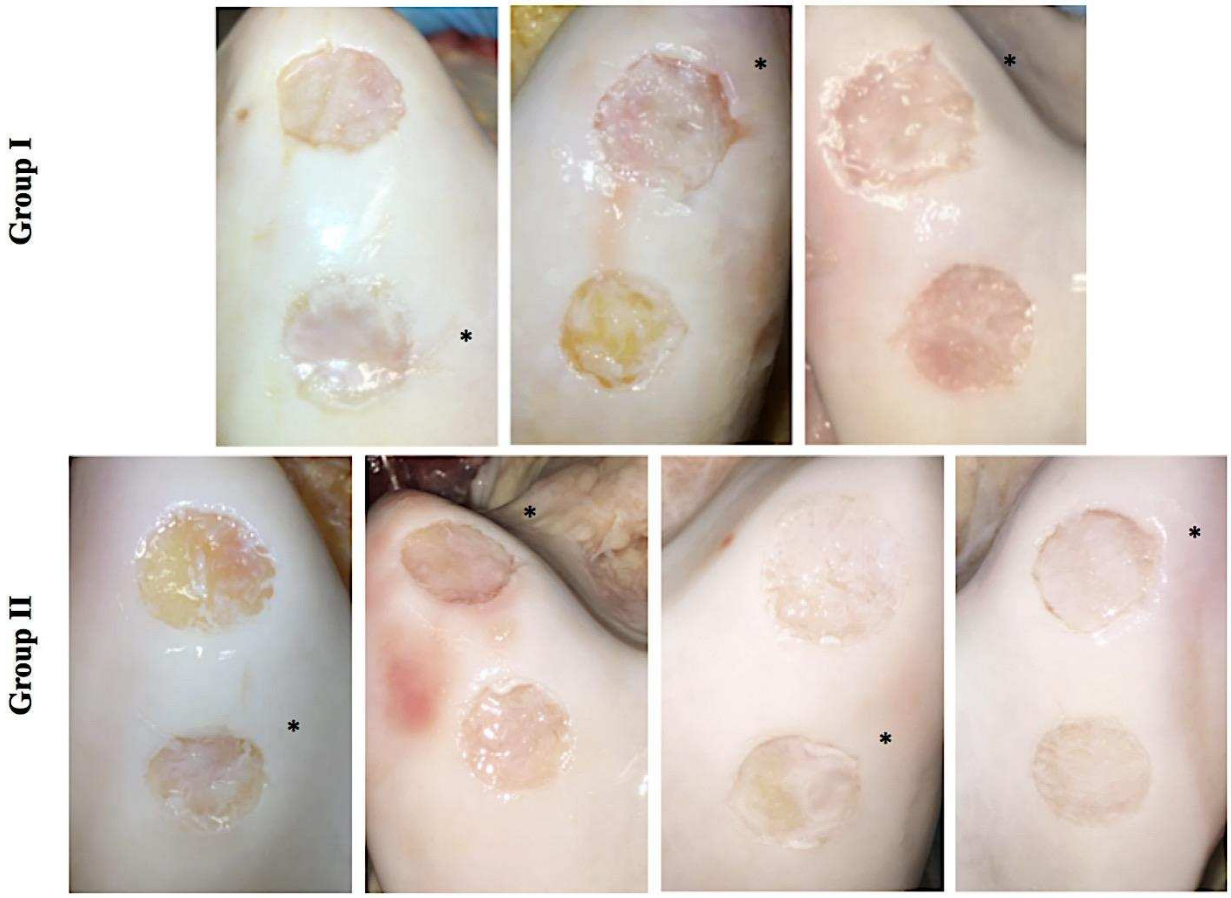

Figure 5.3 – Postmortem photographs of the medial trochlear ridge of the femur showing the appearance of the 2 -15 mm circular defects that were created at four months (Group I) and two months (Group II) after surgery. The asterisk indicates that the defect had calcified cartilage removed (repair 2) and in the other defect the calcified cartilage was retained (repair 1).

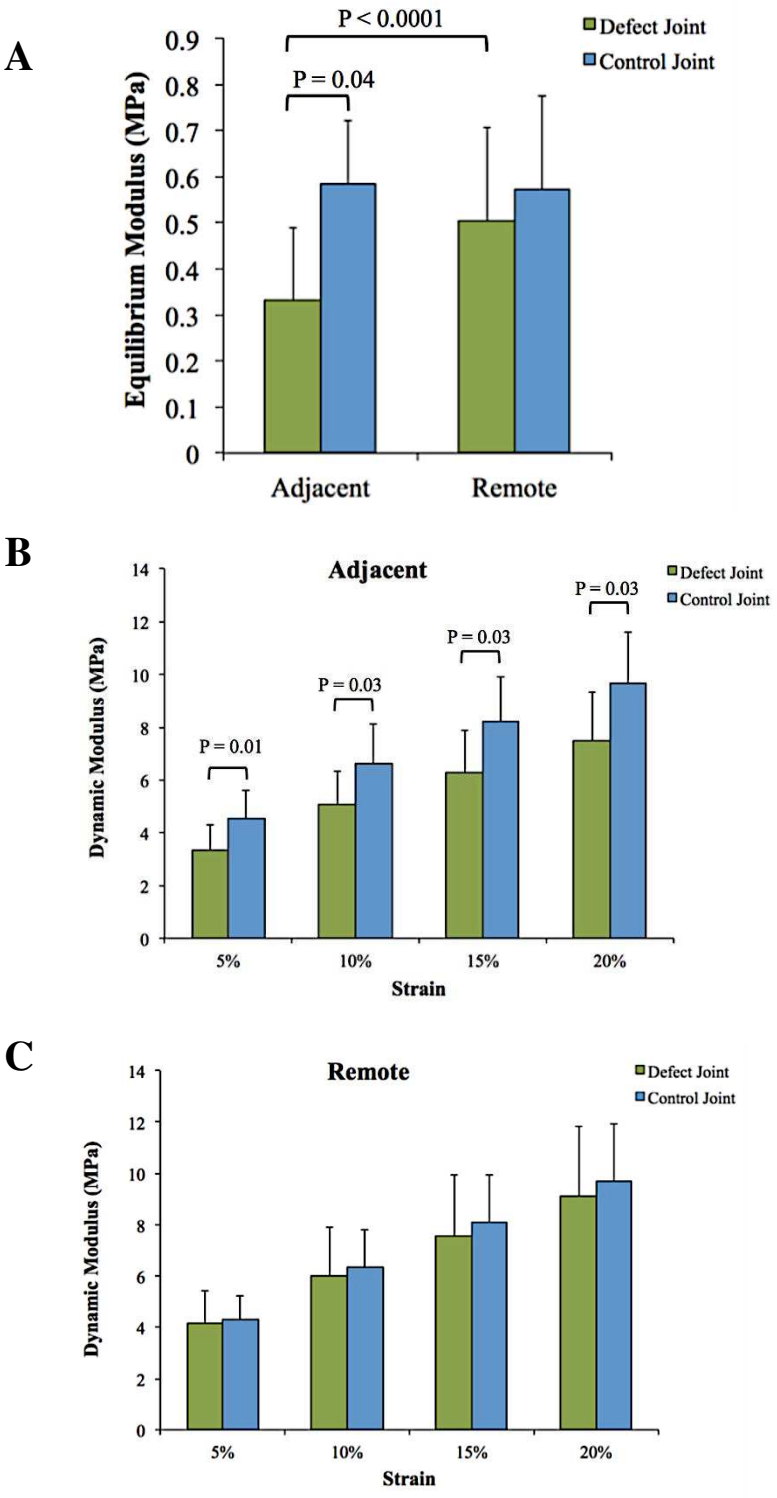

Figure 5.4 – Mean ± s.d. of mechanical data grouped by defect and control joints. (A) equilibrium compressive modulus, (B) dynamic modulus in adjacent (to defect) samples and (C) dynamic modulus in remote (to defect) samples. Significant differences between groups are indicated with brackets.

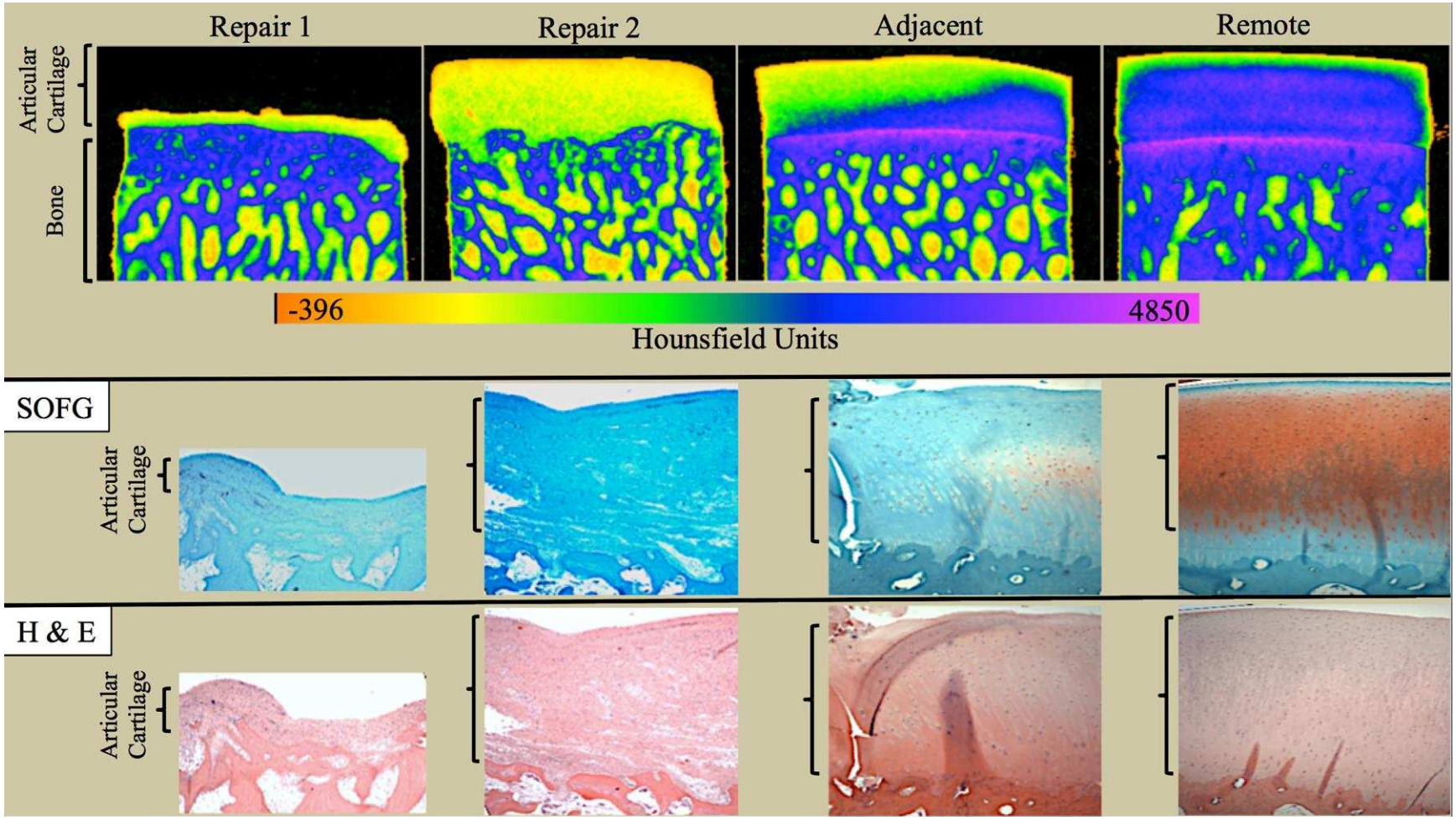

Figure 5.5 – Representative cationic CECT microCT images of the four articular cartilage sample groups showing a continuum of disease states. The repair groups show the healing response after calcified cartilage was retained (repair 1) and after calcified cartilage removed (repair 2). The adjacent sample was collected at a location bordering a critically sized defect and the remote sample was taken > 15 mm from any defect. The grey scale images were transformed into a color map to highlight the range and distribution of x-ray attenuation in and throughout articular cartilage across disease states. Beneath each sampled location is a representative histology image stained with safraninin-O fast green (SOFG) and hematoxylin & eosin (H & E).

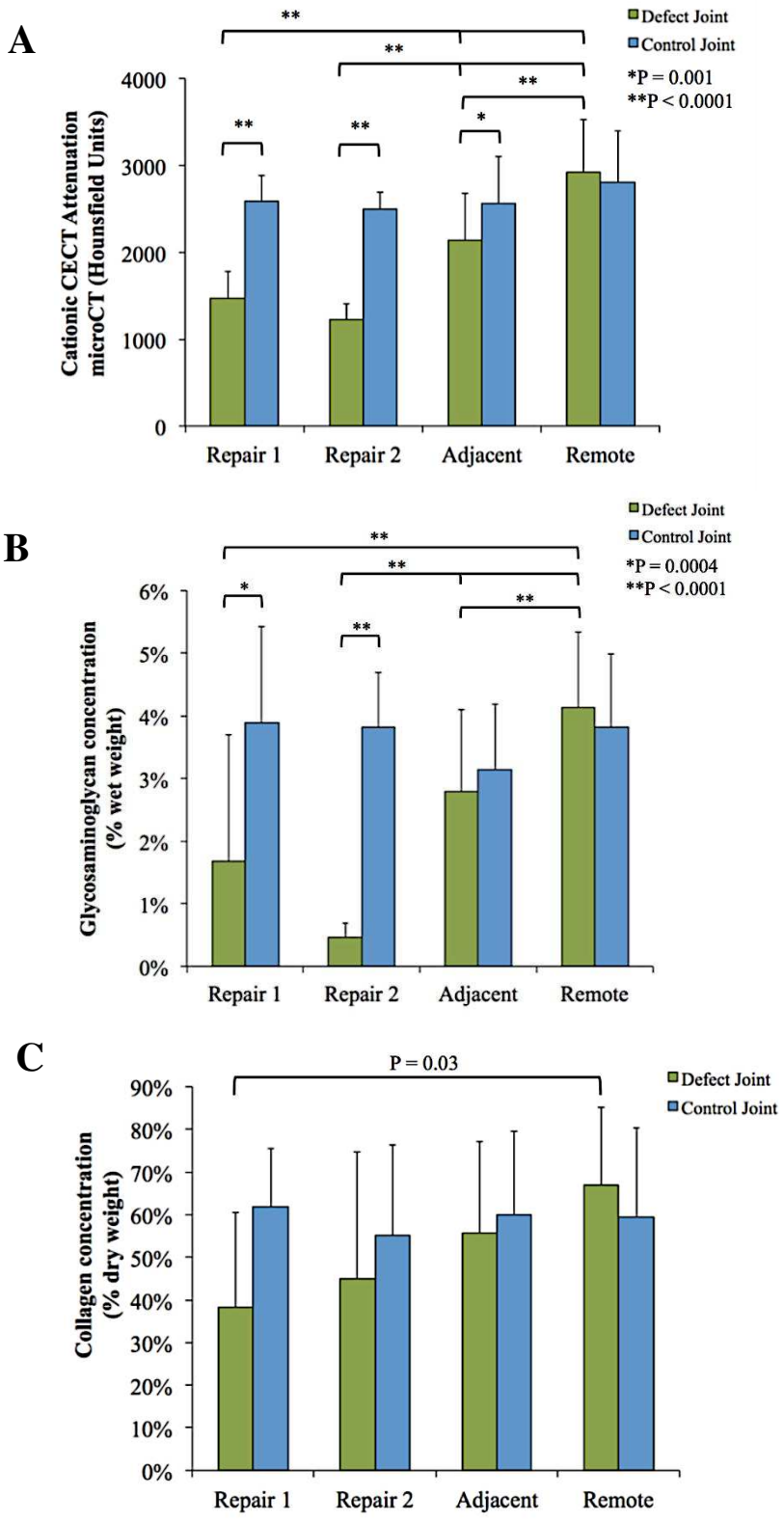

Figure 5.6 – Mean ± s.d of (A) cationic CECT attenuation (microCT), (B) glycosaminoglycan concentration and (C) total collagen content at each sample site grouped by defect or control joint. Significant differences between groups are indicated with brackets.

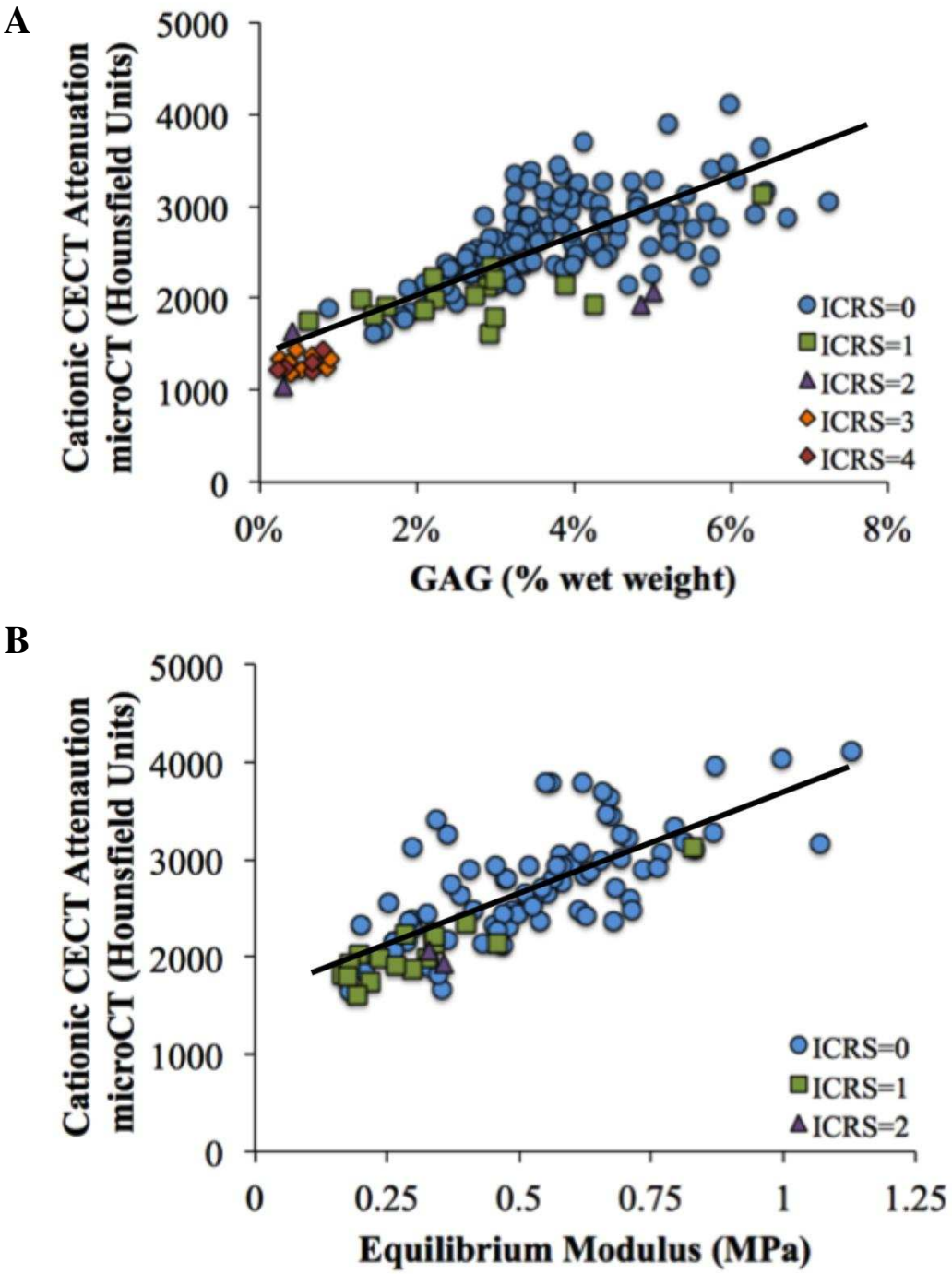

Figure 5.7 – Correlations between cationic CECT attenuation (microCT) and (A) glycosaminoglycan concentration and (B) equilibrium compressive modulus grouped by the macroscopic score from the International Cartilage Repair Society (ICRS).

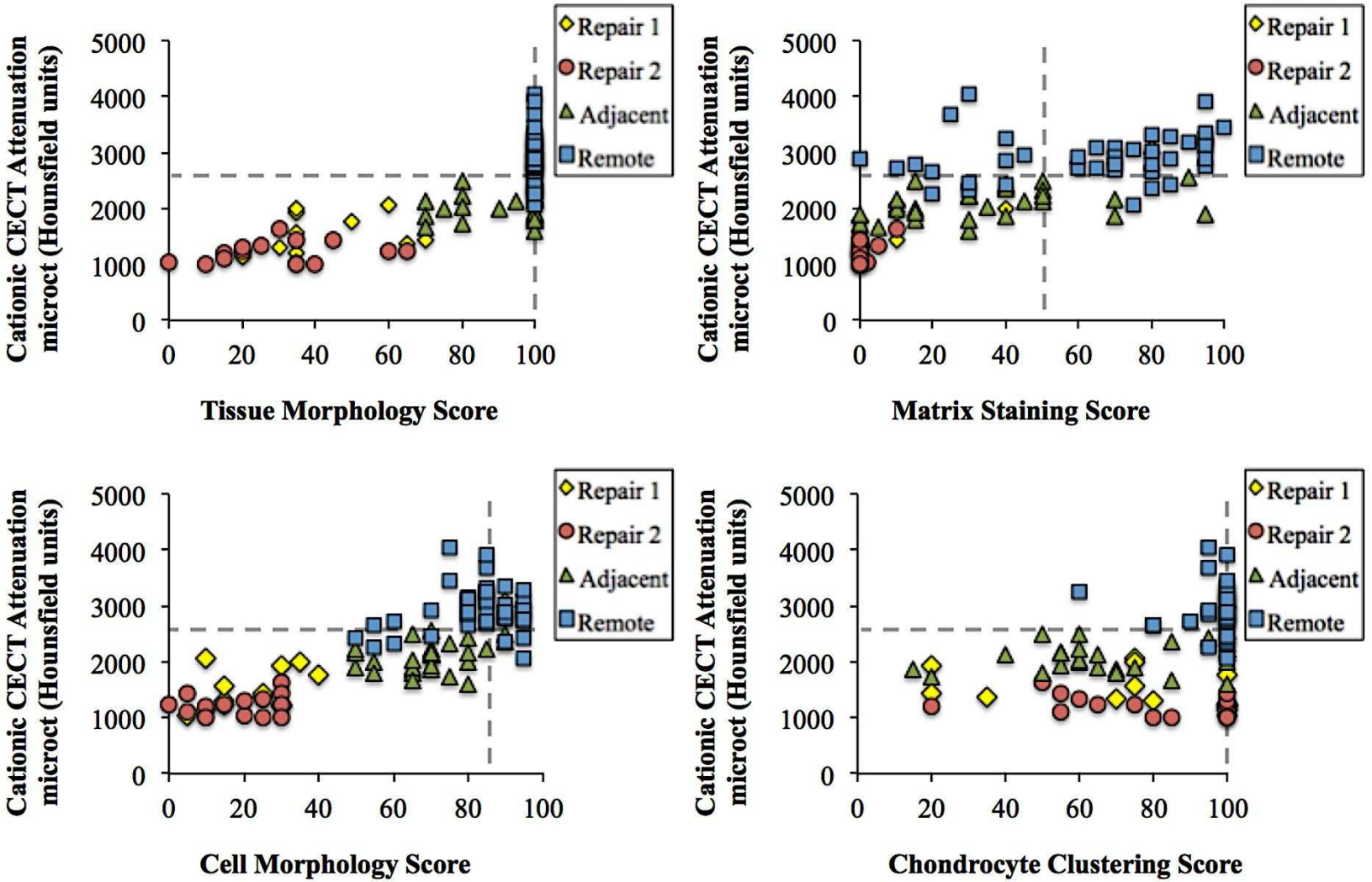

Figure 5.8 – Scatterplot of cationic CECT attenuation (microCT) versus individual histological scoring components from the International Cartilage Repair Society (ICRS) II scoring system in defect joints.[41] The data points are arranged by the sample group designations. The dotted lines indicate the average scores in control joint samples (horizontal: cationic CECT attenuation, vertical: ICRS II score for each parameter).

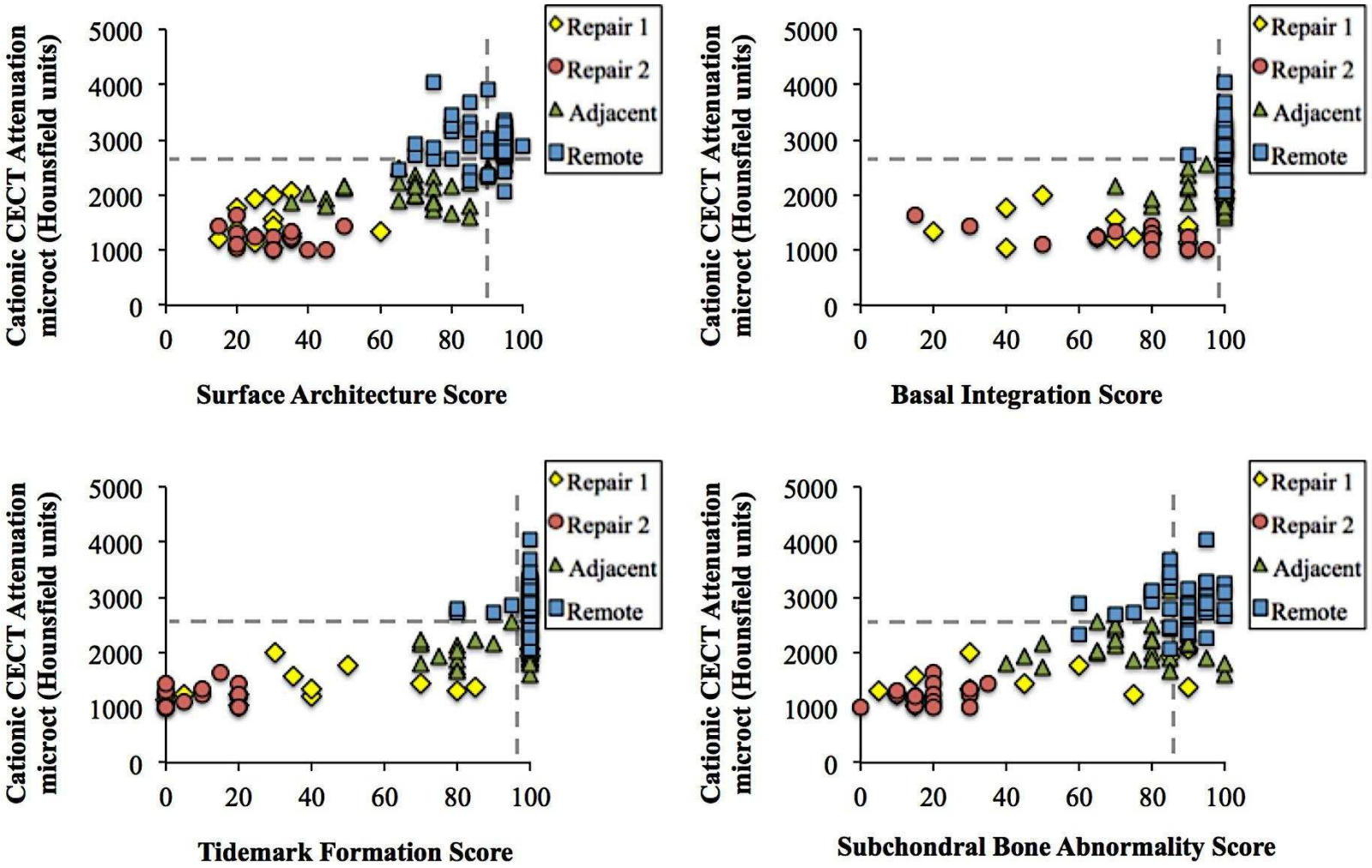

Figure 5.8 – continued. Scatterplot of cationic CECT attenuation (microCT) versus individual histological scoring components from the International Cartilage Repair Society (ICRS) II scoring system in defect joints.[41] The data points are arranged by the sample group designations. The dotted lines indicate the average scores in control joint samples (horizontal: cationic CECT attenuation, vertical: ICRS II score for each parameter).

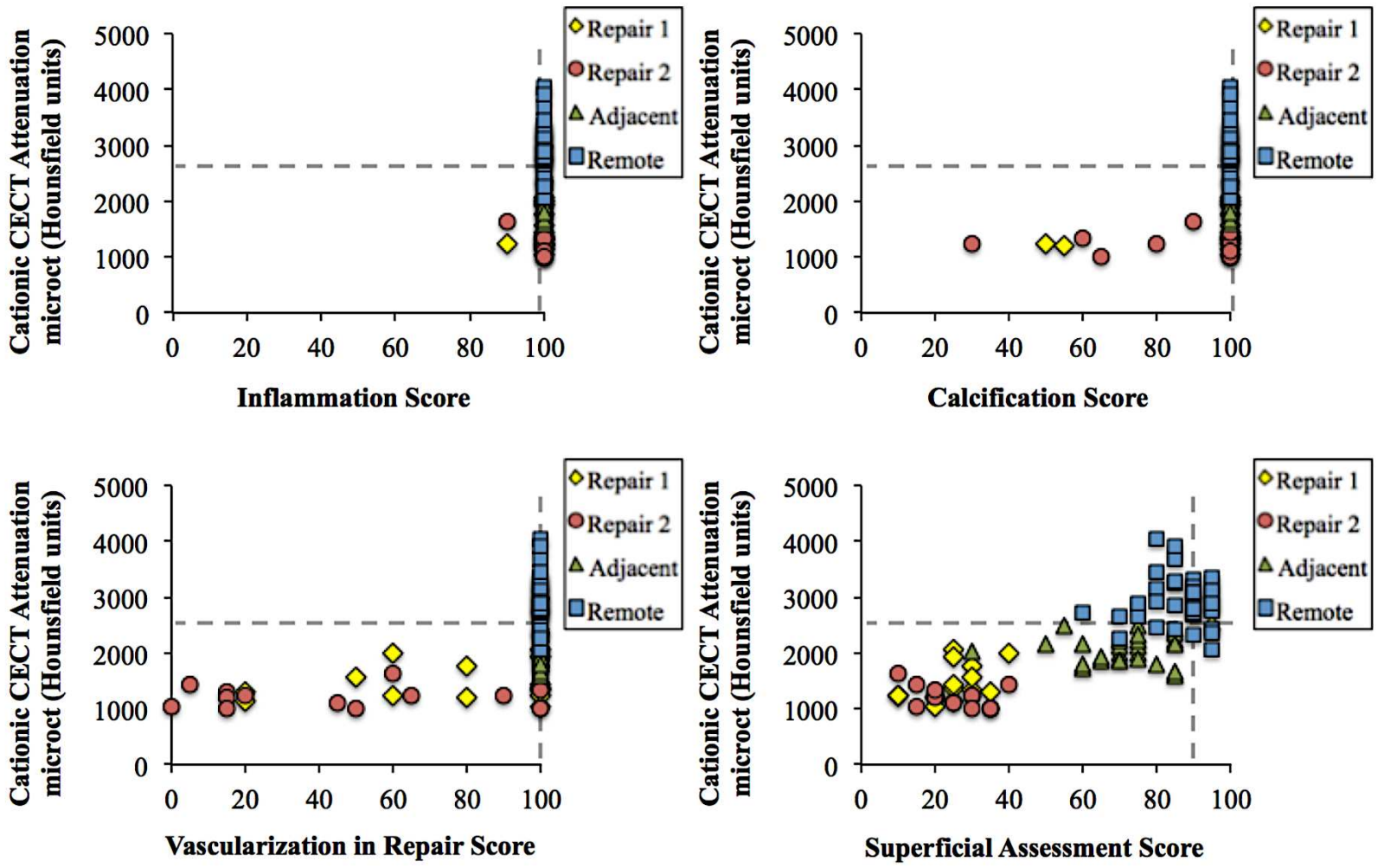

Figure 5.8 – continued. Scatterplot of cationic CECT attenuation (microCT) versus individual histological scoring components from the International Cartilage Repair Society (ICRS) II scoring system in defect joints.[41] The data points are arranged by the sample group designations. The dotted lines indicate the average scores in control joint samples (horizontal: cationic CECT attenuation, vertical: ICRS II score for each parameter).

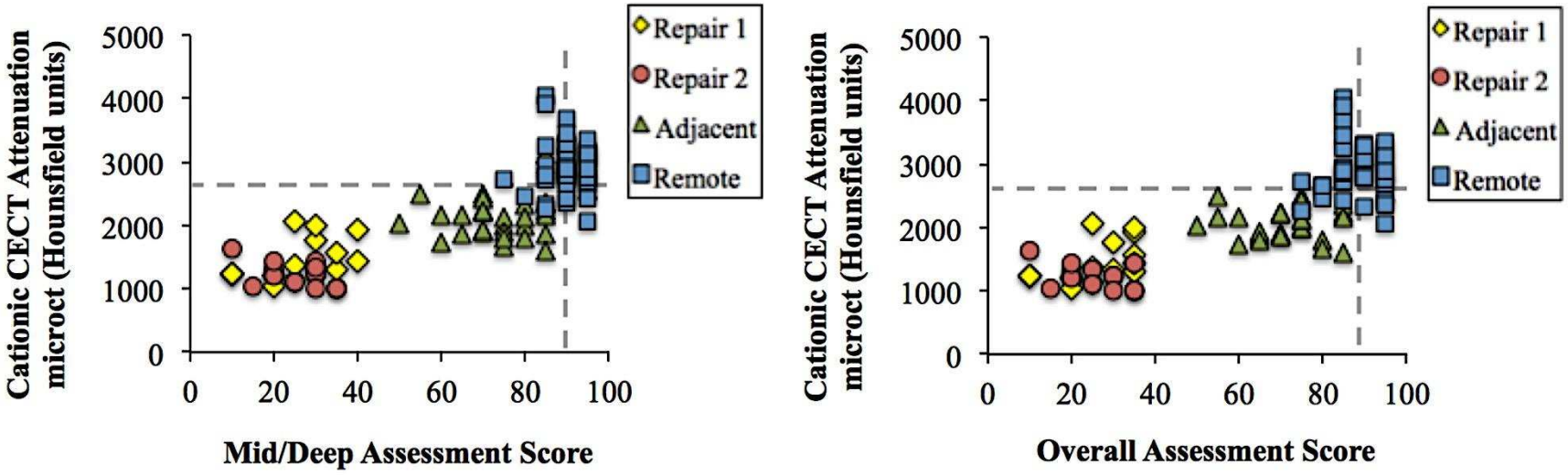

Figure 5.8 – continued. Scatterplots of cationic CECT attenuation (microCT) versus individual histological scoring components from the International Cartilage Repair Society (ICRS) II scoring system in defect joints.[41] The data points are arranged by the sample group designations. The dotted lines indicate the average scores in control joint samples (horizontal: cationic CECT attenuation, vertical: ICRS II score for each parameter).

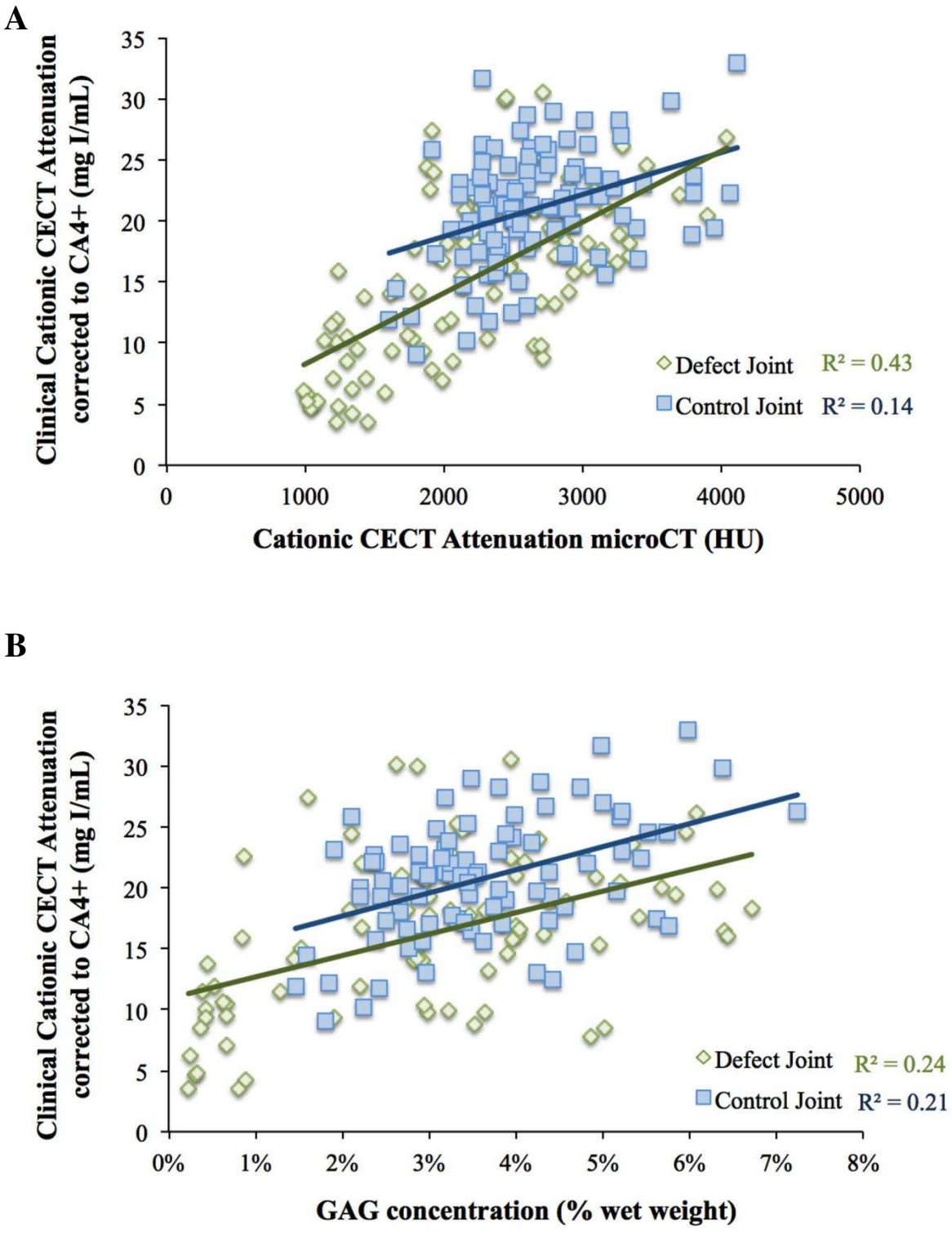

Figure 5.9 – Scatterplots of clinical cationic CECT attenuation corrected to CA4+ concentration versus (A) cationic CECT attenuation microCT and (B) glycosaminoglycan (GAG) concentration.

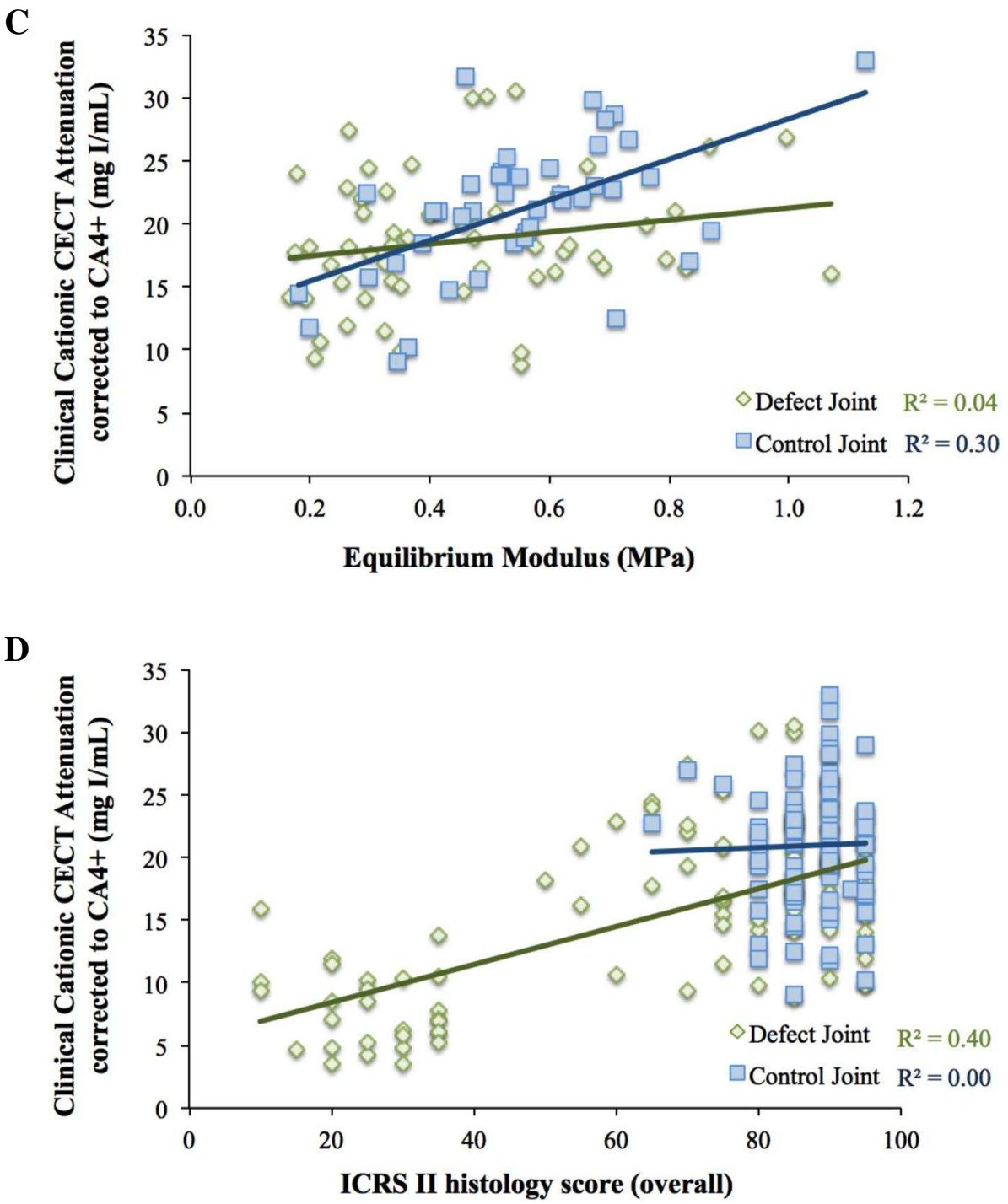

Figure 5.9 – continued. Scatterplots of clinical cationic CECT attenuation corrected to CA4+ concentration versus (C) equilibrium compressive modulus and (D) histologic (overall) score from the International Cartilage Repair Society (ICRS) II system.

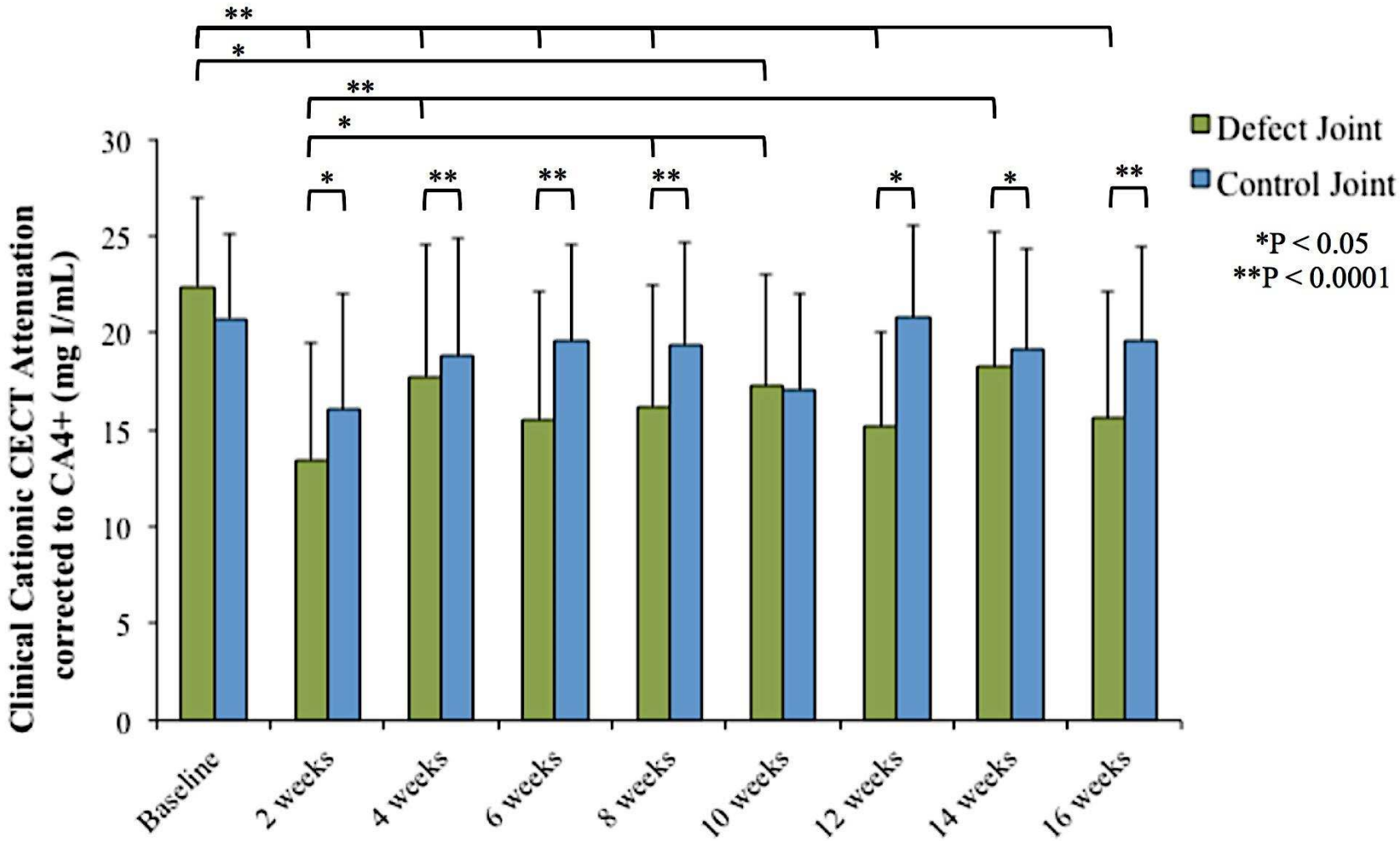

Figure 5.10 – Mean ± s.d. of clinical cationic CECT attenuation corrected to CA4+ concentrations between joint groups and over time. All sampling groups are averaged throughout the joint. Significant differences ($P < 0.05$) between groups are indicated by brackets and asterisks. All horses have data through eight weeks, while group I horses extend over 16 weeks.

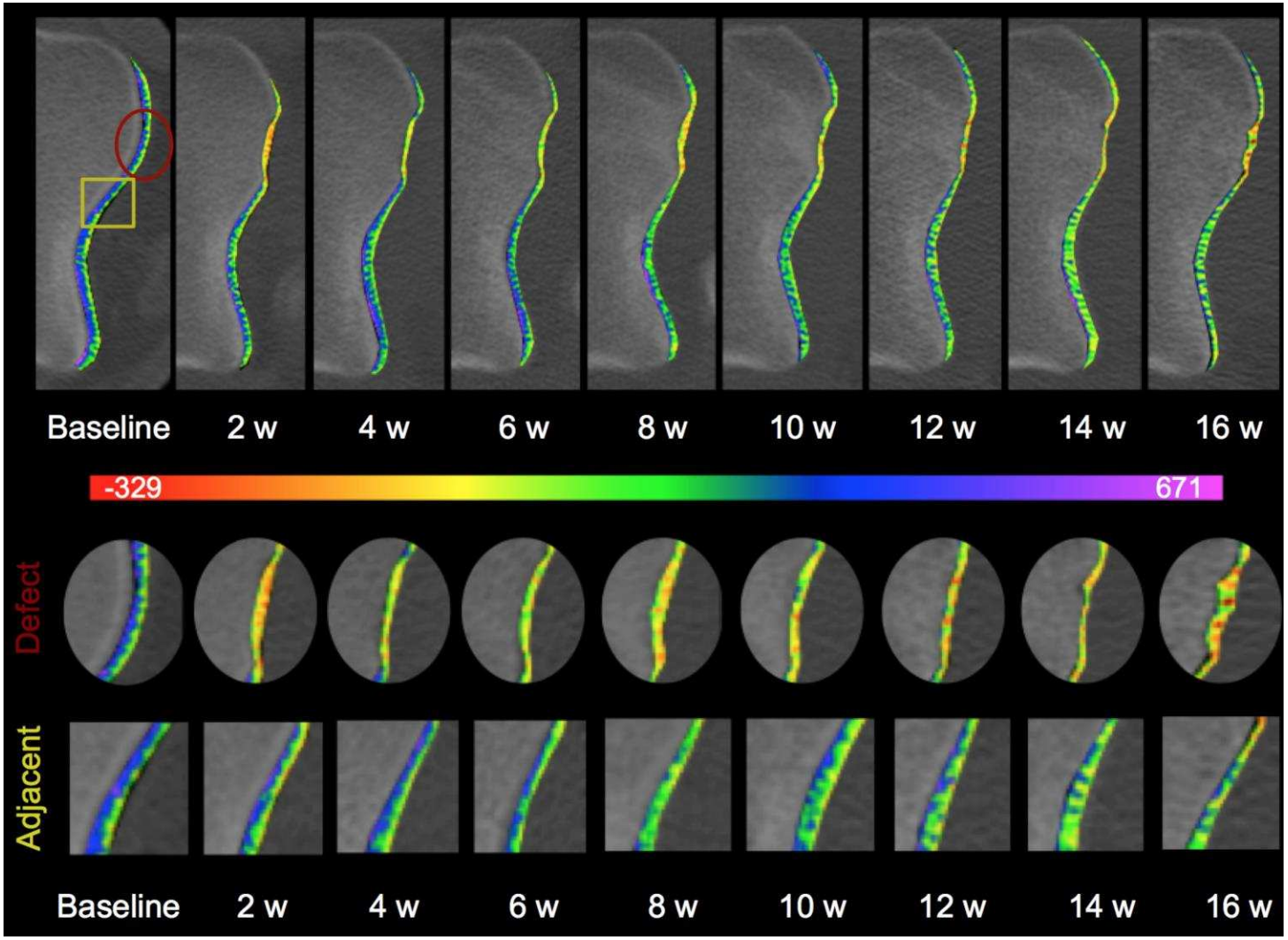

Figure 5.11 – Sequential clinical cationic CECT images of the femoral trochlea in the defect joint from one horse in group I. The top row images are in the transverse plane with a color map representing cationic CECT attenuation values over the articular surface. The red circle denotes the defect (repair 2) and the middle row of images show the magnified defect location over time. The yellow square highlights the location adjacent to the defect with the bottom row of images showing that location magnified. w, weeks after defect.

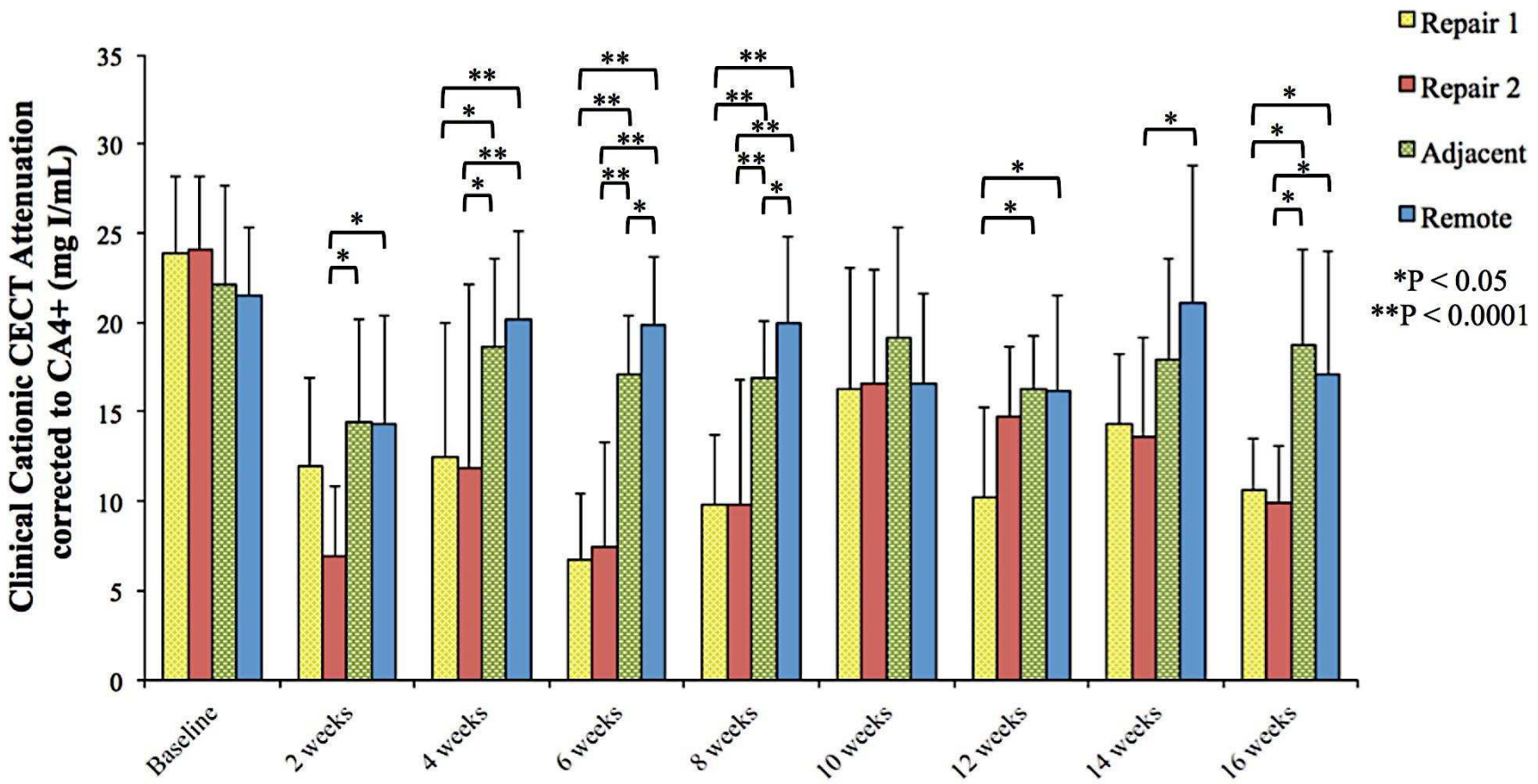

Figure 5.12 – Mean ± s.d. of clinical cationic CECT attenuation corrected to CA4+ concentration in defect joints (control joints excluded) and grouped by time point. Sample location groups are shown at each time point. Significant differences ($P < 0.05$) between groups are indicated by brackets and asterisks. Comparisons between groups across time points are not shown in this chart. All horses have data through eight weeks, while group I horses extend over 16 weeks.

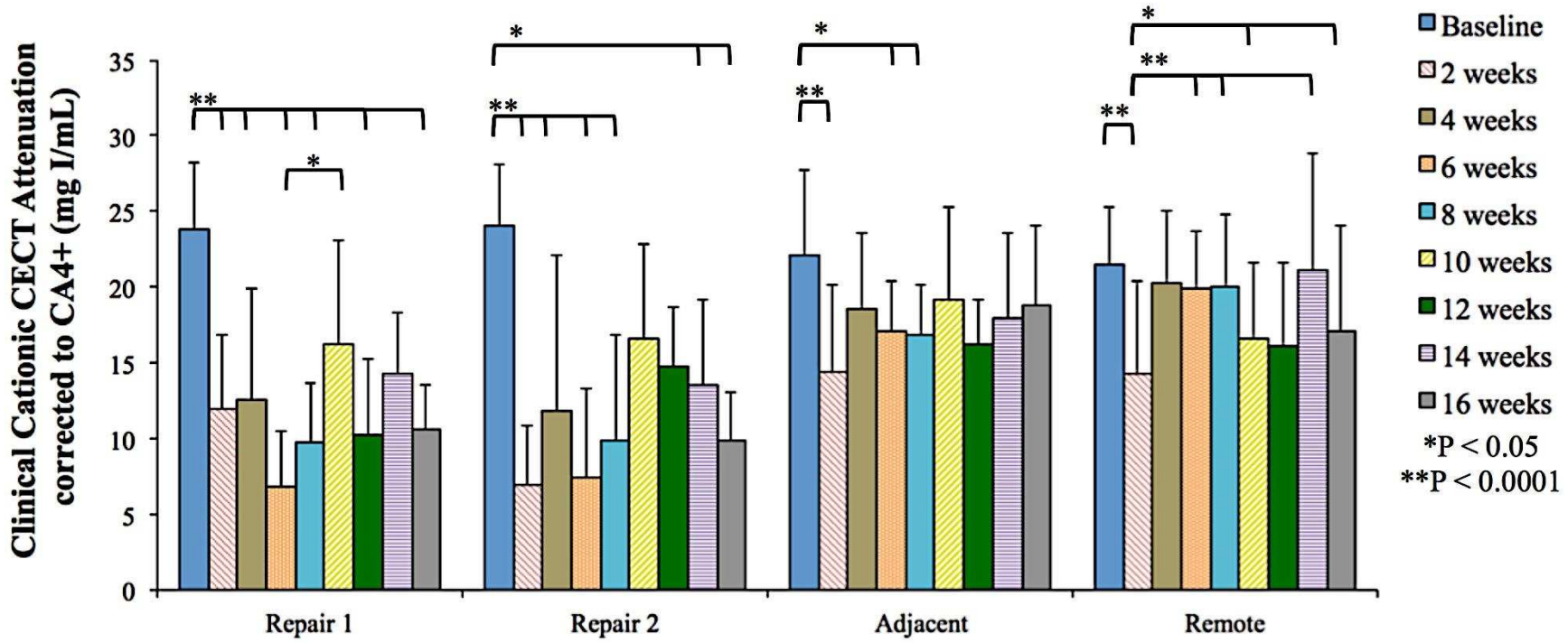

Figure 5.13 – Mean ± s.d. of clinical cationic CECT attenuation corrected to CA4+ concentration in defect joints (control joints excluded) and grouped by sample location. Significant differences ($P < 0.05$) between time points within each sample group are indicated by brackets and asterisks. All horses have data through eight weeks, while group I horses extend over 16 weeks.

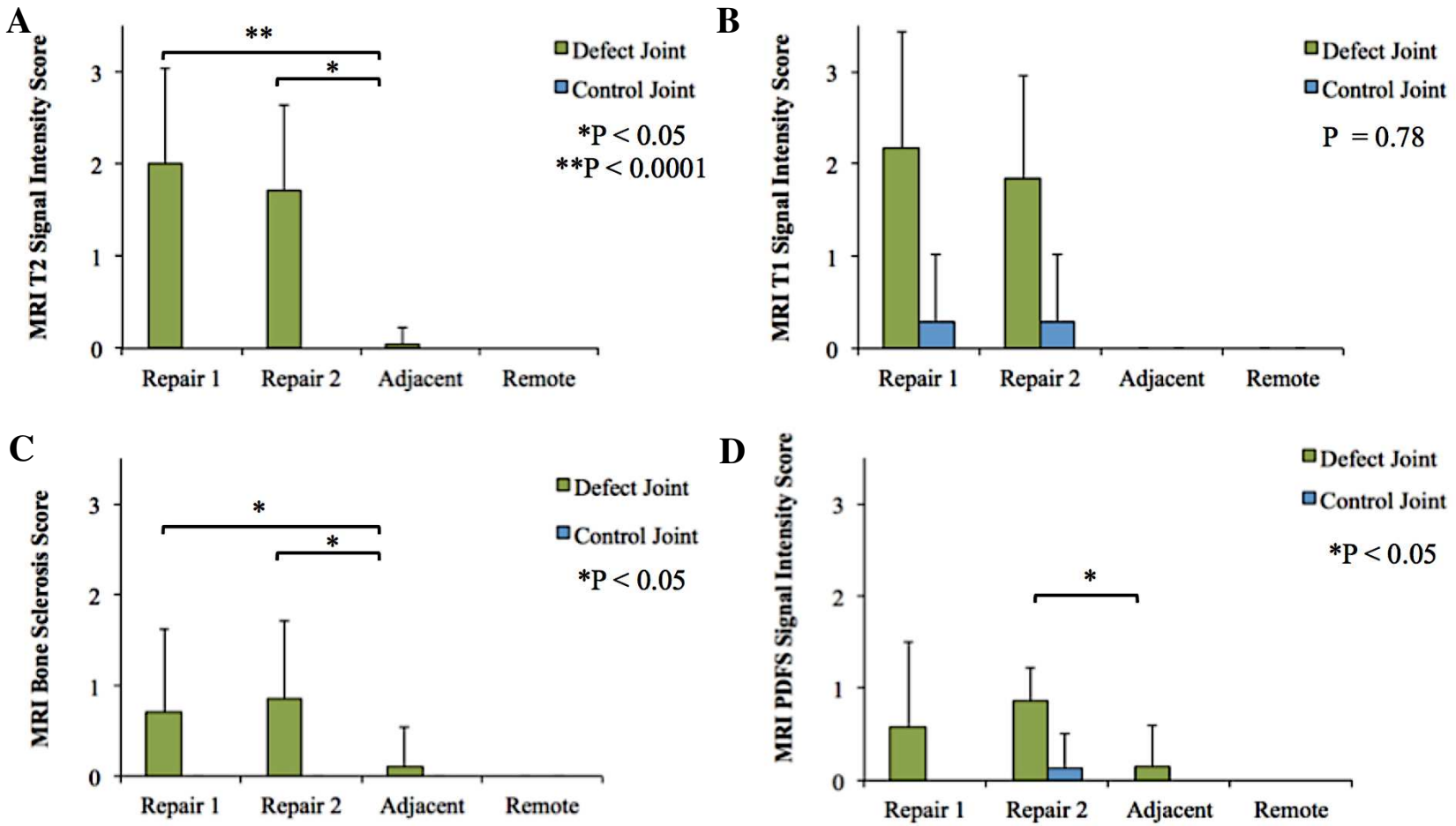

Figure 5.14 – Mean ± s.d. MRI scores at each sample location in defect and control joints: (A) T2 signal intensity, (B) T1 signal intensity, (C) bone sclerosis and (D) proton density with fat suppression (PDFS). MRI scores are 0 – 3: none, mild, moderate and severe.

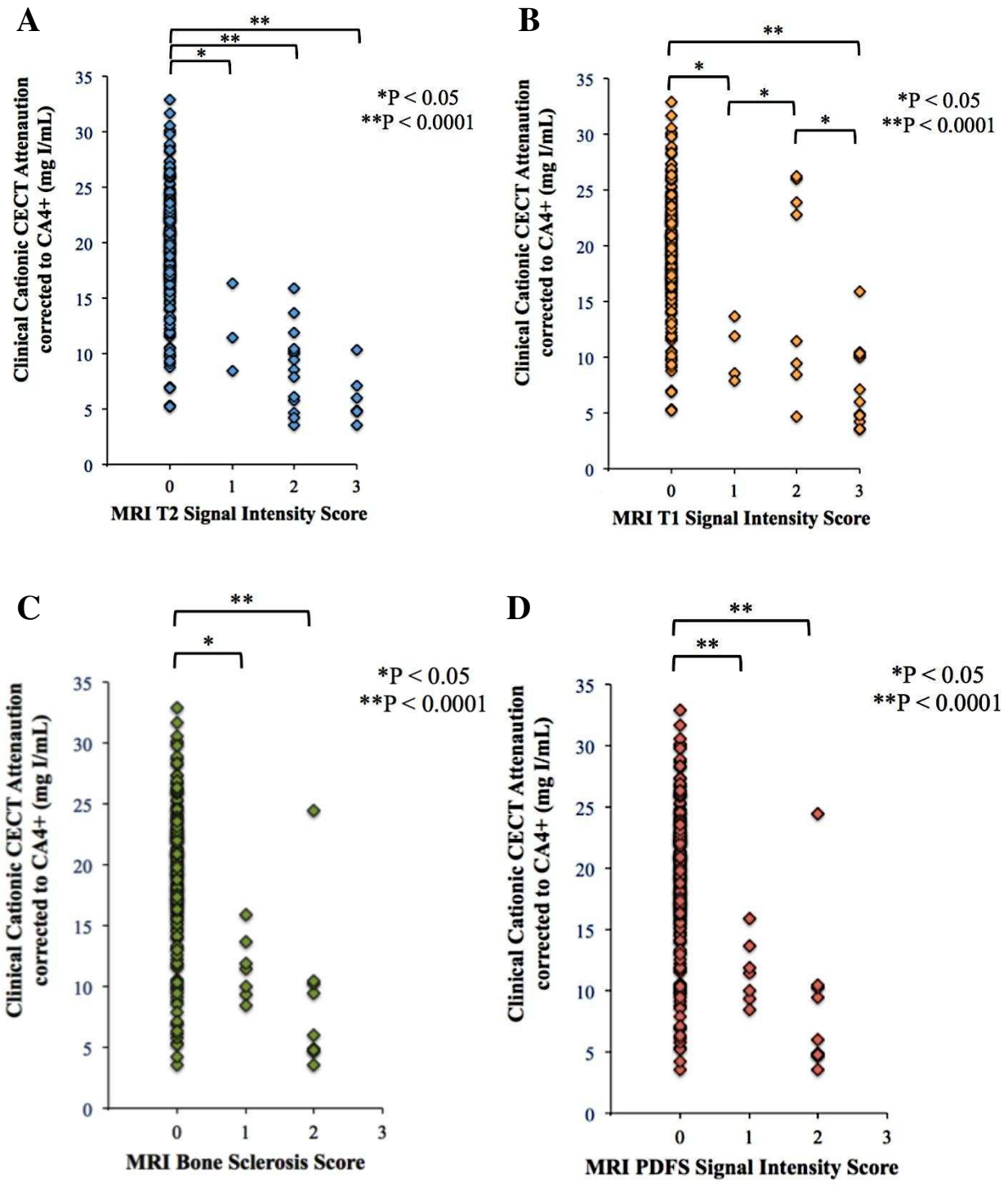

Figure 5.15 – Comparisons between clinical cationic CECT attenuation values and MRI scores: (A) T2 signal intensity, (B) T1 signal intensity, (C) bone sclerosis and (D) proton density with fat suppression (PDFS). The brackets with asterisks indicate a significant difference ($P < 0.05$) of mean cationic CECT attenuation between scores. MRI scores are 0 – 3: none, mild, moderate and severe.

Table 5.1A – Comparisons between joints (P = 0.25) and over time (P = 0.66) were not significantly different using repeated measures mixed model ANOVA

Time Point	**Leukocyte concentration (10^6/μL)**	
	Defect Joint	Control Joint
Baseline (0 weeks)	400 ± 400	400 ± 337
2 weeks	800 ± 497	2,600 ± 2,300
4 weeks	614 ± 302	871 ± 403
6 weeks	914 ± 1,038	2,729 ± 3,280
8 weeks	714 ± 463	1,067 ± 638
10 weeks	433 ± 351	333 ± 252
12 weeks	667 ± 503	533 ± 404
14 weeks	367 ± 208	337 ± 153
Endpoint (16 weeks)	433 ± 115	533 ± 252

Table 5.1B – Comparisons between joints (P = 0.52) and over time (P = 0.63) were not significantly different using repeated measures mixed model ANOVA

Time Point	**Lymphocytes (% of leukocytes)**	
	Defect Joint	Control Joint
Baseline (0 weeks)	29.7 %	35.4 ± 1.8 %
2 weeks	32.3 ± 9.4 %	34.4 ± 5.1 %
4 weeks	32.7 ± 9.8 %	30.8 ± 10.9 %
6 weeks	29.5 ± 9.9 %	25.2 ± 6.2 %
8 weeks	31.6 ± 5.5 %	33.6 ± 7.4 %
10 weeks	27.3 ± 14.3 %	30.0 ± 15.3 %
12 weeks	28.0 ± 0.6 %	31.0 ± 6.4 %
14 weeks	35.0 ± 4.8 %	33.0 ± 9.3 %
Endpoint (16 weeks)	25.8 ± 7.3 %	26.1 ± 2.6 %

Table – 5.1C – Comparisons between joints (P = 0.77) and over time (P = 0.57) were not significantly different using repeated measures mixed model ANOVA

Time Point	**Monocytes (% of leukocytes)**	
	Defect Joint	Control Joint
Baseline (0 weeks)	9.9 %	9.3 ± 0.2 %
2 weeks	5.6 ± 1.6 %	6.1 ± 1.9 %
4 weeks	7.1 ± 1.6 %	5.4 ± 1.4 %
6 weeks	4.7 ± 1.5 %	6.9 ± 3.0 %
8 weeks	6.9 ± 0.9 %	6.1 ± 0.8 %
10 weeks	7.5 ± 2.1 %	4.0 ± 2.1 %
12 weeks	6.6 ± 0.7 %	5.5 ± 1.5 %
14 weeks	9.2 ± 1.6 %	5.2 ± 3.0 %
Endpoint (16 weeks)	5.7 ± 0.4 %	3.5 ± 1.5 %

Table 5.1D – Comparisons between joints (P = 0.38) and over time (P = 0.25) were not significantly different using repeated measures mixed model ANOVA

Time Point	**Neutrophils (% of leukocytes)**	
	Defect Joint	Control Joint
Baseline (0 weeks)	60.4 %	55.4 ± 1.6%
2 weeks	62.0 ± 10.6%	59.6 ± 6.4 %
4 weeks	60.2 ± 9.8 %	63.9 ± 10.9 %
6 weeks	65.9 ± 11.2 %	67.8 ± 8.2 %
8 weeks	61.5 ± 5.8 %	60.3 ± 7.4 %
10 weeks	65.2 ± 16.4 %	66.1 ± 17.4 %
12 weeks	65.5 ± 0.1 %	63.6 ± 5.2 %
14 weeks	55.8 ± 6.4 %	61.9 ± 12.3 %
Endpoint (16 weeks)	68.5 ± 6.9 %	70.4 ± 1.9 %

Table 5.2 – Median (range) scores of variables assessed with arthroscopic examination at the end point. Percent of repair tissue (0-4; 0%, 1-25%, 26-50%, 51-75%, 76-100%), cartilage and bone attachment (0-4; normal, moderate, mild, slight, none), firmness (0-4; similar, slightly soft, mildly soft, moderately soft, markedly soft compared to normal articular cartilage), Level (1-6; mildly recessed, slightly recessed, level, slightly elevated, mildly elevated, moderately elevated), International Cartilage Repair Society (ICRS) score (0-4; normal, nearly normal, abnormal <50% depth, severely abnormal >50% depth, severely abnormal – through subchondral bone), Outerbridge score (0-4; normal, softening, partial thickness 1.5 cm diameter, fissuring >1.5 cm diameter, subchondral bone), Blood (1-3; fresh, old, none), shape (0-1; no increase, degeneration beyond defect), color (1-6; red, red/white, yellow, yellow/white, white/yellow, white), surface (1-4; non-undulating, slightly undulating, mildly undulating, moderately undulating) and grade (0-4; no tissue, poor, fair, good, excellent)

	Group I		**Group II**	
	Defect Joint	**Control Joint**	**Defect Joint**	**Control Joint**
Repair 1 (Calcified cartilage retained)				
Percent repair	1 (1 – 3)	4 (4 – 4)	1 (0 – 1)	4 (4 – 4)
Cartilage attachment	3 (0 – 3)	0 (0 – 0)	4 (1 – 4)	0 (0 – 0)
Bone attachment	3 (0 – 4)	0 (0 – 0)	2.5 (0 – 4)	0 (0 – 0)
Firmness	4 (2 – 4)	0 (0 – 0)	4 (0 – 4)	0 (0 – 0)
Level	1 (1 – 1)	3 (3 – 3)	1 (1 – 1)	3 (3 – 3)
ICRS score	3 (3 – 4)	0 (0 – 0)	4 (4 – 4)	0 (0 – 0)
Outerbridge score	4 (3 – 4)	0 (0 – 0)	4 (4 – 4)	0 (0 – 0)
Blood	1 (1 – 3)	3 (2 – 3)	3 (3 – 3)	3 (2 – 3)
Shape	0 (0 – 0)	0 (0 – 0)	1 (0 – 1)	0 (0 – 0)
Color	6 (6 – 6)	6 (6 – 6)	6 (6 – 6)	6 (6 – 6)
Surface	4 (2 – 4)	1 (1 – 1)	4 (4 – 4)	1 (1 – 1)
Grade	1 (1 – 1)	4 (4 – 4)	1 (1 – 1)	4 (4 – 4)
Repair 2 (Calcified cartilage removed)				
Percent repair	4 (4 – 4)	4 (4 – 4)	3.5 (3 – 4)	4 (4 – 4)
Cartilage attachment	1 (0 – 1)	0 (0 – 0)	1 (1 – 3)	0 (0 – 0)
Bone attachment	0 (0 – 1)	0 (0 – 0)	1 (1 – 1)	0 (0 – 0)
Firmness	2 (2 – 2)	0 (0 – 0)	2.5 (2 – 4)	0 (0 – 0)
Level	2 (1 – 2)	3 (3 – 3)	1.5 (1 – 3)	3 (3 – 3)
ICRS score	1 (1 – 1)	0 (0 – 0)	3 (1 – 3)	0 (0 – 0)
Outerbridge score	1 (1 – 2)	0 (0 – 0)	3 (2 – 3)	0 (0 – 0)
Blood	1 (1 – 3)	3 (2 – 3)	3 (3 – 3)	3 (2 – 3)
Shape	0 (0 – 0)	0 (0 – 0)	0 (0 – 1)	0 (0 – 0)
Color	6 (6 – 6)	6 (6 – 6)	6 (6 – 6)	6 (6 – 6)
Surface	2 (2 – 2)	1 (1 – 1)	3 (2 – 4)	1 (1 – 1)
Grade	3 (3 – 3)	4 (4 – 4)	2 (1 – 3)	4 (4 – 4)

Table 5.3 – Spearman rank (rho) coefficients and associated P – values for correlations between cationic CECT attenuation (microCT) and individual histological scoring components of the International Cartilage Repair Society (ICRS) system. *P < 0.05.

ICRS II histology scoring component	**Rho**	**P - value**
Tissue morphology	0.64	<0.0001*
Matrix staining	0.73	<0.0001*
Cell morphology	0.57	<0.0001*
Chondrocyte clustering	0.42	<0.0001*
Surface architecture	0.55	<0.001*
Basal integration	0.56	<0.0001*
Tidemark formation	0.62	<0.0001*
Subchondral bone abnormalities	0.58	<0.0001*
Inflammation	0.05	0.47
Calcification/Ossification	0.29	<0.0001*
Vascularization in repair	0.48	<0.0001*
Superficial zone Assessment	0.61	<0.0001*
Mid/Deep zone Assessment	0.66	<0.0001*
Overall Assessment	0.67	<0.0001
SOFG superficial zone	0.08	0.25
SOFG middle zone	0.23	0.0015*
SOFG deep zone territorial	0.16	0.03*
SOFG deep zone interterritorial	0.20	0.005*

Table 5.4 – Spearman correlation (rho) coefficients and P – values between clinical cationic CECT attenuation corrected to CA4+, iohexol and calcium hydroxyapatite (CaHA) concentrations, and other measured biochemical, mechanical and histological variables. *P < 0.05.

Variable	**CA4+ corrected**		**Iohexol corrected**		**CaHA corrected**	
	Rho	P - value	Rho	P - value	Rho	P - value
GAG	0.39	<0.0001*	0.39	<0.0001*	0.40	<0.0001*
Equilibrium Modulus	0.36	0.0003*	0.35	0.0004*	0.33	0.001*
MicroCT (cationic CECT) attenuation	0.52	<0.0001*	0.53	<0.0001*	0.53	<0.0001*
Dynamic Modulus 5%	0.39	0.001*	0.37	0.0001*	0.35	0.0003*
Dynamic Modulus 10%	0.41	<0.0001*	0.39	0.0001*	0.37	0.0002*
Dynamic Modulus 15%	0.40	<0.0001*	0.39	0.001*	0.37	0.0002*
Dynamic Modulus 20%	0.39	0.0001*	0.38	0.0001*	0.37	0.0002*
Collagen	-0.03	0.71	-0.04	0.63	-0.03	0.78
ICRS II histology scoring component						
Tissue morphology	0.57	<0.0001*	0.57	<0.0001*	0.57	<0.0001*
Matrix staining	0.32	<0.0001*	0.33	<0.0001*	0.33	<0.0001*
Cell morphology	0.37	<0.0001*	0.37	<0.0001*	0.35	<0.0001*
Chondrocyte clustering	0.31	<0.0001*	0.31	<0.0001*	0.30	<0.0001*
Surface architecture	0.32	<0.0001*	0.34	<0.0001*	0.32	<0.0001*
Basal integration	0.35	<0.0001*	0.35	<0.0001*	0.35	<0.0001*
Tidemark formation	0.36	<0.0001*	0.36	<0.0001*	0.36	<0.0001*
Subchondral bone abnormalities	0.35	<0.0001*	0.35	<0.0001*	0.36	<0.0001*
Inflammation	0.07	0.35	0.06	0.41	0.06	0.42
Calcification/Ossification	0.28	0.0001*	0.28	0.0001*	0.27	0.0001*
Vascularization in repair	0.45	<0.0001*	0.45	<0.0001*	0.44	<0.0001*
Superficial zone Assessment	0.33	<0.0001*	0.34	<0.0001*	0.33	<0.0001*
Mid/Deep zone Assessment	0.36	<0.0001*	0.37	<0.0001*	0.36	<0.0001*
Overall Assessment	0.35	<0.0001*	0.37	<0.0001*	0.36	<0.0001*
SOFG superficial zone	-0.04	0.55	-0.03	0.63	-0.04	0.58
SOFG middle zone	0.11	0.14	0.12	0.1	0.11	0.14
SOFG deep zone territorial	0.14	0.05	0.15	0.04	0.14	0.05
SOFG deep zone interterritorial	0.06	0.44	0.06	0.44	0.05	0.46

REFERENCES

1. Bansal PH, Joshi NS, Entezari V, et al. Contrast enhanced computed tomography can predict the glycosaminoglycan content and biomechanical properties of articular cartilage. *Osteoarthritis Cartilage* 2010;18:184-191.
2. Frisbie DD, Al-Sobayil F, Billinghurst RC, et al. Changes in synovial fluid and serum biomarkers with exercise and early osteoarthritis in horses. *Osteoarthritis and Cartilage* 2008;16:1196-1204.
3. Bekkers JE, Creemers LB, Dhert WJ, et al. Diagnostic modalities for diseased articular cartilage-from defect to degeneration: a review. *Cartilage* 2010;1:157-164.
4. Pease A. Biochemical evaluation of equine articular cartilage through imaging. *Vet Clin N Am-Equine* 2012;28:637-646.
5. Murray RC, Mair TS, Sherlock CE, et al. Comparison of high-field and low-field magnetic resonance images of cadaver limbs of horses. *Vet Rec* 2009;165:281-288.
6. Smith MA, Dyson SJ, Murray RC. Reliability of high- and low-field magnetic resonance imaging systems for detection of cartilage and bone lesions in the equine cadaver fetlock. *Equine Vet J* 2012;44:684–691.
7. Taylor C, Carballido-Gamio, J, Majumdar, S, Li, X. Comparison of quantitative imaging of cartilage for osteoarthritis: T2, T1ρ, dGEMRIC and contrast-enhanced computed tomography. *Mag Res Imag* 2009;27:779-784.
8. Roemer FW, Eckstein F, Hayashi D, et al. The role of imaging in osteoarthritis. *Best Pract Res Clin Rheumatol* 2014;28:31-60.
9. Judy C. The stifle In: Murray RC, ed. *Equine MRI*. Oxford, UK: Wiley-Blackwell, 2011;451-466.

10. Valdés-Martínez A. Computed tomographic arthrography of the equine stifle joint. *Vet Clin N Am-Equine* 2012;28:583-598.
11. Nelson BB, Kawcak CE, Goodrich LR, et al. Comparison between computed tomographic arthrography, radiography, ultrasonography, and arthroscopy for the diagnosis of femorotibial joint disease in western performance horses. *Vet Radiol Ultrasound* 2016;57:387-402.
12. Joshi NS, Bansal PN, Stewart RC, et al. Effect of contrast agent charge on visualization of articular cartilage using computed tomography: exploiting electrostatic interactions for improved sensitivity. *J Am Chem Soc* 2009;131:13234-13235.
13. Bansal PN, Joshi NS, Entezari V, et al. Cationic contrast agents improve quantification of glycosaminoglycan (GAG) content by contrast enhanced CT imaging of cartilage. *J Orthop Res* 2011;29:704-709.
14. Bansal PN, Stewart RC, Entezari V, et al. Contrast agent electrostatic attraction rather than repulsion to glycosaminoglycans affords a greater contrast uptake ratio and improved quantitative CT imaging in cartilage. *Osteoarthritis Cartilage* 2011;19:970-976.
15. Lakin BA, Ellis DJ, Shelofsky JS, et al. Contrast-enhanced CT facilitates rapid, non-destructive assessment of cartilage and bone properties of the human metacarpal. *Osteoarthritis Cartilage* 2015;23:2158-2166.
16. Lakin BA, Grasso DJ, Shah SS, et al. Cationic agent contrast-enhanced computed tomography imaging of cartilage correlates with the compressive modulus and coefficient of friction. *Osteoarthritis Cartilage* 2013;21:60-68.

17. Lakin BA, Patel H, Holland C, et al. Contrast-enhanced CT using a cationic contrast agent enables non-destructive assessment of the biochemical and biomechanical properties of mouse tibial plateau cartilage. *J Orthop Res* 2016;34:1130-1138.
18. Kallioniemi AS, Jurvelin JS, Nieminen MT, et al. Contrast agent enhanced pQCT of articular cartilage. *Phys Med Biol* 2007;52:1209-1219.
19. Kulmala KAM, Karjalainen HM, Kokkonen HT, et al. Diffusion of ionic and non-ionic contrast agents in articular cartilage with increased cross-linking--contribution of steric and electrostatic effects. *Med Eng Phys* 2013;35:1415-1420.
20. Stewart RC, Bansal PN, Entezari V, et al. Contrast-enhanced CT with a high-affinity cationic contrast agent for imaging ex vivo bovine, intact ex vivo rabbit and in vivo rabbit cartilage. *Radiology* 2013;266:141-150.
21. Stewart RC, Patwa AN, Lusic H, et al. Synthesis and preclinical characterization of a cationic iodinated imaging contrast agent (CA4+) and its use for quantitative computed tomography of ex vivo human hip cartilage. *J Med Chem* 2017;60:5543-5555.
22. American Association of Equine Practitioners. *Guide for veterinary service and judging of equestrian events*. Lexington, KY: American Association of Equine Practitioners, 1991.
23. Frisbie DD, Bowman SM, Colhoun HA, et al. Evaluation of autologous chondrocyte transplantation via a collagen membrane in equine articular defects – results at 12 and 18 months. *Osteoarthritis and Cartilage* 2008;16:667-679.
24. Hendrickson DA, Nixon AJ. Comparison of the cranial and a new lateral approach to the femoropatellar joint for aspiration and injection in horses. *J Am Vet Med Assoc* 1994;205:1177-1179.

25. McIlwraith CW, Fortier LA, Frisbie DD, et al. Equine models of articular cartilage repair. *Cartilage* 2011;2:317-326.

26. Hurtig MB, Fretz PB, Doige CE, et al. Effects of lesion size and location on equine articular cartilage repair. *Can J Vet Res* 1988;52:137-146.

27. Frisbie DD, Trotter GW, Powers BE, Rodkey WG, Steadman JR, Howard RD, Park RD, and McIlwraitth CW. Arthroscopic subchondral bone plate microfracture technique augments healing of large chondral defects in the radial carpal bone and medial femoral condyle of horses. *Vet Surg* 1999;28:242-255.

28. Bertone AL, Palmer JL, Jones J. Synvoial fluid cytokines and eicosanoids as markers of joint disease in horses. *Vet Surg* 2001;30:528-538.

29. Farndale RW, Buttle DJ, Barrett AJ. Improved quantitation and discrimination of sulphated glycosaminoglycans by use of dimethylmethylene blue. *Biochim Biophys Acta* 1986;883:173-177.

30. McIlwraith CW, Nixon AJ, Wright IM. Diagnostic and surgical arthroscopy of the femoropatellar and femorotibial joints In: McIlwraith CW, Nixon AJ,Wright IM, eds. *Diagnostic and surgical arthroscopy in the horse*. 4th ed. New York: Mosby Elsevier, 2015;175-242.

31. Brittberg M, Winalski CS. Evaluation of cartilage injuries and repair. *J Bone Joint Surg* 2003;85-A:58-69.

32. Outerbridge RE. The etiology of chondromalacia patellae. *J Bone Joint Surg Br* 1961;43-B:752-757.

33. Edwards RB, Lu Y, Cole BJ, et al. Comparison of radiofrequency treatment and mechanical debridement of fibrillated cartilage in an equine model. *Vet Comp Orthop Traumatol* 2008;21:41-48.

34. Brittberg M, Winalski CS. Evaluation of cartilage injuries and repair. *J Bone Joint Surg Am* 2003;85-A Suppl 2:58-69.

35. Mow V, Hayes W. *Basic Orthopaedic Biomechanics*. New York, NY: Raven Press Ltd., 1991.

36. Mow VC, Ratcliffe A, Poole AR. Cartilage and diarthrodial joints as paradigms for hierarchical materials and structures. *Biomaterials* 1992;13:67-97.

37. Park S, Hung CT, Ateshian GA. Mechanical response of bovine articular cartilage under dynamic unconfined compression loading at physiological stress levels. *Osteoarthritis and Cartilage*;12:65-73.

38. Lippiello L, Hall D, Mankin HJ. Collagen synthesis in normal and osteoarthritic human cartilage. *J Clin Invest* 1977;59:593-600.

39. Venn M, Maroudas A. Chemical composition and swelling of normal and osteoarthrotic femoral head cartilage. I. Chemical composition. *Ann Rheum Dis* 1977;36:121-129.

40. McIlwraith CW, Frisbie DD, Kawcak CE, et al. The OARSI histopathology initiative - recommendations for histological assessments of osteoarthritis in the horse. *Osteoarthritis and Cartilage* 2010;18:S93-S105.

41. Mainil-Varlet P, Van Damme B, Nesic D, et al. A new histology scoring system for the assessment of the quality of human cartilage repair: ICRS II. *Am J Sports Med* 2010;38:880-890.

42. Landis JR, Koch GG. The measurement of observer agreement for categorical data. *Biometrics* 1977;33:159-174.

43. Stewart R. A diagnostic imaging technique and therapeutic strategy for early osteoarthritis. *College of Engineering*. Boston, MA: Boston University, 2014;180.

44. Schmitz N, Laverty S, Kraus VB, et al. Basic methods in histopathology of joint tissues. *Osteoarthritis and Cartilage* 2010;18:S113-S116.

45. Camplejohn KL, Allard SA. Limitations of safranin 'O' staining in proteoglycan-depleted cartilage demonstrated with monoclonal antibodies. *Histochemistry* 1988;89:185-188.

46. Maroudas A. Balance between swelling pressure and collagen tension in normal and degenerate cartilage. *Nature* 1976;260:808-809.

47. Burr DB. The importance of subchondral bone in osteoarthrosis. *Curr Opin Rheumatol* 1998;10:256-262.

48. Li G, Yin J, Gao J, et al. Subchondral bone in osteoarthritis: insight into risk factors and microstructural changes. *Arthritis Res Ther* 2013;15:223.

49. Kawcak CE, McIlwraith CW, Norrdin RW, et al. The role of subchondral bone in joint disease: a review. *Equine Vet J* 2001;33:120-126.

50. van Weeren PR. General anatomy and physiology of joints In: McIlwraith CW, Frisbie DD, Kawcak CE, et al., eds. *Joint Disease in the Horse* 2nd ed. St. Louis, MO: Elsevier, 2016;1-24.

51. Silver FH, Bradica G, Tria A. Relationship among biomechanical, biochemical, and cellular changes associated with osteoarthritis. *Crit Rev Biomed Eng* 2001;29:373-391.

52. Zhu W, Mow VC, Koob TJ, et al. Viscoelastic shear properties of articular cartilage and the effects of glycosidase treatments. *J Orthop Res* 1993;11:771-781.

53. Hoemann CD. Molecular and biochemical assays of cartilage components In: De Ceuninck F, Sabatini M,Pastoureau P, eds. *Cartilage and Osteoarthritis*. Totowa, New Jersey: Humana Press, 2004;127-156.

54. Strauss EJ, Goodrich LR, Chen CT, et al. Biochemical and biomechanical properties of lesion and adjacent articular cartilage after chondral defect repair in an equine model. *Am J Sports Med* 2005;33:1647-1653.

55. Torrie AM, Kesler WW, Elkin J, et al. Osteochondral allograft. *Curr Rev Musculoskelet Med* 2015;8:413-422.

56. Valiyaveettil M, Mort JS, McDevitt CA. The concentration, gene expression, and spatial distribution of aggrecan in canine articular cartilage, meniscus, and anterior and posterior cruciate ligaments: a new molecular distinction between hyaline cartilage and fibrocartilage in the knee joint. *Connect Tissue Res* 2005;46:83-91.

57. Nguyen AM, Levenston ME. Comparison of osmotic swelling influences on meniscal fibrocartilage and articular cartilage tissue mechanics in compression and shear. *J Orthop Res* 2012;30:95-102.

58. LeRoux MA, Arokoski J, Vail TP, et al. Simultaneous changes in the mechanical properties, quantitative collagen organization, and proteoglycan concentration of articular cartilage following canine meniscectomy. *J Orthop Res* 2000;18:383-392.

59. Nelson BB, Kawcak CE, Ehrhart EJ, et al. Radiofrequency probe and sharp transection for tenoscopic-guided desmotomy of the accessory ligament of the superficial digital flexor tendon. *Vet Surg* 2015;44:713-722.

60. Frisbie DD, McIlwraith CW, Kawcak CE, et al. Efficacy of intravenous administration of hyaluronan, sodium chondroitin sulfate, and N-acetyl-d-glucosamine for prevention or treatment of osteoarthritis in horses. *Am J Vet Res* 2016;77:1064-1070.

61. Kawcak CE, Frisbie DD, Werpy NM, et al. Effects of exercise vs experimental osteoarthritis on imaging outcomes. *Osteoarthritis Cartilage* 2008;16:1519-1525.

62. Smith AD, Morton AJ, Winter MD, et al. Magnetic resonance imaging scoring of an experimental model of post-traumatic osteoarthritis in the equine carpus. *Vet Radiol Ultrasound* 2016;57:502-514.

63. Hontoir F, Clegg P, Nisolle JF, et al. Magnetic resonance compositional imaging of articular cartilage: What can we expect in veterinary medicine? *Vet J* 2015;205:11-20.

SUMMARY AND CONCLUSIONS

In summary, this compilation of experiments critically evaluated cationic CECT in equine articular cartilage and supported its ability to distinguish disease states through nondestructive assessment. Additionally, these studies also consistently reinforced the capability of cationic CECT attenuation to reflect the biochemical, mechanical and histological attributes of articular cartilage. The objectives of this work to comprehensively examine the use of this imaging technology in equine articular cartilage were achieved. In the first study, the trajectory of CA4+ diffusion to reach an equilibrated state within articular cartilage was established and also validated the *in vitro* protocols used in the consecutive experiments.

The second study revealed that the *in vivo* diffusion trajectory was predictable in the face of active joint metabolism. Additionally, the intra-articular administration of CA4+ did not cause overt toxicity to articular tissues. However, the high injection frequency and volume administered within a short duration implored by the study design lead to untoward effects in the synovial membrane as determined with histologic assessment. The injection frequency used in this experiment would not be practical in clinical scenarios and coupled with the lack of any other adverse outcomes, it is unlikely that this response in the synovial membrane is clinically relevant, though requires further investigation. Subsequent experiments where administering two doses of CA4+ administered two months apart did not elicit this same histological response and signify that these effects are not directly related to the CA4+ contrast medium.

The two remaining studies used different *in vivo* equine models to investigate the validity of cationic CECT imaging in detecting subtly damaged and reparative articular cartilage from

normal tissue *in vitro* and *in vivo*. Both models were adaptations of previously documented techniques and were modified to address the customized hypotheses for each experiment. The *in vivo* impact model delivered a contusive force to articular cartilage that established a degenerative process. The model did not induce fulminant joint disease in the short term but did permit investigation of subtle articular cartilage injury that could be inspected with *in vivo* cationic CECT imaging. The results of the postmortem analyses confirmed that the mechanically induced impact caused degeneration of the extracellular matrix components and therefore reduced the mechanical stiffness of the tissue, both of which were discernable using cationic CECT (microCT) imaging. *In vivo,* clinical cationic CECT attenuation demonstrated significant fair correlations with GAG content, EM, and SOFG staining scores. Despite these promising results, the clinical CECT attenuations were not of sufficient bandwidth to detect differences between disease states. Further investigations are warranted to determine how focal sites of injury can be identified from the resolution limited by current CT technology. Assessments of tissue volume and automated sampling methods still have the potential to identify these differences between disease states *in vivo* with clinical cationic CECT imaging and require investigation.

The fourth study revealed that cationic CECT imaging uncovered the differences between healing, degenerative and normal articular cartilage by utilizing an *in vivo* chondral defect model. The model effectively provided a spectrum of diseased tissue for evaluation. Both microCT and clinical scanners demonstrated the ability to distinguish these groups. While trends over time revealed a significant difference between groups, the inherent biochemical and biomechanical variation that exists across joints surfaces complicates the detection of subtly

damaged tissue using a single quantitative measurement at a solitary examination. Nonetheless, this study demonstrated that longitudinal examinations of cationic CECT imaging successfully illustrate the degenerative pathophysiological alterations that occur in articular cartilage. Despite these promising results, the use of automated processing algorithms to improve the feasibility of this technique and large-scale studies establishing normal variation across horses with altering ages, athletic status and different joints are required before fulminant use can be instituted into clinical practice.

In conclusion, these studies show the ability of cationic CECT imaging to characterize articular cartilage across a multitude of injured states and further support its use as a research tool for the evaluation of articular cartilage. With continued optimization to establish consistency across inflamed joints and using automated imaging analysis protocols, it also holds considerable promise to traverse research environments and become incorporated into clinical practice. Lastly, with the horse being an established translational research animal for humans, and the similarities in the pathophysiology of osteoarthritis between these two species combined with the safe administration of CA4+ on articular tissues, the exploration of cationic CECT imaging in human tissue can justifiably be considered.

APPENDIX I

PROTOCOLS FOR PROCESSING AND STAINING OF HISTOLOGICAL TISSUES

Table I.1A: Osteochondral tissue processing settings. Tissue processor: Tissue Tec VIP 5 (Leica Model #5A-F1)

Station #	Solution	Concentration %	Duration (h)	Temp (°C)	P/V	Mix
1	Ethanol	70	3 h	--	Off	off
2	Ethanol	80	2 h	--	On	Fast
3	Ethanol	80	3 h	--	On	Fast
4	Ethanol	95	2 h	--	On	Fast
5	Ethanol	95	3 h	--	On	Fast
6	Ethanol	100	1 h	--	On	Fast
7	Ethanol	100	2 h	--	On	Fast
8	Ethanol	100	3 h	--	On	Fast
9	Xylene	100	3 h	--	On	Fast
10	Xylene	100	1 h	--	On	Fast
11	Paraffin	100	1 h	62	On	Slow
12	Paraffin	100	2 h	62	On	Slow
13	Paraffin	100	2 h	62	On	Slow
14	Paraffin	100	0.0 h	62	On	Slow

Table I.1B: Synovial membrane tissue processing settings. Tissue processor: Tissue Tec VIP 5 (Leica Model #5A-F1)

Station #	Solution	Concentration %	Duration	Temp (°C)	P/V	Mix
1	Ethanol	70	1 h 15 min	37	off	off
2	Ethanol	80	1 h 15 min	37	off	off
3	Ethanol	80	1 h 15 min	37	off	off
4	Ethanol	95	1 h 15 min	37	off	off
5	Ethanol	95	1 h 15 min	37	off	off
6	Ethanol	100	1 h 15 min	37	off	off
7	Ethanol	100	1 h 15 min	37	off	off
8	Ethanol	100	1 h 15 min	37	off	off
9	Xylene	100	1 h 15 min	37	off	off
10	Xylene	100	1 h 15 min	37	off	off
11	Paraffin	100	1 h 15 min	62	off	off
12	Paraffin	100	1 h 15 min	62	off	off
13	Paraffin	100	0.0 h	62	off	off
14	Paraffin	100	0.0 h	62	off	off

Appendix I.2**:** Histology slide staining protocols

Hematoxylin and eosin staining (articular cartilage and synovial membrane)

1. Deparaffinize sections through two xylene soaks for 10 minutes each.
2. Serial alcohol hydrations
    i. 100% ETOH 3 minutes
    ii. 100% ETOH 3 minutes
    iii. 90% ETOH 2 minutes
    iv. 90% ETOH 2 minutes
    v. 70% ETOH 2 minutes
    vi. 70% ETOH 2 minutes
    vii. Distilled water 5 minutes
    viii. Distilled water 5 minutes
3. Stain slides in Harris's hematoxylin for 8 minutes
4. Rinse in running tap water for 5 minutes
5. Rinse slides in 1% Acid alcohol for 30 seconds
6. Rinse in running tap water for 1 minutes
7. Stain slides in bluing solution for 1 min
8. Rinse in running tap water for 1 minute
9. Dip slides 10 times into 95% Ethanol
10. Counterstain in Eosin Y for 1 min
11. Dehydrate through serial alcohol steps
    i. 95% ETOH for 2 minutes
    ii. 100 % ETOH for 2 minutes
12. Clear in Xylene for 5 minutes
13. Coverslip

Safranin-O Fast Green staining (articular cartilage)

1. Deparaffinize sections through two xylene soaks for 5 minutes each.
2. Serial alcohol hydrations
    i. 100% ETOH 3 minutes
    ii. 100% ETOH 3 minutes
    iii. 90% ETOH 2 minutes
    iv. 90% ETOH 2 minutes
    v. 70% ETOH 2 minutes
    vi. 70% ETOH 2 minutes
3. Stain slides in working Weigert's hematoxylin working solution for 7 minutes
4. Rinse for 2 minutes
5. Stain in working Fast green solution for 3 minutes
6. Rinse slides in 1% acetic acid solution for 15 minutes
7. Stain in 0.1% safranin O solution for 10 minutes
8. Dehydrate through serial alcohol steps
    i. 90% ETOH dip 10-20 times
    ii. 100% ETOH for 2 minutes
9. Clear in Xylene for 5 minutes
10. Coverslip

APPENDIX II

RESULTS OF THE INTERNATIONAL CARTILAGE REPAIR SOCIETY II HISTOLOGY SCORES COMPARED BETWEEN SAMPLE LOCATIONS (CHAPTER 5 SUPPLEMENTARY FIGURES).

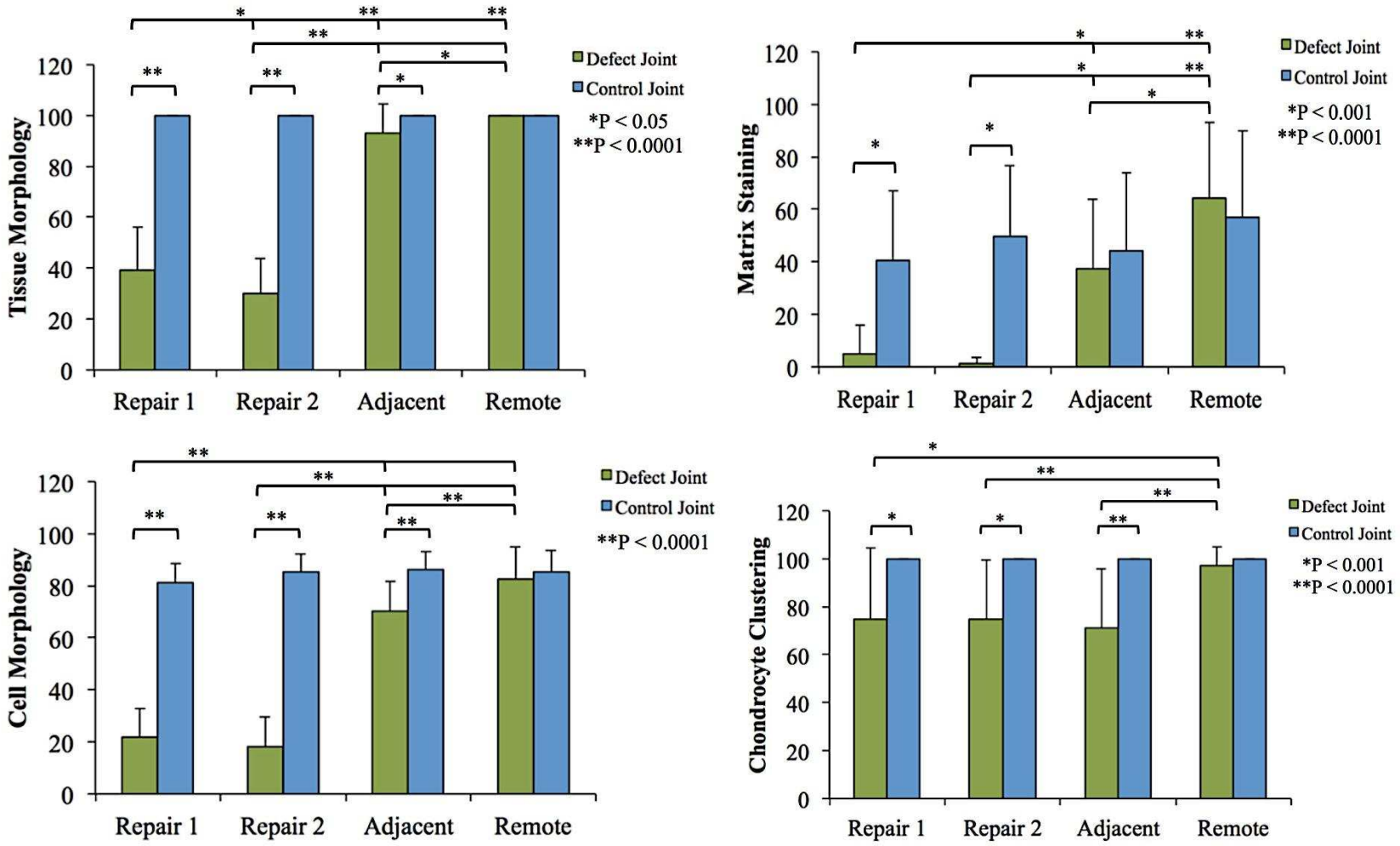

Figure II.1 – Comparisons of individual components of the International Cartilage Repair Society (ICRS) II histology scoring system across sample locations in defect and control joints. Mean ± s.d. SOFG, safranin O fast green.

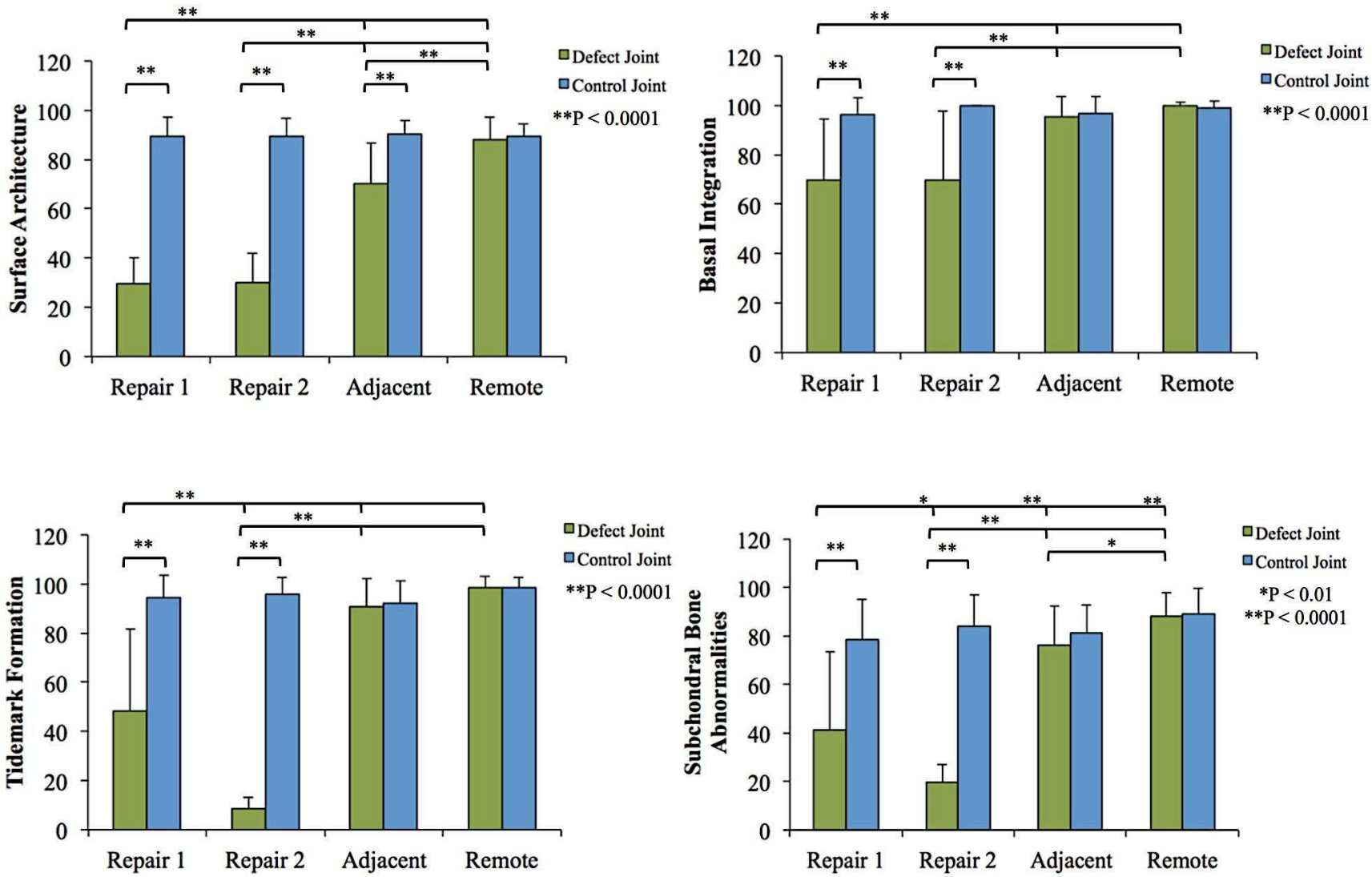

Figure II.1 – continued. Comparisons of individual components of the International Cartilage Repair Society (ICRS) II histology scoring system across sample locations in defect and control joints. Bars represent mean ± s.d. SOFG, safranin O fast green.

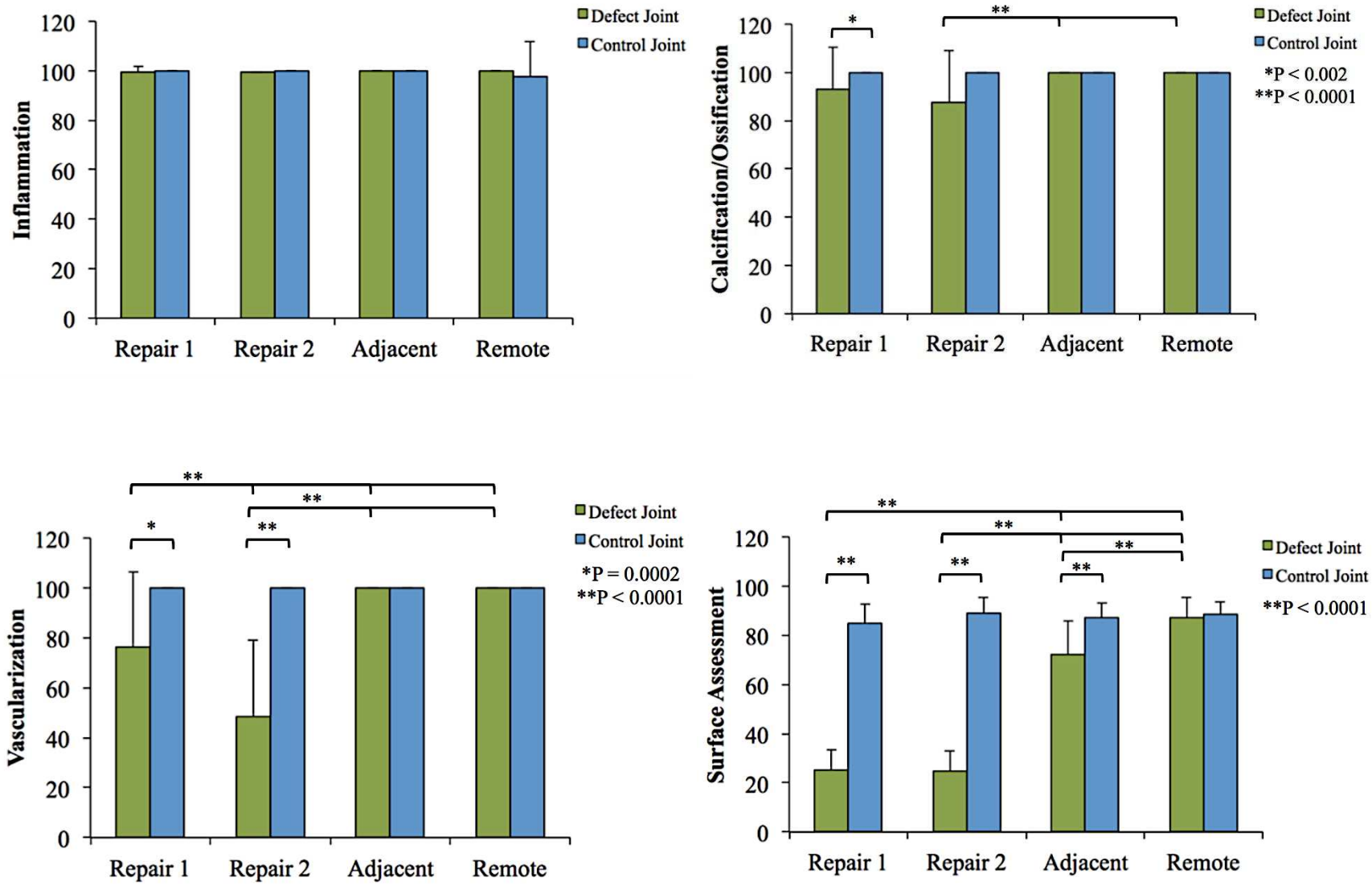

Figure II.1 – continued. Comparisons of individual components of the International Cartilage Repair Society (ICRS) II histology scoring system across sample locations in defect and control joints. Bars represent mean ± s.d. SOFG, safranin O fast green.

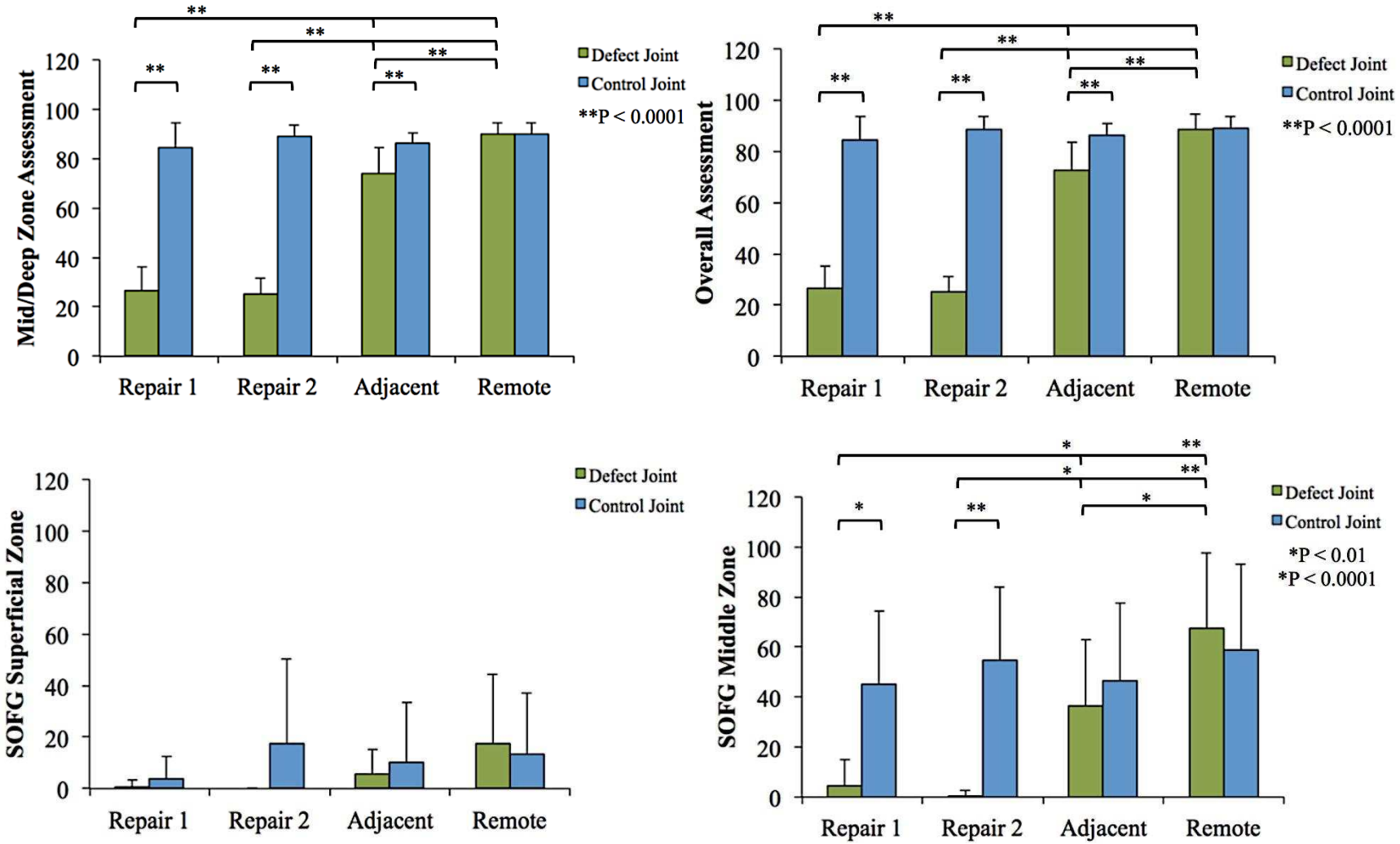

Figure II.1 – continued. Comparisons of individual components of the International Cartilage Repair Society (ICRS) II histology scoring system across sample locations in defect and control joints. Bars represent mean ± s.d. SOFG, safranin O fast green.

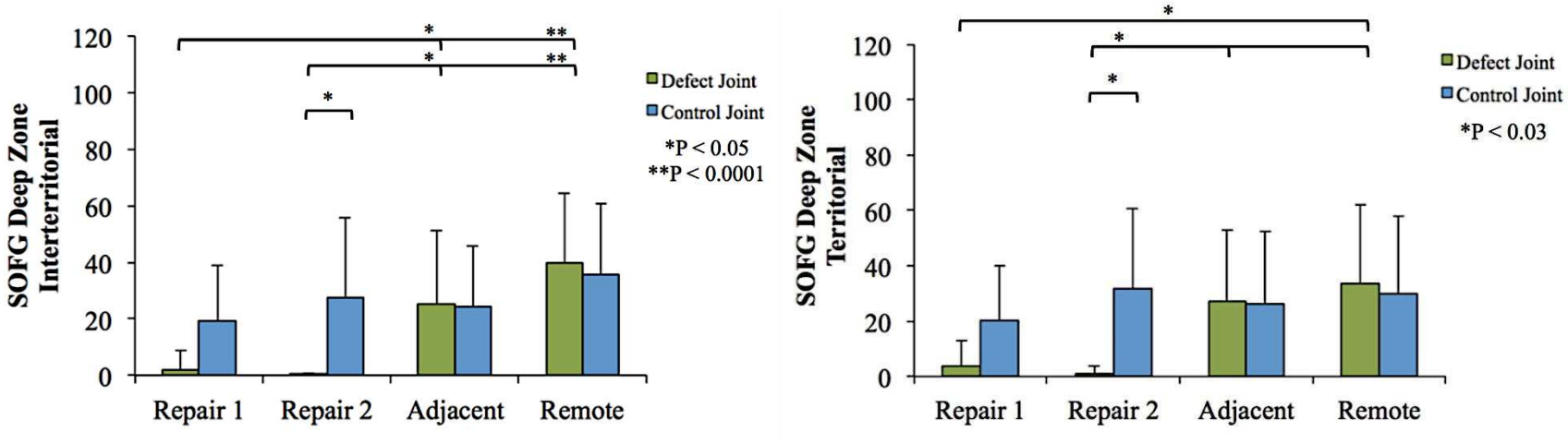

Figure II.1 – continued. Comparisons of individual components of the International Cartilage Repair Society (ICRS) II histology scoring system across sample locations in defect and control joints. Bars represent mean ± s.d. SOFG, safranin O fast green.